Signal Processing for Airborne Bistatic Radar

Kian Pin Ong

A thesis submitted for the degree of Doctor of Philosophy.

The University of Edinburgh.

- June 2003 -

Abstract

The major problem encountered by an airborne bistatic radar is the suppression of bistatic clutter. Unlike clutter echoes for a sidelooking airborne monostatic radar, bistatic clutter echoes are range dependent. Using training data from nearby range gates will result in widening of the clutter notch of STAP (space-time adaptive processing) processor. This will cause target returns from slow relative velocity aircraft to be suppressed or even go undetected. Some means of Doppler compensation for mitigating the clutter range dependency must be carried out.

This thesis investigates the nature of the clutter echoes with different radar configurations. A novel Doppler compensation method using Doppler interpolation in the angle-Doppler domain and power correction for a JDL (joint domain localized) processor is proposed. Performing Doppler compensation in the Doppler domain, allows several different Doppler compensations to be carried out at the same time, using separate Doppler bins compensation. When using a JDL processor, a 2-D Fourier transformation is required to transform space-time domain training data into angular-Doppler domain. Performing Doppler compensation in the space-time domain requires Fourier transformations of the Doppler compensated training data to be carried out for every training range gate. The whole process is then repeated for every range gate under test. On the other hand, Fourier transformations of the training data are required only once for all range gates under test, when using Doppler interpolation. Before carrying out any Doppler compensation, the peak clutter Doppler frequency difference between the training range gate and the range gate under test, needs to be determined. A novel way of calculating the Doppler frequency difference that is robust to error in pre-known parameters is also proposed.

Reducing the computational cost of the STAP processor has always been the desire of any reduced dimension processors such as the JDL processor. Two methods of further reducing the computational cost of the JDL processor are proposed. A tuned DFT algorithm allow the size of the clutter sample covariance matrix of the JDL processor to be reduced by a factor proportional to the number of array elements, without losses in processor performance. Using alternate Doppler bins selection allows computational cost reduction, but with performance loss outside the clutter notch region. Different systems parameters are also used to evaluate the performance of the Doppler interpolation process and the JDL processor. Both clutter range and Doppler ambiguity exist in radar systems operating in medium pulse repetitive frequency mode. When suppressing range ambiguous clutter echoes, performing Doppler compensation for the clutter echoes arriving from the nearest ambiguous range alone, appear to be sufficient.

Clutter sample covariance matrix is estimated using training data from the range or time or both dimension. Investigations on the number of range and time training data required for the estimation process in both space-time and angular-Doppler domain are carried out. Due to error in the Doppler compensation process, a method of using the minimum amount of range training data is proposed. The number of training data required for different clutter sample covariance matrix sizes is also evaluated. For Doppler interpolation and power correction JDL processor, the number of Doppler bins used can be increased, to reduce the amount of training data required, while maintaining certain desirable processor performance characteristics.

Declaration of originality

I hereby declare that the research recorded in this thesis and the thesis itself was composed and originated entirely by myself in the School of Engineering and Electronics at the University of Edinburgh, except Figure 1.5 and Figure 4.17.

Kian Pin Ong

June 2003

Acknowledgements

I would like to extend my sincere thanks to the following people for their invaluable assistance during the course of this PhD:

* Professor Bernard Mulgrew, my supervisor, for his continuous support, guidance and invaluable advice. Also for reading and checking this thesis during time when his attention is greatly demanded by so many other people.

* My 2^{nd} supervisor Professor Steve McLaughlin for his support and guidance, as well as for his constructive comments on the writing for this thesis.

* BAE Systems Edinburgh for providing funding and support for this work.

* My parents for their financial and emotional support during my PhD, without them, completion of this work would not be possible.

* My brother - Ben Ong, sisters: Hui Pin Ong and Mariette Ong, and brothers-in-law: Sam Foo and Jeffery Tan for always be there to give me support and advice. Constantly receiving photographs and stories about my nieces: Glenda Foo, Callista Foo and Ava Tan, never fails to warm my heart.

* My colleagues and academic staffs in the former Signals and System Group, now known as Institute of Digital Communications for their assistance in one way or another during the last three years. Special thanks to Dr. Martin Luna-Rivera, Michael Bennett and Moti Tabulo for providing advice, reading and correcting this thesis.

* The staff of the Institute of Digital Communications, particularly Dr. John Thompson, Dr. Dave Laurenson and Dr. Jimmy Dripps, who have at some stage or another provided valuable assistance.

* David Stewart, Michael Gordon, Chris Rudd and Bryan Tierney for their instantaneous computer support and tolerance towards my high computing usage.

* My friends from Canadian Rendez-Vous 2002, for keep sending their encouragement and thoughts from around the world.

* Jamie Chan, for her love and support during the first $2\frac{1}{2}$ years of this degree.

* Victoria Di*é*guez and others who have one time or another lived in Kitchener House, making it such an interesting place to live in.

* Special thanks to Jürgen Kruse, EADS, Bremen, Germany for the kind permission to reproduce Figure 1.5.

Contents

List of figures

List of tables

Acronyms and abbreviations

2-D	two-dimensional
$\Sigma\Delta$ STAP	Sum and difference STAP
ADC	Angle-Doppler compensation
ADPCA	Adaptive DPCA
AEW	Airborne early warning
AWGN	Additive whit Gaussian noise
CNR	Clutter to noise ratio
CPI	Coherent processing interval
CSM	Cross-Spectral Metric
DOA	Direction of arrival
DOF	Degrees-of-Freedom
DBU	Derivative-based updating
DFT	Discrete Fourier transform
DPCA	Displaced phase centre antenna
DW	Doppler warping
EC	Eigencanceler
EFA	Extended factored approach
ESMI	Extended sample matrix inversion
F/B	Forward-backward
FA	Factored approach
FFT	Fast Fourier transform
FTS	Factored time-space
GSC	Generalized sidelobe canceller
IF	Improvement factor
i.i.d.	Independent identical distribution
JDL	Joint domain localised
LCNR	Load-to-clutter + white noise ratio
LPI	Low probability of intercept
LPR	Localized processing region

MDV	Minimum detectable velocity
ML	Maximum likelihood
MLE	Maximum likelihood estimator
MPRF	Medium PRF
MSWF	Multistage Wiener filter
MVE	Minimum variance estimator
NHD	Non-homogeneity detector
PC	Principal components
PRF	Pulse repetition frequency
PRI	Pulse repetition interval
RCS	Radar cross section
RAM	Radar absorbing material
RAS	Radar absorbing structure
SCNR	Signal-to-clutter+noise ratio
SINR	Signal-to-interference + noise ratio
SLAR	Sidelooking monostatic airborne radar
STAP	Space-time adaptive processing
UAV	Unmanned aerial vehicle
UHF	Ultra high frequency
ULA	Uniform linear array
VHF	Very high frequency

Nomenclature

α	cone angle
α_k	estimation performance factor
α_s	an unknown complex constant representing the amplitude of the target signal
α_{ta}	target direction of arrival of the target
β	the look direction relative to the array
Δ	difference beam
$\Delta\phi$	phase change between pulses
Δ	Doppler frequency shift
Δf_D	change in target Doppler frequency
Δ^i_{fd}	is the time offsets for the ith translation
Δ^i_{fs}	is the space offsets for the ith translation
ΔR	range change between pulses
Δv_t	change in target velocity
δ_t	transmitter flight direction
δ_r	receiver flight direction
λ	wavelength of the radar signal
$\otimes$	Kronecker product
$\circ$	Hadamard product
ψ	crab angle
Σ	sum beam
σ^2_c	clutter variance
σ^2_L	loading noise variance
σ^2_w	white noise variance
θ	depression angle
θ_r	receiver depression angle
θ_t	transmitter depression angle
$\theta_{r,k}$	receiver depression angle from range gate k
$\theta_{r,r}$	receiver depression angle from range gate r
$\theta_{t,k}$	transmitter depression angle from range gate k

$\theta_{t,r}$	transmitter depression angle from range gate r
φ	azimuth angle
φ_r	receiver azimuth angle
φ_t	transmitter azimuth angle
$\varphi_{t,k}$	receiver azimuth angle from range gate k
$\varphi_{t,r}$	receiver azimuth angle from range gate r
a_e	x-axis parameter of an ellipsoid
a_t	acceleration of the target
b_e	y-axis parameter of an ellipsoid
$\mathbf{C}$	clutter matrix
C_k	clutter ridge from neighboring range gates k's
C_r	clutter ridge from range gate r
c	speed of light
c_e	z-axis parameter of an ellipsoid
$\mathbf{D}$	cube data matrix of all range gates
$D(.)$	sensors directivity patterns
D_f	size of DFT process (transform of time domain to Doppler domain
d	distance travelled
d_a	spacing between the elements of the array antenna
$\widetilde{d_T}$	unit vector pointing from the transmitter to P
$\widetilde{d_R}$	unit vector pointing from the receiver to P
$E[\cdot]$	mathematical expectation operator
f_0^d	Doppler frequency of range gate under test
f_0^s	spatial frequency of range gate under test
f_D	clutter Doppler frequency
$\tilde{f}_k^d$	estimated clutter Doppler frequency of range gate k using received data
f_d'	renamed Doppler frequency for scaling method
f_s'	renamed spatial frequency for scaling method
f_d^k , f_k^d	calculated Doppler frequency of range gate k
f_s^k , f_k^s	spatial frequency of range gate k
f_{ss}	target signal spatial frequency
f_{st}	target signal temporal frequency
f_{new}	Doppler frequency of interest

f_r	relative Doppler frequency
$\tilde{f}_r^d$	would be clutter Doppler frequency of range gate r using received data, assuming no target is present
f_r^d	calculated Doppler frequency of range gate r
f_o	operating frequency
f_{old}	Doppler frequency from the old data
$f_s(r,k)$	Doppler shift from range gate k to r
$G(.)$	transmit directivity pattern
G_d	total number of range gate available
g	range gate number
superscript H	Hermitian operator (conjugate transpose)
H	height of platform
H_0	signal-absence hypothesis
H_1	signal-presence hypothesis
H_R	receiver height
H_T	transmitter height
$\mathbf{I}$	identity matrix
IF	improvement factor
K	total number of snapshot
K_{opt}	number of snapshot required to obtain $\mathbf{R}$
k	range gate number
kT_sB_n	thermal-noise power
$L(.)$	reflectivity of the ground
L	time dimension data snapshots
L_e	baseline of an ellipsoid
L_{SINR}	SINR loss
M	number of temporal pulses used in a STAP processor
M_{Db}	number of Doppler bins required for separate Doppler compensation
M_f	number of Doppler bins used in JDL processor
ML	maximum likelihood
$\mathbf{N}$	noise matrix
N	number of antenna array element
N_a	number of angular bins using in JDL processor

N_{dw}	number of pulses within a single dwell
N_p	number of zero padding added to the spatial samples
$O(.)$	of the order of bracketed quantity number of operation
ω	Doppler frequency
P	scatter P
$\widehat{P_{cl_k}}$	power of clutter/interference arriving from training range gate k
P_c	power compensation
P_{cl}	clutter power
P_{cl_k}	calculated clutter power arriving from training range gate k
P_{cl_r}	calculated clutter power arriving from training range gate r
P_t	transmitted power
P_n^{in}	noise power at the input
P_n^{out}	noise power at the output
P_s^{in}	signal power at the input
P_s^{out}	signal power at the output
$\mathbf{Q}$	true clutter/interference + noise covariance matrix
$\widehat{\mathbf{Q}}$	estimated clutter/interference + noise covariance matrix
$\widehat{\mathbf{Q}}_{2D}$	2-D Doppler warped clutter/interference + noise covariance matrix
$\widehat{\mathbf{Q}}_{dw}$	Doppler warped clutter/interference + noise covariance matrix
$\widehat{\mathbf{Q}}_s$	scaled estimated clutter/interference + noise covariance matrix
$\tilde{\mathbf{Q}}_{DBU}$	DBU clutter/interference + noise covariance matrix
$\mathbf{R}$	covariance matrix of signal+ clutter/interference+noise
Rx	receiver position
R_g	ground range
R_{gR}	receiver ground range
R_{gT}	transmitter ground range
R_{ins}	insensitive area
R_s	slant range
R_{sR}	receiver slant range
$R_{sR,k}$	slant distance between receiver and ground from range gate k
$R_{sR,r}$	slant distance between receiver and ground from range gate r
R_{sT}	transmitter slant range
$R_{sT,k}$	slant distance between transmitter and ground from range gate k

$R_{sT,r}$	slant distance between transmitter and ground from range gate r
R_t	clutter range (distance)
r	range gate under test
r_a	range ambiguous index
$\mathbf{S}$	target signal matrix
S_{fd}	the time scaling factor
S_{fs}	the space scaling factor
$S_k[\cdot]$	scaling operator
$SINR_{\tilde{Q}}$	SINR of the estimated clutter sample covariance matrix
$SINR_Q$	Optimum SINR (with target signal absent)
$SINR_{\tilde{R}}$	SINR of the estimated clutter sample covariance matrix with target signal present
$SINR_R$	Optimum SINR (with target signal present)
$\mathbf{s}$	space-time signal vector
$\mathbf{s}_s$	spatial domain target signal
$\mathbf{s}_t$	temporal domain target signal
superscript T	transpose operator
$\mathbf{T}_{2D}$	angle-Doppler compensation transformation matrix
$\mathbf{T}_{dw}$	Doppler warping transformation matrix
$\mathbf{T}_s$	affine transformation for scaling method
$Time(g)$	time taken for the signal to hit the ground in range gate g and back to the receiver
Tx	transmitter position
t_{dw}	dwell time
tr()	trace of a square matrix
v_p	platform velocity for monostatic airborne radar
v_R	receiver velocity
v_{rad}	relative velocity of the target
v_T	transmitter velocity
v_{unamb}	Unambiguity velocity
vec(.)	matrix operation that stacks the columns of a matrix under each other to form a new column vector
$W_s(U_s, V_s)$	scaling window

$\tilde{\mathbf{w}}_{DBU}$	DBU augmented weight vector
$\mathbf{w}$	arbitrary STAP weight vector
$\mathbf{w}_{Ta}$	Taylor series weights
$\mathbf{w}_{DBU}$	DBU weights
$\dot{\mathbf{w}}(n)$	first order weight derivative
$\ddot{\mathbf{w}}(n)$	second order weight derivative
$\mathbf{X}$	range gate under test data matrix
$\mathbf{X}_{\Sigma\Delta}$	stacked data received from Σ and Δ beams
$\mathbf{X}_r$	received signal with target signal present, from the range gate under test (range gate r)
$\tilde{\mathbf{x}}_{DBU}$	DBU augmented data vector
x_p	x-coordinate of scatter P
x_R	x-coordinate of receiver
x_T	x-coordinate of transmitter
$\mathbf{Y}_{2D}$	2-D Doppler warped training data
$\mathbf{Y}_{dw}$	Doppler warped training data
$\mathbf{Y}_k$	training data from range gate k
$\mathbf{Y}_{\mathrm{F}k}$	angle-Doppler domain training data from range gate k
$\mathbf{Y}_{Pk}$	zeroes padded training data matrix
$\mathbf{y}_{DBU}$	output of DBU-STAP
$y_{\mathrm{F}new}$	f_{new} signal magnitude
$y_{\mathrm{F}old}$	f_{old} signal magnitude
y_p	y-coordinate of scatter P
y_R	y-coordinate of receiver
y_T	y-coordinate of transmitter
Z	number of zero padding added to the temporal samples

Chapter 1
Introduction

Radar is often used to detect objects that are not visible to our naked eyes. In a commercial context it is widely used in safety applications, such as in air traffic control or speed cameras. Radar can be used as an offensive or defensive tool in a military context. Controlling the air space is the key element in modern warfare. The start of any modern arms conflict is usually marked with the destruction of the enemy radar system. Having a modern and reliable radar system plays a significant part in determining the outcome of the conflict. With the help of airborne and spaceborne radar, intelligence about the enemy units can be readily available before the battle even begins. Besides being able to look further into the enemy territory and detect low flying aircraft and vehicles in a hilly landscape, an airborne bistatic radar survivability is greatly increased by positioning the transmitter in a "safe" location while the receiver is in the enemy airspace operating in the passive mode. The greatest advantage of an airborne bistatic radar is its ability to possibility detect targets which employ stealth technology. Using stealth technology, the radar cross section (RCS) of target is reduced in the forward scattering direction, making target returns harder to separate from the noise. Examples of targets unable to be detected reliably at significant range, using present radar technology are the stealth aircrafts: F117, F22 fighter plane and B-2 bomber.

Within this thesis, the problem of designing a clutter [i] suppressing filter for an airborne bistatic radar system is considered. The contributions of this work are in the understanding of bistatic clutter echoes of a forward looking airborne bistatic radar, development of Doppler compensation techniques for mitigating the effect of clutter Doppler range dependency and an algorithm for reducing the dimension of a joint domain localised (JDL) processor. A new method of estimating the clutter Doppler frequency difference between range gates is proposed. A new technique for mitigating the effect of clutter Doppler range dependency using Doppler interpolation and power compensation in angle-Doppler domain is also proposed. The alternate Doppler bins selection and the tuned DFT are two proposed algorithms that allow further

[i] Clutter are radar returns due to reflection from the ground and buildings.

dimension reduction of the JDL processor. Further analysis on the proposed Doppler compensation technique as well as its sample requirement will greatly assist in the design of the bistatic clutter suppression filter.

This chapter presents a brief introduction to radar systems, in particular the airborne bistatic radar. It highlights the reasons why airborne bistatic radar is once again gaining researchers' interest after the decline of interest in bistatic radar in the late 1930s. The motivation and aim of this work, simulation assumptions used as well as the thesis layout are also included.

1.1 RADAR

Figure 1.1 shows the different types of radar systems available [2–4]. A monostatic radar refers to a radar system which has the transmitter and receiver located at the same site. It has been the most widely used radar since it was developed in the late 1930s, primarily because it is easier to operate and usually - but not always - performs better than bistatic radar (page 1 of [5]).

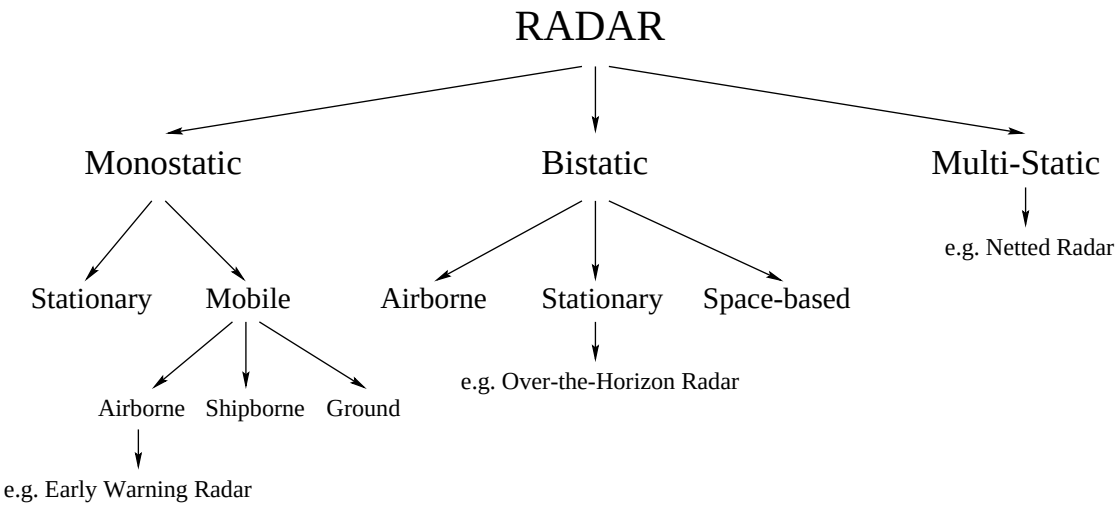

Figure 1.1: *Different types of Radar Systems.*

Airborne early warning (AEW) radar is an example of an airborne monostatic radar. Although monostatic means stationary, in airborne radar engineering it is used to address an individual radar system. By having a radar on an aircraft, it enables the radar to look from above and further into the enemy territory. Looking from above, detection of low flying aircraft and vehicles in a hilly landscape is improved. However, by doing so, two serious problems are encountered.

The signal return from the ground, normally known as clutter return or clutter echoes will be much larger in amplitude because of the steeper aspect angle. Secondly, due to the aircraft motion, the clutter echoes will be Doppler shifted, hence making its suppression more complex. Like any type of radar, a target hiding behind a chaff cloud could not be reliably detected. A chaff cloud is formed by strips of metal foil/wire or clutter of material ejected into the air for reflecting radar wave. It is used to confuse and prevent aircraft from being detected or tracked by an enemy radar [6].

An airborne bistatic radar, as shown in Figure 1.2, generally refers to two airborne radars working together, one as the transmitter and the other as the receiver. As well as having the advantages of an airborne radar, it also has the advantages of a bistatic radar system. When the transmitter and receiver are at different sites, the transmitter could be in a "safe" position, far away from the war zone. While, the receiver is in the enemy airspace, it can only be detected by active means (illuminated by another radar), as it is operating in the passive mode[ii]. With this combination, the airborne bistatic radar system survivability is greatly increased. It is also very attractive to use an unmanned aerial vehicle (UAV) as a passive receiver, thus protecting expensive assets. Being in the passive mode, the receiver is also immune to anti-radiation missiles and is less likely to be jammed by an enemy jammer [7]. An attacking aircraft, being the receiver in such a system, could get around restrictions imposed by the power-aperture product (page 507 of [8]) and yet acquire real-time radar data. Last but not least, airborne bistatic radar is believed to have anti-stealth technology capability. Before we take a look at stealth technology, in order to understand how is this possible, the disadvantages of the airborne bistatic radar shall be investigated.

Beside having the mentioned disadvantages of an airborne monostatic radar, airborne bistatic radar suffers from other disadvantages. Having the transmitter and receiver at different sites, synchronisation between them is required for the operation of an electronically scanned phased array. This requirement further increases the complexity of the radar system. The major problem with the airborne bistatic radar, however, is the range dependent nature of bistatic clutter echoes.

[ii] Passive mode means that the radar does not emit any radar signal.

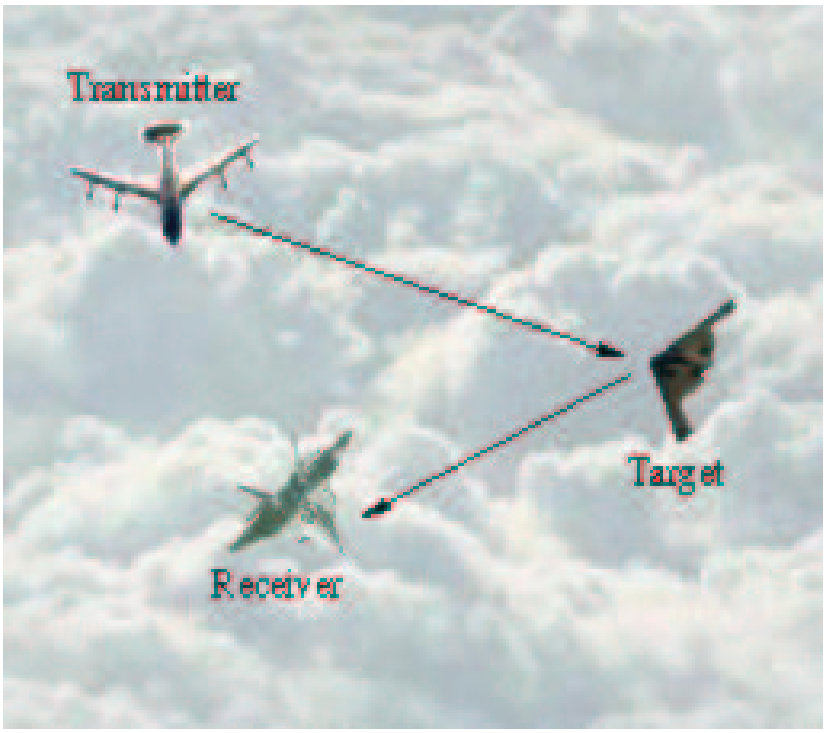

Figure 1.2: *An airborne bistatic radar system.*

1.2 Motivation of this work

Radars are designed to detect, locate and track targets [9–24]. Most targets can be detected as a matter of time. When the target gets nearer to the radar position, its echoes become stronger, making it easier to be detected. The only targets that manage to hide from modern radar are targets which employ stealth technology. Example of such targets are the F117 [iii] fighter / bomber, B-2 bomber and F-22 fighter [25–31]. Finding such targets reliably remains one of the greatest challenges in radar engineering.

Aircraft employing stealth technology are designed to produce a very weak radar return (target echo). In other words, the aircrafts have a very small RCS area, so small that the radar return cannot be differentiated from the clutter/interference and noise. Hence, making it undetectable by a modern radar system reliably. In the following sub-sections, different ways of reducing the RCS will be discussed.

[iii] The F-117 was the first aircraft to strike Baghdad in the opening minutes of the air war in Desert Storm. Footage from cameras on board showed a number of 200 lbs bombs from F-117 scoring direct hits on Iraqi strategic targets and mobile missile launchers.

1.2.1 Antenna RCS

In order to minimise the RCS of the aircraft, several measures must be taken. Firstly, the RCS of the installed antenna is reduced by carefully designing and fabricating the antenna, reducing each of the four components of backscatter as shown in Figure 1.3 [32]. The components of backscatter from a planar array antenna are the edge diffraction, antenna mode reflections, structural mode reflections and random scattering. As seen in Figure 1.4, these mirror like reflections from the antenna structure may be controlled by physically tilting the antenna. The antenna is tilted at an angle, so that the reflections are not directed back in the direction from which the illuminating radiation came from. Although the tilt does not reduce the reflections, it prevents the threat radar from receiving them.

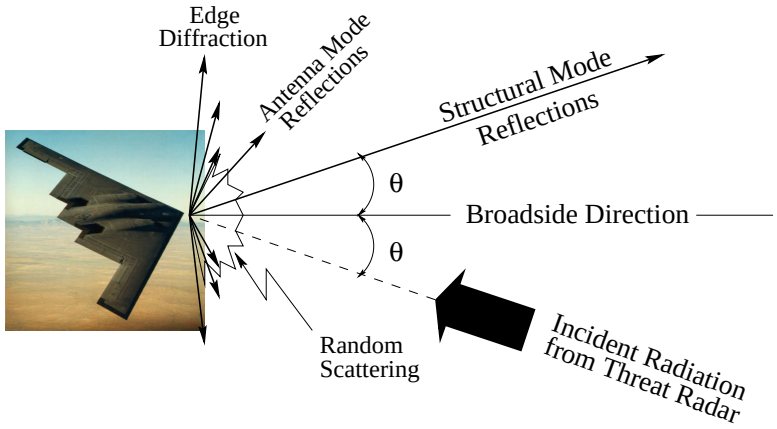

Figure 1.3: *Four basic components of backscatter from a planar array antenna.*

1.2.2 Low Probability of Intercept

Secondly, a low probability of intercept (LPI) strategy is employed. LPI is the term used for there being a low probability that radar emissions will be detected by an intercepting receiver in another aircraft or on the ground. There are a number of design strategies that could be used for LPI. One of them is to trade integration for reduced peak power. For a signal to be usefully detected by an intercepting receiver, the intercepting receiver must detect strong individual pulses. By coherently integrating the echoes received by the radar over a long period, the peak power needed to detect a target can be greatly reduced, thereby reducing the probability of the radar signal being detected [33].

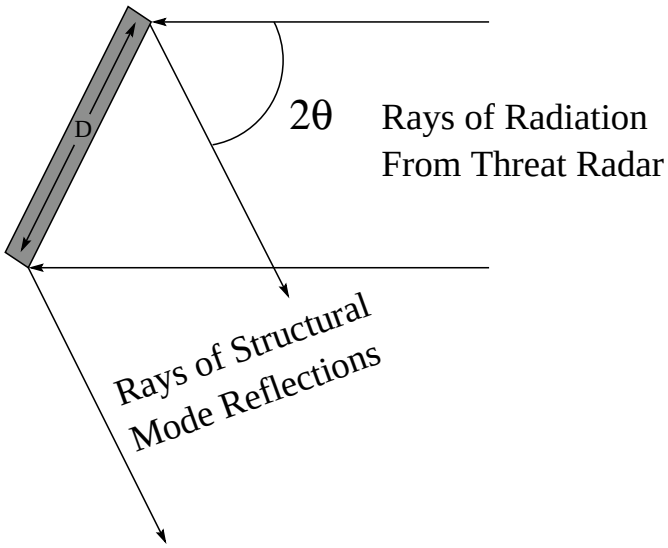

Figure 1.4: *Antenna structural reflection.*

1.2.3 Radar absorbing material (RAM)

Next, a masking technique is used to further reduce the RCS. A special coating known as radar absorbing material is applied on the aircraft to absorb the energy of the incoming electromagnetic wave. Alternatively a radar absorbing structure (RAS) could be used [34]. For any radar absorbing material to be used as a measure to reduce the RCS of any object, it has to be matched to the wavelength of the incoming radar signal. Dielectric absorbers can consist of layers of absorbing material, whose thickness has to be in the order of 0.01 to 0.1 λ (λ being the radar signal wavelength). At very high frequency (VHF)/ultra high frequency (UHF), this is generally too thick to be applied to any aircraft. Magnetic absorbers can be manufactured to be effective in thinner layers; however, they tend to be heavy and eat up a considerable portion of the aircraft payload. Structural absorbers may be considered efficient at low frequencies, since the required thickness can potentially be afforded. The application of state-of-the-art RAM, can reduce the RCS by an average of 10 dB over a fairly large bandwidth at high frequencies. However, it has proven to be ineffective in the VHF/UHF bands [35].

1.2.4 Surface facet shaping

The principal signature reduction technique employed, however, is surface facet shaping. Surface facet shaping relies on shaping the aircraft geometry so as to deflect the electromagnetic

energy impinging on it into directions other than the direction of illumination. By doing so, the monostatic RCS of the aircraft is reduced. Since this cannot be achieved over the full 360° range of aspects of the aircraft, such stealth measures are generally concentrated on the nose-on section in the range of $\pm 30°$ to 60° front aspect.

Scaled measurements of different stealth target models had been performed in an anechoic chamber at DASA, Bremen, to analyse the effect of shaping on RCS reduction as a function of radar frequency. The results obtained from measurements on a metallised 1:10-scale model of an F117 type aircraft are considered in the following [35, 36].

The aircraft geometry was obtained from open literature and hence the target model does not take into account fine structure details and surface materials such as RAM. This model is thus regarded as a good example for demonstrating how a faceted stealth scheme, like that applied in the F117, impacts on the RCS of a target. Figure 1.5[iv] shows the so-called K-plane view for representing the spectral distribution of the target scattering properties as a function of the aspect angle ($0° - 360°$ for 0° elevation). The RCS values are indicated by colour coding and ranged from -18 dBm^2 (dark blue) to +24 dBm^2 (red). The frequency ranges from 100 MHz on the inner circle to 2 GHz on the outer circle. The aspect angle corresponds to the target geometry sketch in the centre of the diagram.

The scaled measurement results presented in Figure 1.5 show that the attempt to reduce the target RCS has been successful in the $\pm 70°$ section around the nose-on aspect and for the frequency range above 400 MHz [v]. High RCS values covering the whole frequency range occur when the direction of illumination is perpendicular to the front or back edges of the wings or other dominant structures of the fuselage. It can be concluded from the above measurement results and the law of physics [vi] that, an airborne bistatic radar flying in certain flight configurations, can be used to detect a target employing stealth technique (primarily, against surface facet shaping) [37, 38].

[iv] Reproduced with permission of Jürgen Kruse, EADS Germany.

[v] Analysis of results are obtained from [35].

[vi] The laws of physics maintain that energy must be conserved. If the monostatic RCS is reduced by shaping, the incident energy must be distributed elsewhere. As such, the target signature is increased at some or all bistatic angles.

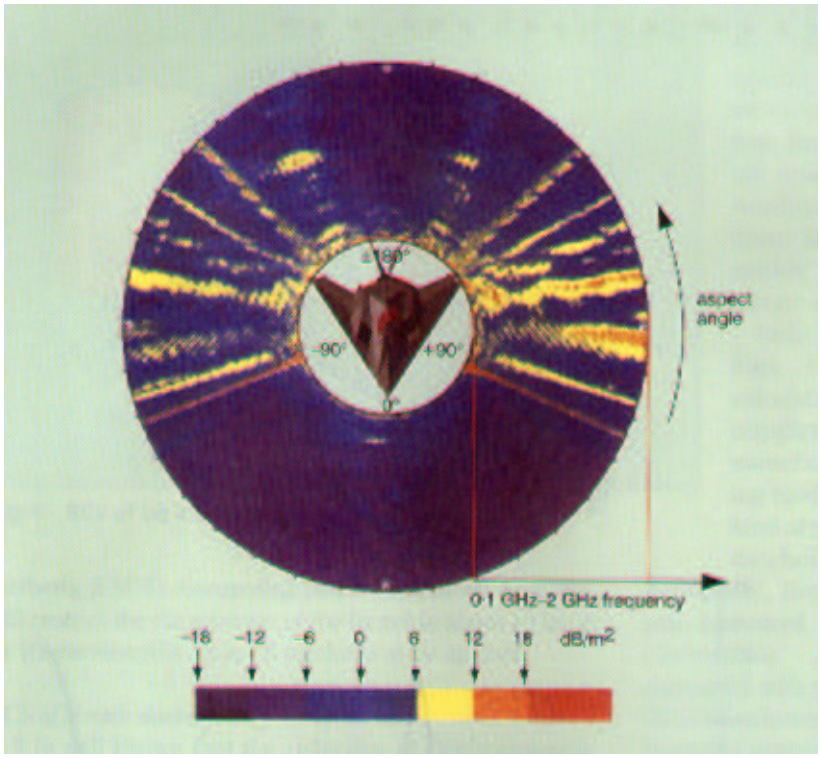

Figure 1.5: *K-plane RCS of F117-like target (courtesy of EADS, Bremen).*

1.3 Aims of this work

The key objective of this thesis is the development of a signal processing system for an airborne bistatic radar. Space-time adaptive processing (STAP) [39] has been shown to be successful in suppressing clutter echoes of a sidelooking airborne monostatic radar. As the airborne monostatic radar is a special case of the airborne bistatic radar, similarities and differences between the two cases first need to be understood. Clutter Doppler range dependency is observed in the forward looking airborne monostatic radar and in both the forward and the sidelooking airborne bistatic radar.

STAP works by assuming knowledge of the true clutter sample covariance matrix. In practice, the true clutter sample covariance matrix is estimated using clutter echoes from other neighbour range gates or from the time dimension or both. The range dependent nature of the clutter echoes will cause incorrect estimation of the true clutter sample covariance matrix and will require continuous estimation of the clutter sample covariance matrix for every range gate under test. Incorrect estimation of the true clutter sample covariance matrix, arising from the use

of statistically different training range gates, will broaden the clutter suppression filter clutter notch and result in a loss of processor performance. Meanwhile continuous estimation of the clutter sample covariance matrix will cause an additional computational load for the adaptation process.

Clutter Doppler range dependency also creates a dilemma. On one hand, the amount of training range gates required to produce a sufficiently narrow clutter notch, may not be enough for the adaptation of the estimated clutter sample covariance matrix, hence a loss in improvement factor (defined in Section 2.5.1) will occur. On the other hand, if a large number of range gates (with different Doppler frequencies) are used, broadening of clutter notch will result in degradation of slow relative velocity target detection.

It is the ultimate goal of this research to study the range dependency of the forward looking bistatic clutter and to develop a Doppler compensation algorithm than can mitigate the bistatic clutter Doppler range dependency. The proposed algorithm should ideally be based on a reduced dimension STAP processor, to reduce the amount of training range gates required for the estimation of the clutter sample covariance matrix, as well as to reduce the computational cost of the clutter suppression filter adaptation with range.

As part of the proposed algorithm system analysis, the processor performance with various system parameters such as the size of Doppler and spatial bins, size of the discrete Fourier transform (DFT) processor, diagonal loading, radar ambiguities shall be investigated. In addition, the number of training data required in both range and time dimensions, for the estimation of the clutter sample covariance matrix shall be studied.

1.4 Assumptions

In order to obtain a simplified understanding of the nature of the bistatic clutter, as well as to develop and test the proposed Doppler compensation method, the radar and clutter models are simplified as much as possible. The following assumptions are made:

1. The clutter statistics are stationary within the dwell time. Thus, adaptation of the clutter sample covariance matrix with time is not considered. The effects of motion on adaptive arrays has been studied extensively by HAYWARD [40]. Changes in the clutter statistic due to such motion can be compensated using extended sample matrix inversion (ESMI)

[41];

2. Interference caused by jamming is not considered in an airborne bistatic radar system, as the location of the receiver is usually unknown to the enemy jammers;

3. Mutual coupling effects between elements of the array have been neglected [42–44];

4. The contributions of different scatterers to the clutter echoes are statistically independent;

5. Since the clutter echoes are a sum over a large number of scatterers, they are assumed asymptotically Gaussian;

6. The reflectivity of the ground is assumed to be independent of the depression angle. In practice, there is a strong dependence which is in turn associated with the kind of clutter background (roughness);

7. Multiple-time around clutter occurs whenever the pulse repetition frequency (PRF) is chosen such that the radar is range ambiguous within the visible radar range. In this work, multiple clutter echoes have been neglected except in Section 4.8.4; and

8. Although range walk can lead to temporal decorrelation of space-time clutter echoes, its effect is neglected. The influence of the range walk on space-time clutter sample covariance matrices and the associated power spectra has been analysed by KREYENKAMP [45].

1.5 Thesis organisation and Original contributions to knowledge

This section summarises the contents of this thesis, as well as highlights the original contributions to knowledge contained within the chapters.

Chapter 2 offers a different perspective of the nature on the clutter echoes in both airborne monostatic and bistatic radar systems from that normally portrayed in other literatures. The space-time adaptive processing processor, which has been widely studied for clutter suppression in airborne monostatic radar is also discussed. In the second part of this chapter, the performance metrics used for evaluating the performance of Doppler compensation schemes are presented. Different methods of mitigating the range dependency are also shown. Lastly, four different types of Doppler compensation algorithms are elaborated.

The clutter Doppler range dependency is often presented in the Doppler-$\cos\beta$ plane. For sidelooking airborne monostatic radar, the clutter echoes are shown to be range independent in the Doppler-$\cos\beta$ plane. Because of this feature, it is attractive to work in the $\cos\beta$ plane rather than the azimuth plane. However for airborne bistatic radar, clutter range independence doesn't exist in either plane. Hence the first contribution of this work is on the illustration of the clutter Doppler range dependency for both airborne monostatic and bistatic radar, in the Doppler-azimuth plane. The azimuth plane is chosen for this work to allow easier visualisation of the angle of arrival. The range dependency of an airborne bistatic radar is widely studied for cases using a sidelooking array and in the Doppler-$\cos\beta$ plane. This work presents the range dependency in Doppler-azimuth plane for a forward looking airborne bistatic radar, with various flight configurations.

Chapter 3 describes a reduced dimension STAP processor called the joint domain localised (JDL) processor [46], an angular-Doppler domain processor. A novel algorithm for estimating the centre clutter Doppler frequency difference between range gates, that is to a certain extent, robust to errors in estimated parameters such as the transmitter velocity is proposed [47]. Using the JDL processor as the base of the clutter suppression filter, a novel way of performing Doppler compensation by Doppler interpolation and power correction is proposed [47]. A method of further reducing the dimension of the JDL processor, called the tuned DFT is also proposed [48]. The computational cost can be further reduced without affecting the processor performance, when using the tuned DFT.

Chapter 4 is dedicated to the investigation of the proposed Doppler interpolation processor performance when using different parameters. Carrying out analyses on the processor parameters allows a better understanding and design of both the proposed Doppler interpolation processor and the JDL processor. Using the proposed alternate Doppler bins selection, a computational cost reduction or processor performance improvement can be achieved. The sensitivity of the processor performance with error in pre-known parameters is also being investigated. The extent to which the processor performance is affected by radar ambiguity, - in particularly range ambiguity, is presented. The last part of this chapter takes a look at the sample requirement (for the estimation of the clutter sample covariance matrix) when using different Doppler compensation processors and different data types. Using correctly selected training range gates in situations where Doppler compensation is required, plays important part in reducing the sample requirement.

Finally, Chapter 5 summaries and concludes the work presented and highlights possible future work.

Chapter 2
Clutter nature of airborne bistatic radar

2.1 Introduction

Clutter suppression in an airborne bistatic radar is very different from that of an airborne monostatic radar. Bistatic clutter echoes are range dependent and change non-linearly with range. Traditional methods of estimating the clutter sample covariance matrix, using training data in the range dimension will only result in the widening of the clutter notch. The widening of the clutter notch will degrade the target detection processor's ability to detect low relative velocity targets.

In this chapter, an insight into the clutter Doppler range dependency (in the Doppler-azimuth plane) for both airborne monostatic and bistatic radar systems will be given. Similarity in terms of range dependency between the clutter echoes received by a forward looking airborne monostatic radar and an airborne bistatic radar (in the Doppler-$\cos\beta$ plane) is observed [49]. Range dependency does exist in airborne monostatic radar (in both a sidelooking and forward looking array). However due to the look angles normally employed, it is only in the forward looking case where the range dependency becomes obvious.

Clutter suppression using space-time adaptive processing (STAP) has been shown to be very successful in airborne monostatic radar systems [46, 47, 50–54]. An introduction to space-time adaptive processing is given. The effects of bistatic clutter Doppler range dependency on the STAP processor will be evaluated. Methods used in overcoming range dependency in forward looking airborne radar provide suggestions on how range dependency in airborne bistatic radar can be solved. Some of these Doppler compensation methods do not produce impressive results when used by the airborne bistatic radar system, as the bistatic clutter echoes are much more complex than the monostatic clutter echoes.

There are a number of ways to mitigate the effect of clutter Doppler range dependency. Some form of Doppler compensation, however, seem to be highly desirable for neutralising the range

dependency. Several compensation methods proposed by various authors (e.g. derivative-based updating, Doppler warping, two-dimensional angle-Doppler compensation and scaling) are explained.

2.2 An airborne monostatic radar

Before analysing the clutter echoes received by an airborne bistatic radar, an understanding of the monostatic clutter echoes is essential. An airborne radar system that uses a common antenna for both transmitting and receiving is called an airborne monostatic radar. It is sometimes referred to as a special case of the airborne bistatic radar, when the distance between the transmitter and receiver equal zero, and both the transmitter and receiver are travelling at the same velocity. Figure 2.1 shows the geometry of an airborne monostatic radar. The radar platform (at position marked O) is assumed to be moving parallel to the ground in the x-direction at velocity v_p. The ground is also assumed to be planar. The scalar φ denotes azimuth angle, R_s is the slant range, R_g the ground range, H is the height of the platform and θ the depression angle.

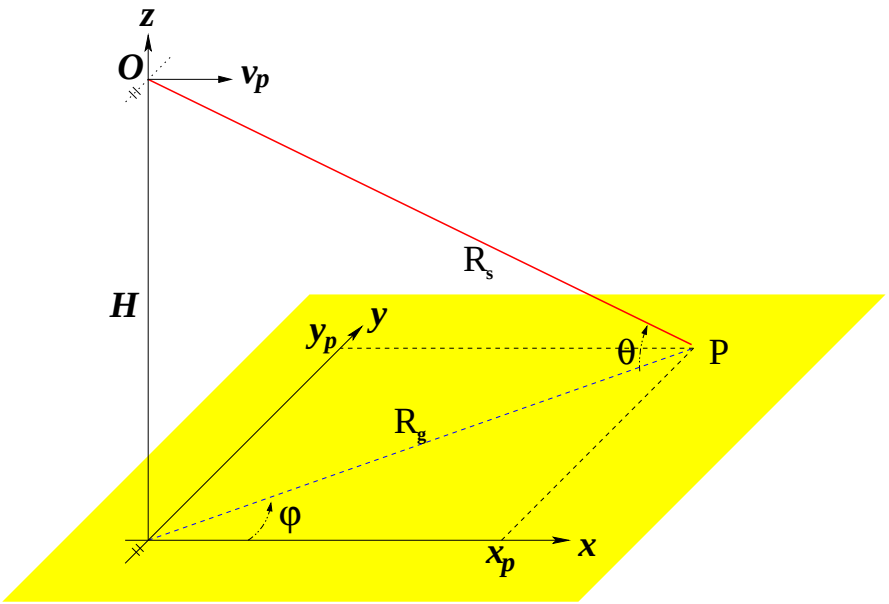

Figure 2.1: *Geometry of an airborne monostatic radar.*

The clutter Doppler frequency, f_D (for an airborne monostatic radar system) due to a certain

stationary scatterer, P on the ground is proportional to the radar system's radial velocity.

$$f_D = \frac{2v_p}{\lambda}\cos\varphi\cos\theta \tag{2.1}$$

where λ is the wavelength of the radar signal. For every pair of angles (φ, θ), f_D denotes an individual clutter Doppler frequency. Curves of constant Doppler frequency on the ground are called isodops, while curves of constant range are called isoranges.

Figure 2.2 shows an isodops and an isoranges plot for an airborne monostatic radar. The positions marked T and R represent the positions of the transmitter and receiver respectively. The isodops consist of symmetric set of hyperbolas, which are obtained for a flight path parallel to the ground. For flight paths including a diving angle, the hyperbolas will become non-symmetric about the y-axis. Parabolas or ellipses may also be obtained, depending on the diving angle. The clutter Doppler frequency tends to be constant with range at a greater distance and at azimuth angles close to 90°.

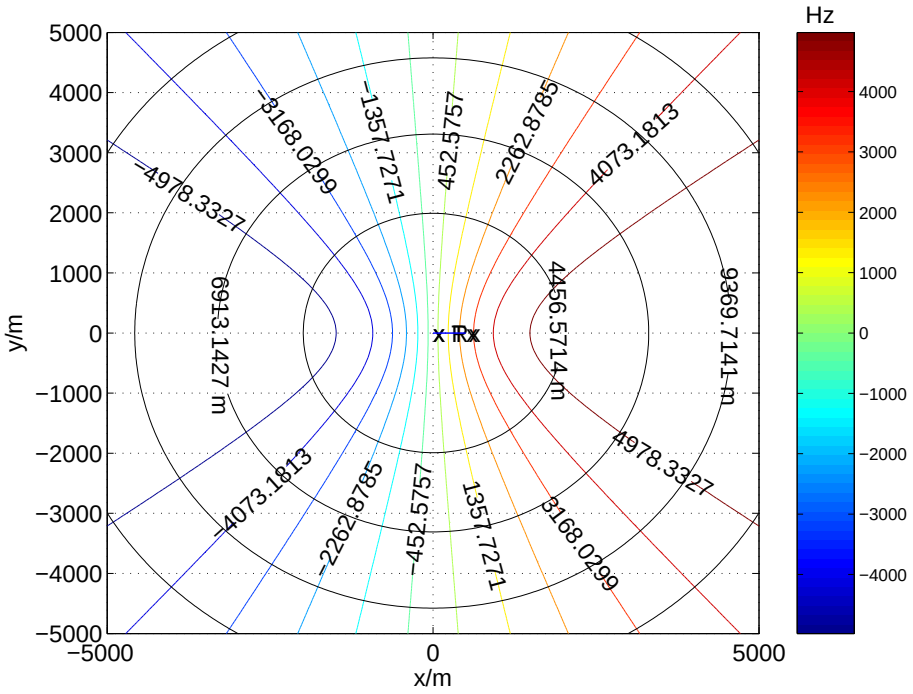

Figure 2.2: *Isodops and isoranges for an airborne monostatic radar.*

Array configurations for sidelooking and forward looking antennas can be seen in Figure 2.3. A sidelooking array (represented by hollow circle) is an array with its elements lying along the

flight path, while a forward looking array (represented by solid circle) has its elements lying perpendicular to the flight path. Zero azimuth is defined as the x-axis. For a sidelooking array, $0^\circ \leq \varphi \leq 180^\circ$ (port side) or $-180^\circ \leq \varphi \leq 0^\circ$ (starboard side), while $-90^\circ \leq \varphi \leq 90^\circ$ for a forward looking array, looking towards the front of the aircraft. Anti-clockwise from the x-axis is the positive φ angle, while clockwise is the negative φ angle.

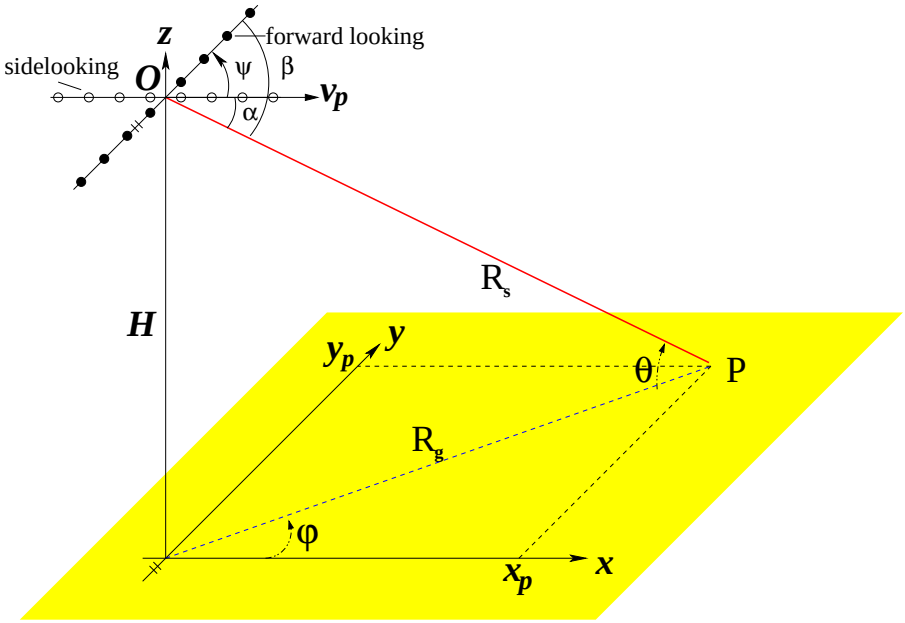

Figure 2.3: *Geometry of a linear airborne array.*

2.2.1 Sidelooking array configuration

Clutter suppression for a sidelooking airborne monostatic radar (SLAR) using the STAP has been shown by a number of authors to be very successful (STAP is explained in Section 2.4). Displaced phase centre antenna technique [55–57] has also been used in SLAR, by exploring the range independent nature of the clutter echoes when operating in Doppler-cone angle plane. An example of a typical Doppler-azimuth clutter spectrum (using the minimum variance estimator (MVE), see Appendix A and page 225-227 of [58]) for a SLAR is given in Figure 2.4 [i].

The clutter echoes are separated by range gates. Range gates are very similar to isoranges, where clutter echoes from ground scatterers in the same range are collected and superimposed

[i] General simulation parameters for the MVE power spectrum plot are given in Table 2.1

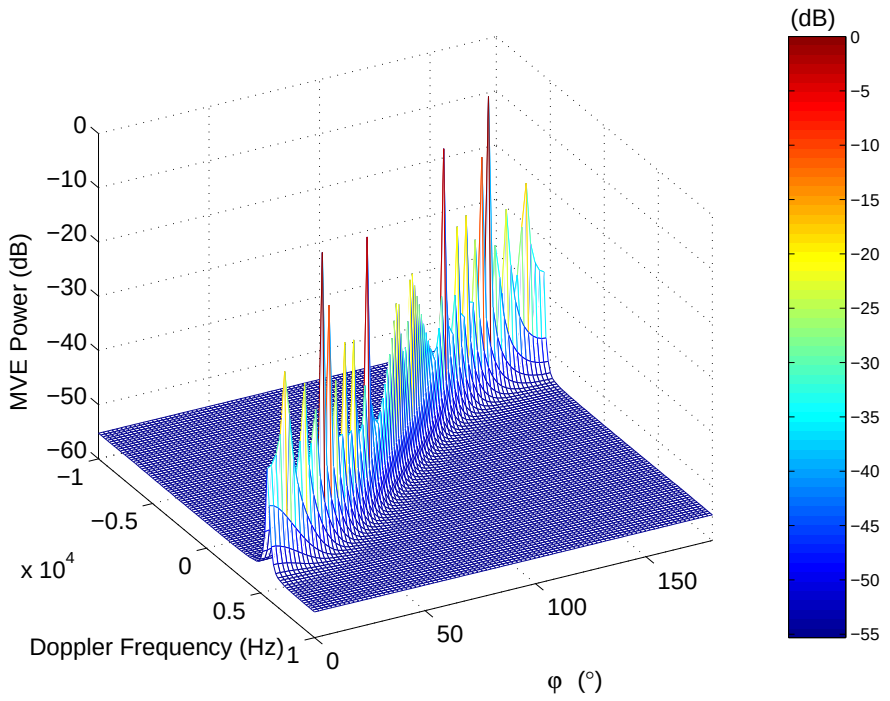

Figure 2.4: *Clutter spectrum of a sidelooking airborne monostatic radar.*

together. The spacing between range gates is normally set approximately equal to the pulse width. Using a single range gate spacing with a 2:1 variation in pulse width (two range gates for one pulse width) is undesirable as it may result in unacceptable range gate straddling losses and perhaps even missing samples. The maximum number of range gates samples possible is determined by the height of the platform, the pulse width and the pulse repetition frequency (PRF), using the following equation

$$\text{Maximum number of range gates possible} \approx \frac{\frac{1}{\text{PRF}} - \frac{2H}{c}}{\text{pulse width}}. \tag{2.2}$$

where c is the speed of light. For PRF = 20kHz, pulse width = 0.5μsec and a platform height of 1km, the maximum number of range gates possible is approximately 86.

Figure 2.5 shows how the clutter Doppler frequency changes in azimuth and with range gate (plotted on a Doppler-azimuth plane). The different colours represent the range gate numbers. The range gate number starts counting from 25 (for this graph) as some of the range gates have

no clutter echoes[ii]. The number of range gates without clutter echoes is generally dependent on the height of the radar platform. The spreading of the colours in the Doppler frequency axis represents the range dependency of the clutter Doppler at a particular φ angle. The wider the spread of the colours, the higher the clutter Doppler range dependency. For $45^\circ \leq \varphi \leq 135^\circ$, there is not much change in Doppler frequency with different range gates, hence the clutter echoes can be assumed to be range independent. Range dependency is obvious for $0^\circ \leq \varphi \leq 15^\circ$ and $165^\circ \leq \varphi \leq 180^\circ$. However due to the difficulty in resolving angles near endfire (near the array axis), clutter echoes from these angles are suppressed. The mainlobe of the transmitter beam pattern is seldom pointed towards the endfire. As a result, the clutter echoes for a sidelooking airborne monostatic radar are generally considered to be range independent.

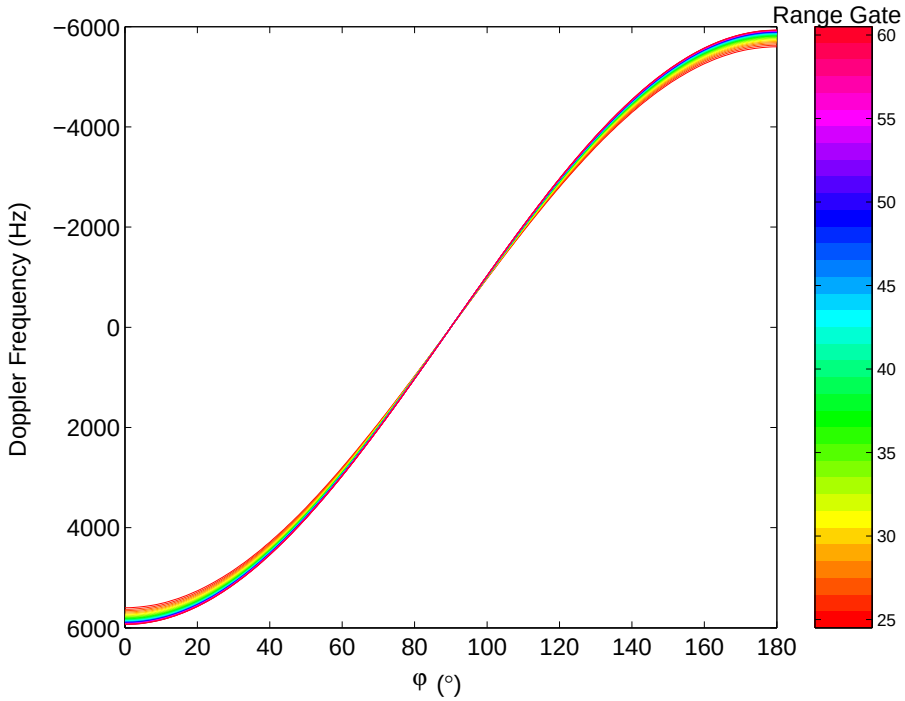

Figure 2.5: *Range dependency of a sidelooking airborne monostatic radar.*

The range dependency of the clutter echoes received by a sidelooking array is explained slightly differently from that given in literature, which uses the cone angle, α, [51, 59–62]. The clutter Doppler range dependency is explained in terms of the look direction relative to the array, β.

[ii] Assuming no range ambiguity.

The relative clutter Doppler frequency is given as

$$f_r = \frac{f_D \lambda}{2 v_p} = \cos \alpha \tag{2.3}$$

and

$$\cos \alpha = \cos \varphi \cos \theta \tag{2.4}$$

The look direction of the array is given by

$$\begin{aligned} \cos \beta &= \cos(\varphi - \psi) \cos \theta \\ &= (\cos \varphi \cos \psi + \sqrt{1 - \cos^2 \varphi} \sin \psi) \cos \theta \end{aligned} \tag{2.5}$$

where β is the look direction relative to the array, ψ is the crab angle. The crab angle is the angle between the antenna array and the flight direction. For sidelooking array, $\psi = 0^\circ$ while for a forward looking array, $\psi = 90^\circ$. For $\beta = 0^\circ$ this means the direction of the array axis.

To relate the relative Doppler frequency, f_r with the look direction, $\cos \beta$, equation (2.5) is solved for $\cos \varphi$ (see Appendix B).

$$f_r = \cos \beta \cos \psi \pm \sqrt{(\cos \beta \cos \psi)^2 - (cos^2 \beta - \cos^2 \theta \sin^2 \psi)} \tag{2.6}$$

For a side looking array, $\psi = 0^\circ$, equation (2.6) reduces to

$$f_r = \cos \beta \tag{2.7}$$

which is a straight line in the $f_r - \cos \beta$ plane and is also known as Doppler-$\cos \beta$ plane with a 45° slope. It means that the clutter Doppler frequency depends only on the look direction, but not on range.

The main difference between a Doppler-azimuth plane and a Doppler-$\cos \beta$ plane is that the azimuth axis in the Doppler -azimuth plane, is independent of the range gate. However, for the look direction ($\cos \beta$) axis in the Doppler-$\cos \beta$ plane, $\cos \beta$ is dependent on the depression angle, which is determined by the range gate in an airborne monostatic radar environment. This indirect dependency of $\cos \beta$ causes the clutter Doppler range dependency presented on the Doppler-$\cos \beta$ plane to be different from that presented on the Doppler-azimuth plane.

The range independence of the clutter Doppler frequency is a unique property of the sidelooking airborne monostatic radar [60]. It has strong implications for the design of an adaptive processor because training data can be obtained directly from the neighbouring range gates.

2.2.2 Forward looking array configuration

The statistics of the clutter echoes do not change when a non-sidelooking array, e.g. a forward looking array, is used instead of a sidelooking array. The only difference is the angle of arrival when different antenna array configurations are used. Figure 2.6 shows a clutter power spectrum (using MVE), when using a forward looking array.

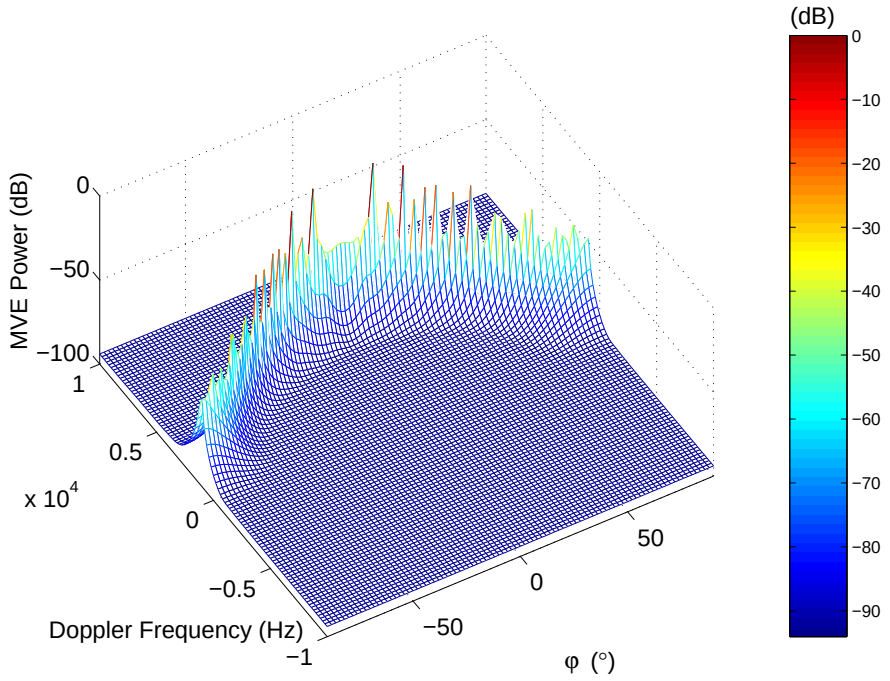

Figure 2.6: *Clutter spectrum of a forward looking airborne monostatic radar.*

When a forward looking array looks toward the flight direction, the clutter power spectrum consists of only positive Doppler frequencies (only true for airborne monostatic radar). The negative Doppler frequency belongs to clutter echoes arriving from the back lobe, which are normally suppressed using a metal reflector.

The range dependent nature for a forward looking array is different from that of a sidelooking array shown on the Doppler-azimuth plane, because of the look angle employed. As mentioned

earlier, a sidelooking array has difficulty in resolving azimuth angles $0° \leq \varphi \leq 15°$ and $165° \leq \varphi \leq 180°$, which are the azimuth angles that experience Doppler frequency variation with range gate. For a forward looking array, azimuth angles $-90° \leq \varphi \leq -75°$ and $75° \leq \varphi \leq 90°$ are the angles of arrival which experience clutter suppression due to the transmitter beam pattern. Strong clutter echoes received by a sidelooking array may appear weak when received by a forward looking array and vice versa. Figure 2.7 shows how the clutter Doppler frequency changes with range gate in the Doppler-azimuth plane when a forward looking array is used.

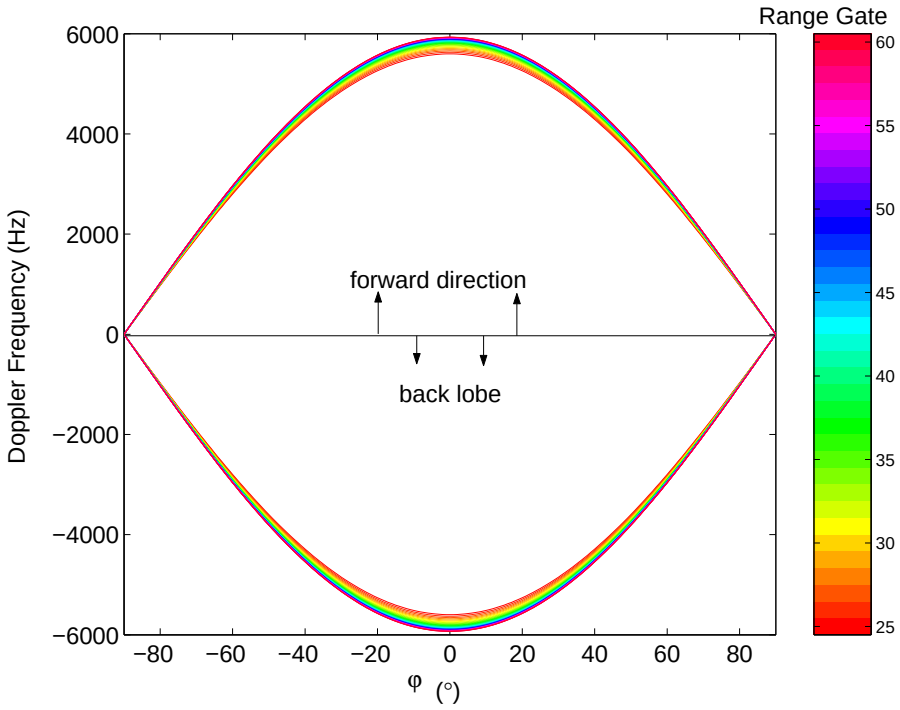

Figure 2.7: *Range dependency of a forward looking airborne monostatic radar.*

Within the azimuth range of $-45° \leq \varphi \leq 45°$, a significant Doppler frequency change with range is observed. These angles being the main look angles of a forward looking array, which implies that the clutter Doppler frequency of a forward looking airborne radar are range dependent.

Looking at the clutter Doppler range dependency on the Doppler-$\cos\beta$ plane, from equation (2.6), with $\psi = 90°$

$$f_r = \pm\sqrt{\cos^2\theta - cos^2\beta} \tag{2.8}$$

Equation (2.8) shows that for a forward looking array, the clutter Doppler frequency is also range dependent even when Doppler-$\cos\beta$ plane is used.

For an airborne monostatic radar, the clutter echoes are considered to be range independent when a sidelooking antenna array is used. On the other hand, when a forward looking antenna array is used, the clutter Doppler is range dependent [63, 64]. Clutter Doppler range dependency can also be observed when an inclined antenna array [52, 62], also known as non-sidelooking antenna array [65, 66], is used. In the next section, the clutter Doppler range dependency for an airborne bistatic radar will be investigated.

2.3 An airborne bistatic radar

The clutter spectrum for an airborne bistatic radar is much more complicated than an airborne monostatic radar. It is dependent on the transmitter and receiver positions, as well as their respective radial velocities. An airborne bistatic radar geometry is shown in Figure 2.8. The receiver is at point Rx, at height, H_R, above the $x-y$ ground plane, and the transmitter is at point Tx, at height, H_T. The receiver moves in the x-direction at speed, v_R, while the transmitter moves at speed, v_T, at flight direction, δ_t. A transmit pulse hits the ground at point P after passing the transmit slant range, R_{sT}, and the reflected pulse is received by the receiver after passing the receiver slant range, R_{sR}.

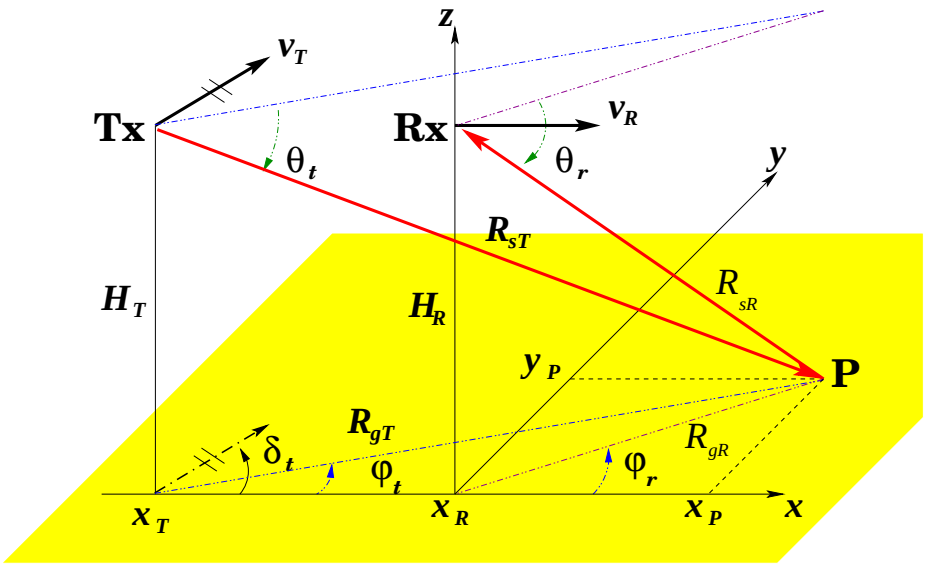

Figure 2.8: *Geometry of an airborne bistatic radar.*

Due to the motion of the two platforms, ground clutter echoes will exhibit a Doppler shift that is proportional to the velocity of both the transmitter and the receiver. For the airborne bistatic radar, the Doppler frequency of the clutter echo is given as follows:

$$f_D = \frac{v_T \cos(\varphi_t - \delta_t) \cos\theta_t + v_R \cos\varphi_r \cos\theta_r}{\lambda} \tag{2.9}$$

where φ_t and φ_r are the azimuth angles of the transmitter and receiver respectively, and θ_t and θ_r are the depression angles of the transmitter and receiver respectively. The scalar φ_r is sometime also referred to the look angle. For $v_T = v_R$, $\varphi_t = \varphi_r$, $\theta_t = \theta_r$ and $\delta_t = 0$, equation (2.9) reduces to the monostatic case.

As observed from equation (2.9), any changes in transmitter and receiver configuration will affect the isodops pattern of the clutter echoes. KLEMM in [49] has discussed the influence of bistatic parameters when using a sidelooking array. He concluded that in bistatic radar, the clutter Doppler frequency is in general range dependent even for a sidelooking array geometry. In the rest of this section, the influence of the airborne bistatic radar configuration on the clutter Doppler range dependency, when using forward looking array, will be investigated. The relationship between the clutter Doppler frequency and the look direction ($\cos\beta$) will not be developed here, as there is no range independent advantage for working in the Doppler-$\cos\beta$ plane for both sidelooking and forward looking array.

2.3.1 Transmitter and Receiver Aligned

Figure 2.9 shows the clutter isodops and the isoranges with both the transmitter and receiver flying at the same speed and in the same direction. The transmitter is 2000 m ahead of the receiver. The bistatic configuration chosen is symmetric about the flight axis. The isodops still look very similar to the hyperbolas shown in Figure 2.2, except the centre region. Figure 2.10 shows the clutter Doppler range dependency of such a bistatic configuration. For the forward direction (front of the receiver), the clutter Doppler frequency varies significantly with range gate, especially in the lower range gates. A relatively uniform Doppler frequency variation can be observed at all φ_r angles, as compared to the airborne monostatic radar using a forward looking array, where the Doppler frequency variation is only observed for $-45^\circ \leq \varphi_r \leq 45^\circ$. A much wider clutter Doppler frequency spreads across range gates, as compare to the airborne

monostatic case, is also observed.

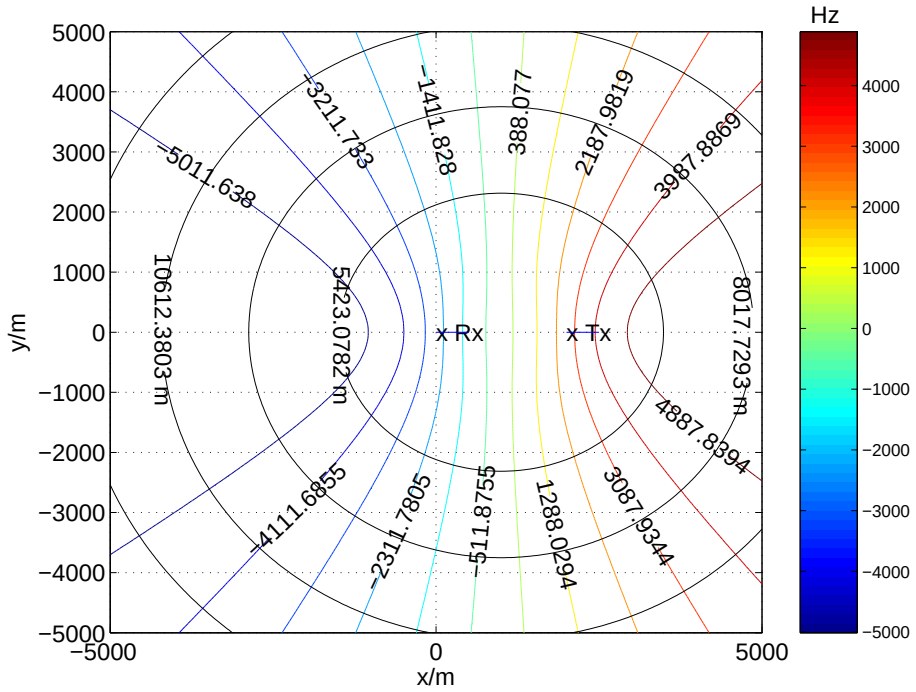

Figure 2.9: *Clutter isodops and isoranges pattern with transmitter and receiver aligned.*

The backlobe clutter Doppler frequency responds in a different manner with range gate than the forward direction clutter. The clutter Doppler frequency increases with range gate at certain azimuth angles, but also decrease with range gate at other azimuth angles. This shows that the clutter Doppler frequency variation is only symmetric about the flight axis and not about the antenna axis. This is totally different when a side looking array is used in an airborne monostatic radar, where the forward direction and backlobe parts coincide. In special applications where omni-directional sensors are used to achieve a 360° coverage, the difference between the forward direction and backlobe will influence the clutter spectra. The adaptive processor will produce a second clutter notch and, therefore requires additional degrees of freedom.

Figure 2.11 shows the clutter Doppler frequency variation when the transmitter is behind the receiver. The clutter Doppler frequency variation at the forward direction is no longer uniform across all φ_r angles. The minimum clutter Doppler range dependency is observed at $\varphi_r \approx \pm 45°$.

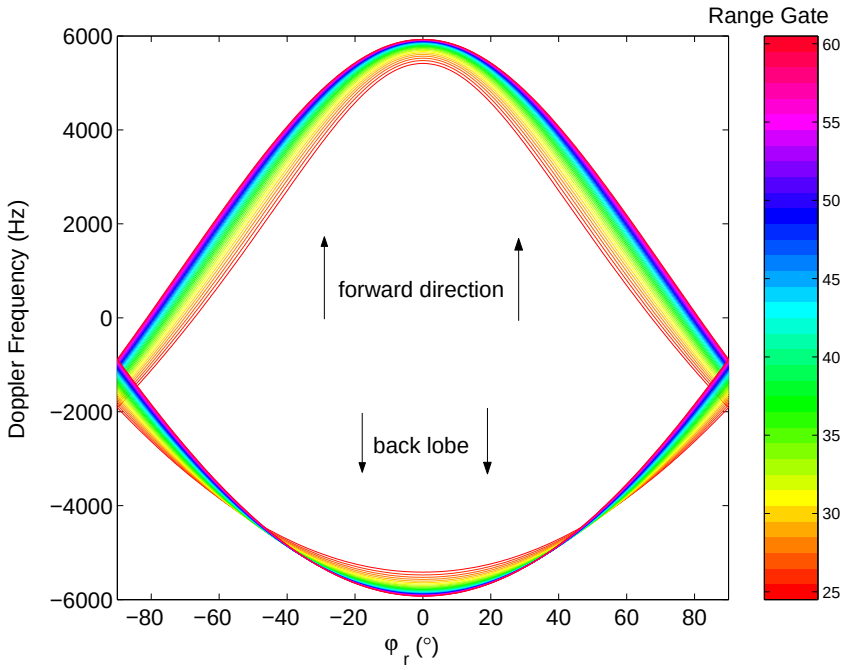

Figure 2.10: *Range dependency for a transmitter ahead of receiver with a forward looking array.*

2.3.2 Transmitter and Receiver on Parallel Flight Paths

The transmitter and the receiver are configured to be on parallel flight paths with a separation of 2000 m. The isodops and isoranges pattern are shown in Figure 2.12.

As it can be seen, the lateral displacement of the transmitter causes the isodops pattern on the ground to be asymmetric about the receiver flight path but symmetric about the antenna array axis. Figure 2.13 shows the clutter Doppler range dependency of such configuration.

For φ_r angles $-35° \leq \varphi_r \leq 80°$, the clutter Doppler frequency varies significantly with range. However on the other side of the receiver (towards the transmitter), $-90° \leq \varphi_r < -35°$, the clutter Doppler frequency variation with range is small. Such small clutter Doppler range dependent can be used to minimise the effect of clutter Doppler range dependency.

KLEMM has shown in [49], that when the displacement between transmitter and receiver becomes small compared with its height, the bistatic configuration approaches the monostatic case. Hence making the clutter Doppler frequency less range dependent.

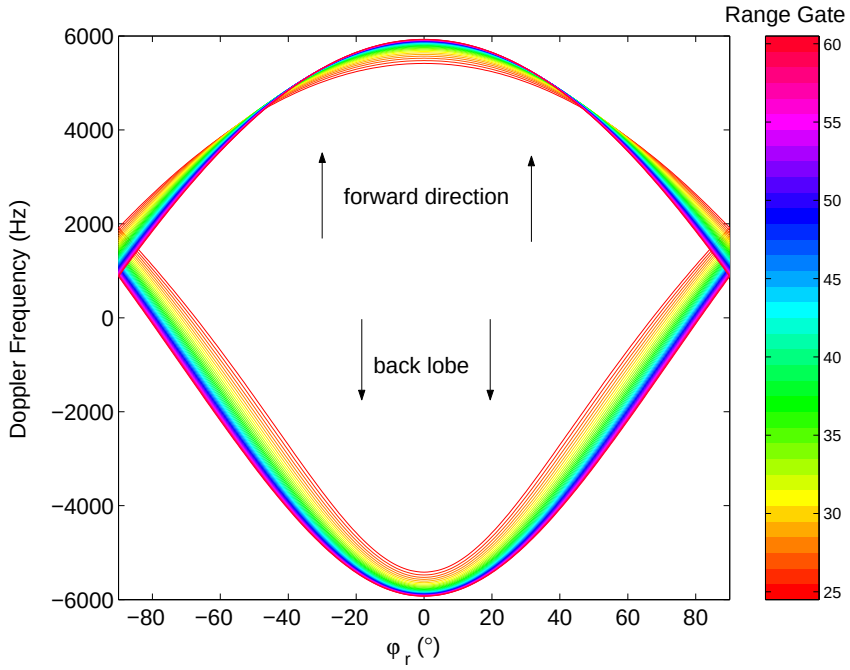

Figure 2.11: *Range dependency for transmitter behind the receiver with forward looking array.*

2.3.3 Transmitter and Receiver on Orthogonal Flight Paths

Figure 2.14 shows the isodops and isoranges pattern of a bistatic transmitter and receiver aligned configuration, with the two flight paths orthogonal to each other (the transmitter's flight direction is 90° from that of the receiver's). This configuration is not very attractive from an operational standpoint, because the configuration and the Doppler characteristics change with time. Besides making the clutter echoes highly non-stationary, bistatic radar operation becomes impossible when the transmitter leaves the radar range. However, such situation may occur during a manoeuvre, and a clutter suppression processor should still operate even under such conditions.

The shape of the isodops is greatly changed. The isodops pattern is rotated by about 45° anticlockwise. There are some ellipse-like forms in the lower left corner, while the isodops field in the upper-right still look like hyperbolas. Figure 2.15 gives more insight on how the Doppler changes with φ_r angle and range gate.

The complex, twist and turn nature of the isodops field is reflected in Figure 2.15 with the crossing of different range gate clutter Doppler frequency at different φ_r angles. At certain φ_r

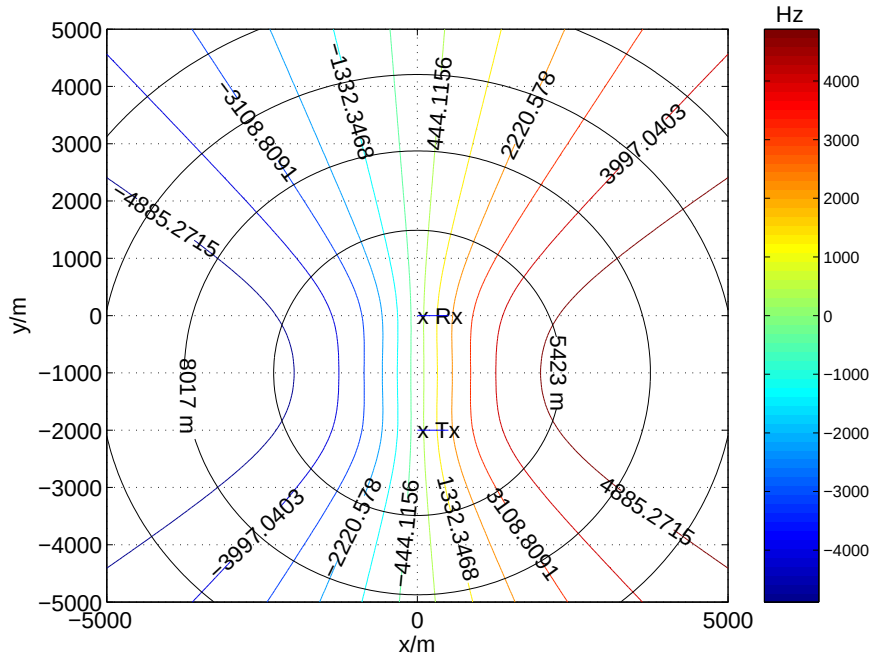

Figure 2.12: *Isodops and isoranges for transmitter and receiver on parallel flight paths with forward looking array.*

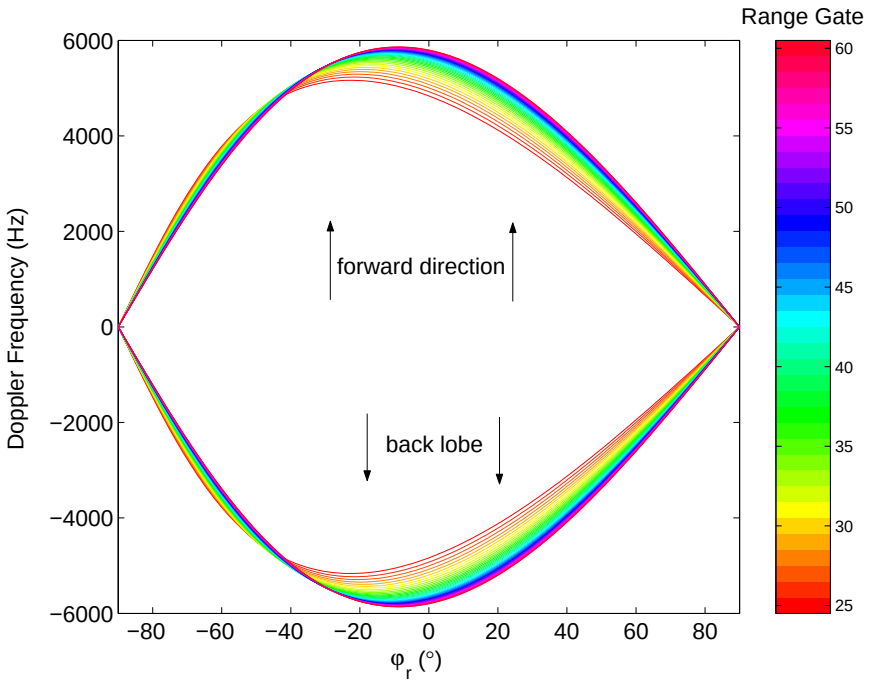

Figure 2.13: *Range dependency for transmitter and receiver on parallel flight paths with forward looking array.*

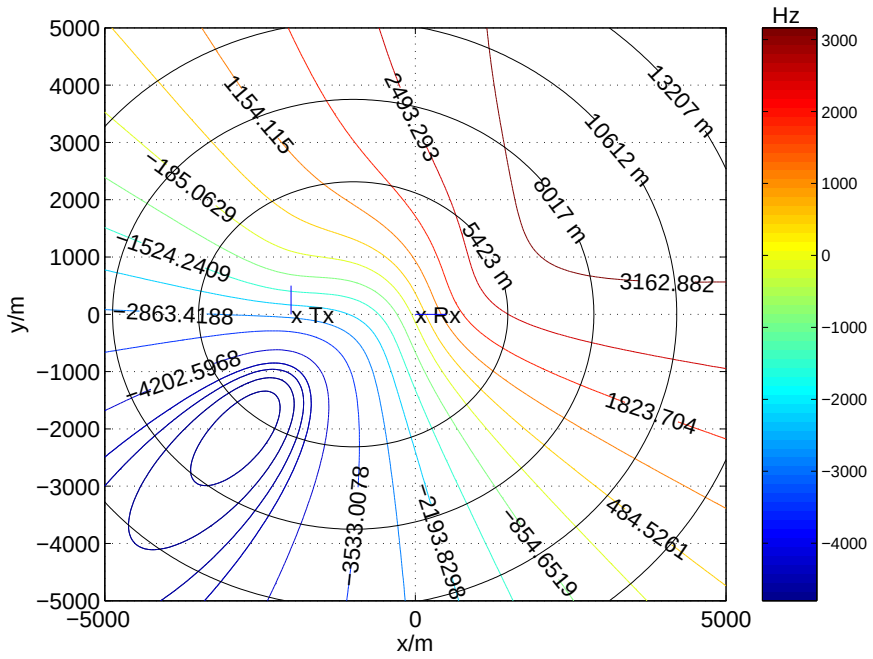

Figure 2.14: *Isodops and isoranges for transmitter and receiver on orthogonal flight paths with forward looking array.*

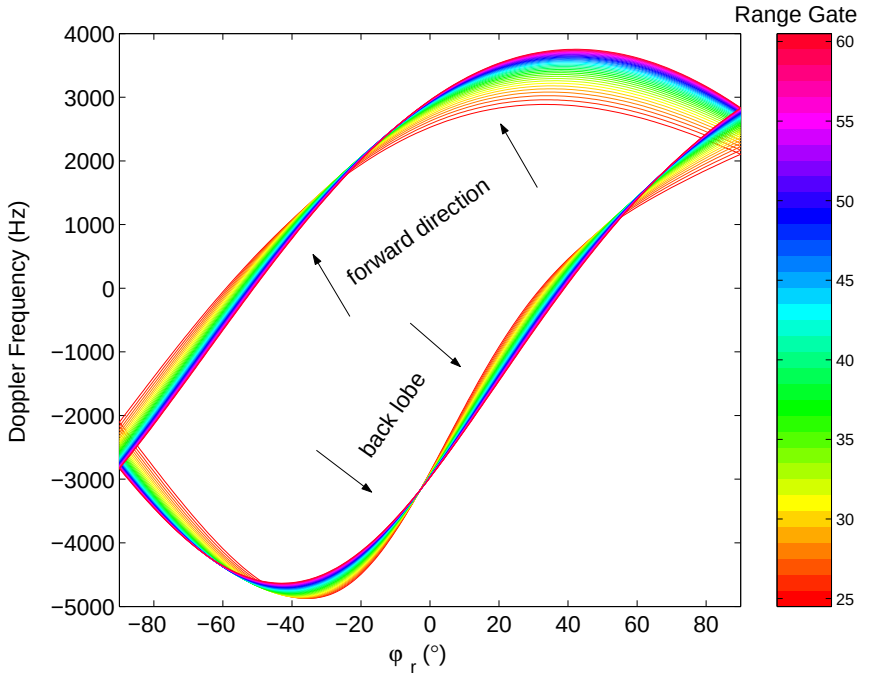

Figure 2.15: *Range dependency for transmitter and receiver on orthogonal flight paths with forward looking array.*

angles, the Doppler frequency increases as range gate increases, while at other angles, the Doppler frequency decreases as the range gate increases. Any assumption about how the Doppler frequency changes (linear or non-linear) with range gate in such configuration will not be true for all φ_r angles. Strong Doppler asymmetry between the forward direction and backlobe is also observed. Minimum clutter Doppler range dependency is observed at $\varphi_r \approx$ -33° for the forward direction and at $\varphi_r \approx 0°$ and at $\varphi_r \approx 55°$ for the backlobe direction. Figure 2.16 shows the corresponding clutter power spectrum using the MVE for clutter return from range gate 27. Omni-directional beam pattern is used for this simulation. The clutter power spectrum forms two ridges in the Doppler-azimuth plane. This shows that the space-time adaptive processing can still be effective in suppressing the clutter echoes.

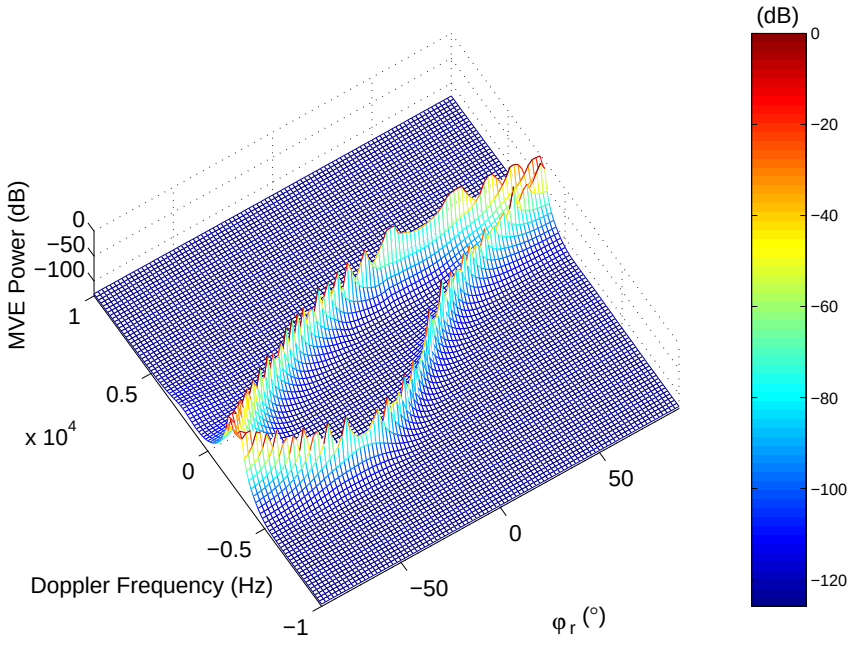

Figure 2.16: *Clutter power spectrum for transmitter and receiver on orthogonal flight paths with forward looking array from range gate 27.*

Figures 2.17 and 2.18 shows the clutter power spectrum from range gates 25 and 29 respectively, using transmitter beamwidth of 3° and 30dB mainlobe to sidelobe ratio. The receiver beam pattern is as defined in Equation (C.5). The ridge pattern appears largely the same in both the figures and the clutter echoes range dependency can hardly be observed using the MVE spectrum plot. On the other hand, the mainlobe to sidelobe ratio tends to be quite different at different range gates. From these two figures, one can expect different processor performance

when using training data from different range gates.

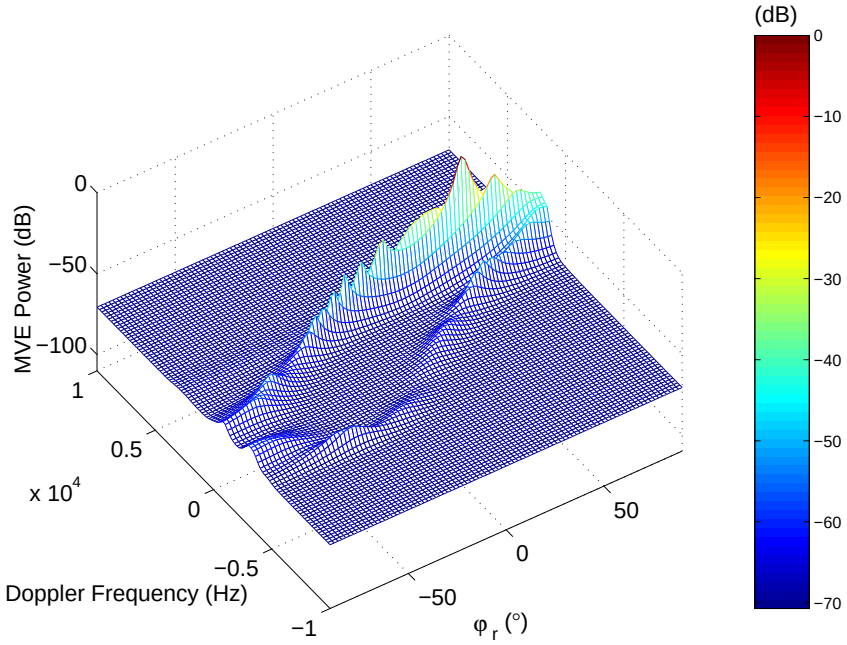

Figure 2.17: *Clutter power spectrum for transmitter and receiver on orthogonal flight paths with forward looking array from range gate 25.*

The clutter Doppler frequency of an airborne bistatic radar, operating in any configuration, is in general range dependent, regardless of using a forward looking array or a sidelooking array antenna [49, 67]. Greater clutter Doppler range dependency exists in the near range and it decreases as range increases. Figure 2.19 shows how the MVE power spectrum varies with range gate. The clutter echoes from range gate 1 to range gate 15 are the results of range ambiguity. KLEMM provides an insight into the clutter Doppler range dependency when the transmitter and the receiver aircraft are flying on parallel paths, with the transmitter above the receiver (page 356 to 357 of [68]). HERBERT and RICHARDSON described the bistatic clutter Doppler range dependency as having regions where small changes of angular location correspond to large changes of clutter Doppler frequency. The variation of the clutter angle-Doppler relationship due to topographic features, e.g. variations in ground height is also studied by HERBERT and RICHARDSON [69, 70].

The clutter Doppler range dependent - non-stationary - nature of the clutter echoes may be mitigated by appropriate choice of the transmitter-receiver configuration or by performing certain Doppler compensation. Examples of such configurations is when the transmitter height is

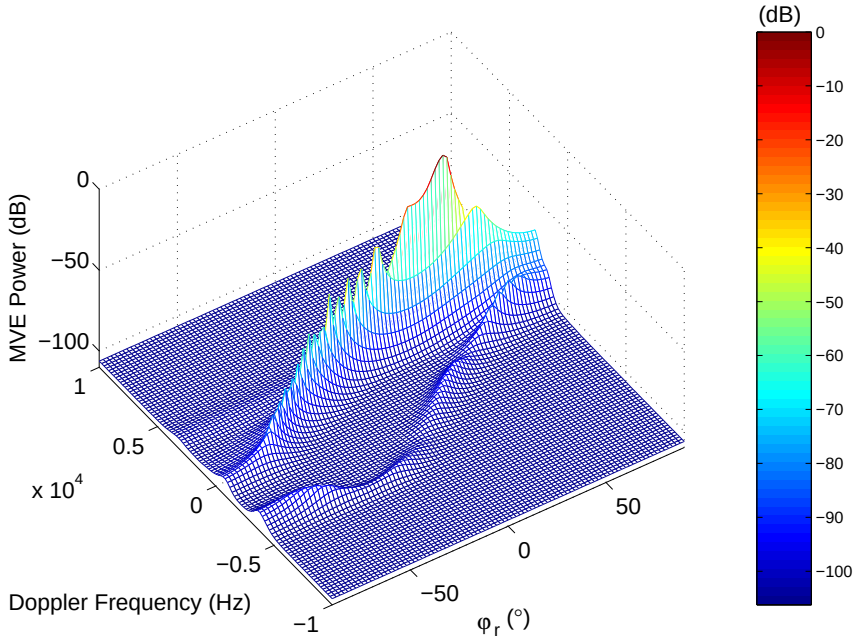

Figure 2.18: *Clutter power spectrum for transmitter and receiver on orthogonal flight paths with forward looking array from range gate 29.*

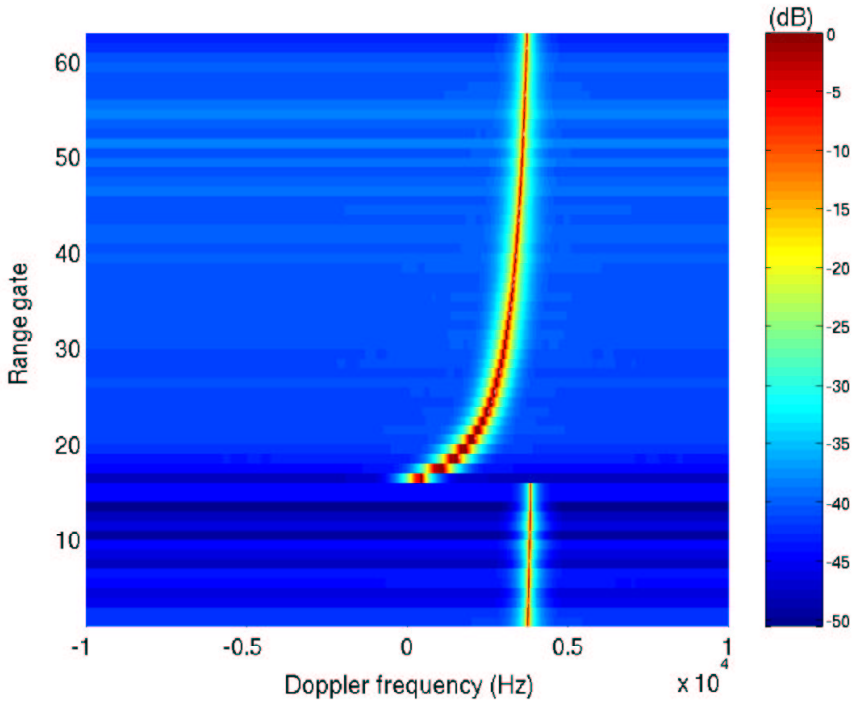

Figure 2.19: *MVE power spectrum varies with range gate.*

much larger than the receiver height. Such configuration might be desirable anyway for operational reasons. Means to mitigate the effect of clutter Doppler range dependency on clutter suppression filters such as the STAP, will be discussed in Section 2.6.

2.4 Space Time Adaptive Processing (STAP)

In an airborne radar, suppression of Doppler spread clutter echoes without minimising the target return (especially for low altitude and low relative velocity targets) has always been one of the important tasks in radar signal processing. Attempts to remove the clutter using one dimensional filtering such as the displaced phase centre antenna (DPCA) technique [55–57], can achieve adequate rejection over the full spectral bandwidth of the clutter. However, this is at the expense of attenuating clutter echoes from low relative velocity targets (i.e. targets possessing the same Doppler frequency as the mainlobe clutter echoes). In contrast, space-time adaptive processing (STAP) [39, 51, 68, 71–74] further distinguishes the clutter and target returns in the angular domain by using antenna array, hence offering the capability of detecting moving targets with low relative velocity. Calculating the two dimensional filter weights adaptively leads to the advantages over DPCA in robustness to errors and capability for simultaneous suppression of jamming and clutter echoes.

Figure 2.20 shows an illustration of spatial and spectral filtering for a sidelooking airborne monostatic radar. The clutter as well as the target returns can be divided into the space and time domains. As the target may be travelling at a different velocity to that of the airborne bistatic radar system (transmitter and receiver), its echo is likely to have a different Doppler frequency from that of the clutter echoes. Filtering the echoes in space and time domain, allows the target return to be separated, even if it has the same direction of arrival (DOA) as the clutter echoes. However, when the target Doppler frequency gets nearer to the clutter Doppler frequency (both with the same DOA), nulling is required to suppress the clutter echoes, in order to detect the target.

Radar systems using STAP typically emit repetitive identical pulses. The reflected echoes (consisting of both target return and clutter echoes) are sensed at each of the N antenna array elements, and the sensed returns are sampled at each of the discrete range gates (total number of range gates is G_d)- covering the range interval of interest, over M successive pulse repetition intervals (PRI) (see Appendix C for the clutter model used).

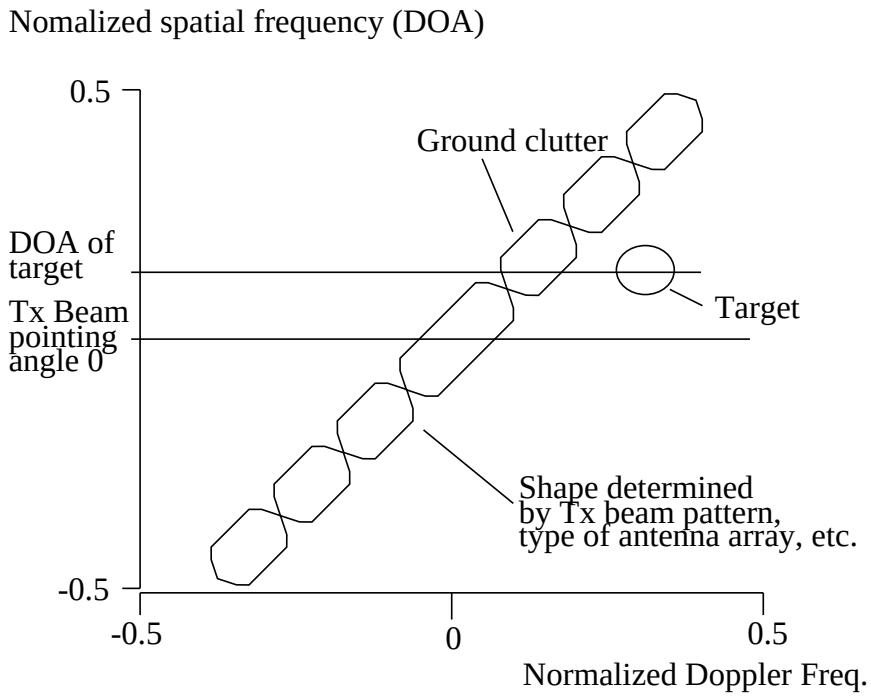

Figure 2.20: *Illustration of spatial and spectral filtering for a sidelooking airborne monostatic radar.*

Let the data received (reflected echoes) from all the range gates be stored in a cube data matrix $\mathbf{D}$ which has a dimension of ($N \times M \times G_d$). The complex scalar $\mathbf{d}_{n,m,g}$, represents the mth baseband complex (I/Q) data samples of the nth array channel in the gth range gate. The cube data matrix $\mathbf{D}$ is defined by

$$\mathbf{D} = [\mathbf{D}(1)\, \mathbf{D}(2)\, \ldots\, \mathbf{D}(G_d)] \tag{2.10}$$

where $\mathbf{D}(g)$ is an $N \times M$ matrix

$$\mathbf{D}(g) = \begin{pmatrix} d_{1,1,g} & d_{1,2,g} & \ldots & d_{1,M,g} \\ d_{2,1,g} & d_{2,2,g} & \ldots & d_{2,M,g} \\ \vdots & \vdots & \ddots & \vdots \\ d_{N,1,g} & d_{N,2,g} & \ldots & d_{N,M,g} \end{pmatrix} \tag{2.11}$$

where $g = 1, \ldots, G_d$ and G_d is the total number of range gates available.

Let the data matrix $\mathbf{X}_r$ = $\mathbf{D}(r)$ where r is the range gate under test. Under the signal-absence hypothesis H_0, the data matrix $\mathbf{X}_r$ consists of clutter (also known as interference) and noise

components only, i.e.,

$$\mathbf{X}_r = \mathbf{C}_r + \mathbf{N} \tag{2.12}$$

where $\mathbf{C}_r$ and $\mathbf{N}$ are the clutter and noise matrices respectively. Both have the same dimension as $\mathbf{X}, (N \times M)$. The elements in matrix $\mathbf{C}_r$ are given by $c_{n,m,r}$ as defined by equation (C.4), while the elements in matrix $\mathbf{N}$ are additive white Gaussian noise (AWGN) with a variance of σ_n^2, generated by the radar receiver which is dominated by the first amplifier in the receiver chain. The noise is assumed to be uncorrelated in time and space.

Under the signal-presence hypothesis H_1, a target signal component also appears in the data matrix, i.e.,

$$\mathbf{X}_r = \alpha_s \mathbf{S}_r + \mathbf{C}_r + \mathbf{N} \tag{2.13}$$

where α_s is an unknown complex constant, representing the amplitude of the target signal and $\mathbf{S}$ is the target signal matrix expressed by

$$\mathbf{S} = \mathbf{s}_t^T \otimes \mathbf{s}_s \tag{2.14}$$

where $\otimes$ is the Kronecker product, $\mathbf{s}_t$ and $\mathbf{s}_s$ is the temporal and spatial dimensions of the target signal respectively,

$$\mathbf{s}_t^T = [1 \ \exp(j2\pi f_{st}) \ \ldots \ \exp(j2\pi(M-1)f_{st})] \tag{2.15}$$

and

$$\mathbf{s}_s = [1 \ \exp(j2\pi f_{ss}) \ \ldots \ \exp(j2\pi(N-1)f_{ss})]^T. \tag{2.16}$$

The superscript T is the transpose operator, f_{st}, the target signal temporal frequency and f_{ss}, the target signal spatial frequency are given as

$$f_{st} = \frac{2v_{rad}\text{PRI}}{\lambda} \tag{2.17}$$

and

$$f_{ss} = \frac{d_a \sin \alpha_{ta}}{\lambda} \tag{2.18}$$

respectively. v_{rad} is the relative velocity of the target, $d_a = \frac{\lambda}{2}$ is the spacing between the elements of the array antenna and α_{ta} is the direction of arrival of the target-return planewave with respect to the broadside of the array for a forward looking array.

In the case of unknown clutter statistics, the data from the adjacent range gates, conventionally referred to as the training data, training range gates or secondary data, is used for the estimation of the clutter sample covariance matrix. The training data (assumed to be free from target signal and derived from a homogeneous clutter environment[iii]) consists of only the clutter/interference and noise components and is denoted by

$$\mathbf{Y}_k = \mathbf{C}_k + \mathbf{N}. \tag{2.19}$$

$\mathbf{Y} = \mathbf{D}(k)$, is a data matrix with dimension ($N \times M$) and k is the training range gate.

Matrices $\mathbf{Y}_k$ and $\mathbf{X}_r$ are assumed to be independent of each other, but process the same clutter statistics, i.e., vec($\mathbf{Y}_k$), a ($NM \times 1$) vector comprising the NM elements of $\mathbf{Y}_k$ should have a complex Gaussian distribution with zero mean and an estimated [iv] clutter sample covariance matrix $\widehat{\mathbf{Q}}$. The notation vec($\mathbf{A}$) = [$\mathbf{a}_1^T, \mathbf{a}_2^T, \ldots, \mathbf{a}_n^T$] where $\mathbf{a}_n$ is a column of the matrix $\mathbf{A}$ and using the maximum likelihood estimator (MLE) [78], $\widehat{\mathbf{Q}}$, a ($NM \times NM$) matrix when using only range dimension training data, is given as

$$\widehat{\mathbf{Q}} = \frac{1}{K} \sum_{\substack{k=r-1-\frac{K+1}{2} \\ k \neq r-1, r, r+1}}^{r+1+\frac{K+1}{2}} \mathrm{vec}(\mathbf{Y}_k)\mathrm{vec}(\mathbf{Y}_k)^H \tag{2.20}$$

where K is the total number of "snapshots" used (or also known as sample support or sample requirement) and $\mathbf{Y}_k$ is the training data matrix from range gate k and r is the range gate under test. The immediate neighbour range gates $r-1$ and $r+1$ are excluded to prevent target self-nulling. Target self-nulling occurs when target energy leaks into neighbour range-gate. These excluded gates are referred to as guard-gates. Snapshots, or samples, are a sequence of ($N \times M$)

[iii] The non-homogeneity detector (NHD) [75–77] can be used to remove non-homogeneous clutter.

[iv] In this thesis, the clutter/interference + noise covariance matrix will be known as the clutter sample covariance matrix $\widehat{\mathbf{Q}}$

data array of samples at successive range gates. In cases where the clutter Doppler frequency is range dependent, snapshots from range gates with clutter echoes statistically different from that of the range gate under test should be excluded. On the other hand, snapshots from the time domain (obtained with a tapped delay line, with a PRI delay between the snapshots) may be required, even though they are not independent identically distributed (i.i.d.). Figure 2.21 and Figure 2.22 show the data snapshots from the range domain and time domain respectively.

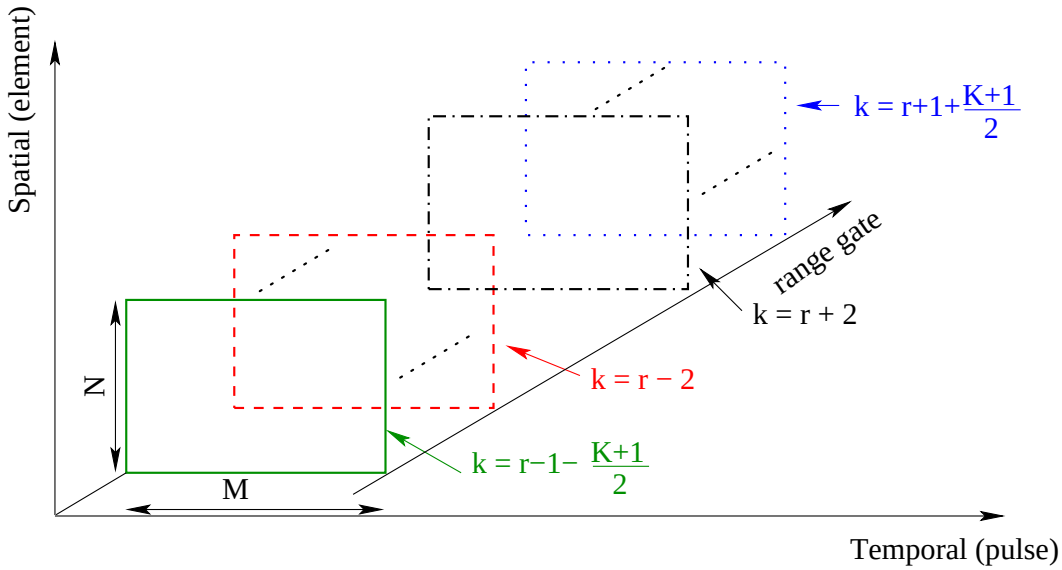

Figure 2.21: *Illustration of snapshots collected in the range domain.*

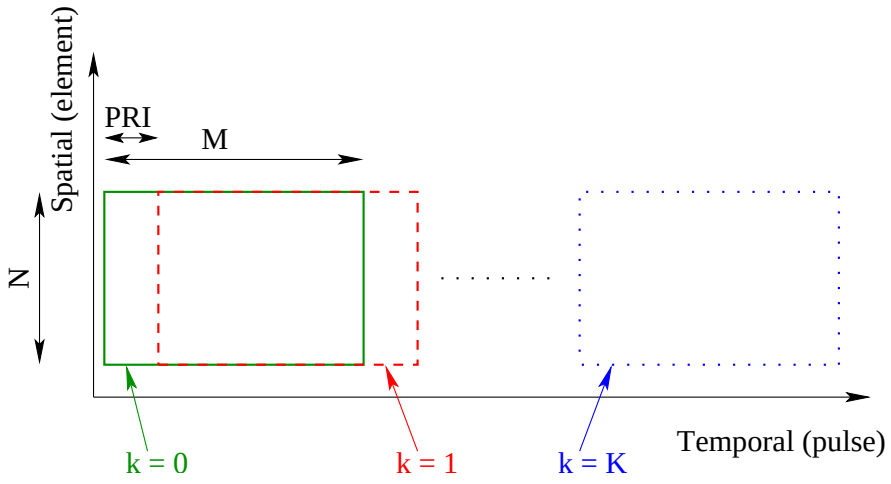

Figure 2.22: *Illustration of snapshots collected in the time domain.*

Due to the clutter Doppler range dependency, the clutter sample covariance matrix may differ

from range gate to range gate. $\widehat{\mathbf{Q}}_r$ is an estimation of $\mathbf{Q}_r$, the true clutter sample covariance matrix from r range gate under test, using the training data and $\mathbf{Q}_r$ is given as

$$\begin{aligned} \mathbf{Q}_r &= \mathbf{R}_r - \mathbf{Q}_s \\ &= \mathrm{E}[\mathrm{vec}(\mathbf{X}_r)\mathrm{vec}(\mathbf{X}_r)^H] - \mathrm{E}[\mathrm{vec}(\mathbf{S}_r)\mathrm{vec}(\mathbf{S}_r)^H] \end{aligned} \tag{2.21}$$

where E[·] means the mathematical expectation, $\mathbf{R}_r$ is covariance matrix of the target signal + clutter + noise, $\mathbf{Q}_s$ is the target signal covariance matrix, both for the range gate under test r and superscript H is the Hermitian operator. For the rest of this thesis, the index r of the clutter sample covariance matrix will be left out, as the STAP processor is always assumed to be designed for the range gate under test.

For an optimum signal-to-clutter + noise ratio (SCNR) STAP processor, the weights are given as

$$\mathbf{w}_{(scnr)} = \mathbf{Q}^{-1}\mathbf{s} \tag{2.22}$$

where $\mathbf{Q}^{-1}$ is the inverse of $\mathbf{Q}$ and $\mathbf{s}$, a $(NM \times 1)$ vector is the signal-steering vector matched to the signal of interest (possible target signal). When the possible target signal is unknown, the signal-steering vector has to sweep through the whole range of Doppler and spatial frequencies.

Theoretically, a fully-adaptive STAP can implement the optimal solution (a Wiener filter). However, in practice, fully-adaptive STAP encounter several problems [79]. First, the number of weights in the linear filter can be extremely large. Even in a radar with the number of antenna elements N of about a thousand, the value of NM may range from tens of thousands to thousands of thousands (page 118 of [68]). Secondly, the adaption of the processor has to be a moderately fast operation which should be able to cope with any changes in the data statistics. Such changes may be the result of inhomogeneity of the clutter background and perturbations caused by the radar motion. Finally, the number of snapshots required (as explained in Section 4.9.2) to obtain a good estimation of the clutter sample covariance matrix, also known as sample support is considered data intensive. The computational cost of directly inverting a $(NM \times NM)$ dimensional matrix, $\mathrm{O}(NM)^3$, is also considered to be too expensive. In this work, direct matrix inversion is used to invert the clutter sample covariance matrix, even though matrix inversion algorithms that use less computational cost are available [80–83]. Both clutter sample covariance matrix estimation and matrix inversion must be performed for every range

gate under test. The weights of the STAP processor must also be calculated for every look angle. All these processes must be carried out in real-time [84–88].

A number of projects which deal with searching for a real time, realizable and reduced rank (or partially adaptive) sub-optimum approach, with low computational cost have been reported. Some of the reduced rank STAPs will be introduced in Section 2.6.4. A number of studies, along with some experimental data, have shown that STAP can be very efficient for clutter suppression as well as target detection for both airborne monostatic and airborne bistatic radar [46, 47, 50, 52–54, 89–93].

2.4.1 Effects on STAP processor caused by clutter Doppler range dependency

The non-stationary nature of the clutter ridge changing with range in Doppler-azimuth space directly violates the intrinsic adaptive algorithm assumption[v], thereby complicating STAP implementation and potentially degrading target detection performance. MELVIN et al. [67] investigated the effect of estimating the clutter sample covariance matrix using range dependent training data. A significantly broadened MVE spectra response is observed. It indicates the clutter sample covariance matrix mismatch with respect to other bistatic ranges of interest. This is a result of the averaging operation in equation (2.20). The broadening of the MVE spectra also implies an increase of minimum detectable velocity (MDV), making it harder to detect slow relative velocity targets (i.e. targets which have only a small component of velocity in the direction of the receiving radar).

The non-stationary clutter behaviour results in clutter sample covariance matrix estimation errors which substantially degrade the target detection performance.

2.5 Performance Metric

Before we look at different methods of mitigating the problem caused by clutter Doppler range dependency, the performance metric used to evaluate the performance of the processors investigated in this work is first described. The four performance metrics used in this work are the improvement factor (IF) [51], improvement factor loss, mean improvement factor loss and signal-to-interference + noise ratio. For all processor performances evaluated in this thesis, the

[v] Assumes a stationary set of training data.

performance of the processors was calculated from an average of 20 independent trials[vi].

2.5.1 Improvement Factor

The efficiency of any linear processor, can be characterised by the improvement factor which is defined as the ratio of signal-to-noise power ratios at the output and input, respectively.

$$\begin{aligned} IF &= \frac{\frac{P_s^{out}}{P_n^{out}}}{\frac{P_s^{in}}{P_n^{in}}} \\ &= \frac{\frac{\mathbf{w}^H \mathbf{s}\mathbf{s}^H \mathbf{w}}{\mathbf{w}^H \mathbf{Q} \mathbf{w}}}{\frac{\mathbf{s}^H \mathbf{s}}{\mathrm{tr}(\mathbf{Q})}} \\ &= \frac{\mathbf{w}^H \mathbf{s}\mathbf{s}^H \mathbf{w} \cdot \mathrm{tr}(\mathbf{Q})}{\mathbf{w}^H \mathbf{Q} \mathbf{w} \cdot \mathbf{s}^H \mathbf{s}} \end{aligned} \tag{2.23}$$

where P_s^{out}, P_n^{out}, P_s^{in}, P_n^{in}, are the signal power at the output, noise power at the output, signal power at the input and noise power at the input respectively. The vector $\mathbf{w}$, a $(NM \times 1)$ vector is the weights of the processor, $\mathbf{s}$, a $(NM \times 1)$ vector is the signal-steering vector, $\mathbf{Q}$ is the true clutter sample covariance matrix and tr() is the trace of a square matrix.

Specifically for the optimum (in the sense of SCNR) processor $\mathbf{w}_{(scnr)} = \mathbf{Q}^{-1}\mathbf{s}$ (equation (2.22))[vii], replacing $\mathbf{Q}$ with $\widehat{\mathbf{Q}}$ when the true clutter covariance matrix is not available, one gets

$$IF_{(scnr)} = \frac{\mathbf{s}^H \widehat{\mathbf{Q}}^{-1} \mathbf{s}\mathbf{s}^H \widehat{\mathbf{Q}}^{-1} \mathbf{s} \cdot \mathrm{tr}(\mathbf{Q})}{\mathbf{s}^H \widehat{\mathbf{Q}}^{-1} \mathbf{Q} \widehat{\mathbf{Q}}^{-1} \mathbf{s} \cdot \mathbf{s}^H \mathbf{s}} \tag{2.24}$$

When $\widehat{\mathbf{Q}}$ is a very good estimate of $\mathbf{Q}$, $\widehat{\mathbf{Q}} = \mathbf{Q}$, then $IF_{(scnr)} = IF_{(opt)}$

$$\begin{aligned} IF_{(opt)} &= \frac{\mathbf{s}^H \mathbf{Q}^{-1} \mathbf{s}\mathbf{s}^H \mathbf{Q}^{-1} \mathbf{s} \cdot \mathrm{tr}(\mathbf{Q})}{\mathbf{s}^H \mathbf{Q}^{-1} \mathbf{Q} \mathbf{Q}^{-1} \mathbf{s} \cdot \mathbf{s}^H \mathbf{s}} \\ &= \frac{\mathbf{s}^H \mathbf{Q}^{-1} \mathbf{s} \cdot \mathrm{tr}(\mathbf{Q})}{\mathbf{s}^H \mathbf{s}} \end{aligned} \tag{2.25}$$

IF is normalised by the theoretical maximum which is approximately $CNR \times N \times M$, where CNR is the clutter to noise ratio (see page 114 of [51]). When using reduced dimension STAP processor such as the joint domain localized (JDL) processor, the reduced dimension

[vi] An error of about 5% may be expected when using 20 trials (see page 691-698 of [94])

[vii] The processor is assumed to be perfectly matched to the expected target signal. In practice some losses occur owing to the finite set of Doppler and spatial filters.

clutter sample covariance matrix and steering vector would be concatenated with zeroes (at the appropriate position) and expanded into a full dimension (NM) matrix and vector respectively.

2.5.2 Improvement factor loss (IF loss)

The loss incurred due to the difference between the true ($\mathbf{Q}$) and estimated ($\widehat{\mathbf{Q}}$) clutter sample covariance matrix is shown by the improvement factor loss (IF loss). In the context of clutter suppression in a range-dependent clutter environment, IF loss is a measure of the loss due to imperfect Doppler compensation. While in the context of reduced dimension STAP, it shows loss in processor performance in return for lower computational cost. IF loss is typically evaluated for a single look angle for all possible Doppler frequencies. The resulting IF loss curve then gives an indication of the performance in terms of minimum detectable velocity for a specified, maximum tolerable IF loss. IF loss is given by

$$\begin{aligned} IF\ loss &= \frac{IF_{opt}}{IF_{scnr}} \\ &= \frac{\frac{\mathbf{s}^H\mathbf{Q}^{-1}\mathbf{s}\cdot\mathrm{tr}(\mathbf{Q})}{\mathbf{s}^H\mathbf{s}}}{\frac{\mathbf{s}^H\widehat{\mathbf{Q}}^{-1}\mathbf{s}\mathbf{s}^H\widehat{\mathbf{Q}}^{-1}\mathbf{s}\cdot\mathrm{tr}(\mathbf{Q})}{\mathbf{s}^H\widehat{\mathbf{Q}}^{-1}\mathbf{Q}\widehat{\mathbf{Q}}^{-1}\mathbf{s}\cdot\mathbf{s}^H\mathbf{s}}} \\ &= \frac{\mathbf{s}^H\mathbf{Q}^{-1}\mathbf{s}\mathbf{s}^H\widehat{\mathbf{Q}}^{-1}\mathbf{Q}\widehat{\mathbf{Q}}^{-1}\mathbf{s}\cdot\mathbf{s}^H\mathbf{s}}{\mathbf{s}^H\mathbf{s}\mathbf{s}^H\widehat{\mathbf{Q}}^{-1}\mathbf{s}\mathbf{s}^H\widehat{\mathbf{Q}}^{-1}\mathbf{s}} \end{aligned} \tag{2.26}$$

The minimum IF loss is unity or 0 dB, when $\widehat{\mathbf{Q}} = \mathbf{Q}$. All compensation algorithms will try to achieve 0 dB IF loss (assuming that the number of samples used to estimate the clutter sample covariance matrix is $\gg 2NM$)[viii]. However, when using reduced dimension STAP, the minimum IF loss achievable by the compensation process is often higher than the minimum IF loss achievable with a full dimension STAP. In this work, the desired minimum IF loss is still considered to be the 0 dB, even when using a reduced dimension STAP.

2.5.3 Mean IF loss

It is sometime desirable to obtain a number that can be used to describe the performance of the processor. Mean IF loss is used for such a purpose. It is the mean of the improvement factor loss across all Doppler frequency (-PRF/2 $\leq f_D \leq$ PRF/2) at a particular look angle, φ_r. The

[viii] Refer to Section 4.9 for details

finer is the separation between the Doppler frequency, the better is the mean IF loss estimation.

$$Mean\ IF\ loss = \frac{1}{\mathrm{PRF}} \int_0^{\mathrm{PRF}} Mean\ IF(\omega) d\omega \tag{2.27}$$

$$= \frac{1}{\mathrm{PRF}} \int_0^{\mathrm{PRF}} \frac{\mathbf{s}(\omega)^H \widehat{\mathbf{Q}}^{-1} \mathbf{Q} \widehat{\mathbf{Q}}^{-1} \mathbf{s}(\omega)}{\mathbf{s}(\omega)^H \mathbf{Q}^{-1} \mathbf{s}(\omega)} d\omega \tag{2.28}$$

where ω is the Doppler frequency.

2.5.4 Signal-to-interference+noise power ratio

Signal-to-interference+noise power ratio is sometimes also used to determine the performance of a processor. The signal-to-interference+noise power ratio is given as

$$SINR = \frac{P_s^{(out)}}{P_n^{(out)}} = \frac{\mathbf{w}^H \mathbf{s}\mathbf{s}^H \mathbf{w}}{\mathbf{w}^H \mathbf{Q} \mathbf{w}} \tag{2.29}$$

With the performance metrics defined, methods of mitigating the clutter Doppler range dependency - for improving the clutter suppression performance - can now be investigated.

2.6 Mitigating clutter Doppler range dependency

Figure 2.23 shows the performance of the STAP processor without compensation, using radar parameters shown in Table 2.1. The curve labelled “Ideal STAP processor” (in Figure 2.23(a)) assumed that the clutter sample covariance matrix is known. The curve labelled “without compensation” in Figure 2.23(a) shows the improvement factor of the STAP processor when mitigation of the non-stationarity nature (in range) of the clutter echoes is not taken into consideration. The range gate under test is chosen to be range gate 27. There are two reasons for this selection: The range dependence of the clutter echoes tends to be more significant in the near range than the far range. Choosing range gate under test to be range gate 27 will allow significant clutter range dependency to be observed; Due to the computational power available, the number of clutter return is finite[ix]. The nearer the range gate, the lesser the number of clutter returns. Range gate 27 being approximately 1/3 of the total number of range gates available, is hence

[ix] The simulated ground is formed using a grid system.

the appropriate choice to being use as the range gate under test. Training data from neighbour range gates 25 & 29 is used in this simulation. The curve in Figure 2.23(b) shows the degradation in performance in terms of IF loss, when any form of compensation is not used. Significant performance loss of up to 25 dB is observed at the clutter notch region. The objective of any mitigation or compensation method, will be to obtain an IF loss of 0 dB for all Doppler frequency.

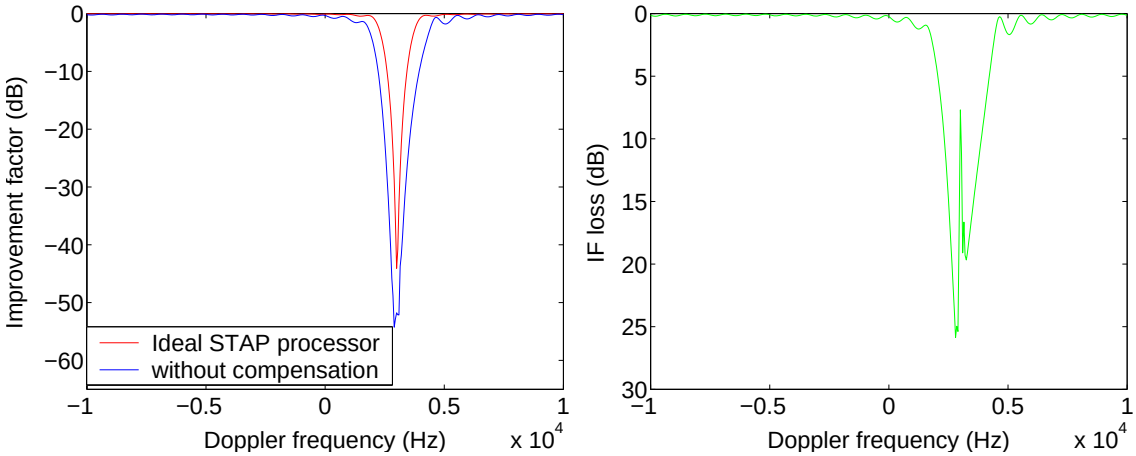

Figure 2.23: *STAP processor performance without compensation, using training data from neighbour range gates 25 & 29 (a) Improvement factor plot, and (b) Improvement factor loss plot.*

To mitigate the impact of clutter echoes range dependency on clutter suppression, a number of approaches can be used. They are:

1. Increasing the Degrees-of-Freedom;
2. Using variable range dimension training data size;
3. Using multiple staggered medium PRF;
4. Using reduced-dimension algorithm in order to reduce the amount of samples / training range gates required;
5. Time-varying the adaptive filter response; and
6. Deterministically modifying the data or filter notch to account for the non-stationary behaviour.

number of antenna elements	N	8
number of pulses delay	M	24
pulse repetition frequency	PRF	20 kHz
operating frequency	f_o	10 GHz
wavelength	λ	0.03 m
array geometry		linear forward looking
receiver & transmitter height	H_R, H_T	1000 m
receiver & transmitter velocity	v_R, v_T	90 m/s
receiver flight angle	δ_r	0°
transmitter flight angle	δ_t	90°
receiver look angle	φ_r	45°
baseline separation (along flight direction)		2000 m
total number of range gates		64
testing range gate	r	27
training range gates	k	25 & 29

Table 2.1: *Radar Parameters.*

2.6.1 Increasing the Degrees-of-Freedom

One method of reducing the degradation of MDV is to increase the number of degrees-of-freedom (DOF) available to the STAP algorithm [62]. RICHARDSON had shown that, for forward looking airborne monostatic radar with transmitter and receiver beams oriented at a steep grazing angle to the ground (approximately 30°) and scanned off at an angle of 60° from broadside to the array, slow-moving target detection can be achieved using both azimuth and elevation degrees of freedom (using a planar array) [95]. However with the increase of DOF, more data samples are required and the computation cost will increase because of a bigger covariance matrix size. Limited fundamentally by the non-stationary nature of the training data over range, more DOFs will provide a narrower clutter notch about the broaden clutter ridge but nothing is done to address the difference between clutter ridges of different range gates. As a result, increasing the degrees-of-freedom is effective when there is only a single training range gate.

2.6.2 Variable range dimension training data size

Reducing the number of range dimension training data and the number of range gates under test in a training set is another technique to lessen the effects of range dependency. In sidelooking airborne monostatic radar, a certain amount of range gates under test are grouped as a training

set, and each training set uses the same adaptive weights. Clutter non-stationarity is most severe at the near range. Using less range training data at short range will minimise the spread of the clutter ridge. The size of the range training data can increase with increasing range since clutter non-stationary is less severe at long range. This technique however has two disadvantages. More adaptive weight vectors need to be computed because of the increased number of training sets used. The sample support consideration must also be taken into account when deciding the number of training range gates required in each training set [52].

2.6.3 Multiple PRF

As discussed before, the clutter spectrum changes less significantly with range at far range, adaptive processing without any Doppler compensation can hence be carried out at far range. Unfortunately, it is very difficult to perform adaptive processing at near range because there are not enough stationary data vectors. The area within this special near range is referred as the insensitive area (R_{ins}). For medium PRF (MPRF) mode, the lower range of MPRF can be used to decrease the insensitive zones. Considering the range ambiguity and Doppler ambiguity in MPRF radar, multiple staggered PRFs can be adopted to make the insensitive areas staggered. This method of combining STAP with range-dimension information is called the multiple-PRF STAP scheme [96]. The multiple-PRF STAP scheme may be described as follows. Beyond the special range, adaptive processing is performed directly. For the special near range, the insensitive areas could be directly given up or the receiver can adopt the conventional non-adaptive method (using pre-designed filters). Multiple staggered PRFs are used to make the insensitive and blind zones staggered [66].

2.6.4 Reduced dimension processing

Reducing the dimension of the STAP processor is often used to reduce the computational cost of the processor. The inverse of the clutter sample covariance matrix is required when calculating the STAP processor weights coefficient. As mentioned before, the inversion of a ($NM \times NM$) dimension covariance matrix (using direct inversion) requires a computational cost of $O(NM)^3$, which is considered too expensive for real time implementation. In order to build a practical STAP processor, dimensional reduction is often used. Using reduced dimension STAP, also known as reduced rank STAP, means that less training data will be required (as explained in Section 4.9.2).

In a non-stationary clutter environment, using less training data from different range gates will minimise the widening of the clutter ridge. Compared with full dimension STAP, reduced dimension STAP processor may suffer from some degradation in clutter suppression performance especially when system errors, such as array errors and channel mismatch are in existence [97]. However, in situations where there are a limited amount of training data available for the estimation of the clutter sample covariance matrix, reduced-dimension methods outperform full-dimension space-time adaptive processing. It is important to note that dimension-reduction is not the only method for reducing sample support requirement. Other examples of minimising the sample support, include methods which exploit properties of uniformly sampled spatial-temporal array such as Block-Block-Toeplitz estimation [98], persymmetry and forward-backward (F/B) smoothing [99, 100], as well as parametric and multichannel modelling methods [101, 102]. Sample support requirement for reduced dimensional STAP is given in Section 4.9.3, Section 4.9.4 and Section 4.9.6 . A number of reduced dimensional or suboptimal methods have been proposed by several authors. Some of them are:

1. Sum and difference STAP ($\Sigma\Delta$ STAP) [51, 103–109];
2. Factored approach (FA) [110–112];
3. Extended factored approach (EFA) [110, 113];
4. Eigencanceler (EC) [114];
5. Factored time-space (FTS) [112, 115];
6. Pre-Doppler [116–118] and post-Doppler STAP [84, 119];
7. Space-time subspace transforms (see Chapter 5 of [51]);
8. Principal-components (PC) [120, 121];
9. Cross-spectral metric (CSM) [122–124];
10. Multistage wiener filter (MSWF) [125–127];
11. Joint-domain processing approach with multiple Doppler bins (mDT-SAP) [62, 105, 128];
12. hybrid STAP [73, 105];
13. Reduced-rank generalized sidelobe canceller (GSC) [129–131];

14. Joint domain localised processor (JDL) [46, 132–134]; and

15. Modified joint domain localised STAP [54, 135].

Various reduced-rank STAP performances had been analysed and compared by numerous researchers. Some of the researchers are PECKHAM et al. [136], GUERCI et al. [125], WANG et al. [132, 137], GOLDSTEIN et al. [115, 138], HIMED et al. [139], GU et al. [71], ZULCH et al. [140] and BAO et al. [105].

2.6.5 Derivative-based updating

Another approach that addresses the non-stationary clutter is to use STAP weights that vary linearly from range gate to range gate. The entire interval of K range gates centred at range gate r (range gate under test) is used to compute the range-varying STAP weights. The range-varying STAP weights can be rewritten as a Taylor series expansion.

$$\mathbf{w}_{Ta}(k) = \mathbf{w}_0 + k\dot{\mathbf{w}}_0 + \frac{k^2}{2}\ddot{\mathbf{w}}_0 + \dots \tag{2.30}$$

where $\mathbf{w}_0 = \mathbf{w}(r)$, $\dot{\mathbf{w}}_0 = \dot{\mathbf{w}}(r)$ and $\ddot{\mathbf{w}}_0 = \ddot{\mathbf{w}}(r)$ are the weight vector, first order derivative (in range) and second order derivative (in range) of the STAP weight vector at $k = r$, i.e. the centre of the training interval, respectively.

This expansion can be approximated using only the first-order derivative provided that the higher order terms are negligible. The result, known as derivative-based updating (DBU) [141–144], can be written as a linearly range-varying weight vector

$$\mathbf{w}_{DBU}(k) = \mathbf{w}_0 + k\dot{\mathbf{w}}_0 \tag{2.31}$$

The output of DBU-STAP processor is obtained by multiplying the range-varying weight vector

from equation (2.31) with the rth data snapshot (range gate under test)

$$\begin{aligned} y_{DBU}(r) &= \mathbf{w}_{DBU}^{H}(r)\mathrm{vec}(\mathbf{X}_{\mathrm{r}}) \\ &= \mathbf{w}_{0}^{H}\mathrm{vec}(\mathbf{X}_{\mathrm{r}}) + r\dot{\mathbf{w}}_{0}^{H}\mathrm{vec}(\mathbf{X}_{\mathrm{r}}) \\ &= \begin{bmatrix} \mathbf{w}_0 \\ \dot{\mathbf{w}}_0 \end{bmatrix}^{H} \begin{bmatrix} \mathrm{vec}(\mathbf{X}_{\mathrm{r}}) \\ r\mathrm{vec}(\mathbf{X}_{\mathrm{r}}) \end{bmatrix} \\ &= \tilde{\mathbf{w}}_{DBU}^{H}\tilde{\mathbf{x}}_{DBU}(r) \end{aligned} \tag{2.32}$$

where $\tilde{\mathbf{x}}_{DBU}(r)$ is the augmented data vector and $\tilde{\mathbf{w}}_{DBU}$ is the augmented STAP weight vector. Note that $\tilde{\mathbf{w}}_{DBU}$ is not a function of r. Rather, the augmented data vector absorbs the varying component. The clutter sample covariance matrix of the augmented data vector is computed by using equation (2.20). This clutter sample covariance matrix can be modelled by using the estimated clutter sample covariance matrix of each range gate

$$\tilde{\mathbf{Q}}_{DBU} = \frac{1}{K} \sum_{\substack{k=r-1-\frac{K+1}{2} \\ k\neq r-1,r,r+1}}^{r+1+\frac{K+1}{2}} \begin{bmatrix} \widehat{\mathbf{Q}}_k & k\widehat{\mathbf{Q}}_k \\ k\widehat{\mathbf{Q}}_k & k^2\widehat{\mathbf{Q}}_k \end{bmatrix}. \tag{2.33}$$

The resulting DBU-STAP weight vector is then found to be

$$\tilde{\mathbf{w}}_{DBU} = \begin{bmatrix} \mathbf{w}_0 \\ \dot{\mathbf{w}}_0 \end{bmatrix} = \tilde{\mathbf{Q}}_{DBU}^{-1} \begin{bmatrix} s \\ 0 \end{bmatrix} \tag{2.34}$$

Note that the degrees of freedom for the DBU-STAP weights is now twice that of the other STAP methods considered, since both the weights and their first-order derivative have to be computed at range gate r. The number of data snapshots must also be doubled to ensure that $\tilde{\mathbf{Q}}_{DBU}$ is full rank. In practice, as K increases, the condition number of $\tilde{\mathbf{Q}}_{DBU}$ increases due to the k^2 term in equation (2.33) and to avoid ill-conditioning, a scaling factor $\propto \frac{1}{K}$ is used in the calculation of the $\tilde{\mathbf{x}}_{DBU}(k)$ (see page 481 of [141]).

DBU can be extended to cope with any suitably smooth non-linear range-variation by using more terms from the series expansion of equation (2.30). Range-varying STAP weights raise several issues, including the availability of sufficient training data as well as the computational complexity.

2.6.6 Doppler warping

Doppler warping [52, 143] also known as Doppler compensation [145], attempts to align the clutter ridge using a range-dependent transformation on the data prior to STAP. It is based on shifting the clutter echoes as a function of range such that the shifting follows the movement of the clutter ridge over range. The clutter sample covariance matrix is computed by averaging over a range interval, training data with the priori transformation.

This method takes data from each range gate and applies a Doppler shift to align the clutter ridge at a common Doppler frequency for a given look angle, e.g., array broadside. If the clutter ridge has a similar shape but is only displaced in Doppler over range, then this Doppler shift will realign the clutter ridge for all ranges. Though this will perfectly align the clutter ridge at one angle, for other angles the alignment is only approximate. Doppler warping incorporates a Doppler shift by producing a phase ramp across pulses. The Doppler shift can be formulated using the transformation matrix $\mathbf{T}_{dw}(r,k)$, which is given as

$$\mathbf{T}_{dw}(r,k) = \begin{pmatrix} t_0(r,k) & & & & & & & & \\ & \ddots & & & & & & & \\ & & t_0(r,k) & & & & 0 & & \\ & & & t_1(r,k) & & & & & \\ & & & & \ddots & & & & \\ & & & & & t_1(r,k) & & & \\ & & & & & & \ddots & & \\ & & & & & & & \ddots & \\ & & 0 & & & & & t_{M-1}(r,k) & \\ & & & & & & & & \ddots \\ & & & & & & & & t_{M-1}(r,k) \end{pmatrix} \tag{2.35}$$

where

$$t_m(r,k) = e^{j2\pi f_s(r,k) m PRI} \qquad \text{for } m = 0 \ldots M-1 \tag{2.36}$$

and $f_s(r,k)$ is the Doppler shift to range gate r from range gate k and M is the number of

successive pulses,

$$f_s(r,k) = f_k^d - f_r^d. \tag{2.37}$$

f_k^d and f_r^d is the Doppler frequency of the clutter echo arriving from angle $\varphi_{r,k}$ for range gate k and from angle $\varphi_{r,r}$ for range gate r respectively.

The Doppler warping transformation matrix $\mathbf{T}_{dw}$ ($NM \times NM$) simply Doppler shifts the entire training data snapshot from range gate k to range gate r. The resulting Doppler warped output to range gate r is

$$\text{vec}(\mathbf{Y}_{dw}(r,k)) = \mathbf{T}_{dw}^H(r,k)\text{vec}(\mathbf{Y}_k) \tag{2.38}$$

where $\mathbf{Y}_k$ is the training data from range gate k.

Likewise, the clutter sample covariance matrix for range gate under test, r, following the Doppler warping is given by

$$\widehat{\mathbf{Q}}_{dw}(r,k) = \mathbf{T}_{dw}^H(r,k)\widehat{\mathbf{Q}}(k)\mathbf{T}_{dw}(r,k) \tag{2.39}$$

2.6.7 Two-dimensional angle-Doppler compensation (ADC)

A two-dimensional angle-Doppler compensation (ADC) approach for pre-processing the secondary data was proposed by HIMED et al. [1, 53]. The intention of the compensation is to co-locate the clutter spectral centres in both angle and Doppler, thus reducing bistatic geometry-induced dispersion. The clutter spectral centre is defined as the peak position of the clutter spectrum for a specified range gate. If the clutter echoes are range independent (only true for side looking monostatic radar), the clutter spectral centres for different range gates should be co-located. However, as the clutter spectrum for a specified range gate is modulated by the transmitter antenna pattern and because of the nature of bistatic radar, the clutter centres usually vary in both angle and Doppler. In order to obtain a good estimate of the covariance matrix using the secondary data from adjacent range gates, these clutter centres should be overlapping (ideal case) or are as close to each other as possible.

Doppler warping manages to align the clutter spectrum in the Doppler domain only, the clutter spectral centres from different range gates still do not overlap.; i.e., although the clutter Doppler

frequencies aligns over range gates, its peak power in the angle domain remains different. Therefore, a two-dimensional (2-D) compensation scheme is required to bring these clutter centres together, rather than just Doppler compensation.

Denote the k-th realization of an NM-dimensional, complex baseband signal vector at spatial frequency, f_k^s, and Doppler frequency, f_k^d, as vec($\mathbf{Y}_k(f_k^s, f_k^d)$). The proposed angle-Doppler warping consists of obtaining transformation $\mathbf{T}_{2D,k}(f_k^s, f_k^d; f_r^s, f_r^d)$, such that

$$\text{vec}(\mathbf{Y}_{2D,k}(f_r^s, f_r^d)) = \mathbf{T}_{2D,k}(f_k^s, f_k^d; f_r^s, f_r^d) \circ \text{vec}(\mathbf{Y}_k(f_k^s, f_k^d)), \tag{2.40}$$

where "$\circ$" denotes the Hadamard product, f_r^s and f_r^d are the spatial and Doppler frequencies of the range gate under test (range gate r), respectively. The transformation $\mathbf{T}_{2D,k}(f_k^s, f_k^d; f_r^s, f_r^d)$ can be generated in the following manner:

$$\begin{aligned}\mathbf{T}_{2D,k}(f_k^s, f_k^d; f_r^s, f_r^d) &= e^{j\frac{2\pi m}{\text{PRF}}(f_r^d - f_k^d)} \otimes e^{j\frac{d_a n}{\lambda}(f_r^s - f_k^s)}; \\ m = 0, 1, \ldots, (M-1), &\qquad n = 0, 1, \ldots (N-1)\end{aligned} \tag{2.41}$$

The maximum likelihood (ML) estimate of the clutter sample covariance matrix is then given by

$$\begin{aligned}\widehat{\mathbf{Q}}_{2D,r}(f_r^s, f_r^d) = \frac{1}{K} \sum_{k=r-1-\frac{K+1}{2}}^{r+1+\frac{K+1}{2}} &\text{vec}(\mathbf{Y}_{2D,k}(f_r^s, f_r^d))\text{vec}^H(\mathbf{Y}_{2D,k}(f_r^s, f_r^d)); \\ &k \neq r-1, r, r+1\end{aligned} \tag{2.42}$$

2.6.8 Scaling

Doppler compensation using the scaling method was initially developed by Lapierre et al. for airborne / space-base monostatic radar [146]. It was then applied to selected bistatic configurations in [147]. The scaling method works by co-locating C_k with C_r, where C_k denotes the clutter ridge (as shown in Figure 2.15) from neighbour range gate k and C_r denotes the clutter ridge from range gate r (assuming that range gate r is the range gate under test). To do so in the space-time frequency domain (power spectrum plot), the following steps have to be carried out:

1. Rename the original variables (f_s^k, f_d^k) for each clutter ridge as (f_s', f_d'), where f_s^k and f_d^k

are the spatial frequency and Doppler frequency of the clutter echo in neighbour range gate k respectively.

2. Bringing the "centre" (defined here to be the centre of the clutter ridge bounding rectangle) of each C_k to the origin of its (f'_s, f'_d) axes.

3. Scaling this translated clutter ridge, possibly inequally along f'_s and f'_d.

4. Bringing the scaled clutter ridge to the "centre" of C_c.

Steps 2-4 transformed all the clutter ridges C_ks into the common system of coordinates (f_s, f_d), which is also that of C_r. This is done by using a particular transformation $\mathbf{T}_s(k)$. Using homogeneous coordinates for convenience, we have

$$(f'_s \; f'_d \; 1)^T = \mathbf{T}_s(k)(f_s \; f_d \; 1)^T \tag{2.43}$$

where $\mathbf{T}_s(k)$ is of the form

$$\begin{pmatrix} 1 & 0 & \Delta^2_{fs} \\ 0 & 1 & \Delta^2_{fd} \\ 0 & 0 & 1 \end{pmatrix} \begin{pmatrix} S_{fs} & 0 & 0 \\ 0 & S_{fd} & 0 \\ 0 & 0 & 1 \end{pmatrix} \begin{pmatrix} 1 & 0 & \Delta^1_{fs} \\ 0 & 1 & \Delta^1_{fd} \\ 0 & 0 & 1 \end{pmatrix}. \tag{2.44}$$

Δ^i_{fs} and Δ^i_{fd} are the space and time offsets for the ith translation respectively and S_{fs} and S_{fd} the space and time scaling factors respectively.

In practice, we only have access to the estimated clutter sample covariance matrix $\widehat{\mathbf{Q}}$, and not the clutter ridges of power spectral density. The spectral-domain affine transformation is expressed in the space-time domain of $\widehat{\mathbf{Q}}$ by the following procedure:

1. Each $\widehat{\mathbf{Q}}(k)$ (from range gate k) is regarded as a 2D sequence with finite support and is converted to a 2D continuous function by applying an interpolation filter to the elements of the sequence.

   The interpolation in the space-time domain corresponds to applying a window $W_s(U_s, V_s)$ in the Fourier or spectral domain, where U_s and V_s are two axes.

2. The continuous 2D function obtained following the interpolation process is then subjected to the transformations corresponding to the translations and scaling that are required

in the spectral domain.

The transformations that are needed are the phase shifts and scaling suggested by the following Fourier transform pairs

$$f(x,y)e^{j2\pi(u_0x+v_0y)} \quad \rightleftharpoons \quad F(u_s-u_0, v_s-v_0) \tag{2.45}$$

$$f(\frac{x}{S_x}, \frac{y}{S_y}) \quad \rightleftharpoons \quad S_xS_yF(S_xu, S_yv). \tag{2.46}$$

3. The transformed 2D function is then resampled on a grid identical to that of the original matrix $\widehat{\mathbf{Q}}(k)$.

The whole transformation described can be represented by some operator $S_k[\cdot]$, so that

$$\widehat{\mathbf{Q}}_s(k) = S_k[\widehat{\mathbf{Q}}(k)]. \tag{2.47}$$

where $\widehat{\mathbf{Q}}_s(k)$ is the scaled estimated clutter sample covariance matrix.

Since the algorithm was initially developed for monostatic cases, where all the clutter ridge in a given range interval are exact scaled versions of each other, the algorithm works well in certain, but not all bistatic cases.

2.7 Discussion on mitigating clutter Doppler range dependency in airborne bistatic radar

Among the six methods of mitigating the effect of clutter Doppler range dependency, methods that use reduced-dimension STAP, time-varying adaptive filter response and deterministically modifying data or filter notch to account for non-stationary behaviour are widely used in airborne bistatic radar system. Very often, several of these methods are used together, in order to achieve better clutter suppression performance.

MELVIN et al. [148] compared the performance of EFA and JDL algorithms and concluded that the 5×5 JDL algorithm provides the best blend of adaptive DOFs and minimal sample support requirement in the case studied. When investigating the time-varying weight method, modest tracking of bistatic clutter features at range gates where clutter characteristics slowly change was observed. As anticipated, the time-varying weight method appears to suffer in regions

where clutter properties vary most dramatically .

MELVIN et al. [67] evaluated the suitability of JDL, EFA and adaptive DPCA (ADPCA) [149] in bistatic environments. The reduced-dimension STAP investigated have shown greatly improved detection capability. Implementing the time-varying weight scheme with JDL, further improves the performance by up to 10 dB. This is possible as it takes advantage of the strengths of both methods.

HIMED [150] studied performance of using the FTS, JDL, EFA, parametric adaptive matched filter (PAMF)[151] and MSWF in a bistatic STAP processor. The MSWF, JDL and the PAMF are shown to be data efficient approaches due to their low secondary data size requirement in the vicinity of the range gate under test.

HIMED et al. [152] extended the Doppler warping and 2-D angle-Doppler compensation to the FTS, EFA, JDL, EC and the PAMF approaches. For both cases, the PAMF follows by the JDL provide superior performances when using ADC.

The clutter Doppler range dependency has been shown to vary with the angle of arrival. Performing Doppler frequency compensation in the angle-Doppler domain may therefore be required. Hence, a reduced-dimension clutter suppression processor, operating in the angle-Doppler domain appears to be a natural choice. Impressive performance of the angle-Doppler domain JDL processor (as shown by MELVIN et al. and HIMED et al.) resulted in the use of JDL as the reduced-dimension processor in this work.

2.8 Summary

In this chapter, the nature of the monostatic and bistatic clutter was investigated. Monostatic clutter echoes tends to be range dependent, although the range dependency is more obvious when using a forward looking than a sidelooking linear array antenna. The problem of range dependency appears to be more serious in an airborne bistatic radar system. Several bistatic radar configurations seem to experience more dramatic range dependency fluctuation than others.

Clutter Doppler range dependency has a significant effect on the performance of the STAP processor. Some form of Doppler compensation is desirable, although it requires extra computational cost. A derivative-based updating approach may face difficulty in coping with the

complex nature of the bistatic clutter. Until a better or more general affine transformation is proposed, the scaling method can only work well in some, but not all bistatic configurations. Doppler warping and ADC are the two proposed techniques for performing Doppler compensation.

The performance metrics used to evaluate the processor performance were also introduced. Towards the end of this chapter, the performance of clutter Doppler range dependency mitigation methods (for bistatic STAP), evaluated by MELVIN et al. and HIMED et al. are included. This set forms the base for the proposed Doppler compensation using interpolation for JDL processor, described in the next chapter.

Chapter 3
Doppler and Power compensation for JDL processor

3.1 Introduction

Doppler compensation has so far shown promising results in mitigating the impact of range dependent clutter/interference statistics. Doppler compensation designed for the joint domain localized (JDL) processor, using interpolation is now proposed. As the clutter power varies with range gates due to the distance travelled, transmitter and receiver antenna patterns, clutter power correction is also required. Doppler compensation methods that modify the data or filter notch deterministically need to know the clutter Doppler frequency difference between range gates (at the look angle). In this chapter, an algorithm that is robust to estimated parameter error is proposed, to determine this Doppler frequency differences. A tuned discrete Fourier transform (DFT) is also proposed to further reduce the size of the JDL processor.

3.2 Joint domain localized processor

The JDL algorithm was first introduced by Wang and Cai in [46]. It works by transforming the space-time signal vector into angle-Doppler domain using a two-dimension (2-D) DFT. The angle-Doppler data is then grouped into regions called the localised processing regions (LPR). Adaptive processing is restricted to the LPRs, as shown in Figure 3.1. Forming LPRs significantly reduces the number of unknowns while retaining maximal gain against thermal noise. The reduced number of degrees of freedom leads to a corresponding reduction in the required sample support and computational cost.

In practice, only a few angular bins covering the angle section centred around the look direction/angle, φ_r (where most of the transmitted energy is contained), are of interest. On the other hand, all Doppler bins must be analysed as the target Doppler frequency is unknown to the processor. The angle-Doppler domain training data, $\mathbf{Y}_{\mathrm{F}k}$, obtained by transforming space-time domain signal into angle-Doppler domain signal, are divided to form L sub-groups, $\mathbf{Y}_{\mathrm{L}l,k}$,

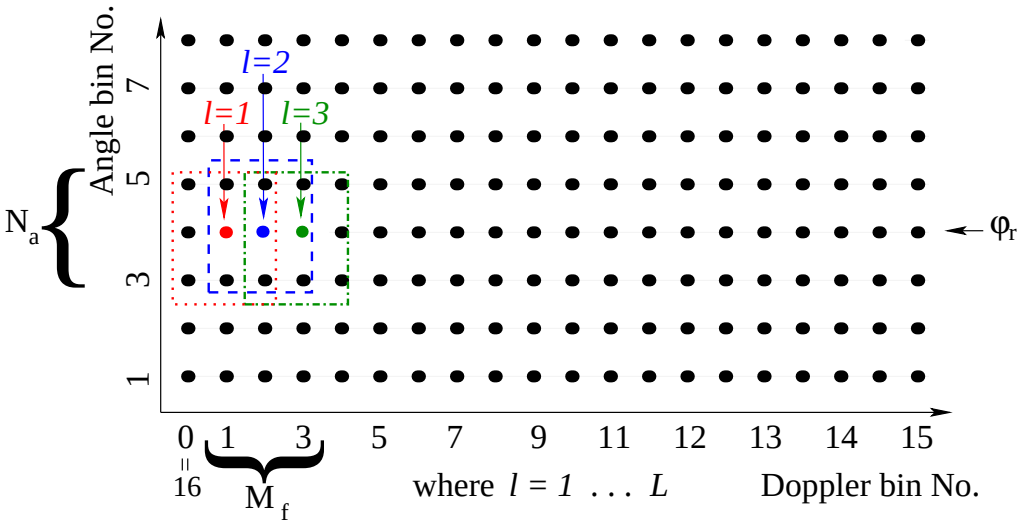

Figure 3.1: *An example of localised processing regions.*

centred around the look direction. Each LPR consists of N_a angular bins and M_f Doppler bins. The choice of N_a and M_f are not directly dependent on the system and environment parameters (e.g. large number of antenna array elements and pulses). The localisation of the target to a small number of angular - Doppler bins decouples the number of adaptive degrees of freedom necessary for handling clutter suppression from the size of the data matrix, $\mathbf{D}(g)$, defined by equation (2.11), while retaining maximal gain against thermal noise. This is however, achieved at the price of using a fast Fourier transform (FFT) (Chapter 10 of [153]) processor or a sliding DFT [154].

The indices k in the data matrix are taken out in order to simplify the expression. The divided $N_a \times M_f$ training data $\mathbf{Y}_{\mathrm{L}_l}$, and the clutter/interference sample covariance matrix, $\widehat{\mathbf{Q}}_{\mathrm{L}_l}$ with dimensions $(N_a M_f \times N_a M_f)$ (using only the range dimension snapshots), are given as

$$\mathbf{Y}_{\mathrm{L}_l} = \begin{pmatrix} y_{b,u_l}^{\mathrm{F}} & y_{b,u_l+1}^{\mathrm{F}} & \cdots & y_{b,u_l+M_f-1}^{\mathrm{F}} \\ y_{b+1,u_l}^{\mathrm{F}} & y_{b+1,u_l+1}^{\mathrm{F}} & \cdots & y_{b+1,u_l+M_f-1}^{\mathrm{F}} \\ \vdots & \vdots & \ddots & \vdots \\ y_{b+N_a-1,u_l}^{\mathrm{F}} & y_{b+N_a-1,u_l+1}^{\mathrm{F}} & \cdots & y_{b+N_a-1,u_l+M_f-1}^{\mathrm{F}} \end{pmatrix} \tag{3.1}$$

and

$$\widehat{\mathbf{Q}}_{\mathrm{L}l} = \frac{1}{K} \sum_{k=r-1-\frac{K+1}{2}}^{r+1+\frac{K+1}{2}} \mathrm{vec}(\mathbf{Y}_{\mathrm{L}l,k})\mathrm{vec}(\mathbf{Y}_{\mathrm{L}l,k})^H \quad \text{for } (k \neq r-1,\ r,\ r+1) \tag{3.2}$$

respectively. The scalar y_{F} in equation (3.1) is the element of the angle-Doppler domain training data given by

$$y_{\mathrm{F}a,f} = \sum_{i=0}^{N-1} \left[\sum_{m=0}^{M+Z-1} y_{\mathrm{P}}(i,m) e^{\frac{-j2\pi mf}{M+Z-1}} \right] e^{\frac{-j2\pi ia}{N}},$$
$$a = b, b+1, \ldots, b+N_a \qquad f = u_l, u_l+1, \ldots, u_l+M_f-1 \tag{3.3}$$

and

$$l = 1, \ldots, L \tag{3.4}$$
$$b = \text{look angular bin} - \mathrm{int}(\frac{N_a}{2}) \tag{3.5}$$
$$u_l = l - \mathrm{int}(\frac{M_f}{2}). \tag{3.6}$$

$\mathbf{Y}_{\mathrm{L}l}$ is a $(N_a \times M_f)$ matrix. The scalar K is the number of training data, the superscript H is the conjugate transpose operator and int() is the integer operation. Let the indices of y_{F} be a_l and f_l, where $a_l \in \{r \ldots r+N_a-1\}$ and $f_l \in \{u_l \ldots u_l+M_f-1\}$ respectively. If $l < \mathrm{int}(\frac{M_f}{2})$, f_l may be less than 1. As the Doppler bins repeat themselves every pulse repetition frequency (PRF), the value of $y_{\mathrm{F}a_l,f_l}$ when $f_l < 1$ is given as:

$$y_{\mathrm{F}a_l,f_l} = y_{\mathrm{F}a_l,D_f+f_l}, \tag{3.7}$$

with D_f as the size of the DFT process (transform of time domain to Doppler domain).

The testing data, $\mathbf{X}$ $(N \times M)$, must also be transformed into angle-Doppler domain, $\mathbf{X}_{\mathrm{F}}$ $(N \times M)$, and then divided into LPRs similar as that of the training data, $\mathbf{Y}_{\mathrm{L}l}$. Assuming that there are no targets present, the true clutter/interference sample covariance matrix of the range gate under test for each LPR is given as

$$\mathbf{Q}_{\mathrm{L}l} = \mathrm{E}[\mathrm{vec}(\mathbf{X}_{\mathrm{L}l})\mathrm{vec}(\mathbf{X}_{\mathrm{L}l})^H] \tag{3.8}$$

where $l = 1, \ldots, L$, $\mathbf{X}_{\mathrm{L}l}$ is the l^{th} LPR testing data. Figure 3.2 shows the forming of a

localised processing region.

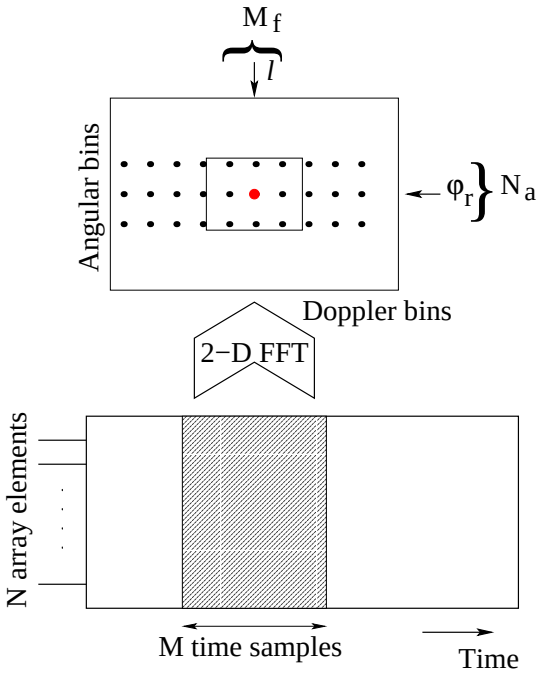

Figure 3.2: *Forming of a localised processing region.*

3.3 Clutter Doppler frequency difference between range gates

For any kind of Doppler compensation, the clutter Doppler frequency difference between range gate r and range gate k needs to be determined. The clutter Doppler frequencies from range gate k can be determined through calculation using estimated parameters, such as the velocity and position of both the transmitter and receiver, as well as the clutter angle of arrival, or from the received data. The disadvantage of just using a pre-calculated clutter Doppler frequency is the inability to adapt to the physical environment. Any errors in the estimation of the estimated parameter will not be detected and will affect the overall Doppler compensation performance. Estimating the clutter Doppler frequency from the received data (assuming that no target is present in that range gate) is hence preferred, although it represents an increase in real time computation cost. The minimum variance estimator (MVE)[i] is used for the mainlobe clutter Doppler frequency estimation, because of its high resolution spectrum. MVE tries to decompose a signal into single peaks. This leads to very realistic spectra without sidelobes. The

[i] Also referred to as "maximum-likelihood" estimator [155, 156].

sidelobes of the transmitter and receiver beam can be noticed as clusters of peaks.

Unfortunately, the clutter Doppler frequency from range gate r cannot be estimated using the received data due to the fact that the target signal may also be present. Therefore, it can only be estimated by using estimated parameters.

Modifying equation (2.37) to take into account of any change in the physical environment, the difference in clutter Doppler frequency at a particular angle of arrival/look angle between range gate under test r and training range gate k is

$$f_s(r,k) = \tilde{f}_k^d - f_r^d \tag{3.9}$$

where $\tilde{f}_k^d$ is the estimated clutter Doppler frequency from the received data obtained from range gate k using MVE, and f_r^d is the calculated clutter Doppler frequency from range gate r using estimated parameters, which is given as:

$$f_r^d = \frac{v_T \cos(\varphi_{t,r} - \delta_t)\cos\theta_{t,r} + v_R \cos(\varphi_r - \delta_r)\cos\theta_{r,r}}{\lambda}, \tag{3.10}$$

where $\varphi_{t,r}$ and $\theta_{t,r}$ are the transmit azimuth and depression angles from range gate r respectively. The clutter azimuth angle of arrival is given by φ_r and $\theta_{r,r}$ is the depression angle of arrival from range gate r. The scalars δ_t and δ_r denote the flight directions of the transmitter and receiver respectively

Alternatively, the Doppler frequency difference, also known as Doppler frequency shift, can be obtained (see Appendix D) using

$$\Delta_f = \tilde{f}_k^d \left(1 - \frac{f_r^d}{f_k^d}\right) \tag{3.11}$$

where f_k^d is the calculated clutter Doppler frequency from range gate k using estimated parameters and is given as:

$$f_k^d = \frac{v_T \cos(\varphi_{t,k} - \delta_t)\cos\theta_{t,k} + v_R \cos(\varphi_r - \delta_r)\cos\theta_{r,k}}{\lambda}. \tag{3.12}$$

The scalars $\varphi_{t,k}$ and $\theta_{t,k}$ are the transmit azimuth and depression angles from range gate k respectively. The depression angles of arrival from range gates k is given as $\theta_{r,k}$.

Substituting equations (3.10) and (3.12) into equation (3.11) and simplifying it,

$$\Delta_f = \tilde{f}_k^d \left(1 - \frac{v_T \cos(\varphi_{t,r} - \delta_t) \cos\theta_{t,r} + v_R \cos(\varphi_r - \delta_r) \cos\theta_{r,r}}{v_T \cos(\varphi_{t,k} - \delta_t) \cos\theta_{t,k} + v_R \cos(\varphi_r - \delta_r) \cos\theta_{r,k}} \right) \tag{3.13}$$

It can be shown that using equation (3.11), instead of equation (3.9), a better Doppler shift estimation is obtained when there is any error in the estimated parameters. Assuming that the only error in the estimated parameters is the transmitter velocity, the change in $f_s(r,k)$, $|\Delta E_{f_s(r,k)}|$, and the change in Δ_f, $|\Delta E_{\Delta_f}|$, due to error in v_T, Δv_T are given as:

$$|\Delta E_{f_s(r,k)}| = | - \frac{C_{Tr}}{\lambda}| \cdot |\Delta v_T|. \tag{3.14}$$

and

$$|\Delta E_{\Delta_f}| = | - \tilde{f}_k^d \left(\frac{C_{Tr}(v_T C_{Tk} + C_{Rk}) - C_{Tk}(v_T C_{Tr} + C_{Rr})}{(v_T C_{Tk} + C_{Rk})^2} \right) | \cdot |\Delta v_T| \tag{3.15}$$

respectively (see Appendix E for the derivation). The scalars C_{Tr}, C_{Rr}, C_{Tk} and C_{Rk} are given as:

$$C_{Tr} = \cos(\varphi_{t,r} - \delta_t) \cos\theta_{t,r} \tag{3.16}$$

$$C_{Rr} = v_R \cos(\varphi_r - \delta_r) \cos\theta_{r,r} \tag{3.17}$$

$$C_{Tk} = \cos(\varphi_{t,k} - \delta_t) \cos\theta_{t,k} \tag{3.18}$$

$$C_{Rk} = v_R \cos(\varphi_r - \delta_r) \cos\theta_{r,k} \tag{3.19}$$

Figure 3.3 shows the change in $f_s(r,k)$ and Δ_f due to error in the transmitter velocity. An error in the transmitter velocity hardly affects the Doppler frequency shift estimation when using equation (3.11). On the other hand, Doppler frequency shift estimation error is about 670 Hz (at the limit of the transmitter velocity error simulated) is observed, when using equation (3.9).

The azimuth and depression angles in equation (3.13) can be expressed, with the clutter P coordinates x_p, y_p (determined by φ_r and the range gate under test) and slant range R_{sT}, R_{sR},

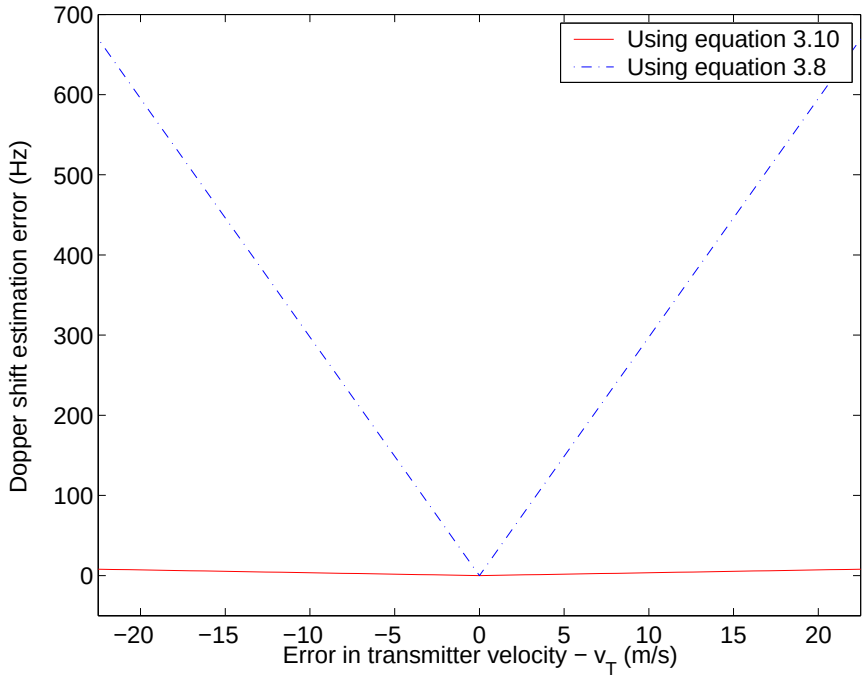

Figure 3.3: *Error in estimation of Doppler frequency difference between range gates k and r, due to error in transmitter velocity.*

using equations (3.20)-(3.27).

$$\Delta_f = \tilde{f}_k^d \left(1 - \frac{v_T(\frac{x_{TP}(r)}{R_{sT}(r)}\cos(\delta_t) + \frac{y_P(r)}{R_{sT}(r)}\sin(\delta_t)) + v_R(\frac{x_{RP}(r)}{R_{sR}(r)}\cos(\delta_r) + \frac{y_P(r)}{R_{sR}(r)}\sin(\delta_r))}{v_T(\frac{x_{TP}(k)}{R_{sT}(k)}\cos(\delta_t) + \frac{y_P(k)}{R_{sT}(k)}\sin(\delta_t)) + v_R(\frac{x_{RP}(k)}{R_{sR}(k)}\cos(\delta_r) + \frac{y_P(k)}{R_{sR}(k)}\sin(\delta_r))} \right) \tag{3.20}$$

where

$$x_{TP}(g) = x_P(g) - \frac{L}{2} - x_T \qquad g \in \{r, k\} \tag{3.21}$$

$$y_P(g) = x_{RP}{}^{\text{ii}}(g)\tan(\varphi_r) \tag{3.22}$$

$$x_{RP}(g) = x_P(g) - \frac{L}{2} - x_R \tag{3.23}$$

$$L = \sqrt{(x_T - x_R)^2 + (y_T - y_R)^2 + (z_T - z_R)^2} \tag{3.24}$$

$$x_P(g) = \frac{1}{2}\left(\frac{4\frac{tan(\varphi_r)^2 L}{d(g)^2-L^2}}{(4\frac{1}{d(g)^2}+4\frac{\tan(\varphi_r)^2}{d(g)^2-L^2})} \pm \frac{4\frac{\sqrt{-2dtanL^2-4d(g)^2H_R^2+d(g)^4-2d(g)^2L^2+L^4\tan(\varphi_r)^2+4L^2H_R^2+L^4-4dtan\,H_R^2+dtan\,d(g)^2)}}{d(g)(-d(g)^2+L^2)}}{(\frac{4}{d(g)^2}+4\frac{\tan(\varphi_r)^2}{d(g)^2-L^2})}\right) \quad (3.25)$$

$$dtan = d(g)^2\tan(\varphi_r)^2 \quad (3.26)$$

$$d(g) = c\,Time(g) \quad (3.27)$$

The function $Time(g)$ is the time taken for the signal to hit the ground in range gate g and back to the receiver. The derivation of equation (3.25) is shown in Appendix F. The symbol $\pm$ in equation (3.25) represents an addition operation for $-\frac{\pi}{2} \leq \varphi_r \leq \frac{\pi}{2}$ and a subtraction operation for $\frac{\pi}{2} < \varphi_r < \frac{3\pi}{2}$.

3.4 Interpolation of Doppler domain data and Doppler bins shifting

Doppler compensation in the space-time domain is obtained using the transformation matrix $\mathbf{T}_{dw}$ or $\mathbf{T}_{2D}$ as described in Sections 2.6.6 and 2.6.7 respectively. However, Doppler compensation can also be achieved by performing interpolation of data in the angle-Doppler domain and applying Doppler bin shifting (re-addressing of Doppler bins). There are some advantages for using the latter compensation technique. When a JDL processor is used as the base of the clutter suppression filter, a 2-D discrete Fourier transformation is required to transform the training data from the space-time domain into the angle-Doppler domain. Performing Doppler compensation in the space-time domain requires Fourier transformations of the Doppler compensated training data to be carried out for every training range gate. The whole process is repeated for every range gate under test. On the other hand, Fourier transformations of the training data are required only once for all range gates under test, when using Doppler interpolation and bins shifting. Doppler compensation in angle-Doppler domain also allows multiple Doppler bin compensation as explained in Section 3.8 and possibly multiple angular bin compensation as explained in Section 5.2.

Performing the Doppler interpolation and bin shifting processes, the training data, $\mathbf{Y}_k$ (equation

[ii] assuming that transmitter and receiver are aligned

(2.19)), in the space-time domain, is first padded with zero padding to the temporal samples. The zeroes padded training data matrix, $\mathbf{Y}_{\mathrm{P}_k}$, is then transformed to the angle-Doppler domain by applying DFT in both time and space domains (from equation 3.3)

$$y_{\mathrm{F}_{a,f}} = \sum_{i=0}^{N-1} \left[\sum_{m=0}^{M+Z-1} y_{\mathrm{P}}(i,m) e^{\frac{-j2\pi mf}{M+Z-1}} \right] e^{\frac{-j2\pi ia}{N}},$$
$$a = b, b+1, \ldots, b+N_a \qquad f = u_l, u_l+1, \ldots, u_l+M_f-1 \tag{3.28}$$

where $N_a = N$, $M_f = M + Z$, a and f are indices of the matrix $\mathbf{Y}_{\mathrm{F}_k}$, while Z is the number of zero padding added to the temporal samples. The emphasis of this work is on the Doppler compensation in the Doppler domain at the main spatial bin, corresponding to the mainbeam centre, therefore spatial zero padding is not used. The Doppler domain DFT size, D_f, is $Z+M$, while the spatial domain DFT size is still determined by the number of array elements N. The angle-Doppler domain training data matrix, $\mathbf{Y}_{\mathrm{F}_k}$, with dimension ($N_a \times M_f$), represents the data at the M_f Doppler bins, N_a angular bins and k the snapshot number.

Next, Doppler bin data interpolation is performed, followed by Doppler bins shifting, carried out by re-addressing the Doppler bins indexes. Interpolation of data allows signal components at Doppler frequencies which lie between the Doppler bins to be determined and by using interpolation, such as the cubic spline interpolation [157], a smooth fit between Doppler bins is achieved. An illustration of the shifting process at one of the angular bins is given in Figure 3.4.

Let the Doppler frequency f_{new} be the frequency of interest, and its signal component be $y_{\mathrm{F}_{new}}$. The steps to determine $y_{\mathrm{F}_{new}}$ is given as follows:

1) The corresponding Doppler frequency from the old data, f_{old} is defined as:

$$f_{old} = f_{new} + \Delta_f \tag{3.29}$$

2) Given the signal components at Doppler frequencies around f_{old}, the signal component $y_{\mathrm{F}_{old}}$ at f_{old}, could be found using cubic spline interpolation.

3) The shifting process of Doppler frequency f_{new} is completed by assigning $y_{\mathrm{F}_{new}} = y_{\mathrm{F}_{old}}$.

The process of frequency shifting of the training data with cubic spline interpolation across each angular bin (N_a) is carried out as explained next. For simplicity, the indices (a and k) for

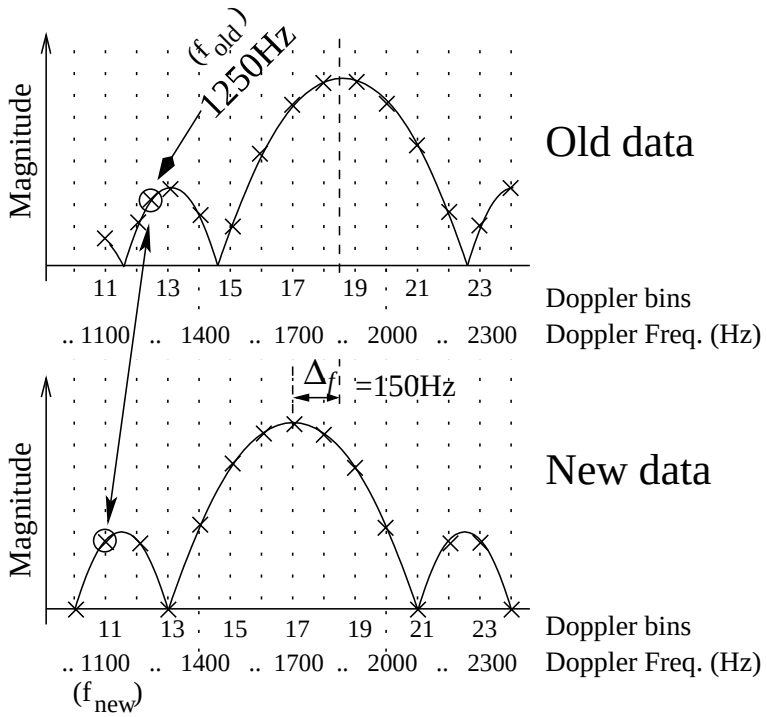

Figure 3.4: *Illustration of frequency shifting at one of the angular bins.*

$\mathbf{y}_{\mathrm{F}}$ will be dropped, i.e

$$\mathbf{y}_{\mathrm{F}f} = \mathbf{y}_{\mathrm{F}a,k,f} \tag{3.30}$$

where $\mathbf{y}_{\mathrm{F}}$ is a row vector from matrix $\mathbf{Y}_{\mathrm{F}}$, with a dimension of $1 \times M_f$. The scalar $y_{\mathrm{F}old}$ is given as

$$y_{\mathrm{F}old}(i) = A_i y_{\mathrm{F}j} + B_i y_{\mathrm{F}j} + C_i y_{\mathrm{F}j}^{''} + D_i y_{\mathrm{F}j}^{''} \tag{3.31}$$

where

$$A_i = \frac{f_{old,j+1} - f_{new,i}}{f_{old,j+1} - f_{old,j}} \tag{3.32}$$

$$B_i = 1 - A_i = \frac{f_{new,i} - f_{old,j}}{f_{old,j+1} - f_{old,j}} \tag{3.33}$$

$$C_i = \frac{1}{6}(A_i^3 - A_i)(f_{old,j+1} - f_{old,j})^2 \tag{3.34}$$

$$D_i = \frac{1}{6}(B_i^3 - B_i)(f_{old,j+1} - f_{old,j})^2 \tag{3.35}$$

and $y_{\mathrm{F}_j}^{''(k)}$ is obtained by solving the equation below using back substitution

$$\frac{f_{old,j} - f_{old,j-1}}{6} y_{\mathrm{F}_{j-1}}^{''} + \frac{f_{old,j+1} - f_{old,j-1}}{3} y_{\mathrm{F}_j}^{''} + \frac{f_{old,j+1} - f_{old,j}}{6} y_{\mathrm{F}_{j+1}}^{''}$$
$$= \frac{y_{\mathrm{F}_{j+1}} - y_{\mathrm{F}_j}}{f_{old,j+1} - f_{old,j}} - \frac{y_{\mathrm{F}_j} - y_{\mathrm{F}_{j-1}}}{f_{old,j} - f_{old,j-1}} \qquad \text{for } (j=2, \ldots, M_f - 1) \tag{3.36}$$

with

$$\mathbf{f}_{old} = \frac{i}{PRI \times M_f} \qquad \text{for } i = 1 \text{ to } M_f \tag{3.37}$$
$$\mathbf{f}_{new} = \mathbf{f}_{old} + \Delta_f \tag{3.38}$$
$$f_{old,j} < f_{new,i} \text{ [iii]} < f_{old,j+1} \tag{3.39}$$

The scalar PRI is the pulse repetition interval. There are M_f-2 linear equations in M_f unknowns, $y_{\mathrm{F}_i}^{''}$, i = 1, . . . , M_f. Two more equations are required. The 'not-a-knot' end condition is used, where the second and second-last points is ignored [157]. Interpolation processes using the cubic spline can be considered computationally intensive, therefore, there are other simpler intensive interpolation methods that can be used, if it does not result in significant loss in processor performance. Examples of other interpolation methods are: linear interpolation, cubic interpolation and sinc interpolation [158, 159].

3.5 Power correction

For any radar system, the power of the clutter/interference differs from range gate to range gate due to the difference in distance travelled. However for an airborne bistatic radar, the situation becomes more complicated. The clutter/interference power also changes with direction of arrival in each range gate [160].

According to the radar range equation (see pages 2.4 - 2.15 in [161]), the power of the clutter/interference arriving at the range gate under test (range gate r), is estimated by multiplying the power of the clutter/interference arriving from training range gate k, $\widehat{P_{cl_k}}$, with the power

[iii] at the boundary, this condition might not be met (for all i values)

correction, P_c, defined as

$$\begin{aligned} P_c &= \frac{P_{cl_r}}{P_{cl_k}} \\ &= \frac{\frac{P_t G(\varphi_{t,r},\theta_{t,r}) D(\varphi_{r,r},\theta_{r,r}) L(\varphi_{r,r},\theta_{r,r})}{(4\pi)^3 k T_s B_n R_{sT,r}^2 R_{sR,r}^2}}{\frac{P_t G(\varphi_{t,k},\theta_{t,k}) D(\varphi_{r,k},\theta_{r,k}) L(\varphi_{r,k},\theta_{r,k})}{(4\pi)^3 k T_s B_n R_{sT,k}^2 R_{sR,k}^2}} \end{aligned} \tag{3.40}$$

where P_{cl_r} and P_{cl_k} are the clutter echoes power received from range gates r and k respectively. P_t stands for transmitted power, $G(.)$ for the transmit directivity pattern, $D(.)$ as the sensors directivity patterns, $L(.)$ represents the reflectivity of the ground, kT_sB_n is the thermal-noise power and $R_{sT,k}$, $R_{sR,k}$, $R_{sT,r}$ and $R_{sR,r}$ are slant distance between transmitter (T) / receiver (R) and the ground from range gate k / r respectively.

Assuming that the sensors' directivity pattern and the reflectivity of the ground do not change significantly with a small change in the range gate number and $G(\varphi_{t,r},\theta_{t,r})$ = 1 (since the mainlobe is pointing at that azimuth and depression angles), the power compensation becomes

$$\begin{aligned} P_c &= \frac{\frac{1}{R_{sT,r}^2 R_{sR,r}^2}}{\frac{G(\varphi_{t,k},\theta_{t,k})}{R_{sT,k}^2 R_{sR,k}^2}} \\ &= \frac{R_{sT,k}^2 R_{sR,k}^2}{G(\varphi_{t,k},\theta_{t,k}) R_{sT,r}^2 R_{sR,r}^2}. \end{aligned} \tag{3.41}$$

Finally, an overall view of the joint Doppler and power correction for JDL processor for a single range gate under test in shown in Figure 3.5. In practice, training data from several range gates are used to form the clutter sample covariance matrix. For the rest of this thesis, the joint Doppler interpolation and power correction for JDL processor will be known as the Doppler interpolation processor.

3.6 Simulation Results

The radar parameters shown in Table 2.1 are given for the case of a pulsed Doppler airborne bistatic radar. As defined in Chapter 2, the performance matrices like the improvement factor (IF), IF loss and averaged IF loss, are used whenever appropriate. Unless otherwise stated, simulation results related to the JDL processor in this and next chapter are performed with M_f (Doppler bins used) = 9, N_a (angular bins used) = 3, K (sample support size) = 384 when using

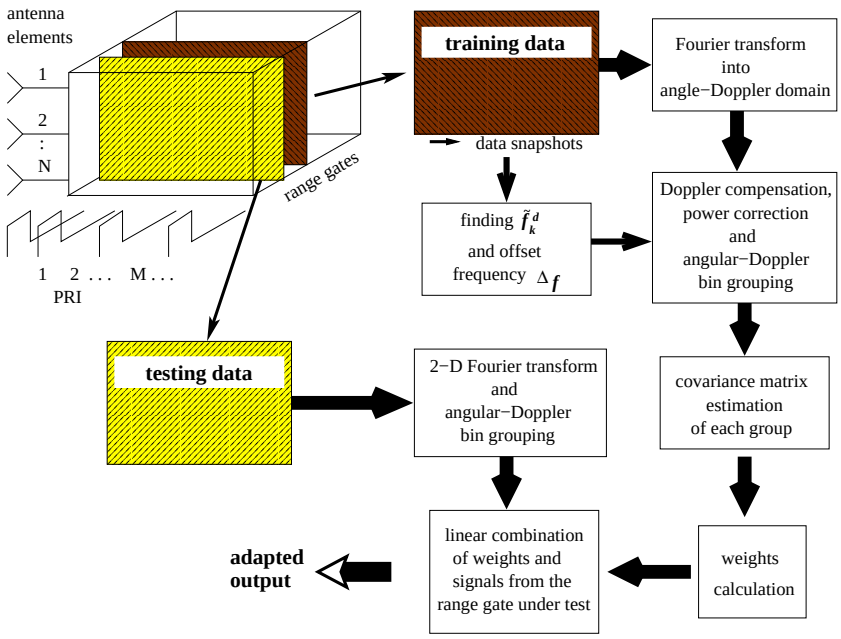

Figure 3.5: *Block diagram of Doppler and power correction for JDL processor.*

one training range gate; K = 768 when using both training range gates 25 & 29, D_f (DFT size) = 128 and the load-clutter to white noise ratio (LCNR) discussed in Section 4.7 = -30 dB. The snapshots used are obtained in both range and time dimension.

Figure 3.6(a) plots improvement factor vs Doppler frequency for the Doppler interpolation processor. The red curve shows the ideal JDL processor performance (assuming knowledge of the true clutter sample covariance matrix), while the blue and green curves show the Doppler interpolation processor performance with and without Doppler interpolation respectively.

The JDL processor, without Doppler interpolation, experienced a drop in improvement factor of about 3 dB in most regions, and up to about 32 dB in the clutter notch region (also shown in Fig. 3.6(b) - which shows the IF loss of the Doppler interpolation processors with (represented by the blue curve) and without (represented by the red curve) Doppler interpolation). A drop of 3 dB in the improvement factor is caused the reduction of Doppler bins used, as explained in Section 4.2, while the IF loss in the clutter notch region is the result of inaccurate estimation of the clutter sample covariance matrix. The degradation in the clutter notch region will cause a slow relative velocity target signal to be attenuated. However, with the proposed Doppler interpolation processor, the biggest IF loss is reduced to less than 10 dB, as shown by the blue curve in Fig. 3.6(b).

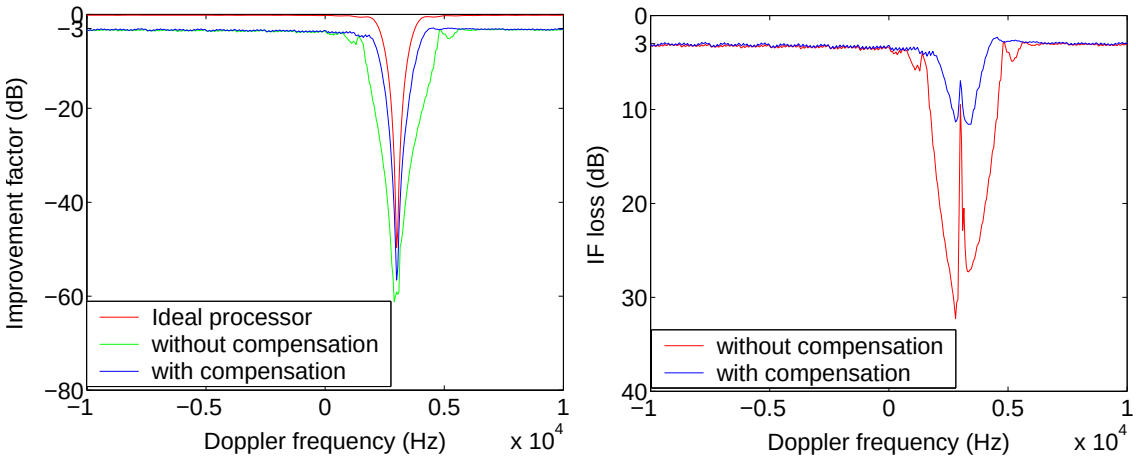

Figure 3.6: *JDL processor performance (a) with improvement factor (b) Improvement factor loss.*

3.6.1 Power correction

Figure 3.7 shows the Doppler interpolation processor performance with and without power correction. The blue and red curves show the processor performance with and without power correction respectively. Figure 3.7(a) and Figure 3.7(b) use training data from range gate 29 and range gate 25 respectively, while Figure 3.7(c) uses training data from both range gates 29 & 25. In Figure 3.7(a), using power correction reduces the IF loss by average of about 1 dB. On the other hand, Figure 3.7(b) shows that power correction does not result in any performance improvement. This is due to the close proximity of the training range gate and the target range gate, as there is not significant power difference between them. Similar performance is obtained when using both training range gates as shown in Figure 3.7(c).

The performance of the proposed Doppler interpolation processor depends on a number of parameters which will be analysed in the next chapter. In the next section, the performance of the Doppler interpolation processor will be compared with Doppler warping compensation and angle-Doppler compensation (ADC).

3.7 Comparison with other compensation methods

When comparing the proposed Doppler interpolation processor with other compensation methods, it is important to compare them on the same baseline. As the proposed compensations are based on JDL which is a reduced dimension processor, we could either apply other compensa-

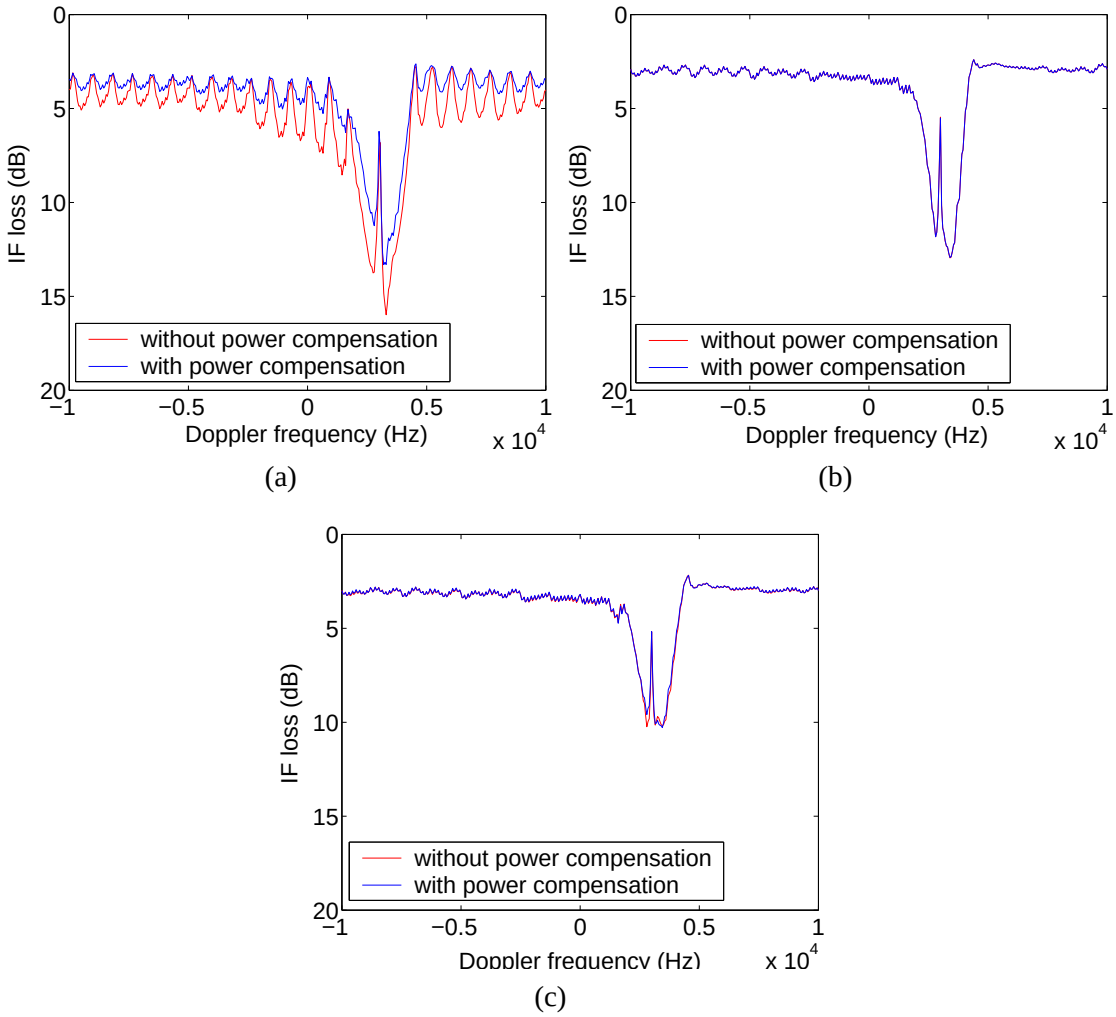

Figure 3.7: *Doppler interpolation processor performance with and without power correction, using (a) training data from range gate 29, (b) training data from range gate 25, and (c) training data from range gates 25 & 29.*

tion methods to JDL processor or uses a full dimension JDL processor. Among all compensation methods mentioned in Chapter 2, Doppler warping and two-dimensional ADC have so far shown the most promising performance, and will be used as performance references.

3.7.1 Doppler warping

Doppler compensation using interpolation is quite similar to Doppler warping, as both shift the Doppler frequency of the clutter return. The difference between the two methods are: Doppler interpolation compensation is performed in the angle-Doppler domain, while Doppler warping is carried out in the space-time domain; Doppler warping is an exact frequency shift, while

Doppler interpolation compensation is an approximation of the frequency shift. As the discrete Fourier transformation is a linear transform, performing compensation in the angle-Doppler domain should ideally produce a similar performance as the space-time domain (assuming that the approximation error is negligible). However, in certain situations, the approximation error is significant enough to cause a difference between the two compensation methods.

Figure 3.8, shows the IF loss of JDL processors using the two methods discussed. The red curve shows the Doppler interpolation processor performance, while the blue curve shows JDL processor performance using Doppler warping. Figure 3.8(a) and (b) show the use of training data from range gate 29 and from range gate 25 respectively. Figure 3.8(c) shows the processors' performance when using training data from both range gates 29 & 25. In Figure 3.8(a), we can see that the Doppler interpolation processor has lower IF loss than the JDL Doppler warping processor across the frequency range outside the clutter notch region. For Figure 3.8(b), the JDL Doppler warping processor has lower IF loss than interpolation, but only in the clutter notch region. Similar performance is observed in other regions of the graph. When using training data from both range gates 29 & 25, as shown in Figure 3.8(c), both methods show improvement when using both training range gates. However, the JDL Doppler warping processor still shows better performance in the clutter notch region.

The reason why both methods behave differently to different training data is still not well understood. More investigation is required to have a better insight of what is happening in this situation. A possible answer however, may lie in the statistics of the training data. This is an area of possible further work as indicted in the conclusion section.

Figure 3.9 shows the comparison of a full dimension Doppler interpolation processor (M_f = 128) and a space-time Doppler warping adaptive processor. The red curve shows JDL processor performance using Doppler interpolation and the blue curve shows space-time adaptive processor (STAP) performance using Doppler warping compensation. Figure 3.9(a) and (b) show the use of training data from range gate 29 and from range gate 25 respectively. Figure 3.9(c) shows the case using training data from both range gates 29 & 25. In practice, a full dimension Doppler interpolation processor would not be used at all, as the JDL processor is designed as a reduced dimension processor. However, in order to compare using Doppler warping compensation for the STAP processor with Doppler interpolation processor, a full dimension Doppler interpolation processor is required.

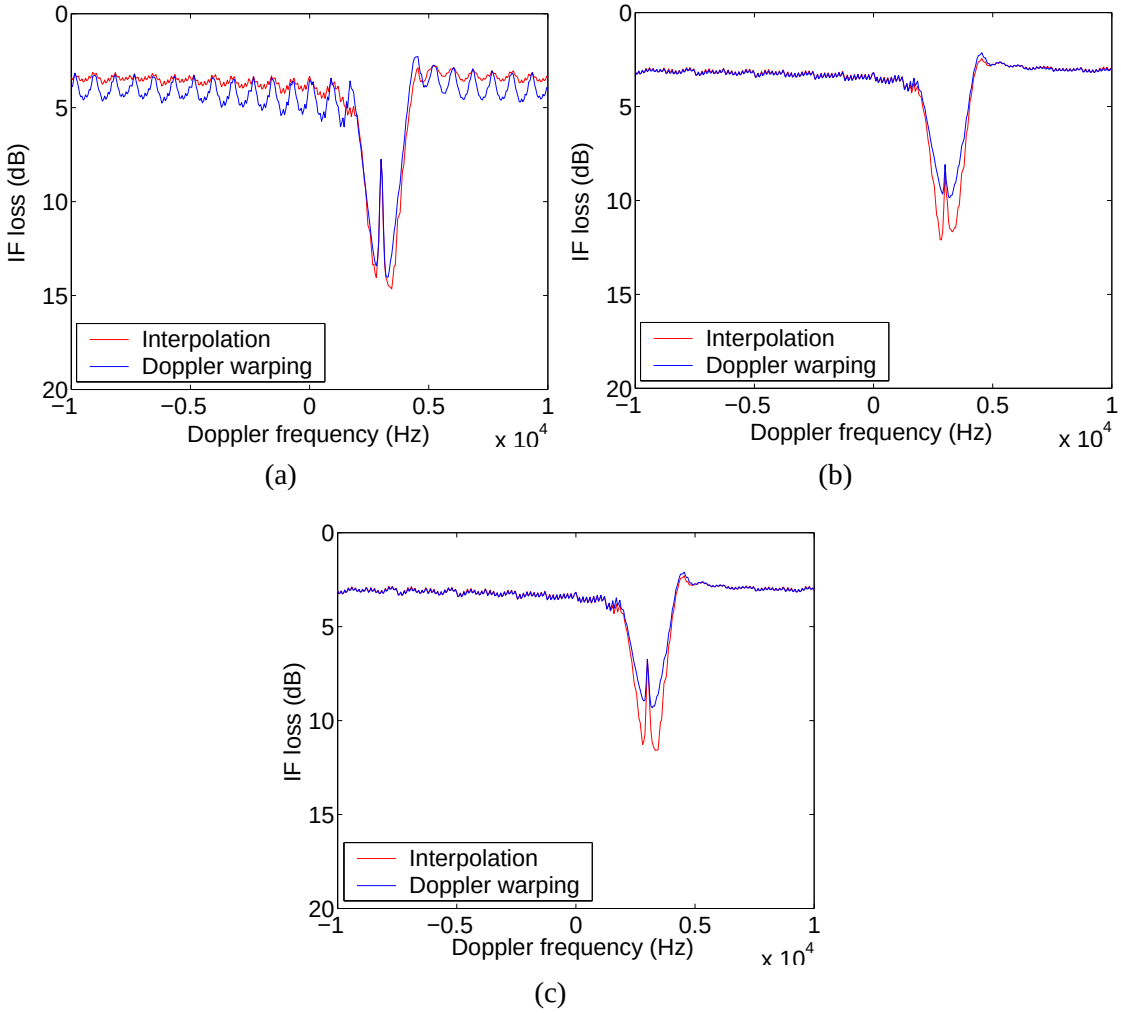

Figure 3.8: *Doppler interpolation and JDL Doppler warping processors' performance, using training data from (a) range gate 29, (b) range gate 25, and (c) range gates 25 & 29.*

The performance of full dimension processors will be better than any reduced dimension processor, but at the price of much higher computational cost. It can be seen from Figure 3.9(a) that the Doppler interpolation processor using training data from range gate 29 produced a similar shape clutter notch as Doppler warping. On the other hand, when using training data from range gate 25 (Figure 3.9(b)), the clutter notch of Doppler interpolation processor has a wider clutter notch than STAP with Doppler warping compensation. The IF loss of the Doppler interpolation processor reduces when both range gates are used (as shown in Figure 3.9(c)). This shows that, the Doppler interpolation processor is only suitable to be used as a reduced dimension processor.

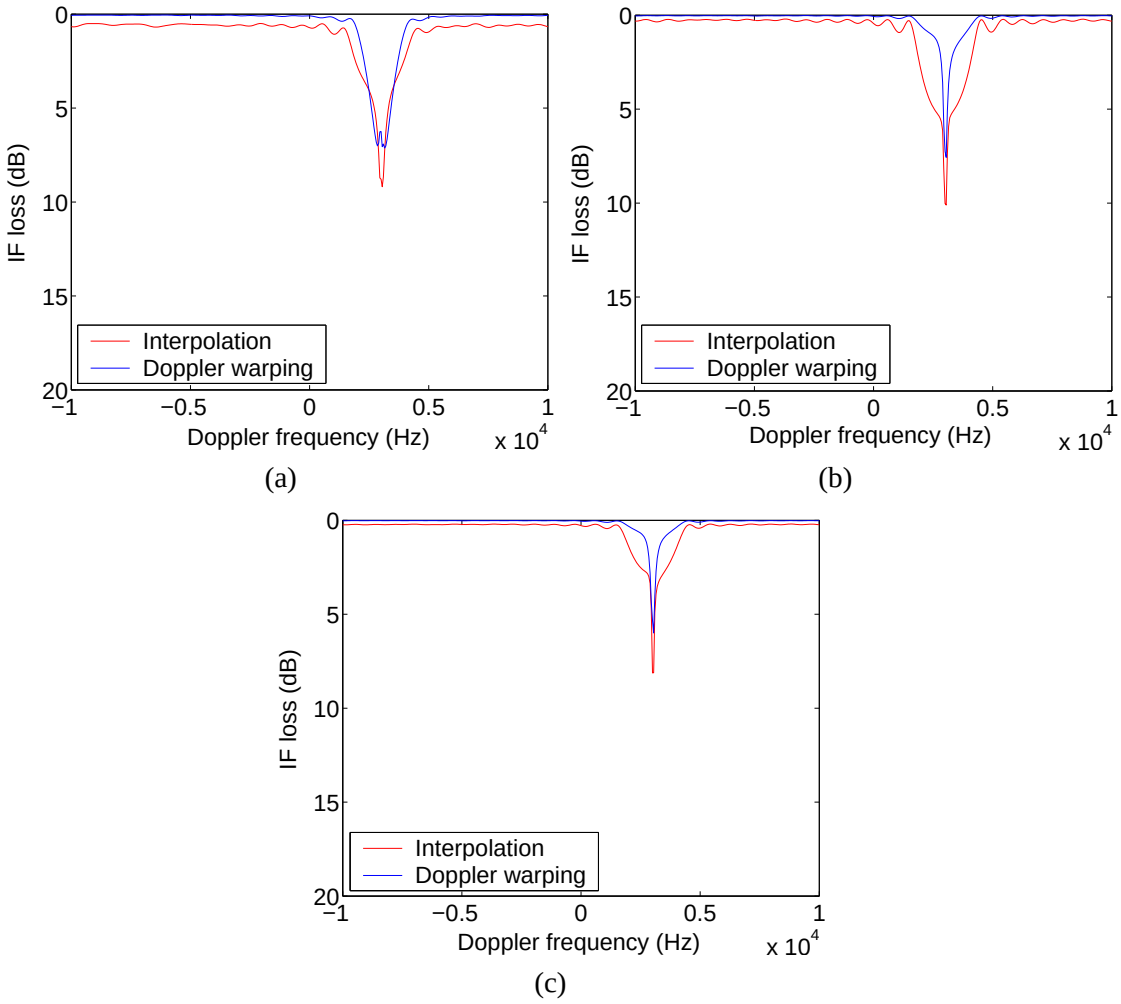

Figure 3.9: *Full dimension Doppler interpolation processor performance and STAP processor performance with Doppler warping compensation, using training data from (a) range gate 29, (b) range gate 25, and (c) range gates 25 & 29.*

3.7.2 Two-dimensional angle-Doppler compensation (ADC)

Angle and Doppler compensations in the ADC co-locates the clutter spectral centres from different range gates. For our simulation, with training data from range gates 29 and 25, the azimuth and depression angles differ from the range gate under test (range gate 27) by -0.8°, -2.6° (azimuth angle) and 3.8°, 2.9° (depression angle) respectively. The angles difference between the range gates are considered to be not significant. Figure 3.10 shows the comparison between Doppler interpolation, Doppler warping and ADC applied to JDL processor. Once again, cases (a), (b) and (c) show the use of different training data. Figure 3.10 is similar to Figure 3.8 except with the addition of the curve labelled “ADC”, which shows the performance

of using the ADC.

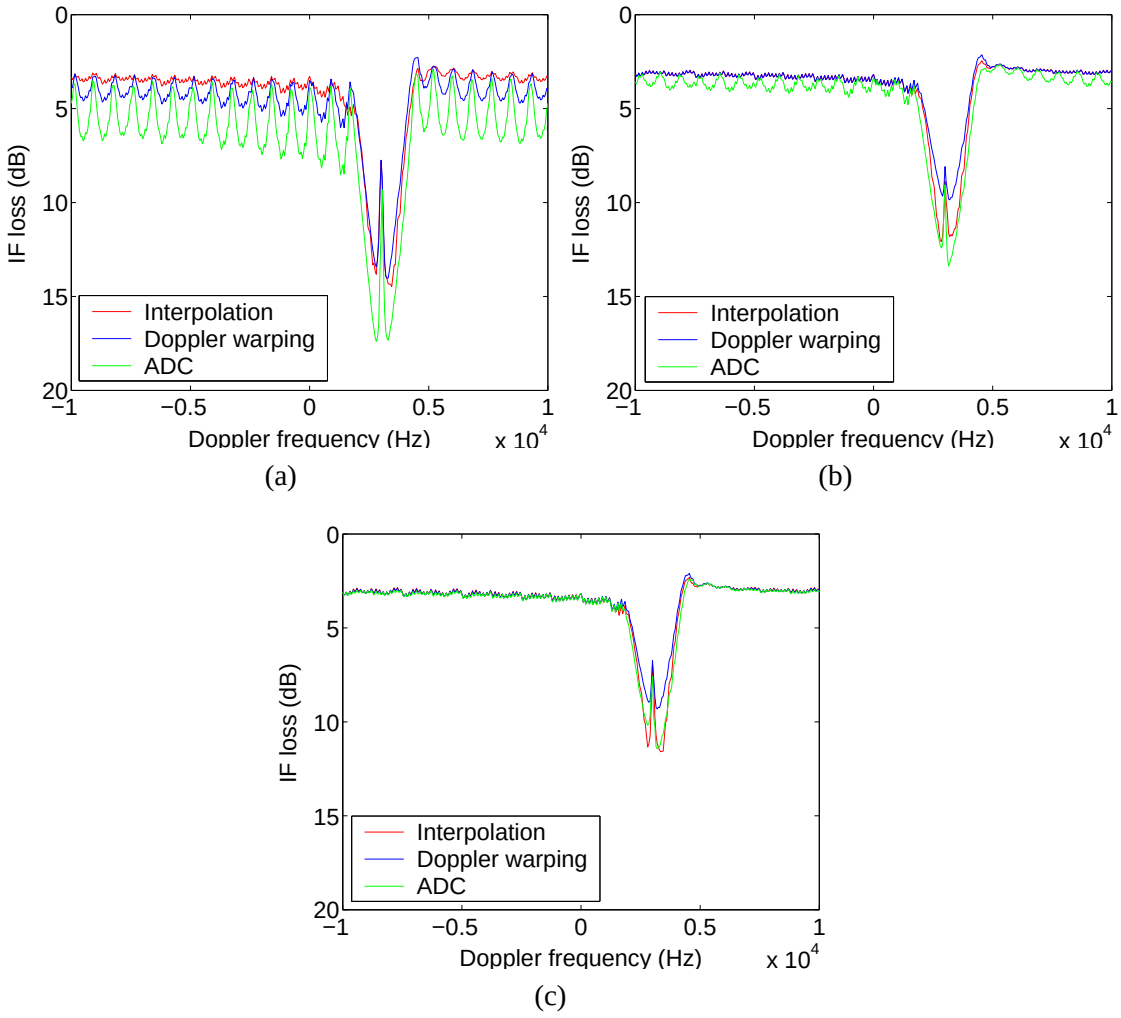

Figure 3.10: *Comparison between JDL processor performance with Doppler interpolation, Doppler warping and ADC, using training data from (a) range gate 29, (b) range gate 25, and (c) range gates 25 & 29.*

From Figure 3.10(a), when using training data from range gate 29, the ADC processor has the worst performance among the three compensation methods. On the other hand, the Doppler interpolation processor offers the lowest IF loss. When using training data from range gate 25 (Figure 3.10 (b)), using the ADC does not offer the same performance as using the Doppler warping compensation method. However, significant improvement is observed for the ADC processor using training data from range gate 29. Similar performance among the three different compensation methods, for regions other than clutter notch region, is observed when both range gates 29 and 25 are used. In the case of the ADC processor having a poorer performance than

the Doppler warping processor, this is due to the close proximity of the range gate under test and the training range gates. The benefit of using ADC over Doppler warping can be observed when the clutter spectral centres from the training range gates are not in the mainbeam [1, 53].

3.7.3 Processor performance at different look angles

As discussed in Section 2.3.3 and illustrated in Figure 2.15, the clutter Doppler range dependency changes with the look angle, φ_r. At certain φ_r angles, the corresponding clutter Doppler frequency varies significantly with range gate, while at some other φ_r angles, the corresponding clutter Doppler frequency remains almost constant across range gates. A clear example of this situation where there is almost no Doppler frequency difference (between range gates 27 and 29), is when φ_r = -33.48°.

For clutter echoes arriving from angles near φ_r, its Doppler frequencies will still be to a certain extent range dependent. Depending on the beamwidth and mainlobe to sidelobe ratio, these clutter echoes may be of a comparable strength to the clutter echo arriving from φ_r. For the particular bistatic configuration considered in Table 2.1, at φ_r = -33.48°, there is no significant Doppler difference between the training range gates 29 & 25 and the range gate under test, range gate 27, $\Delta_f \approx 0$ Hz (see Figure 2.15). In such a situation, all current Doppler compensation processors would not attempt to carry out any Doppler compensation process[iv]. By doing so, those range dependent clutter echoes arriving from angles near the look angle φ_r would not be compensated properly. This will have a significant effect on the processor performance.

Figure 3.11 shows the JDL processor performance using both the training range gates 25 & 29, where φ_r = -33.48°. Figure 3.11(a) and Figure 3.11(b) show the use of a narrow beam with beamwidth = 4° and a widebeam with beamwidth = 16° respectively. The red curve labelled "Ideal JDL processor" assumes that the JDL processor processes the true clutter sample covariance matrix. This serves as the performance upper bound when perfect Doppler compensation is achieved. The blue curve labelled "uncompensated" shows the JDL processor performance when no Doppler compensation is carried out. The green curve labelled "Doppler interpolation" and black dashed curve labelled "Doppler warping" show the performance of the Doppler interpolation processor and JDL Doppler warping processor respectively.

From Figure 3.11(a), it can be observed that none of the Doppler compensation methods provide

[iv] ADC may still carry out angle compensation.

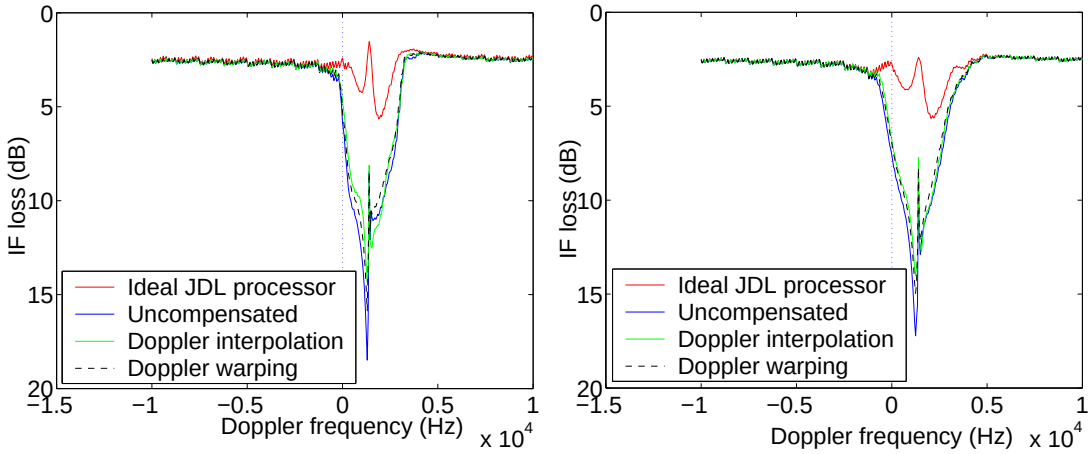

Figure 3.11: *JDL processor performance with φ_r = -33.48°, using (a) Narrow beam - 4° (b) Widebeam - 16°.*

any significant performance gain. These results are not surprising as the clutter Doppler frequency difference between the training range gates and the range gate under test, at φ_r = -33.48° is about 0 Hz. With a Doppler compensation of 0 Hz, those range dependent clutter echoes will not experience any Doppler compensation, hence no significant performance improvement can be achieved. In Figure 3.11(a) we can notice a performance difference of about 8 dB between the ideal JDL processor (upper bound) and the Doppler compensated processor in the clutter notch region. This performance gap can still be reduced using a more effective Doppler compensation method.

Using a wider transmit mainbeam with beamwidth of 16 ° (as shown in Figure 3.11(b)) results in widening of the clutter notch region. This is caused by receiving more range dependent clutter echoes with signal strength comparable to that of the peak clutter echo. Widening of clutter notch means that it is harder to detect targets travelling at small relative velocities, corresponding to the widened Doppler region. On the other hand, wider beamwidth is sometimes required to allow shorter scanning duration and longer dwell time. Separate Doppler bins compensation is hence proposed to perform different Doppler compensation for different Doppler bins.

3.8 Separate Doppler bins compensation

Due to the complex range dependency of the bistatic clutter, there are clutter echoes from certain look angles that are range independent, while from other look angles, they are range depend-

ent. Performing 0 Hz Doppler compensation on clutter echoes received from such look angles (with range dependent clutter echoes), will not be able to correctly Doppler compensate range dependent clutter echoes arriving from such range dependent angles. When processing signals received from such look angles, several different Doppler compensations may be required, depending on the range dependency of the clutter echoes from those angles.

Performing Doppler compensation in the space-time domain (e.g. Doppler warping or ADC), only allows one Doppler compensation per range gate. However, for Doppler compensation using Doppler interpolation, different amounts of Doppler interpolation can be carried out at different Doppler bins. In a very general sense[v], different Doppler bins correspond to clutter echoes arriving from different angles of arrival, even through clutter echoes arriving from different angles of arrival are also separated in the angle domain. By Doppler compensating Doppler bins differently, those range dependent clutter echoes can be Doppler compensated separately, depending on their range dependency, while those range independent clutter echoes are still being Doppler compensated with 0 Hz Doppler frequency shift. However, separate angular bins compensation may also be desirable.

Separate Doppler bins compensation is carried out as follows:

1. The number of Doppler bins required for separate Doppler bins compensation, M_{Db} is determined by the beamwidth of the mainlobe (assuming high mainlobe to sidelobe ratio),

$$M_{Db} = \frac{\text{beamwidth} \times D_f}{360^\circ} \tag{3.42}$$

   where D_f is the size of the DFT process (transform of time domain to Doppler domain).

2. Determine the individual Doppler bins that require separate Doppler bins compensation. This is achieved by centralising M_{Db} Doppler bins to the Doppler bin corresponding to the look angle φ_r (clutter notch Doppler bin), D_c. For φ_r = -33.45°, D_c is Doppler bin 10.

3. Determine φ_{Db} ($M_{Db} \times 1$), the angles of arrival (with respect to the range gate under test) corresponding to these individual M_{Db} Doppler bins.

[v] The signal component of each Doppler bin depends on the clutter echo Doppler frequencies, as well as the size and shape of the DFT windowing

4. The Doppler frequency shift required at each of the φ_{Db} angles is

$$\Delta f_{Db}(i) = f_k^{d\ \text{vii}} - f_r^{d\ \text{viii}}, \quad i = 1, \ldots, M_{Db} \tag{3.43}$$

   As Δf_{Db} is calculated without using the received clutter echoes, it will be affected by any error in the estimated parameters.

5. Perform Doppler interpolation with the respective calculated Δf_{Db}, on each of the M_{Db} Doppler bins.

6. Some of the Doppler bins, which are not compensated separately, are compensated by Doppler interpolation with a particular Doppler frequency shift, Δf_{Dc}, while the rest of the Doppler bins are compensated with the original amount of Doppler frequency shift Δ_f. The number of Doppler bins that are compensated by Δf_{Dc}, M_{Dc}, as well as the value of Δf_{Dc}, have yet to be precisely determined.

Figure 3.12 shows an illustration of the separate Doppler frequency shifting, while Figure 3.13 shows the JDL processor using training data from range gate 29 (range gate under test = 27), with beamwidth = 16 ° and a different amount of Δf_{Dc}. The red curve labelled “Ideal JDL processor” shows the JDL processor performance with true clutter sample covariance matrix. The blue curve labelled “uniformed bins compensated” shows the processor performance when using the originally proposed Doppler interpolation algorithm. The rest of the curves show the processor performance using separate Doppler bins compensation with different amount of Δf_{Dc} ranging from 23.45 Hz to 53.45 Hz. The objective of performing separate Doppler bins compensation is to obtain processor performance as close as possible to that represented by the ideal case.

A secondary notch at the frequency region of about -3000 Hz, determined by the value of M_{Dc} (M_{Dc} = 101 for this simulation) , is caused by sudden change in the Doppler bins compensation, from Δf_{Dc} to Δ_f. The size of this secondary notch can be reduced by a gradual change in Doppler bins compensation or it can be ignored using some kind of hybrid system. Other processors that can produce ideal performance at the frequency region of about -3000 Hz, can be used to replace the separate Doppler bins compensation processor (only for this secondary notch region).

[vi] calculated from equation (3.12)
[vii] calculated from equation (3.10)

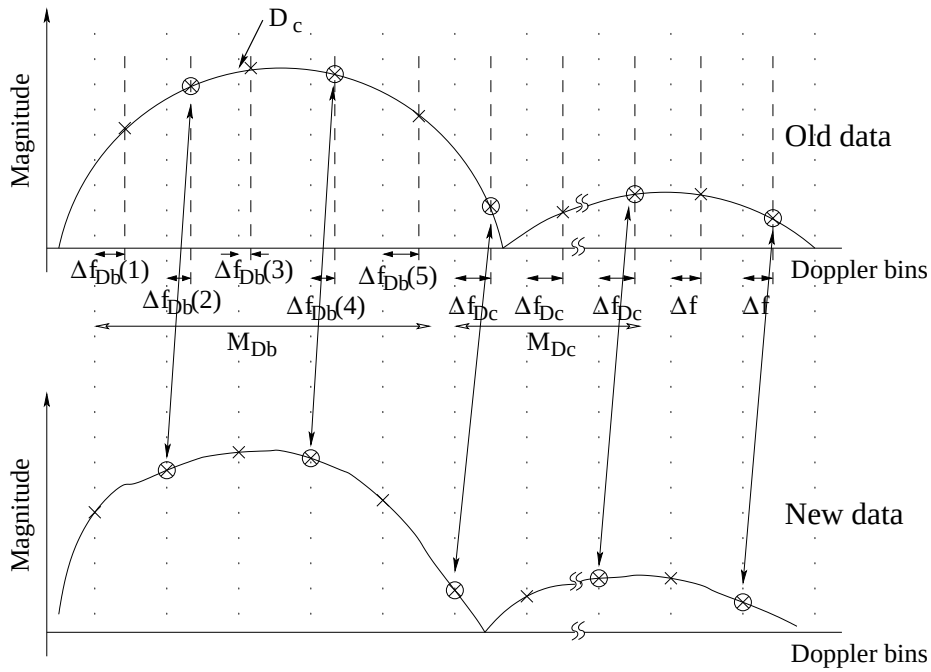

Figure 3.12: *Illustration of the separate Doppler frequency shifting.*

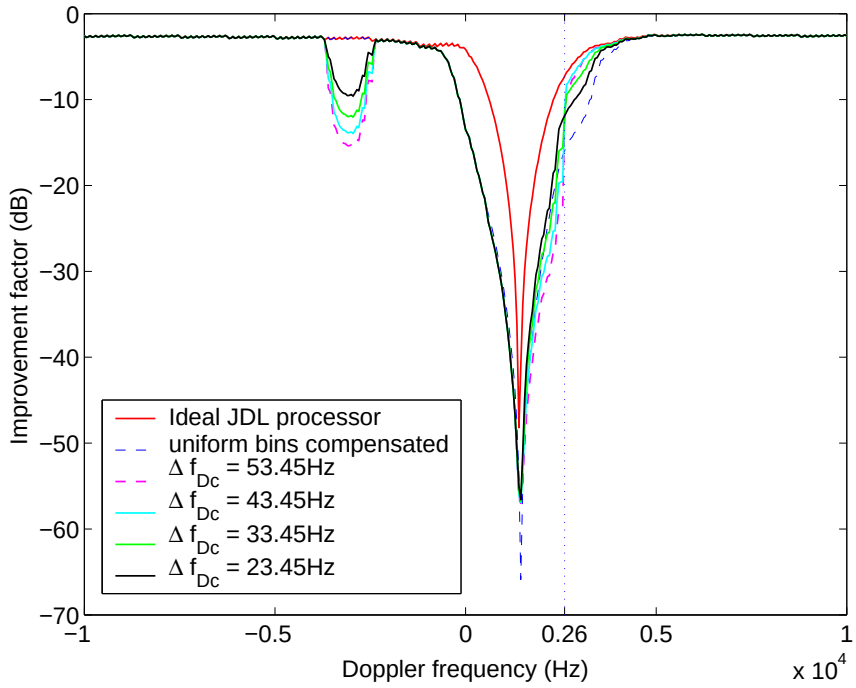

Figure 3.13: *JDL processor with beamwidth = 16 ° and different amount of* Δf_{Dc}.

When using different amount of Δf_{Dc}, performance differences at the right side of the clutter notch are observed. With a high value of Δf_{Dc} (e.g. Δf_{Dc} = 53.45 Hz), the separate Doppler bins processor compensation performance in the region between 2600 Hz to 3500 Hz gets very close to the ideal JDL processor performance. Maximum IF performance improvement of about 8 dB can be achieved in this region. However, in the region between 1500 Hz to 2600 Hz, a loss of about 5 dB in term IF is observed. On the other hand, when using smaller value of Δf_{Dc}, e.g. Δf_{Dc} = 23.45 Hz, a performance improvement is observed in the region between 1500 Hz to 2600 Hz, but with a smaller processor performance improvement in the region between 2600 Hz to 3500 Hz. The processor performance shown in Figure 3.13 is not the optimum performance. Instead, it shows the possibility of improving the processor performance with different Δf_{Dc}. To obtain a good processor performance, some kind of hybrid system that uses different Δf_{Dc} for different Doppler frequency regions, may be desirable.

Figure 3.14 shows the JDL processor performance using both separate bins compensation and Doppler warping. These results are obtained using both the training range gates 25 and 29. Figure 3.14(a) and Figure 3.14(b) illustrate the performance for the cases of using a narrow beam (beamwidth = 4°) and a widebeam (beamwidth = 16°) respectively. The red curve labelled "Ideal JDL processor", once again shows the JDL processor performance when it processes the true clutter sample covariance matrix. The blue curve labelled "separate bins" and green curve labelled "Doppler warping" show the JDL processor using separate bins compensation and Doppler warping respectively.

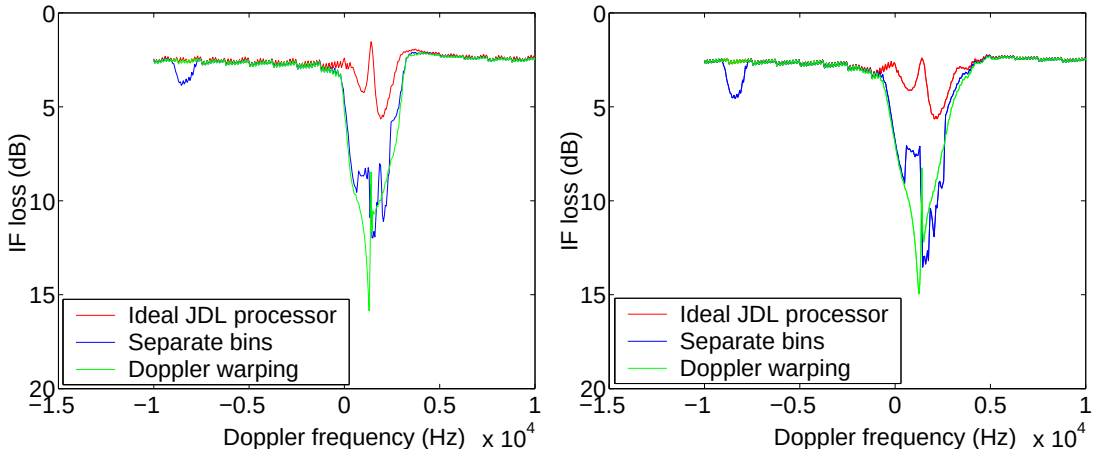

Figure 3.14: *JDL processor performance with separate bins compensation, using (a) Narrow beam - 4° (b) Widebeam - 16°.*

The secondary notch now appears at -8500 Hz as M_{Ds} = 67 is used for these simulations. For both cases (narrowbeam and widebeam), separate bins compensation clearly out-performs Doppler warping in the region between 600 Hz and 1350 Hz for narrowbeam and between 500 Hz and 1350 Hz for widebeam. In these regions, separate bins compensation seems to be more effective when a widebeam is used. The minimum IF loss in these regions falls to about 8.5 dB when using narrowbeam and about 7.5 dB when using widebeam.

3.9 Tuned DFT

Transforming spatial samples into the angular domain using the DFT with a rectangular window often results in smearing across several angular bins. The smearing depends on a number of factors, such as: the number of antenna array element, N; the size of the DFT; the angle of arrival, φ_r; the spatial sampling rate which is determined by the separation between the antenna elements; windowing used; and zero padding added on the spatial samples. As a result of the smearing, a number of angular bins, N_a, (normally N_a, = 3) are grouped into each LPR in order to gather a significant portion of the spatial energy.

Figure 3.15 shows the (angle-domain) 8-point DFT outputs of signals received by a forward looking array. Five individual signals arriving from five different φ_r, with depression angle, θ = 27°, are received during five different experiments and plotted together. It can be seen that, for the signals arriving at φ_r = 35° and φ_r = 55°, the DFT outputs concentrate at bin 3 and bin 4 respectively. On the other hand for the signal arriving at φ_r = 45°, it is attenuated and spread widely across bin 2 and bin 6. This attenuation of the measured value of an angular component that falls in between the DFT bins is known as scalloping loss [153]. Scalloping loss can be reduced by using a tapered window function as well as performing zero padding. Window tapering will however, widen the mainlobe, while zero padding will increase the DFT size, hence increasing the computational cost.

A tuned DFT processor that minimises the scalloping loss and reduces the computational cost significantly is proposed. The tuned DFT obtains an unattenuated angular component value by matching the angular bin to the angular component. The system performance penalty of using only one angular bin is offset by the reduction in scalloping loss. Using just one angular bin allows the computational cost of calculating output at other angular bins to be saved. For N = 8, computational cost saving of up to 87.5% maybe be achieved at this stage. Further

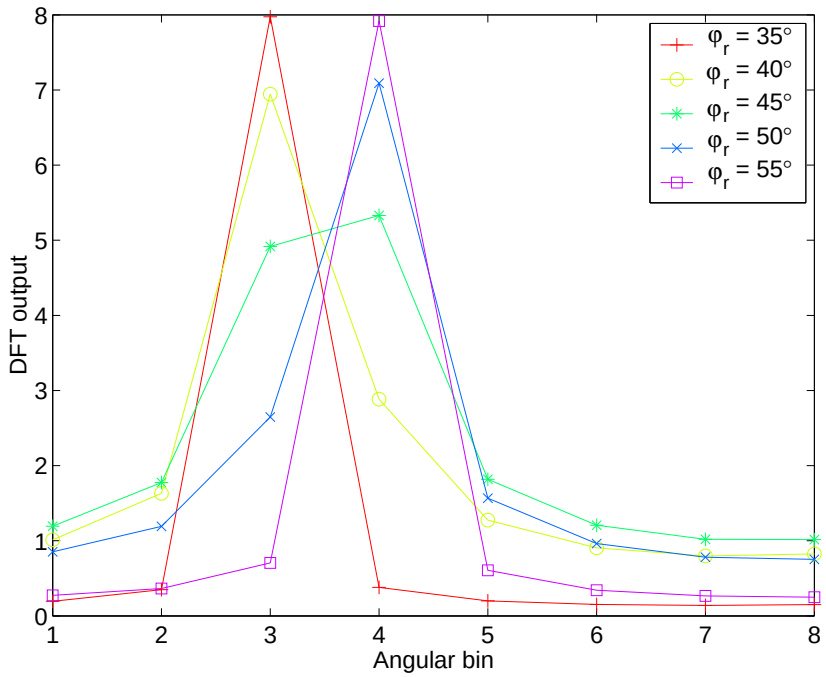

Figure 3.15: *Output of DFT with varies angle of arrival.*

computational saving is expected when the dimensions of the LPR are reduced from $(N_a \times M_f)$ to $(1 \times M_f)$.

The output of a tuned DFT for a spatial signal received by a linear array is given as

$$y\mathrm{F}a = \mathbf{w}_{tF}^{H}\mathbf{y}_s \tag{3.44}$$

where $\mathbf{y}_s$ represents a $(N \times 1)$ spatial signal vector. The weight vector of the tuned DFT, $\mathbf{w}_{tF}$, is given as

$$\mathbf{w}_{tF} = \left(w_{tF1}, w_{tF2}, \ldots, w_{tFN}\right)^{H} \tag{3.45}$$

where

$$w_{tFn} = \exp(-j2\pi k(n-1)), n \in \{1 \ldots N\}. \tag{3.46}$$

For a forward looking linear antenna array, k is defined as

$$k = \frac{\sin \varphi_r \cos \theta_{r,r}}{2}, \qquad k \in \Re \tag{3.47}$$

while for a sidelooking linear antenna array, this is given as

$$k = \frac{\cos \varphi_r \cos \theta_{r,r}}{2}, \qquad k \in \Re. \tag{3.48}$$

The different k values for different linear antenna arrays arises from the ability of the antenna to differentiate between angles. By definition of φ_r, a forward looking array is only able to differentiate $-90 \leq \varphi_r \leq 90$, while a sidelooking array is able to differentiate $0 \leq \varphi_r \leq 180$. The factor of $\frac{1}{2}$ in equations (3.47) and (3.48) is due to the $\lambda/2$ spacing between the antenna elements.

Back to the context of STAP, instead of performing a 2-dimensional DFT for space and time transformation, a normal DFT will follow after the tuned Fourier transform. The normal DFT will transform the time sample output of the tuned DFT ($\mathbf{y}_{\mathrm{F}a}$) into Doppler domain, $\mathbf{y}_{\mathrm{F}}$. Re-writing equation (3.44) to take into account of the temporal samples, the output of tuned DFT becomes

$$\mathbf{y}_{\mathrm{F}a} = \mathbf{w}_{tF}^{H} \mathbf{Y} \tag{3.49}$$

where $\mathbf{Y}$ (from equation (2.19)), a $(N \times M)$ matrix represents the space-time data samples.

The training data in each LPR becomes

$$\mathbf{y}_{\mathrm{L}_l} = \begin{pmatrix} y_{\mathrm{F}_{u_l}} & y_{\mathrm{F}_{u_l+1}} & \dots & y_{\mathrm{F}_{u_l+M_f-1}} \end{pmatrix} \tag{3.50}$$

3.9.1 Simulation Results

In order to compare the difference between JDL processors that use all angular bins, N_a = 3 angular bins, one angular bin and the tuned DFT angular bin, common ground must be established among them. The common ground is achieved by replacing $\mathbf{Q}_{\mathrm{L}_l}$ (from equation (3.8))

with $\mathbf{Q}_{\mathrm{LP}_l}$, $\mathbf{Q}_{\mathrm{LP}_l}$ is given as

$$\mathbf{Q}_{\mathrm{LP}_l} = \mathrm{E}[\mathrm{vec}(\mathbf{X}_{\mathrm{LP}_{l,k}})\mathrm{vec}(\mathbf{X}_{\mathrm{LP}_{l,k}})^H] \tag{3.51}$$

where $\mathbf{X}_{\mathrm{LP}_{l,k}}$, a $((N + N_p) \times M_f)$ matrix is the data samples in the l-th LPR group, grouped from angle-Doppler data samples $\mathbf{X}_{\mathrm{P}_k}$. The scalar N_p is the number of padding zeroes added to the spatial samples and $\mathbf{X}_{\mathrm{P}_k}$, a $((N + N_p) \times M)$ matrix is obtained by transforming $\mathbf{X}_k$ (from equation (2.12)) into the angle-Doppler domain using a 2-dimensional DFT with zero padding on the spatial samples. Zero padding is added to the spatial samples in order to obtain a better estimate of the energy between the original (without zero padding) DFT angular bins. All $N + N_p$ angular bins are included so that the performance upper bound can be established.

The signal-steering vector $\mathbf{s}_{l_{pq}}$ is replaced by the zero padded angle-Doppler signal-steering vector, $\mathbf{s}_{l_{p_{zq}}}$, which includes N angular bins as well as the N_p angular bins created by the zero padding, where index $z \in \{1 \ldots (N + N_p)\}$. Lastly, $\widehat{\mathbf{Q}}_{\mathrm{L}_l}^{-1}$ needs to be modified in order to achieve the same matrix size as $\mathbf{Q}_{\mathrm{LP}_l}$. The reconstructing is carried out by adding zero into angular and Doppler bins that is assumed to be zero. This is reasonable as the assumption of using less angular bins assumes that the energy in the rest of the angular bin (unwanted bins) is negligible (≈ 0).

Figure 3.16 shows the improvement factor for the Doppler interpolation processor using different number of angular bins as well as the proposed tuned DFT angular bin. The parameters used are: M (number of temporal pulses) = 128, N (number of antenna array element) = 8, M_f (Doppler bins used) = 9, N_p = 8, φ_r (look angle) = 55°. The training data is obtained from range gates 29 & 25. The curve labelled "All bins with zero padding" uses all 16 angular bins ($N + N_p$), to form the processor performance upper limit. The curve labelled "All bins without zero padding", uses 8 angular bins formed without zero padding. Of the two curves, the latter shows a performance degradation of about 3 dB, which is caused by the scalloping loss.

From Figure 3.15, we can see that for $\varphi = 55°$, most of the spatial energy concentrates in bin 4, and very little in bin 3 and bin 5. When angular bins 3,4 and 5 are used to calculate the weights of the processor, identical performance as compared with using 8 angular bins is achieved. Slight performance degradation around the notch region is observed when using just one angular bin (bin 4 is chosen as it has the highest energy). This is so, as some energy is lost when the energy in bin 3 and bin 5 is assumed to be zero. As expected, the tuned DFT did not

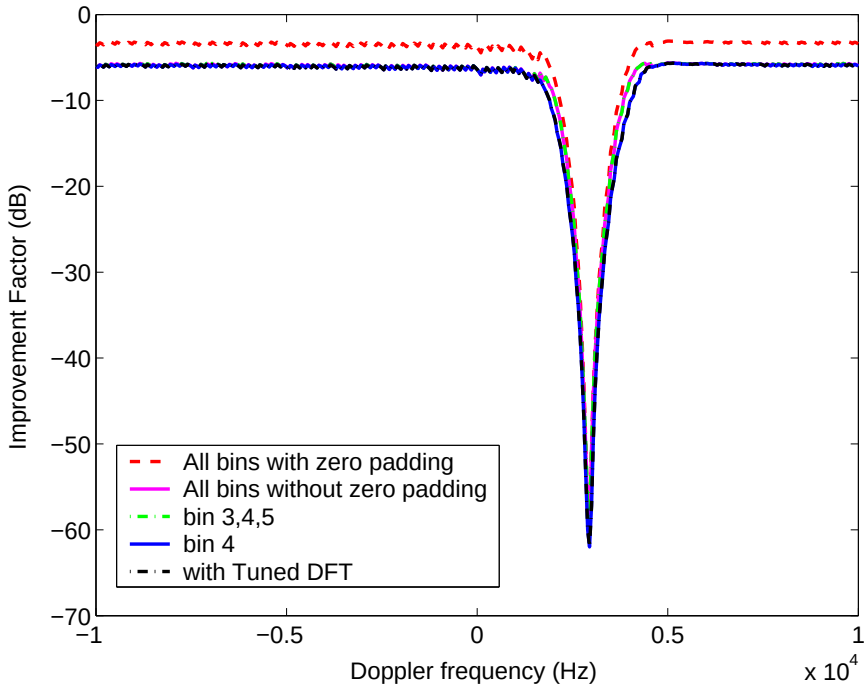

Figure 3.16: *Performance of angular bin reduction processor with* $\varphi_r = 55°$.

manage to have any performance improvement over using one angular bin (bin 4), since the energy concentration in bin 4 is already very high.

Figure 3.17 shows the improvement factor for the Doppler interpolation processor with $\varphi_r = 45°$. Using bins 3,4 and 5 shows that a comparable performance (as compare to using 8 angular bins) can be achieved by assuming the energy in the rest of the angular bins is approximately zero. A 3 dB degradation in performance is however observed when only one angular bin (bin 4) is used. From Figure 3.15, we can see that significant energy is also present in bins 3 and 5, excluding this energy will no doubt degrade the processor performance. The curve that uses the angular bin output from the tuned DFT (labelled "with tuned DFT") shows that by using one angular bin which is tuned to the maximum energy, processor performance as good as using 8 angular bins can be achieved. However small performance degradation is observed at the notch region.

This shows that very significant computational cost saving, in both the transformation of space-time samples into angle-Doppler samples and calculation of the inverse of sample covariance matrix can be achieved when using the propose tuned DFT. Degradation in processor performance due to using less angular bins is offset by reduction of scalloping loss. Reducing the

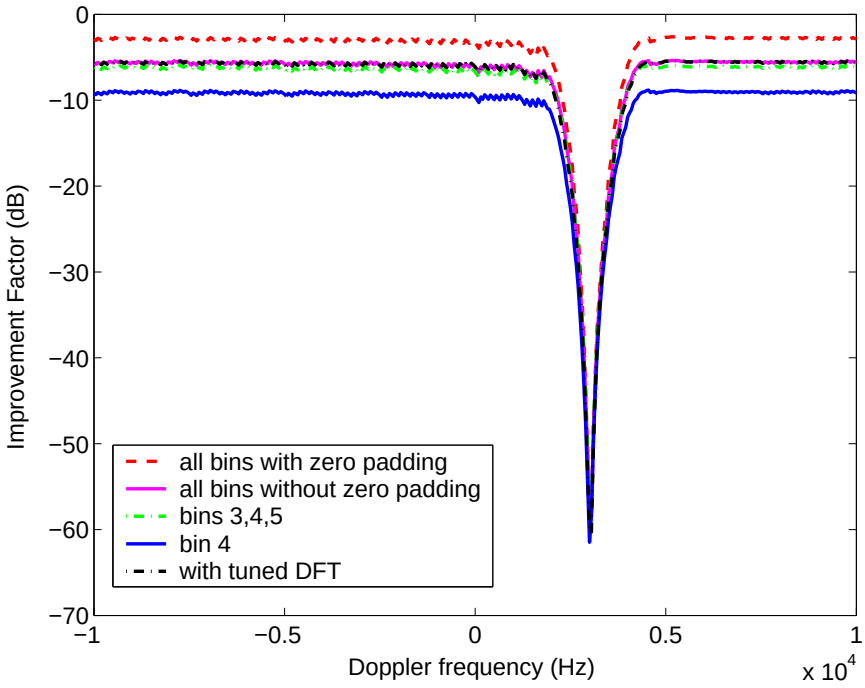

Figure 3.17: *Performance of angular bin reduction processor with* $\varphi_r = 45°$.

sample covariance matrix size to $(1 \times M_f)$ may further reduce the training data support size, hence improving the JDL processor performance in a non-homogeneous environment.

3.10 Summary

The proposed joint Doppler and power correction offers an alternative compensation method in the angle-Doppler domain to the Doppler warping compensation and ADC in the space-time domain. When using training data from range gate 29, Doppler interpolation achieved lower IF loss as compared with Doppler compensation methods using Doppler warping and ADC. This advantage reduces when training data from range gate 25 is used individually or together with training data from range gate 29. Doppler interpolation and ADC processors produce similar IF loss when training data from both range gates 29 & 25 is used. The proposed method of estimating the Doppler frequency shift shows robustness to errors in estimated parameters. For the range of the transmitter velocity error considered, the proposed method of estimating the Doppler frequency shift has an error of not more than 10 Hz. On the other hand, Doppler frequency shift estimation using equation (3.9) has an estimation error of about 670 Hz at the

transmitter velocity error range limit. Performing separate Doppler bins compensation allows Doppler interpolation to Doppler compensate clutter echoes with different range dependency. Significant processor performance improvement can be observed when comparing with Doppler warping compensation processor. The tuned DFT allows significant computational cost saving without reducing the processor performance by reducing the scalloping loss.

Chapter 4
System performance analysis

4.1 Introduction

The performance of the proposed Doppler interpolation processor depends on a number of parameters, such as the size of Doppler bins used, M_f, angular bins used, N_a, zero padding used Z, errors in estimated parameters (e.g. transmitter velocity, flight direction and position), load-to-clutter + white noise ratio (LCNR) and interpolation algorithm. In this chapter, the performance of the Doppler interpolation processor using different parameters will be investigated. Due to the characteristics of a particular radar system, the statistics of the received signal may be interpreted incorrectly and hence result in ambiguity. Ambiguity in a MPRF airborne radar system, as well as the performance of the proposed Doppler interpolation processor in an ambiguous environment shall be evaluated. It has always been believed that a reduced dimension processor will reduce the amount of training data required [140]. The performance of different processors with different amounts and types of training data for an airborne bistatic radar is also analysed. A general overview of the computational cost difference between the Doppler warping processor and the Doppler interpolation processor is also given.

4.2 Doppler bins, M_f

The number of Doppler bins, M_f, used by the Doppler interpolation processor determines a significant part of the processor computational cost as the size of the clutter sample covariance matrix is directly proportional to M_f. On the other hand, the size of M_f also directly affects the performance of the processor as shown in Figure 4.1 (using $N_a = 3$).

Using temporal zero padding, Z = 104, Doppler domain DFT size, D_f, of 128 and a maximum M_f of 128 are obtained. The curve labelled "M_f = 128" shows the best processor performance when all the Doppler bins were used. Its computational cost will be even greater than that of a full space-time STAP processor, because of a bigger matrix dimension, so it is only used to provide the performance upper bound. The curve labelled M_f = 1, shows the worst processor

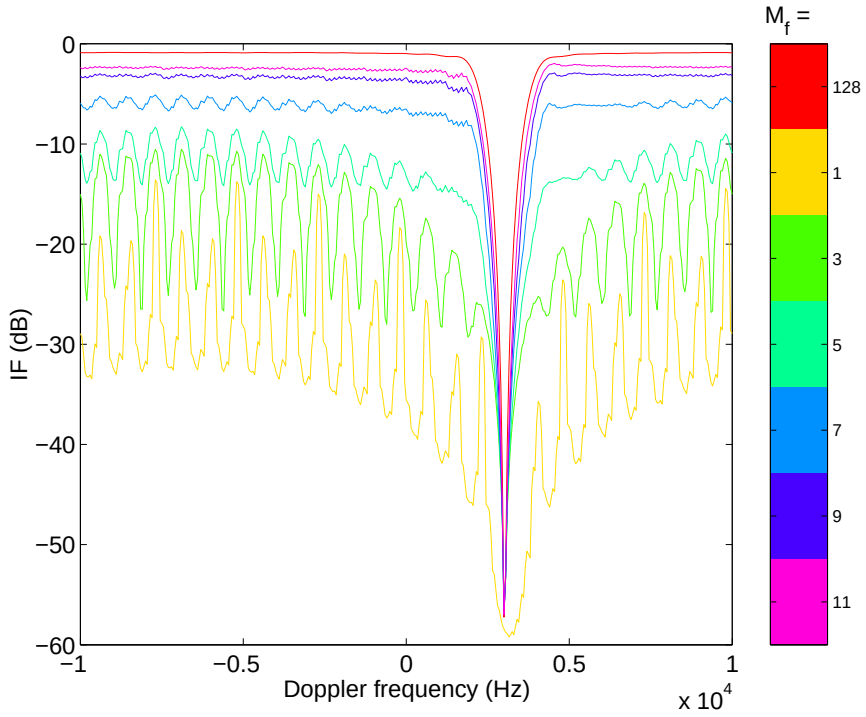

Figure 4.1: *Doppler interpolation processor performance varies with* M_f.

performance that can be expected when using the minimum number of Doppler bins. Curves plotted using M_f = 5 shows the improvement factor (IF) varying in a 5 dB range, centred around -12 dB, for the Doppler frequency regions outside the clutter notch region. Such IF variation is the result of significant difference between the neighbouring JDL localised processing region (LPR). This difference decreases with the increases of LPR size. Therefore, these variations are greatly reduced with increase M_f. For example, with M_f = 9, there is hardly any fluctuation in IF. The performance is within 3 dB of the upper bound.

Figure 4.2 shows how the mean IF loss varies with M_f for two different DFT sizes. For the curve labelled "DFT size = 64", using M_f greater than 5 does not offer significant mean IF loss reduction with increases in computational cost. However with "DFT size = 128", M_f needs to be greater than 9, before the reduction in the mean IF loss becomes less significant. The high minimum mean IF loss when using "DFT size = 64", is due to the interpolation error as explained in Section 4.5.

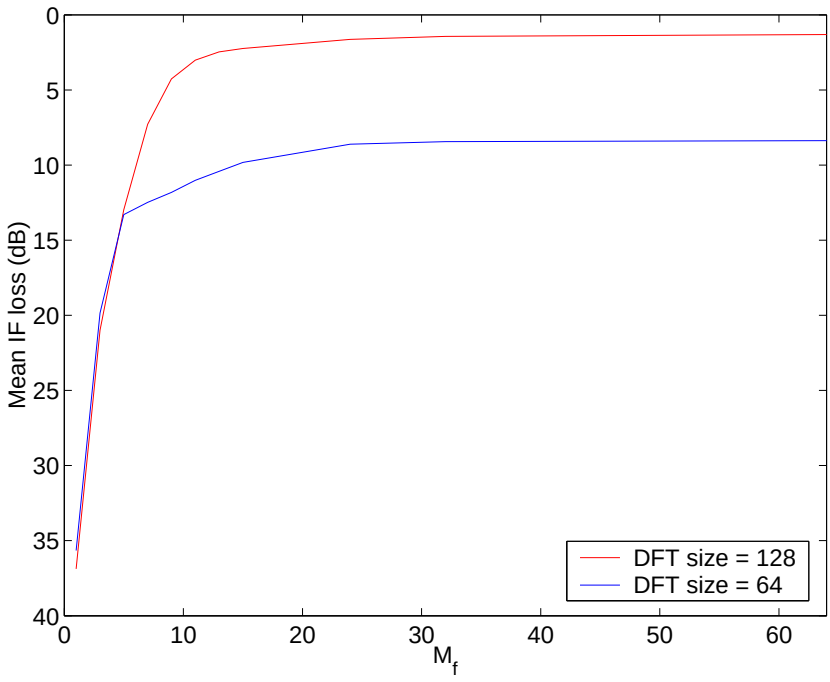

Figure 4.2: *Doppler interpolation processor performance (IF loss mean) varies with* M_f.

4.3 Alternate Doppler bins selection

Using alternate Doppler bins (either the odd or even Doppler bins) in each LPR can reduce the computational cost by about a factor of two. Figure 4.3 shows the processor performance when alternate Doppler bins selection are used. The red solid curve shows the IF of the Doppler interpolation processor that uses "full" Doppler bins (M_f = 9) in each LPR. The green solid curve shows the IF of the same processor, except that only alternate Doppler bins are used in each LPR. A 2.5 dB degradation in the IF is observed in the region outside the clutter notch when using alternate Doppler bins selection. Within the clutter notch region, no obvious difference in processor performance is observed. The blue dashed line represents the Doppler interpolation processor with M_f = 18, using alternate Doppler bins selection. The computational cost for this processor is the same as that using M_f = 9 with "full" Doppler bins. However an IF degradation of 1.5 dB (with respect to the IF with M_f = 9, "full" Doppler bins) is observed in the region outside the clutter notch. Some performance improvement is however, obtained on the right side of the clutter notch. With lower computational cost, Doppler bins alternation offers same low relative velocity target (in the clutter notch region) detection capability as that using "full" Doppler bins. On the other hand, with the same amount of computational cost, using alternate

bins selection offers better detection of low relative velocity targets.

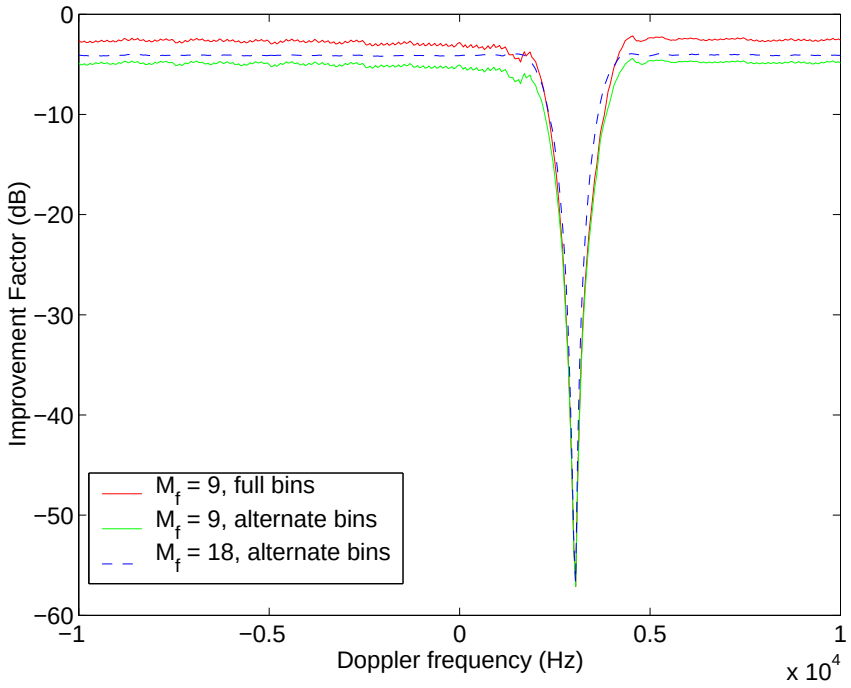

Figure 4.3: *Doppler interpolation processor performance using alternate Doppler bins.*

4.4 Spatial bins, N_a

Two issues arise when discussing spatial bins. The first issue is whether different Doppler compensation should be applied to different spatial bins, while the other issue is the size of spatial bins, N_a, required. With a beamwidth of 4°, the mainlobe clutter is likely to arrive within $\pm 2°$ of the look angle. Assuming that the sidelobe clutter strength is significantly lower than the mainlobe clutter and the number of antenna elements used is small, most of the clutter energy will be concentrated in one spatial bin, with some leakage into the nearby spatial bins. In this case, using the same amount of Doppler compensation for all the spatial bins, will be sufficient to mitigate the effect of the mainlobe clutter Doppler range dependency.

However, if a widebeam mainlobe or a large number of antenna elements are used, some of the clutter energy will fall into the neighbouring spatial bins (around the spatial bin corresponding to the look angle). On the other hand, if the mainlobe to sidelobe clutter ratio is small, the clutter returns from the sidelobe may also exist in some of the neighbouring spatial bins. In

these situations, the clutter Doppler range dependency in each spatial bin may be different from one another. This is so, as these clutter echoes arrive from different angles of arrival. Different amount of Doppler compensations for different spatial bins may hence be required to mitigate the effect of different clutter Doppler range dependency. Separate spatial bins compensation is not considered in this work due to time constraints.

Figure 4.4 shows the mean IF loss when different N_a sizes are used. Due to the nature of the sine function, the spatial bin does not correspond linearly with the signal angle of arrival. For φ_r = 45°, the spatial bin with the most energy is spatial bin 4. When using N_a less than the total number of antenna array elements, N, special care must be exercised when choosing which spatial bins to use. For odd N_a, the selected spatial bins are the spatial bin with the highest energy and an equal number of its left and right spatial bins. However when using even N_a, choosing one more left or one more right spatial bin can make a difference in the processor performance. The red solid line shows the use of spatial bins 3 and 4 when N_a = 2, while the blue dashed line shows spatial bins 4 and 5 being selected for N_a = 2. A difference of 2 dB mean IF loss is observed when different spatial bins were used.

The rate of change of mean IF loss, is reduced significantly for N_a greater than 3. Increasing N_a beyond 3 at the expense of higher computational cost does not yield proportional performance improvement.

4.5 Size of DFT processor, D_f

The accuracy of the Doppler interpolation process is very much influenced by the frequency separation between the Doppler bins. A small frequency separation between Doppler bins will result in better Doppler compensation. The frequency separation is determined by the size of the Doppler domain DFT, D_f, and the PRF. The signal component changes between Doppler bins depends upon the frequency separation as well as the DFT resolution (defined by the number of temporal pulses, M, used). Very often, the amount of temporal pulses available for signal processing are limited, as it is related to the dwell time of the radar system (as mentioned in Section 4.9.1). Zeroes are added to the temporal data to obtain a bigger Doppler domain DFT. That computational cost increases, due to a bigger Doppler domain DFT size, is not a big issue, as the fast Fourier transform (FFT) is widely used in modern radar systems.

Figure 4.5 shows the IF loss when using Doppler interpolation processor with different Doppler

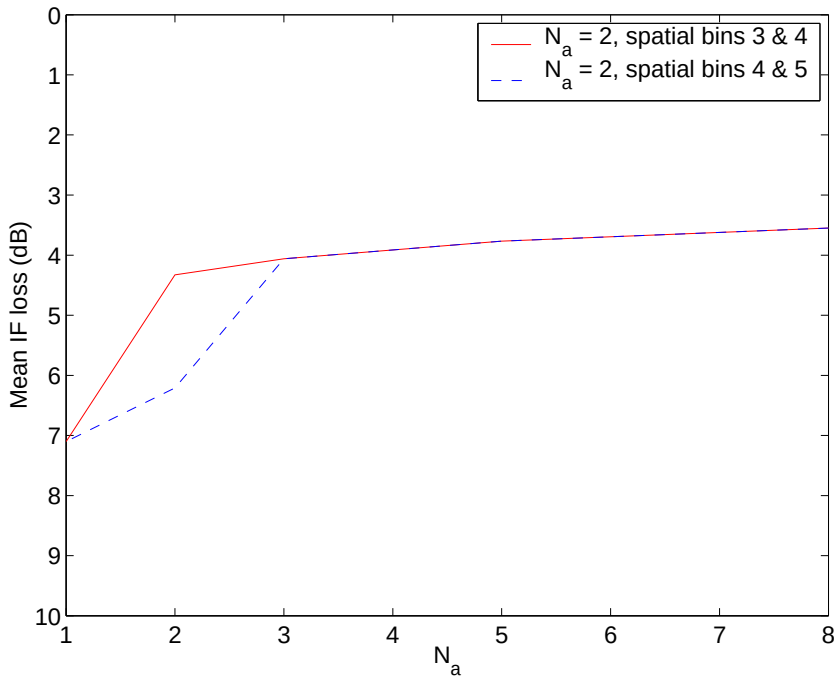

Figure 4.4: *Doppler interpolation processor performance (IF loss mean) varies with N_a, at $\varphi_r = 45°$.*

domain DFT sizes (with $M_f = 9$ and $N_a = 8$). Using a D_f of 24 and 32, represented by curves labelled "D_f = 24" and "D_f = 32" respectively, IF loss of up to about 30 dB is observed in the clutter notch region. This amount of IF loss is even greater than the IF loss from the STAP processor without any compensation (shown in Figure 2.23(b)). The notch region is also widened due to the interpolation error. Using D_f of 64, does reduce the IF loss. However, the notch region is still too wide, as compared to using processor without any compensation. With D_f of 96 or 128, much better performance is obtained. Although the curve labelled "D_f = 96" shows better performance than the curve labelled "D_f = 128", a D_f of 128 should be used, as it can be implemented using a FFT processor, which is not the case with D_f = 96.

About 3 dB IF loss in the region outside the notch is observed when D_f = 128 is used. For this region, using a reduced dimensional STAP, without compensation, may be a better choice. Good interpolation performance can be achieved when D_f is very much greater than the number of temporal pulses M used.

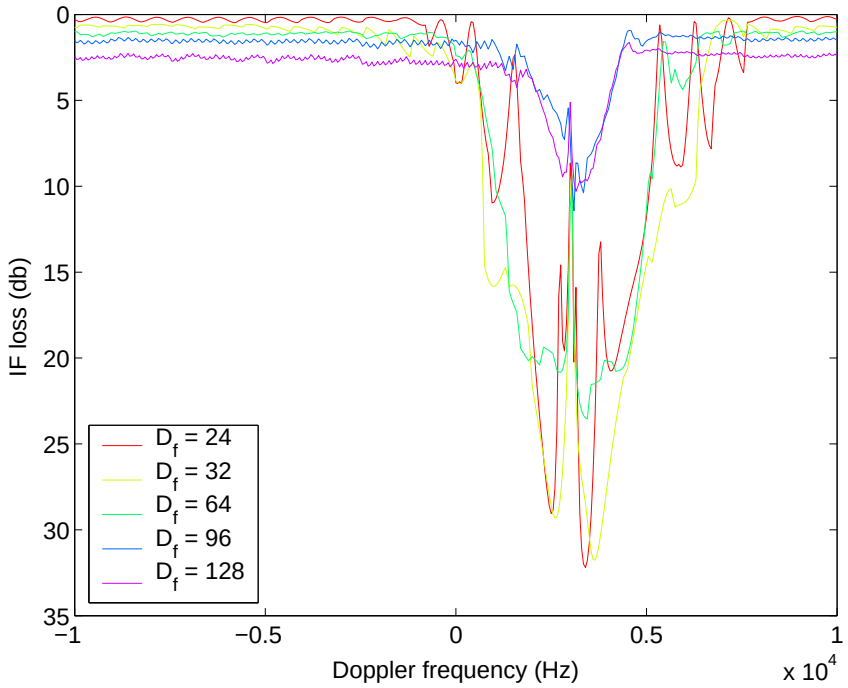

Figure 4.5: *Doppler compensation with different Doppler domain FFT sizes.*

4.6 Errors in estimated parameters

The outcome of the interpolation process, besides depending on the Doppler domain DFT size, D_f, number of temporal pulses used, M, and the interpolation algorithm, is also influenced by the estimation of the clutter Doppler shift, Δ_f. From equation (3.20), Δ_f is a function of $\tilde{f}_k^d$, φ_r, v_T, v_R, δ_t, δ_r, position of the transmitter and receiver, and both the range gate under test and the training range gate. The likely source of errors in these estimated parameters are the value of $\tilde{f}_k^d$, v_T, δ_t and positions of the transmitter. Error in $\tilde{f}_k^d$ maybe be caused by the presence of a target in the training range gate, while transmitter parameters may change in a continuously changing environment. Figure 4.6 shows the Doppler interpolation processor performance (in term of mean IF loss) when experiencing errors in some of the estimated parameters (with $M_f = 9, N_a = 8$).

The curve labelled "v_T" represents mean IF loss caused by error in the estimation of the transmitter velocity. Curves labelled "δ_t" and "x_t" show mean IF loss due to errors in estimating the transmitter flight direction and the transmitter x-axis position respectively. For all the three curves, the simulated error used is in a $\pm 20\%$ range, e.g. 72 m/sec $< v_t <$ 108 m/sec.

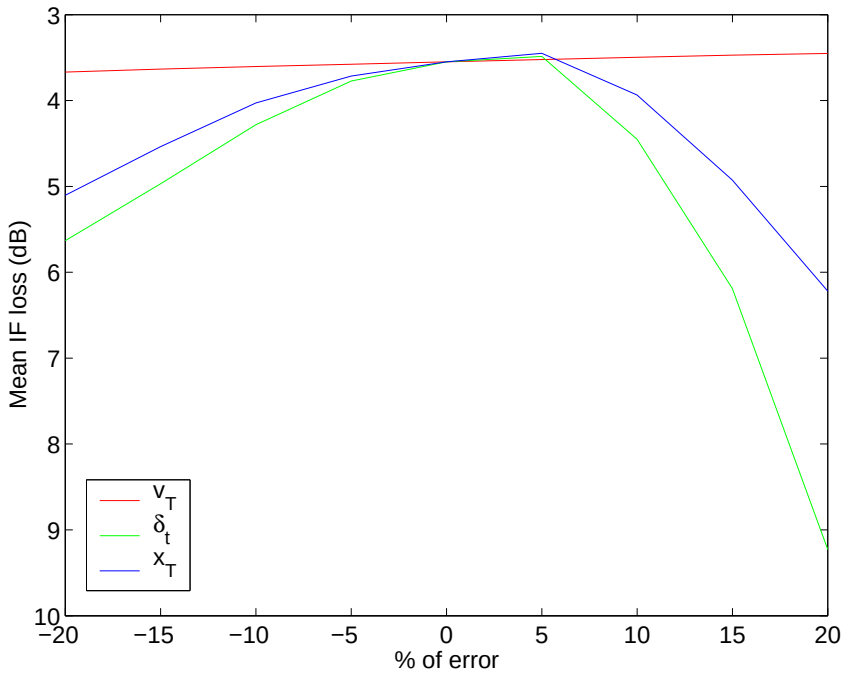

Figure 4.6: *JDL processor performance (IF loss mean) with various different errors.*

The processor is not sensitive to error in the transmitter velocity. While error in the transmitter flight direction will result in a significant loss of performance. A maximum mean IF loss of 9.2 dB and 6.2 dB is observed for errors in transmitter flight direction and transmitter x-axis position respectively. It is also observed that the drop in performance is not symmetric about the 0 % error axis. 0 % error should yield the best processor performance, however this is not the case due to inaccuracy in the interpolation process.

4.7 Diagonal loading

Diagonal loading is a technique that designs adaptive processors by assuming that the white noise is higher than its actual value. It makes the processor robust by attempting to preserve good processor performance in the presence of any mismatch. In this work, the primary mismatch is the mismatch between the estimated and the true clutter sample covariance matrix. This technique is called regularisation in the statistical literature. In this work, diagonal loading, adds an artificial noise to the diagonal elements of the estimated clutter sample covariance matrix. Beside making the processor robust, it also helps to prevent inversion of a singular matrix. The disadvantage of diagonal loading is that there is not enough prior information, to

determine the ideal fixed loading level, as the environment changes over time. Although this approach is not optimum, it is adequate in many cases and is widely used in practice [162]. When using an angle-Doppler domain processor, diagonal loading should be performed after the Fourier transforms.

The load-to-clutter+white noise ratio is defined as

$$\text{LCNR} = \frac{\sigma_L^2}{\sigma_C^2 + \sigma_w^2} \tag{4.1}$$

where σ_L^2, σ_C^2 and σ_w^2 are the loading noise variance, clutter variance and white noise variance respectively. Bigger LCNR represents the use of bigger diagonal loading.

Figure 4.7 shows how the ideal JDL processor performance (assuming knowledge of true clutter covariance matrix) varies with LCNR. Figure 4.7(b) shows a zoom in version of the processor performance. The curve labelled "LCNR = -50 dB" shows the processor produces the deepest clutter notch with this LCNR value. On the other hand, with LCNR = -30 dB, the clutter notch is reduced by about 10dB. A deeper clutter notch means that the target echo needs to be stronger before it can be detected. From Figure 4.7(a), an improvement in IF of about 1 dB is observed in the Doppler frequency region outside the clutter notch, when bigger diagonal loading (LCNR = -30 dB) is used.

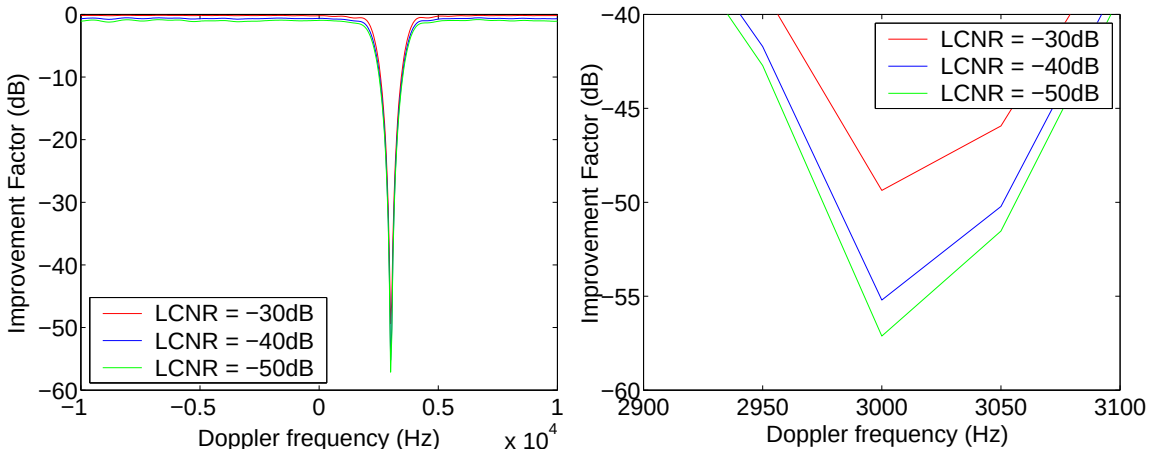

Figure 4.7: *Ideal JDL processor performance with various LCNR (a) full scale (b) zoom in.*

Figure 4.8(a) shows the improvement factor of an uncompensated JDL processor with various LCNR. With the increase of diagonal loading, from LCNR = -50 dB to LCNR = -30 dB, the improvement factor improves by at least 7dB across the whole spectrum. This shows the in-

crease in robustness of the processor when experiencing mismatch between the uncompensated and the true clutter sample covariance matrix (with the increase in diagonal loading).

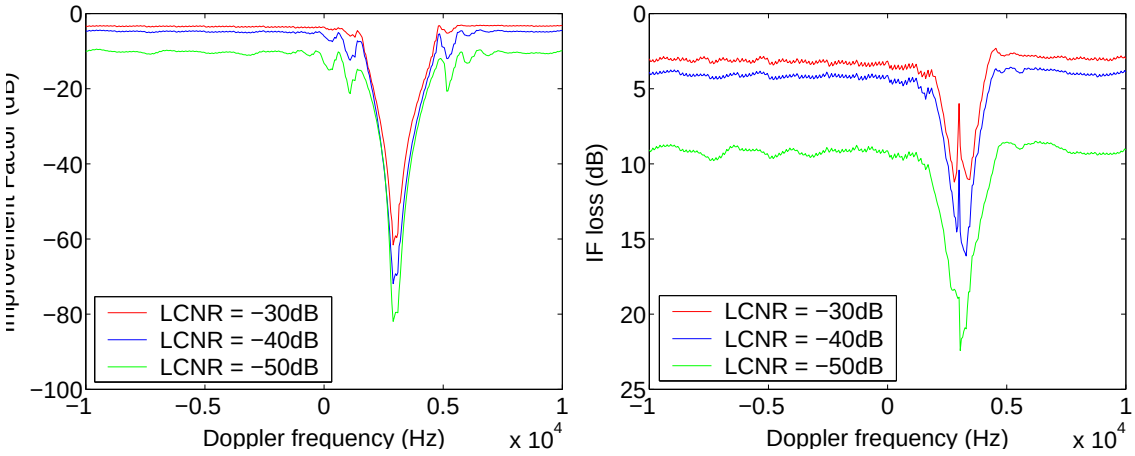

Figure 4.8: *Ideal JDL processor performance with various LCNR (a) uncompensated (b) compensated.*

Figure 4.8(b) shows the IF loss of the Doppler interpolation processor. Increase of diagonal loading once again shows an improvement in the processor performance. The IF loss reduces by about 7 dB in the region outside the clutter notch and by about 10 dB in the clutter notch region, when the LCNR is increased from -50 dB to -30 dB. These show that diagonal loading helps to mitigate clutter Doppler range dependency.

4.8 Radar Ambiguities

Ambiguity refers to the concept that a reflector at one point on the ground reflects the transmitted radar signal that, due to deficiency of the radar, is interpreted by the radar signal processor as caused by another reflector at a different position. There are three kinds of ambiguity in a pulse Doppler radar system. They are:

- Angle ambiguity,
- Range ambiguity, and
- Doppler ambiguity.

4.8.1 Angle ambiguity

Angle ambiguity is often a result of using an antenna pattern with high-gain mainbeam and sidelobes. The mainbeam is steered to a specific angle location. If a target is then detected, the target angle would be assumed to be the same as the steering angle. However due to the high sidelobe level, the target signal maybe reflected by a large cross section target at the sidelobe angle. The target angle is incorrectly registered as the mainbeam steered angle. This is an angle ambiguity. Although a mainbeam to sidelobe level ratio of more than 30 dB is typical in high-performance airborne radar [163], the design of an airborne radome does have a certain impact on the mainbeam to sidelobe level ratio [164]. In this work, angle ambiguity is not a problem, as it is assumed that using a mainbeam to sidelobe level ratio of 30 dB is sufficient to prevent any angle ambiguity.

4.8.2 Range ambiguity

For conventional pulse Doppler radar, range ambiguity occurs because of the transmission of repetitive pulses, which are used to resolve the reflections from targets at different ranges. Using a Medium PRF (MPRF) radar with a pulse repetition interval (PRI) of 100 μs for example, this duration is equal to the time required for a two-way transmission to reach an object in the range of 15km (obtained using equation (4.2)).

$$\begin{aligned} \text{Unambiguous distance} &= \frac{\text{Distance travelled}}{2} \\ \text{Distance travelled} &= \text{Velocity of light} \times PRI \end{aligned}$$

hence,

$$\text{Unambiguous distance} = \frac{\text{Velocity of light} \times PRI}{2} \tag{4.2}$$

If a reflector is more than 15km away, e.g. 20km, it will be assumed to be at a distance of 5km. In other words, reflectors whose range exceeds that defined as the maximum instrumented range are termed range ambiguous. Multiple-time-around echo is also used to describe the echo from a range ambiguous reflector. Figure 4.9 is a curve of the unambiguous range versus pulse repetition frequency (PRF).

Range ambiguities may theoretically be resolved, by observing the variation of the echo signal strength with time (range). This is not always a practical technique, since the echo-signal

amplitude can fluctuate strongly for reasons other than a change in range.

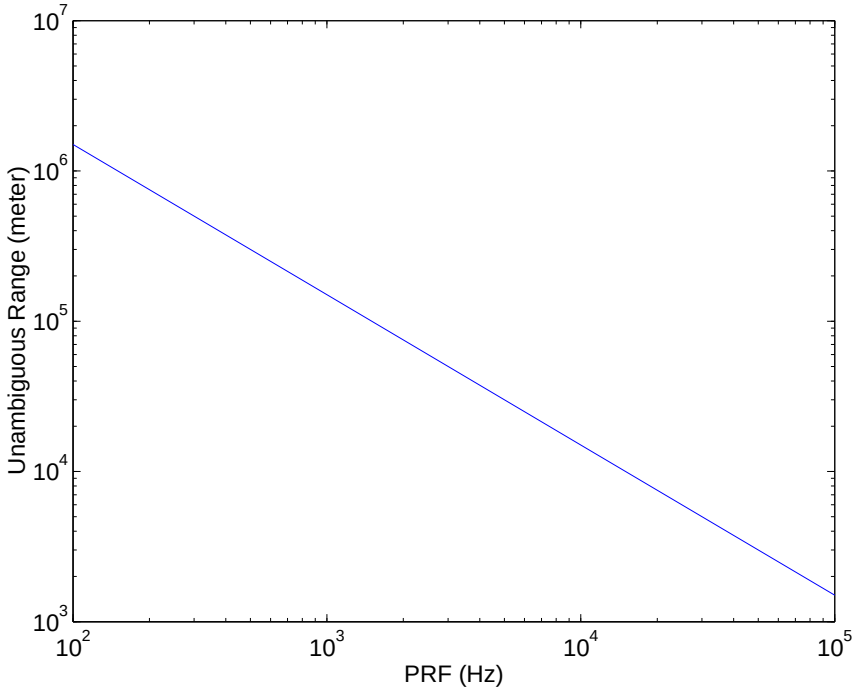

Figure 4.9: *Unambiguous range verse PRF.*

One method of distinguishing multiple-time-around echoes from unambiguous echoes is to operate with a varying PRF. The echo signal from an unambiguous range target will appear at the same place on each sweep no matter whether the PRF is modulated or not. However, echoes from multiple-time-around targets will be spread over a finite range. Using a planar array with additional vertical adaptivity has been proven, to be successful in reducing the effect of multiple-time-around clutter (see page 360 of [68]).

4.8.3 Doppler ambiguity

The Nyquist criterion states that the minimum sampling frequency needed to capture correctly the frequency content of a signal is equal to twice the signal bandwidth. For a pulse Doppler radar, the sampling frequency is the PRF. A simple single-channel radar extracts one data sample in each PRI. It can therefore measure the Doppler shift over an unambiguous frequency interval equal to PRF/2. A radar that extracts two samples per PRI (i.e., an I and a Q sample) has an effective sampling rate of twice the PRF and provides an unambiguous frequency interval of PRF.

Equation (4.3) shows the phase change between pulses (i.e., samples).

$$\Delta\phi = 2\pi\left(\frac{2\Delta R}{\lambda}\right) \tag{4.3}$$

where ΔR is the range change between pulses. If the phase change between pulses is less than 2π, the Doppler frequency can be measured unambiguously. If the phase change is equal to 2π, then the Doppler frequency equals the PRF. Obviously, a shift of 2π cannot be distinguished from a shift of any integral multiple of 2π, including zero. If the phase change is greater than 2π, the observed Doppler frequency will not correctly represent the target speed. The observed Doppler frequency will be incorrect by an integral multiple of the PRF.

Multiple PRFs (usually seven to nine) are used to resolve ambiguous target speed measurement. The maximum resultant unambiguous velocity is

$$v_{unamb} = \pm\frac{PRF \times \lambda}{4}. \tag{4.4}$$

The factor of 1/4 arises from the forward and return path travel by the radar signal, while the $\pm$ sign depends on the target flight direction and its position, if it is in front or behind the airborne radar. The maximum resultant unambiguous velocity, v_{unamb} is the maximum resultant velocity of the radar system and that of the target or clutter. Examples of the Doppler unambiguity velocity are given in Table 4.1, where f_o is the radar operating frequency.

f_o**(GHz)**	**PRF(Hz)**	$\mathbf{v_{unamb}}$**(m/sec)**
3	300	$\pm$7.5
3	20000	$\pm$500
10	20000	$\pm$150

Table 4.1: *Unambiguous Doppler velocity.*

Since the maximum unambiguous range is inversely related to the PRF while the maximum unambiguous Doppler velocity is directly related to the PRF, there is no single PRF that can maximise both at the same time. By using MPRF pulse Doppler radar, a compromise between unambiguous range and Doppler velocity can be achieved. The main advantage of the MPRF is the capability it provides to detect a slow-closing rate target from a high-speed platform (operating in tail chase mode). In tail chase mode, the target needs to travel at a very high relative velocity before its Doppler frequency becomes ambiguous.

4.8.4 Ambiguity in MPRF airborne bistatic radar

For airborne bistatic radar signal processing considered in this work, it is the widening of the clutter notch, that is of concern. Detection of low relative velocity targets tends to be difficult in such situations. As a result, Doppler ambiguity is not as big a concern as range ambiguity in the airborne bistatic radar system considered. For an airborne bistatic radar operation with PRF = 20kHz and f_o = 10 GHz, the unambiguous range can be divided into 64 range gates. Clutter or target returns received in range gate 27 for example, can possibly be originated from a distance equivalent to that of range gates 27 + 64$\times r_a$, where $r_a \in (0, 1, \ldots, \infty)$. The same applies to clutter returns received in the neighbour range gates. The clutter Doppler frequencies difference between range gates 27 and 29 is not the same as that between range gates 91 (27 + 64) and 93 (29 + 64), as shown in Figure 4.10. Compensating the two clutter Doppler frequencies differences with the same Doppler frequency shift, does not seem to be a logical choice. We shall now look at reasons why it might be justified to do so.

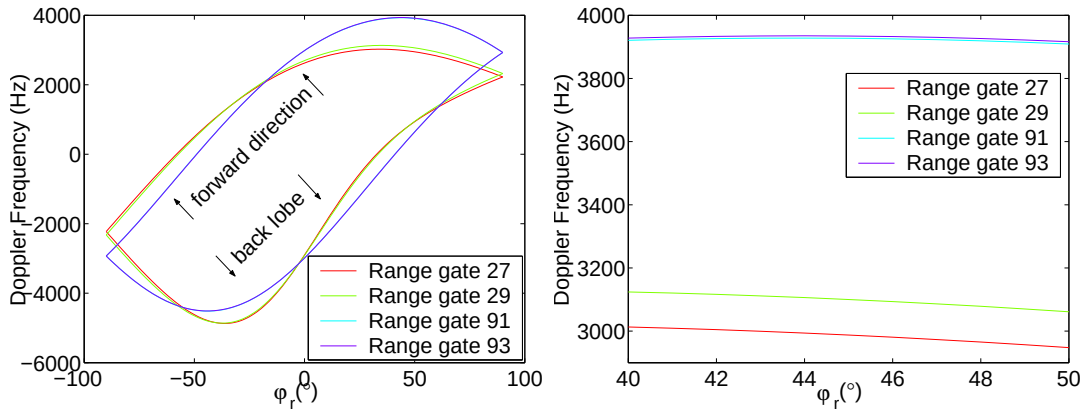

(a) (b)

Figure 4.10: *Isodops pattern of airborne bistatic radar (a) for selected range gates (b) zoomed version.*

From Figure 4.10(b), which is a zoom-in version of Figure 4.10(a), the clutter Doppler frequency difference between range gates 27 and 29 at φ_r = 45° is about 110Hz. On the other hand, there is hardly any Doppler frequency difference between range gates 91 and 93 (at φ_r = 45°). This is because, as the clutter distance gets further, the change in clutter Doppler frequency with range gate gets smaller. The clutter power also decreases significantly as the clutter distance increases. As a result, clutter power from range gates 27 and 29 will be much stronger than that from range gates 91 and 93. Although Doppler shifting the clutter spectrum from training range gate 29 to range gate 27 (range gate under test) by the amount of Doppler

frequency shift determined from the Doppler frequency difference between range gates 27 and 29, will cause the clutter echoes from range gate 93, to be compensated wrongly, the clutter power difference between these ambiguous range gates will make this effect insignificant.

Figure 4.11 shows the JDL processor performance in the assumed situation, with and without range ambiguity. The ideal processor performance (assumed knowledge of the true clutter sample covariance matrix) is shown in Figure 4.11(a). There is no obvious difference between the processors in the situation with and without range ambiguity. The clutter echoes from range gate 91 is much weaker than the clutter echoes from range gate 27, to have any significant effect on the processor weights. If the clutter power from range gate 91 is of the same order of magnitude as that from range gate 27, we will expect the curve with range ambiguity to have a notch at about 3930 Hz.

Figure 4.11(b) shows the IF loss of the Doppler interpolation processor. Although the Doppler compensation for the clutter echoes from range gate 93 is compensated incorrectly, no significant difference between the two curves is observed. Figure 4.11(c) shows a similar range ambiguous conclusion when the Doppler warping - JDL processor is used.

KLEMM's observation on range and Doppler ambiguities for an airborne bistatic STAP radar is quite different from what is observed in this work (see page 357 to 360 of [68]). Ambiguous clutter responses cause a broadening of the clutter notch or create secondary clutter notches. In KLEMM's simulations, the clutter power varies with range according to the radar range equation, i.e., the power due to a single point scatterer on the ground is $P_{cl} \propto \frac{1}{R_t^4}$, where R_t is the distance travelled by the single point scatterer. The sensor pattern used is according to equation (C.5). However, in this work, the clutter power is determined by the radar range equation, the receive sensor pattern[i] and a spotlight shape transmitter beam pattern (4° beamwidth in both azimuth and depression axes, with 30 dB mainlobe to sidelobe ratio). The difference in the transmitter beam pattern used in both cases, may cause the clutter power from range gates far away from the range gate under test, to be significantly different from one another. Because of the transmit beam pattern used, as well as the Doppler compensation process performed on the training data, neither broadening of the clutter notch nor presence of multiple clutter notches is observed in this work.

[i] According to equation (C.5).

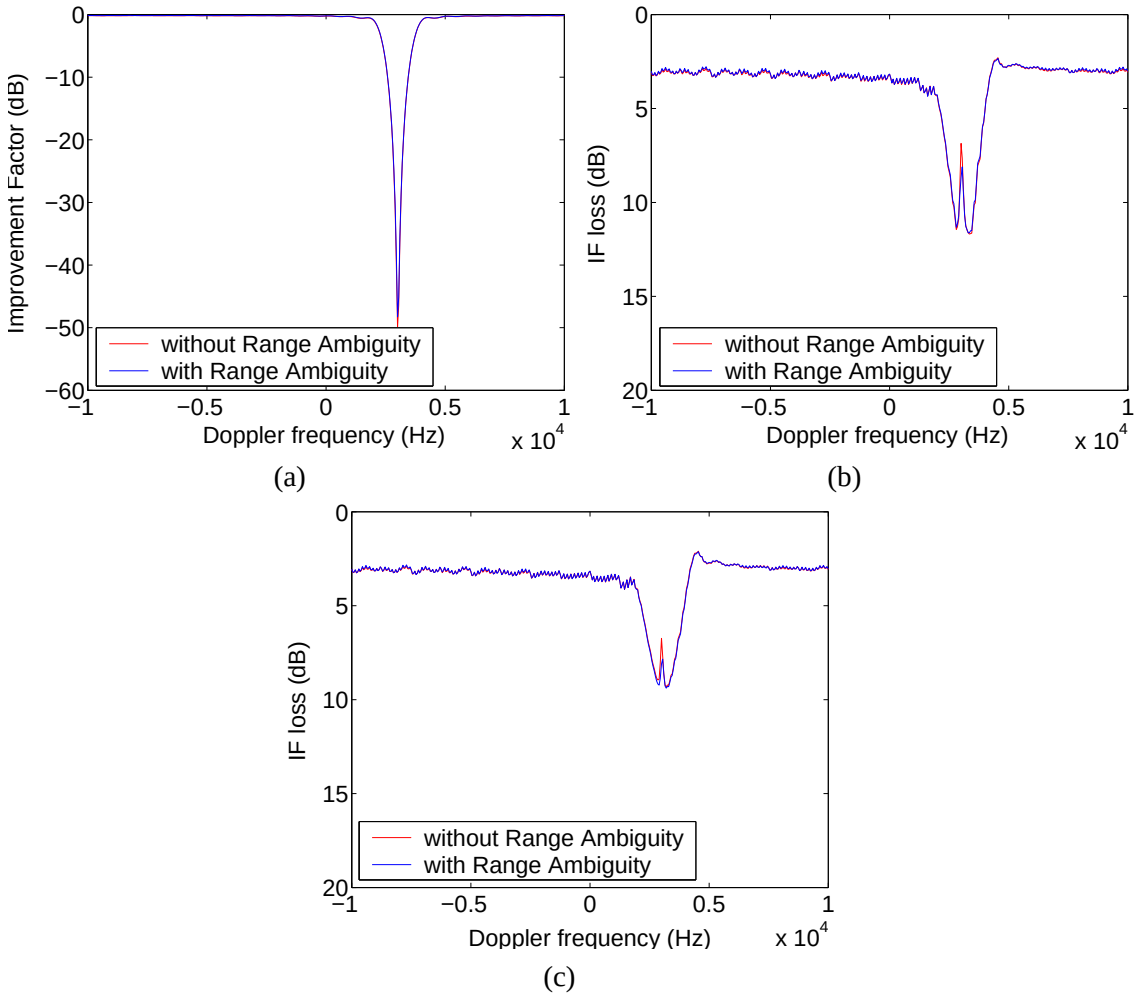

Figure 4.11: *JDL processor performance using Doppler interpolation, in situation with and without range ambiguity, (a) Ideal processor, (b) Doppler Interpolation using training data from range gates 25& 29, (c) Doppler warping using training data from range gates 25 & 29.*

4.9 Sample support for clutter sample covariance matrix estimation

In the number of literature regarding STAP processing, training data for the STAP processor is normally collected in the range dimension. For a sidelooking airborne monostatic radar, where the clutter statistic is range independent, large amounts of training data can be collected in the range dimension especially when operating in low PRF mode. The range samples/training data are generally assumed to be independent identically distributed (i.i.d.), although Zatman and Marshall [99] noted otherwise.

As mentioned in the previous chapter, the clutter statistic of an airborne bistatic radar is range dependent. Use of range samples require compensation to be performed on each of the range gates used, which is rather computationally intensive. An airborne bistatic radar operating in MPRF mode faces additional constraints. The low range ambiguity as well as finite pulse width, limit the number of range gates available. As a result, obtaining additional training data in the time dimension is highly necessary. The number of time samples available, depends on the dwell time, scanning rate, mainlobe beamwidth of the radar and the coverage area (area of interest).

In this section, we shall investigate the number of time samples available (considering only the dwell time), as well as the number of training data required by the STAP processor and the JDL processors.

4.9.1 Dwell Time

A phased-array pulse Doppler radar receiver receives discrete coherent bursts at the antenna look angle. The duration of the bursts is specified by the coherent processing interval (CPI). The measure of the signal-handling rate of a receiver, for a given reception from a particular beam position is termed a dwell. A pulse Doppler dwell consists of a coherent bursts of duration equal to the radar CPI. MPRF coherent bursts are typically transmitted and received within a single dwell [165]. The duration of the dwell is known as the dwell time, t_{dw}.

$$t_{dw} = N_{dw} \times PRI \tag{4.5}$$

where N_{dw} is the number of pulses within a single dwell.

Dwell time is often limited by the acceleration of the target, assuming that the radar system is travelling at a constant velocity. From the beginning of the dwell till the end of it, the change of target velocity, Δv_t, should not cause a significant change in its Doppler frequency. Significant change is defined as a Doppler frequency change that is greater than the filter frequency resolution [166]. It also assumes that the target does not exceed the range increment during the dwell time.

Change of target velocity, Δv_t is given as

$$\Delta v_t = a_t \times t_{dw} \tag{4.6}$$

where a_t is the acceleration of the target.

The change of the target Doppler frequency, Δf_D

$$\Delta f_D = \frac{2 \times \Delta v_t}{\lambda}. \tag{4.7}$$

Substituting equations (4.5) and (4.6) into equation (4.7),

$$\Delta f_D = \frac{2 a_t N_{dw} PRI}{\lambda}. \tag{4.8}$$

The Doppler frequency bin separation, Δf_b, is given as

$$\Delta f_b = \frac{1}{N_{dw} \times PRI}. \tag{4.9}$$

In order to reduce the possibility of the target Doppler frequency from ending up in another Doppler bin at the end of the dwell time,

$$\Delta f_D < \Delta f_b. \tag{4.10}$$

Substituting equations (4.8) and (4.9) into equation (4.10) and solve for N_{dw},

$$\begin{aligned} \frac{2 a_t N_{dw} PRI}{\lambda} &= \frac{1}{N_{dw} PRI} \\ N_{dw}^2 &= \frac{\lambda}{2 a_t PRI^2} \\ N_{dw} &= \sqrt{\frac{\lambda}{2 a_t PRI^2}}. \end{aligned} \tag{4.11}$$

A combat pilot is capable of withstanding an acceleration of 9 $\times$ the gravitational pull for a couple of seconds. Let PRF = 20 kHz, a_t = 90 meter/sec^2 and λ = 0.03 meter, therefore the number of time samples available for signal processing, N_{dw} is 258.

4.9.2 Samples requirement for STAP processor

The true signal+clutter/interference+noise sample covariance matrix is given by

$$\mathbf{R} = \mathrm{E}[\mathrm{Vec}(\mathbf{X}_s)\mathrm{Vec}(\mathbf{X}_s)^H] \tag{4.12}$$

where E[·] is the mathematical expectation operator and $\mathbf{X}_s$ is the received signal with target signal present, from the range gate under test.

When the target signal is absent, then only the clutter/interference and noise are present, and

$$\mathbf{R} = \mathbf{Q} \tag{4.13}$$

where $\mathbf{Q}$ is the true clutter/interference + noise clutter sample covariance matrix.

In practice, $\mathbf{Q}$ is estimated by

$$\widetilde{\mathbf{Q}} = \frac{1}{K}\sum_{k=0}^{K-1}\mathrm{Vec}(\mathbf{Y}_s)\mathrm{Vec}(\mathbf{Y}_s)^H \tag{4.14}$$

where $\mathbf{Y}_s$ is the received signal from the training range gate (assuming that the target is absent).

Samples requirement is defined as the number of K snapshots (in both time and range dimension) required, such that the estimated clutter sample covariance matrix $\widetilde{\mathbf{Q}}$ can be assumed to be the true clutter sample covariance matrix $\mathbf{Q}$. A mean IF loss of less than 3 dB from that of using the true clutter sample covariance matrix, is used to determine the samples requirement.

REED et al. [167] have shown that a adaptive system can achieve a performance roughly 3 dB below the optimum signal to interference + noise ratio (SINR) (with the target signal absent), $SINR_Q$ when the number of i.i.d. training data, is twice the order of the sample covariance matrix: $K \geq 2NM$. N stands for the number of antenna array elements, while M stands for the number of temporal pulse. If we want the SINR of the estimated clutter sample covariance matrix, $SINR_{\tilde{Q}} = \alpha_k SINR_Q$, then we require (see p.733 of [162]),

$$K \simeq \frac{1}{1-\alpha_k}NM \tag{4.15}$$

where α_k is the estimation performance factor. Table 4.2 shows the loss of performance with various K values.

K	Loss of performance
$20NM$	0.22 dB
$10NM$	0.46 dB
$7NM$	0.67 dB
$2NM$	3 dB

Table 4.2: *Performance loss for various K values.*

This leads to the "rule of thumb" that the number of i.i.d. samples required to obtain a useful clutter sample covariance matrix estimation (when the desired signal is absent) is at least twice the number of adaptive degrees of freedom (DOF), for $NM \geq 2$ and $K \geq NM$.

Monzingo and Miller (see p.298 of [168]) extended the result to include the case of a target signal present. Feldman and Griffiths develop an approximate expression for K when the target signal is present in the clutter sample covariance matrix estimation (see p.871 of [169]).

$$K = (SINR_R)(NM - 1) \tag{4.16}$$

to be within 3 dB of the optimum SINR (with target signal present), $SINR_R$. $SINR_{\hat{R}}$ is the SINR using the estimated clutter sample covariance matrix with the target signal present. Equation (4.16) is valid when

$$\begin{aligned} N &\gg 1, \\ K &\gg NM, \\ SINR_R &\gg NM. \end{aligned}$$

This will be significantly larger than the previous $K = 2NM$ result, in most cases of interest.

In practice, obtaining lots of i.i.d. samples within the allowed time frame is not feasible. Data samples are obtained with a tapped delay line, as shown in Figure 4.12. Data samples obtained in this way are correlated with each other, hence are not i.i.d.-(independent). From Section 4.9.1 on dwell time, we know that a maximum number of 258 samples are available for signal processing.

Let K_{opt} be the number of snapshots required to obtain the true clutter sample covariance matrix. Figure 4.13 shows the number of K_{opt} used to obtain the "optimum" STAP performance,

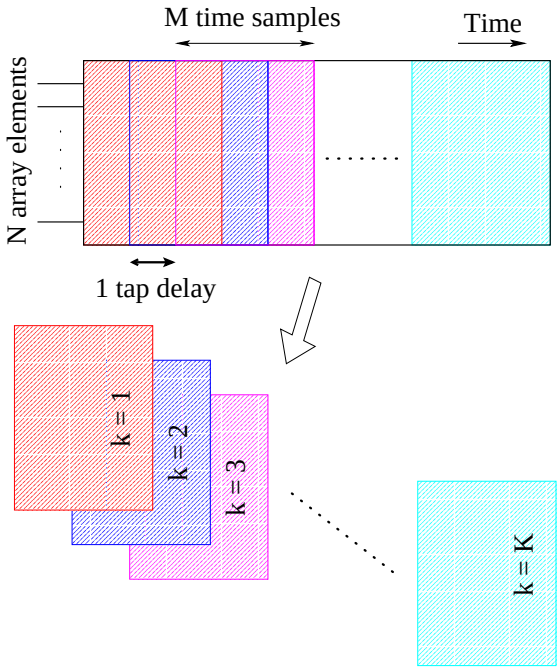

Figure 4.12: *Data samples from one of the training range gates.*

with $N = 8, M = 24$. With $K_{opt} = 20NM$ the convergence rate (using ideal training data[ii]) is more gentle than the curve using $K_{opt} = 7NM$. The amount of change in the mean IF loss from using $K_{opt} = 7NM$ to using $K_{opt} = 10NM$ is about the same as that from using $K_{opt} = 10NM$ to using $K_{opt} = 20NM$, but with significantly less simulation cost. Choosing $K_{opt} = 10NM$ reduces the amount of training data required as well as the computational cost, without significantly affecting the convergence rate. As a result, for the rest of this work, the optimum processor performance is assumed to be achieved when using the clutter sample covariance matrix estimated, with $K_{opt} = 10NM$.

Figure 4.14 shows the convergence rate of a STAP processor (with $N = 8, M = 24$ and 20 Monte Carlo simulations), using different kinds of training data. The curve labelled "Ideal training data", assumes knowledge of the clutter statistic in the range gate under test, range gate 27. In order to reach the 3 dB point, about 440 ideal data samples are required. In this section, the 3 dB point is always defined as 3 dB below the mean IF loss of the processor using K_{opt} number of training samples. This amount of training data looks reasonable, as from the "rule of thumb", 384 i.i.d. samples are required to achieve a 3 dB performance loss. Keeping in mind

[ii] Assuming having training data from the range gate under test, but without target signal.

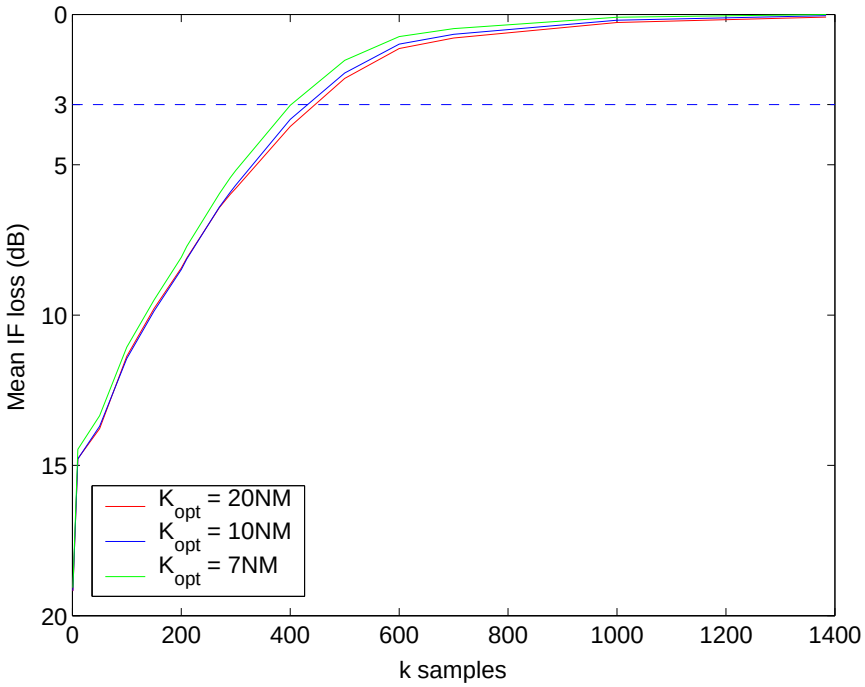

Figure 4.13: *STAP processor convergence rate with various* K_{opt}.

that the ideal training data samples used are correlated with each other. When using training data from the neighbour range gates, compensation using Doppler warping is carried out instead of Doppler interpolation, as Doppler interpolation is not suitable to be used in straightforward space-time processing.

The curves labelled “training range gate = 29” and “training range gate = 25,” show the convergence rate using training data from only one of the neighbour range gates. Their convergence rate to the 3 dB point (from the optimum mean IF loss), at about 3.68 dB (0.68 dB + 3 dB) and 3.25 dB (0.25 dB + 3 dB) respectively, varies quite significantly from each other, by about 200 samples. This provides us with the first insight, that the statistic of the training data does have certain influence over the convergence rate, assuming the Doppler compensation errors in both cases are negligible. From earlier simulations in the previous chapter, we observed that the Doppler warping compensation using training data from range gate 29, is not as good as that using training data from range gate 25. It is therefore not surprising to see that the optimum mean IF loss when using training data from range gate 29, is higher than that of using training data from range gate 25.

The curve labelled “training range gates = 25 & 29”, shows the Doppler warping STAP pro-

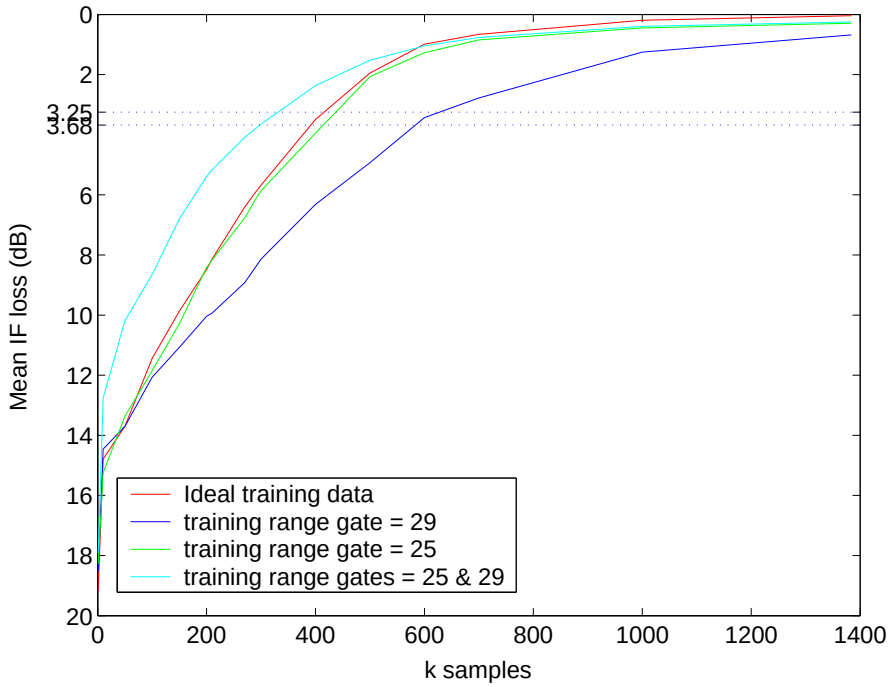

Figure 4.14: *Mean IF loss plots with various training data.*

cessor using training data from both range gates, range gates 25 & 29. The number of data samples obtained from each training range gate (for this case when using training data from two range gates) is half of that used when using training data from only one range gate. The total number of K samples used for this case is therefore the same number of K samples used in other cases. As both training range gates are far apart from each other, it can be can assumed that half of the training data is to a certain extent, independent from the other half. The convergence rate to the 3 dB point is observed to be about 320 samples, which is slightly less than the value of $2NM$. Using training data that is less correlated with or independent from each other, produces a faster convergence rate as well as reducing the number of samples required to reach the 3 dB point.

Figure 4.15 shows how the Doppler warping STAP processor performance varies with M (using training data from range gates 25 & 29). According to the "rule of thumb" given by REED et al., the number of samples required to reach the 3 dB point for each of the M values are 320, 384 and 448 i.i.d. samples respectively. Simulations, however show that less samples are required with the increase of M values. For $M = 20, M = 24$ and $M = 28$, the number of samples required to obtain a 3 dB mean IF loss, from that of the optimum mean IF loss point, are 348,

337 and 324 respectively. In this case, the simulations result is not consistent with the REED rule. The clutter statistic may have not changed significantly, with the increase in M, that may cause an increase in K samples.

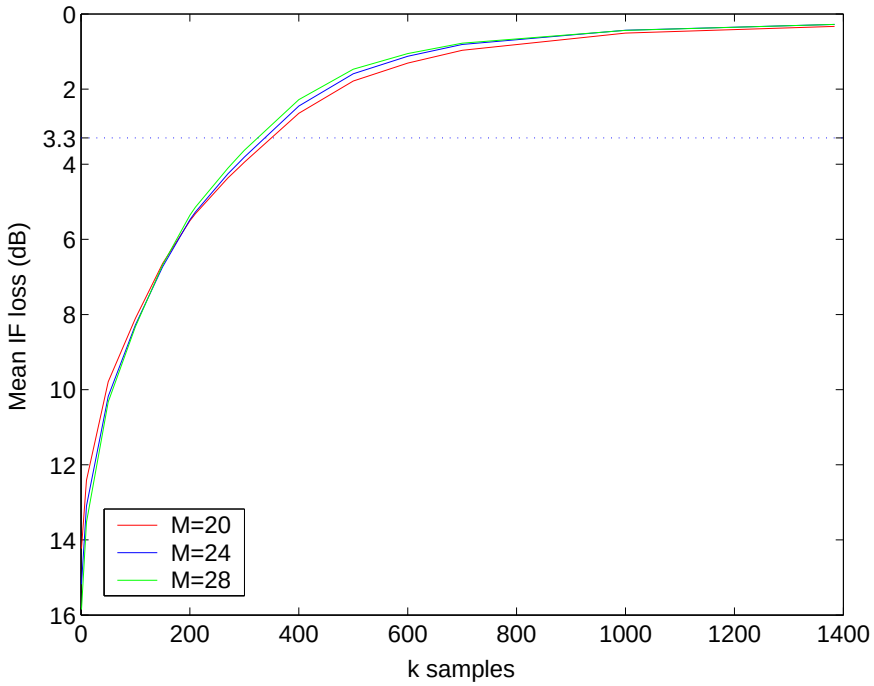

Figure 4.15: *Mean IF loss plots with various M.*

4.9.3 Samples support for Doppler warping JDL processor (using i.i.d. samples)

Next, the convergence rate for the angle-Doppler domain STAP processor, when i.i.d. samples obtained from the range dimension are used will be determined. How similar is it when comparing with similar work done by other researchers?

Figure 4.16 shows the number of i.i.d. samples required to obtain the minimum mean IF loss when using the JDL processor with Doppler warping (DW) compensation. Two different kinds of i.i.d. sample selection methods are used. Due to the distance of the transmitter and receiver from the ground, the first range gate available for sampling is range gate 16. Range gates far away from the range gate under test (assumed to be range gate 27) are also excluded, as the clutter peak (required to perform Doppler warping) is too small to be correctly identified by a 2-D DFT processor. As a result, only a maximum of 32 range gates are available. For the simulations shown in Figure 4.16, the following parameters are used: $M = 64$, $N = 8$,

$M_f = 3$ and $N_a = 3$ (to be as similar as possible with the simulations discussed in Section 4.9.4).

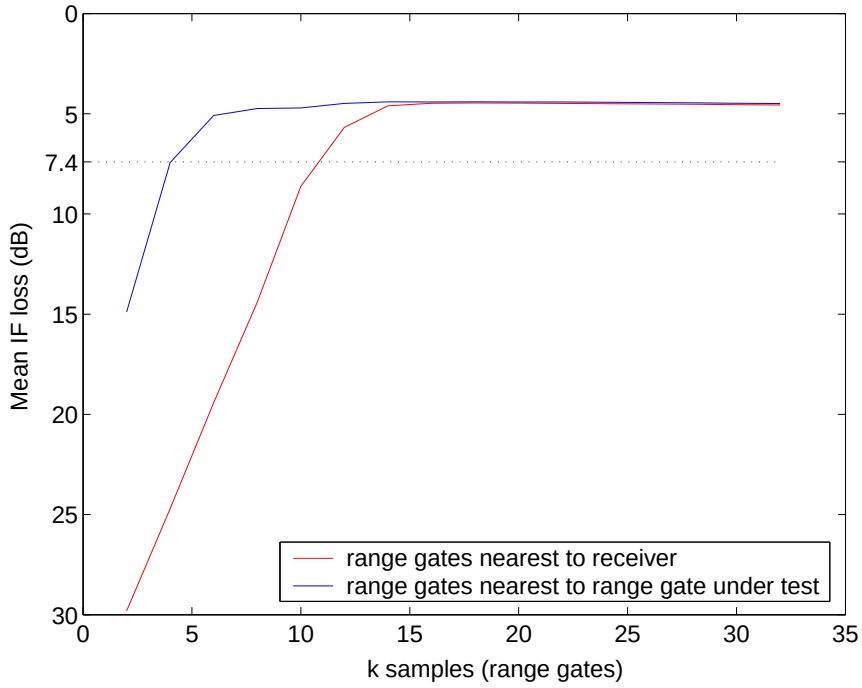

Figure 4.16: *Mean IF loss plots with various combinations of using different training range gates.*

The red curve shows the convergence rate when the i.i.d. samples are obtained from range gates nearest to the receiver (irrespective of the range gate under test). For example, when K samples = 4, range gates 16, 17, 18 and 19 are used; when K samples = 12, range gates 16, 17, 18, 19, 20, 21, 22, 23, 24, 25, 29, 30 are used. The blue curve shows the convergence rate when the i.i.d. samples are obtained from range gates nearest to the range gate under test. For example, when K samples = 4, range gates 24, 25, 29, 30 are used; when K samples = 12, range gates 20, 21, 22, 23, 24, 25, 29, 30, 31, 32, 33, 34. The range gates beside the range gate under test - the guard gates are excluded.

The Doppler warping JDL processor requires about 11 i.i.d. samples nearest to the receiver, to obtain a 3 dB mean IF loss from the minimum mean IF loss. However, when using i.i.d. samples nearest to the range gate under test, only 4 i.i.d. samples are required to achieve the same performance. These simulations show that the “rule of thumb” does not apply to these simulations because the samples are not completely i.i.d.-(identical). Errors in the Doppler compensation process make the training range gates selection critical. The nearer the training

range gate is to the range gate under test, the less is the error caused by the Doppler compensation process. Using training data with minimum error will reduce the number of i.i.d. samples required. For the rest of the simulations explained in this thesis, i.i.d. training data should first be obtained from the training range gates nearest to the range gate under test (when determining the processor convergence rate).

4.9.4 Samples support for Angle-Doppler compensation (ADC) - JDL processor (using i.i.d. samples)

Figure 4.17 shows the convergence rate of the JDL-ADC processor in two different bistatic cases simulated and produced by HIMED et al.[1]. Figure 4.17(a) shows the convergence rate of case 1 - the receiver is assumed to be moving at a velocity of 100 m/sec while the transmitter velocity is 0 m/sec. Figure 4.17(b) shows the convergence rate of case 2 - the receiver is assumed to be moving at a velocity of 100 m/sec while the transmitter velocity is 100 m/sec, with an offset angle of 45 °. Other parameters used are: $N_a = 3$, $M_f = 3$, $M = 64$, $N = 32$, the transmitter center frequency is $f_o = 1.24$ GHz, $PRF = 400$ Hz, receiver height = 3.1 km, transmitter height = 4 km, and baseline separation = 100 km. Due to the geometry of the airborne bistatic radar, the first range gate / smallest secondary data size, K, is 20.

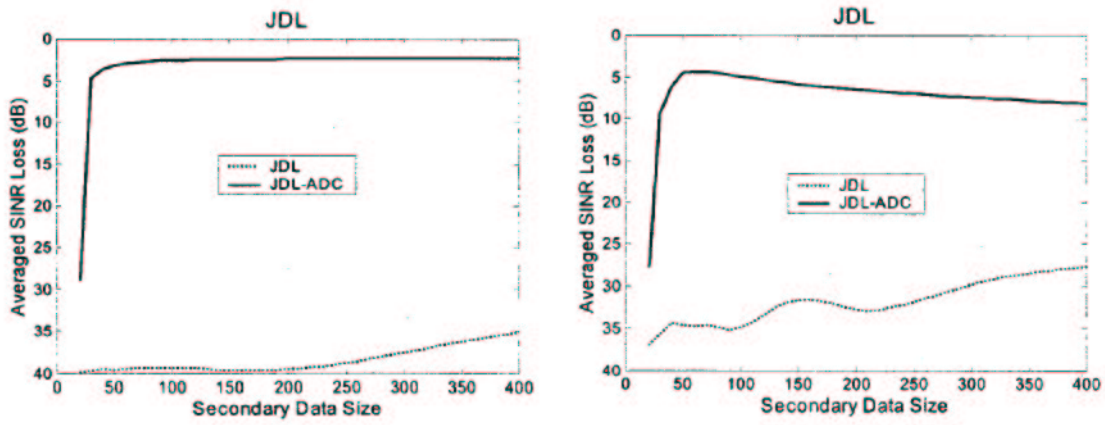

(a) (b)

Figure 4.17: *Convergence rate of JDL-ADC processor with receiver is assumed to be moving at a velocity of 100 m/sec (a) case 1 - while the transmitter velocity is 0 m/sec (b) case 2 - transmitter velocity is 100 m/sec, with an offset angle of 45 °. (Figure obtained from [1]).*

For case 1, it requires about 5 secondary data (K samples) to reach the 3 dB average SINR loss point, from the minimum mean SINR loss (from the solid line labelled "JDL-ADC"). On

the other hand, for case 2, it requires about 15 secondary data to reach the 3 dB mean SINR loss point, from the minimum average SINR loss (from the solid line labelled "JDL-ADC"). According to the "rule of thumb", the number of secondary data should be greater than 18 ($2 \times 3\ (M_f) \times 3\ (N_a)$) for both cases. Once again, the difference in the number of secondary data may be the result of not having completely i.i.d.-(identical) data. It is interesting to note that, for both cases, the number of secondary data required is less than 18, with case 1 - very much less than 18. The use of diagonal loading may be the cause of this.

Comparing the convergence rate using training data obtained from range gates nearest to the receiver (red curve) in Figure 4.16, with Figure 4.17(b), a similar convergence rate is achieved. This similarity shows that the results obtained from the simulation carried out in this work (with regard to the sampling requirement) is in line with the results obtained by other researchers.

4.9.5 Samples support for Doppler interpolation processor (using i.i.d. samples)

Figure 4.18 shows the convergence rate of the Doppler interpolation processor, with various M_f using i.i.d. training data. The red, blue and magenta curves show the convergence rate using $M_f = 9$, $M_f = 12$ and $M_f = 15$ respectively, with $M = 24$, $N = 8$, $N_a = 3$, $\varphi_r = 45°$ and mainlobe beamwidth = $4°$.

It is observed that with the increase of K samples beyond 15, the mean IF loss increases significantly. This is due to errors arising from the interpolation process. The further the range gate is from the range gate under test, the more compensation required. Hence, the harder it is for it to be compensated correctly.

From Section 4.2, it is not surprising to observe that using $M_f = 9$ produces the biggest mean IF loss across most K samples range, and the mean IF loss decreases with the increase in M_f. However, with the increase in M_f, the number of K samples required to obtain a 3 dB mean IF loss from the minimum mean IF loss remains the same, at about 5. This is different from what is expected - an increase in K samples with the increase in M_f.

The convergence rate of the Doppler interpolation processor, with various M_f using non-independent data (with tapped delay line), from both training range gates, range gates 25 & 29, shall next be investigated.

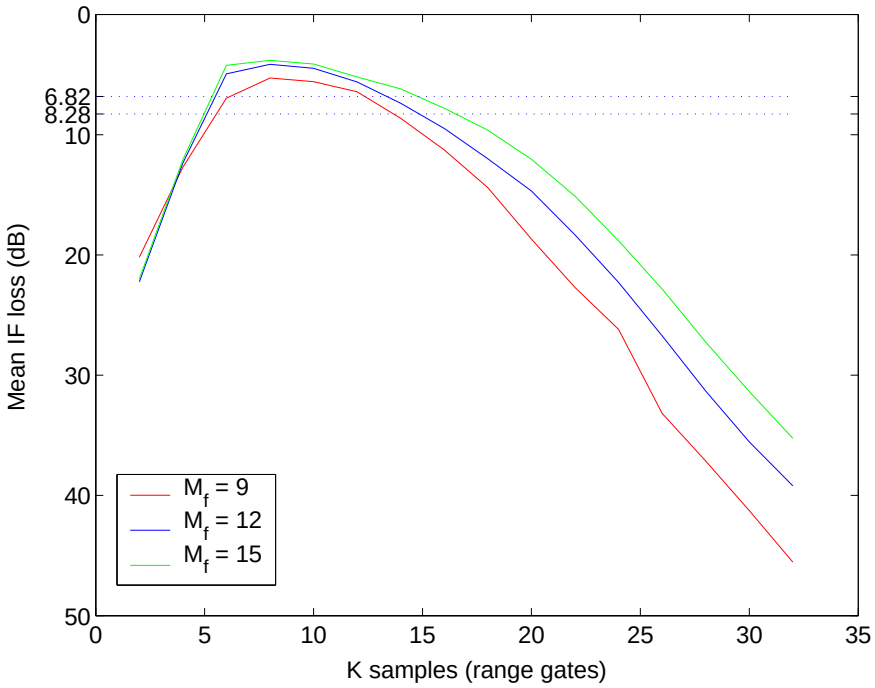

Figure 4.18: *Mean IF loss curves of Doppler interpolation and power correction JDL processor with various M_f using i.i.d. training data.*

4.9.6 Samples support for Doppler interpolation processor (using non-independent data)

Figure 4.19 shows the convergence rate of the Doppler interpolation processor (using non-independent data) with various M_f. The non-independent data are obtained from range gates 25 and 29, with tapped delay line (the dimension sample). The different colour curves: red, blue, magenta, cyan and black shows the convergence rate of the processor using $M_f = 6, M_f = 9, M_f = 12, M_f = 15$ and $M_f = 18$ respectively. For all cases, the number of angular bins used, N_a, is 3. The respective colour arrows indicate the 3 dB mean IF loss from the minimum mean IF loss of each curve.

With the increase of M_f, the number of K samples required to reach the 3 dB mean IF loss from the minimum mean IF loss reduces. It reduces from 426 with $M_f = 6$ to 340 with $M_f = 18$. This is about the same amount of K samples required by the STAP processor (shown in Figure 4.14). This number may be slightly bigger than what the dwell time can offer. But from Section 4.9.5, we know that, by using more nearby range gates, e.g. range gates 24 and 30, the number of K samples required can be further reduced.

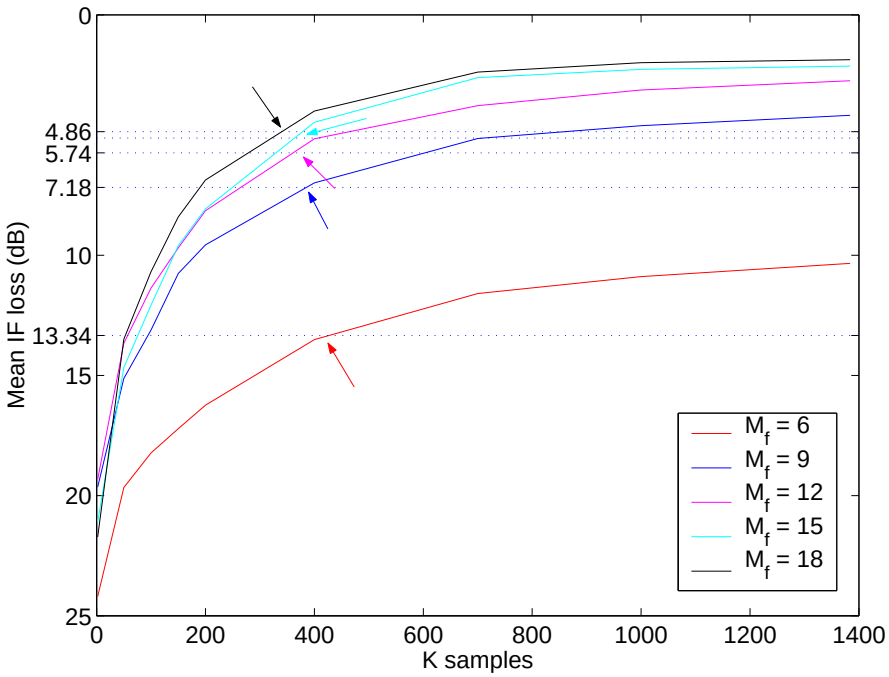

Figure 4.19: *Mean IF loss plots of Doppler interpolation processor with various M_f using non-independent data.*

It is also interesting to note that, to obtain a mean IF loss of 13.34 dB, 426 K samples are required when using $M_f = 6$. However by increasing M_f to 18, only 52 K samples are required.

4.9.7 Discussion on samples support

The samples support for an airborne bistatic clutter suppression processor can be quite different from a sidelooking airborne monostatic clutter suppression processor. In the sidelooking airborne monostatic radar, the clutter echoes are assumed to be range independent. No Doppler compensation is required for the training data and hence, no Doppler compensation error will occur. On the other hand, the range dependent nature of the bistatic clutter echoes makes Doppler compensation a necessity.

All Doppler compensation methods currently available are only an approximation. A certain amount of error is to be expected. Different Doppler compensation methods produce different amounts of error when dealing with different training range gates, in different radar configurations and at different look angles. Comparing ADC and Doppler warping, ADC offers

considerable improvement, especially when $K > 200$ (K samples are obtained in the range dimension) [152]. Several airborne bistatic radar configurations can be used to mitigate the range dependency of the clutter Doppler (page 361 of [68]). They operate by reducing the statistical differences between clutter echoes in different training range gates. Section 3.7.3 shows the Doppler compensation error when using Doppler warping and Doppler interpolation with power correction, at φ_r = -33.48°. When using training data from range ranges 25 & 29, Doppler warping produces smaller error than Doppler interpolation at φ_r = 45°. This advantage disappears at φ_r = -33.48°. The use of separate Doppler bins compensation allows Doppler interpolation processor to offer better performance than Doppler warping processor at φ_r = -33.48°. Because of the above reasons, the samples support analysis carried out in this work may be different from the analysis carried out by other researchers, when different parameters, Doppler compensation methods or assumptions are used.

The blue line in Figure 4.16 (using Doppler warping) and Figure 4.18 (using Doppler interpolation) show the amount of error produced by different Doppler compensation processors. Doppler interpolation seems to produce more error when performing Doppler compensation for further training range gates (with respect to the range gate under test) then Doppler warping. Some kind of error detector may be required to prevent incorrectly Doppler compensated training range gates from being used and degrading the clutter suppression processor performance.

Using a value of K less than the dimension of the covariance matrix will result in a singular matrix. Overcoming this problem using diagonal loading, allows the use of a smaller training sizes.

Similar convergence rate graphs obtained from the blue curve in Figure 4.16 and from the solid line in Figure 4.17(b) provides confidence in the convergence simulations carried out in this work. The solid line in Figure 4.17 (a) and (b) show that the samples support varies with the airborne bistatic radar configuration, when using the ADC - JDL processor. This observation is not reflected by REED's "rule of thumb". HALE et al. further investigated the REED "rule of thumb" for cross spectral metric (CSM) - a kind of reduced dimension STAP algorithm - and concluded that REED rule does not hold for the reduced dimension STAP algorithm studied [124]. Using JDL with Doppler interpolation and power correction, the sample support is shown to be about 5, when using i.i.d. training data, for all M_f values investigated (as shown in Figure 4.18). This shows that REED rule also does not hold for the situation simulated in this case.

Figure 4.18 also shows that the minimum mean IF loss achievable with M_f = 15 using only range samples is 3.82 dB. On the other hand, when using non-independent training data - training data obtained in both range dimension (range gates 25 & 29) and time dimension - a smaller minimum mean IF loss of 2.13 dB is obtained. The slight disadvantage of using training data from both dimensions is the increase in the number of K samples used, which increases the computational cost of forming the estimated clutter sample covariance matrix.

Direct comparison between the samples support for (when using non-independent training data) the STAP processor and the Doppler interpolation processor can not be made, as the processor dimension used in each case are different. However, Figure 4.19 shows that the samples support (when using non-independent training data) for the Doppler interpolation processor is comparable to the samples support for the STAP processor (shown in Figure 4.15). The reduction in the clutter sample covariance matrix size from $M = 20, N = 8$ to $M_f = 6, N_a = 3$, does not seem to reduce the sample support.

4.10 Computational cost

For the JDL based processor, the computational cost of performing Doppler compensation in angle-Doppler domain (Doppler interpolation), is considered to be much less than that of performing in space-time domain (Doppler warping). This may sound rather surprising, as complex phasor multiplication is less computationally intensive than the interpolation process. The reason lies in the fact that, for Doppler warping, a 2D DFT/FFT process must be carried out after the multiplication process for every training range gate undergoing Doppler compensation. Assuming that 10 training range gates are required to obtain a good estimation of the clutter sample covariance matrix (for both Doppler warping and Doppler interpolation processor) and power correction is not used.

When performing Doppler compensation for 48 (for PRF = 20 kHz) different range gates under test, the number of 2D-FFT process required to transform space-time domain data to angle-Doppler domain is as follow:

For Doppler compensation using Doppler warping, the 2D-FFT process can only be carried out after the Doppler warping process has been carried out. For every range gate under test, each training range gate needs to be compensated differently. Therefore, 10 (for 10 training range gates) 2D-FFT processes are required for each range gate under test. 48 different range gates

under test will hence require 48 (number of range gate under test) $\times$ 10 (number of 2D-FFT processes per range gate under test) = 480 2D-FFT processes.

On the other hand, for Doppler compensation using Doppler interpolation, the 2D-FFT process is carried out before the Doppler compensation process. With 48 different range gates under test, we can assume that there are 48 training range gates (although not all training range gates will be used by each range gate under test). Regardless of the number of range gate under test, only 1 2D-FFT process is required for each available training range gate. As a result, 48 different range gates under test will require only 48 (training range gates) $\times$ 1 (number of 2-D FFT processes per training range gate) = 48 2-D FFT processes.

The number of 2D FFT processes required when using Doppler warping will be much larger when low PRF is used. This is because, there will be more range gates under test when operating in low PRF mode. This comparison is only fair when mention is made about the possibility that the FFT processor size, when using Doppler warping, may be smaller than that used by the Doppler interpolation compensation.

4.11 Summary

This chapter has presented an investigation on a variety of parameters that will affect the performance of the proposed Doppler interpolation processor.

The number of Doppler bins (M_f) used will directly determine the computational cost and the processor performance. $M_f = 9$ out of a maximum M_f of 128 is shown to offer the best performance versus computational cost trade off. Using alternate Doppler bins selection offers better detection of low relative velocity targets, without increasing computational cost. If a tuned DFT is not being used, use of 3 spatial bins ($N_a = 3$) proves to be sufficient.

The performance of the interpolation process is greatly determined by the algorithm used as well as the DFT size, D_f. With temporal pulse M = 24 and D_f = 128, the processor performance manages to obtain a maximum IF loss of 10 dB at the clutter notch region. The compensation process is shown to be most sensitive to error in the transmitter flight direction, among the estimated parameters investigated. Diagonal loading increases the robustness of the processor when experiencing mismatch between the estimated and the true clutter sample covariance matrix.

Range ambiguity is the major concern for a MPRF airborne bistatic radar. Due to weaker clutter power arriving from further range gates, range ambiguity has no obvious effect on the compensation performance. When using i.i.d. training data from the range dimension, the Doppler interpolated processor required a sample support of about 5 K samples for various M_f values considered. On the other hand, when using non-independent training data (obtained from the time and range dimension), reducing the rank of the Doppler interpolated processor does not reduce the amount of samples required to form a good clutter sample covariance matrix estimation. For M_f = 18 and N_a = 3, the number of K samples required to reach the 3 dB point is 340 non-i.i.d. samples. The computational cost of using the Doppler interpolation compensation for a JDL processor is shown to be much less than that required by the Doppler warping compensation.

Chapter 5
Conclusion

This chapter serves three purposes. First, to present a summary of the work that has been conducted in each of the previous chapters. Secondly, to highlight the main conclusions drawn from the novel findings. Finally, to conclude the chapter with suggestions on future research options.

5.1 Summary

Chapter 1 described different kinds of radar systems, primarily the airborne monostatic radar and the airborne bistatic radar. The advantages and disadvantages of using an airborne bistatic radar, as well as the motivation of this work - to increase the probability of detecting targets employing stealth technology, are highlighted. Scaled measurements of a stealth target performed in an anechoic chamber at DASA, Bremen, provides very strong evidence that airborne bistatic radar may indeed be used to detect stealth targets, if the bistatic clutter can be properly suppressed. Assumptions made in this work are also stated.

Chapter 2 investigated the clutter Doppler range dependency in the Doppler-azimuth plane. Relationships between the clutter Doppler range dependency for a sidelooking airborne monostatic radar, a forward looking airborne monostatic radar and a forward looking airborne bistatic radar are established. In the Doppler-azimuth plane, clutter Doppler range dependency exists in both airborne monostatic and bistatic radar systems. However due to the look angles normally employed, clutter echoes for a sidelooking airborne monostatic radar appear to be range independent. Clutter echoes for a forward looking airborne monostatic radar and an airborne bistatic radar (for both sidelooking and forward looking) are in general range dependent. The change in range dependency fluctuates widely with azimuth angle for an airborne bistatic radar, but not as much for a forward looking airborne monostatic radar. It is also observed that the clutter Doppler range dependency depends on the bistatic radar configuration. Certain bistatic configurations can be chosen to minimise the range dependency.

Clutter Doppler range dependency will widen the clutter notch of the STAP processor, and cause slow-relative velocity targets to be suppressed, or even go undetected. A number of different methods can be used to mitigate the clutter Doppler range dependency. Among them, the derivative-based updating, Doppler warping, 2-D angle-Doppler compensation and the scaling method offer some form of Doppler compensation. The Derivative-based updating and scaling method may not be able to react to the widely fluctuating nature of bistatic clutter Doppler range dependency.

Chapter 3 begins with a description of the JDL processor, a reduced dimension angle-Doppler domain STAP processor used as the clutter suppression filter in this work. The peak clutter Doppler frequency difference between the training range gates and the range gate under test is determined using the proposed equation (3.11). Equation (3.11) is shown to be more robust to error in estimated parameters than equation (3.9), which is used in the Doppler warping and the ADC Doppler compensation. Doppler compensation in the angle-Doppler domain is carried out by interpolation of Doppler domain data. Angle-Doppler domain compensation is highly desirable when using the JDL processor, as it removes the need of performing Fourier transformations after each training range gate space-time Doppler compensation, and for every range gate under test. Power correction is used to compensate for the difference in range gates clutter echoes power, caused by the distance travelled and the beam pattern of the transmitting and receiving antenna.

While Doppler interpolation may be considered to be an approximation of the Doppler warping process, and hence likely to have a poorer performance than Doppler warping, it was noted that when using a particular range gate for training (range gate 29), Doppler interpolation outperforms Doppler warping in the region outside the clutter notch. This shows the limitation of Doppler warping when processing certain training data. The advantage of using 2-D ADC over Doppler warping is not significant in the cases considered here, as the training range gates used are in close vicinity to the range gate under test. Another advantage of performing Doppler compensation in the angular-Doppler domain is the ability to carry out different amounts of Doppler compensation in each of the two domains. Doppler warping and ADC are only capable of performing an actual Doppler compensation on the peak clutter echoes, compensation on other clutter echoes is only approximated. Separate Doppler bins compensation has shown to offer better processor performance when Doppler warping fails to make any obvious improvement. Tuned DFT is proposed to further reduce the dimension of the localized processing

region (LPR) clutter sample covariance matrix. By reducing scalloping loss, similar processor performance can be obtained with great reduction in computational cost.

In Chapter 4, the performance of the JDL processor using Doppler interpolation and power correction is analysed. Different parameters such as the number of Doppler bins used, M_f, the number of spatial bins used, N_a, the size of the DFT, D_f, errors in estimated parameters and the size of the load-to-clutter+white noise ratio (LCNR), are used to determine its influence over the processor performance. It is observed that processor performance of within 3 dB of the optimum performance is achieved when M_f is between 9 and 13. This observation may be different for other JDL processors, as the proposed processor performance is determined by the Doppler interpolation compensation process. Using alternate Doppler bins selection allows computational reduction, but with performance loss at the region outside the clutter notch, or same computational cost, but with better slow relative velocity target detection ability. Besides, using the tuned DFT, the number of spatial bins used by the Doppler interpolation processor, N_a can be reduced to 2 (with the number of antenna array element used, N = 8) when the spatial bins used are selected carefully. The accuracy of the interpolation process depends greatly on the size of the DFT, D_f, in relation with the amount of temporal pulse (M) used, and the interpolation method used. The size of the DFT processor, which in turn determines the number of temporal zero padding, Z, required, should be of size 2^N [i] (in order to apply the fast Fourier transformation) and very much greater than M.

Among the three estimated parameters examined, the processor performance is greatly affected by errors in the flight direction and position of the transmitter platform. It is also observed that the processor performance is not directly influenced by the absolute error value, as the mean IF loss is not symmetrical about the 0% error axis. Diagonal loading (decrease in clutter to noise ratio) is often used to make the processor robust to signal mismatch. Diagonal loading is used in this work to ensure that the clutter sample covariance matrix is not singular and to reduce the difference between the estimated and true clutter sample covariance matrix.

The effect of range ambiguity on Doppler compensation is studied. Bistatic clutter Doppler range dependency shows that different amounts of Doppler compensation are required for clutter echoes from different range distances but which fall in the same range gate. However, with the significant reduction of power with distance and transmitter beam pattern, Doppler compensation error caused by using a single Doppler compensation does not have any obvious

[i] where N is a positive real number

effect on the processor performance.

The assumption of having i.i.d. training samples is hardly fulfilled in this work. Training data obtained from the range dimension is not identical to each other even after Doppler compensation process, because of imperfect Doppler compensation. Greater Doppler compensation errors are experienced by training range gates further away from the range gate under test. As a result, training data from range gates nearest to the range gate under test (excluding the guard gates) should always be used first in the estimation of the clutter sample covariance matrix. Due to the limited number of suitable range gates available for clutter sample covariance matrix estimation, time dimension data is often required for the estimation process, even though they are not independent from each other. Simulation results show that, when using both range and time dimension training data, the number of samples required to reach the 3 dB point below the optimum processor performance is not directly proportional to the size of M_f (the size of the clutter sample covariance matrix). On the other hand, bigger M_f value seems to require lesser training data to obtain similar processor performance as those obtained using smaller M_f value, but at the expense of higher computational cost.

5.2 Suggestion on future research options

To conclude this thesis, a couple of suggestions on future research options are given.

As discussed in Section 3.7.1, the Doppler interpolation processor and the Doppler warping processor performance vary with the training data used. Further research into why the Doppler interpolation processor performs better than Doppler warping when using training data from range gate 29 should be carried out.

With the land area consisting of only less than 30% of the total earth surface area, it will be desirable to operate the airborne bistatic radar above sea/ocean surfaces. Sea clutter is known to be quite different from land clutter. Doppler compensation algorithms developed for the suppression of land clutter may not be suitable for sea clutter suppression. Further research may concentrate on studying Doppler compensation algorithms for suppression of sea clutter for an airborne bistatic radar system. In addition to this, clutter echoes from a coastal area, when the airborne bistatic radar system approaches the land from the sea or operating along the international sea boundary, may require different types of Doppler compensation algorithm.

Due to time constraints, the algorithm for separate bins compensation is not fully developed. Among all Doppler compensation algorithms currently available, separate bins compensation seems to be the only algorithm that offers the possibility of performing multiple Doppler compensations on each training range gate, at the same time. Multiple Doppler compensation plays an important role in clutter suppression when significant changes in clutter Doppler range dependency occur as the azimuth angle changes or when a wide mainbeam is used. This is because the clutter echoes from different azimuth angles, require different amounts of Doppler compensation. Further investigation on the clutter echoes relationship with each Doppler bin (due to the Fourier transform) may provide better insight on the precise amount of Doppler compensation required for each Doppler bin.

When using a small number of array elements (e.g. $N = 8$), the angular bins after Fourier transformation corresponds to wide angles of arrival. Increasing the number of array elements can be used to reduce the angle coverage by each of the angular bins. If the mainlobe and significant sidelobe [ii] clutter echoes are spread across two or more angular bins, different Doppler compensations may be required for each of those angular bins. This is because different angular bins correspond to different azimuth angles, which have clutter echoes with different range dependencies. Further exploiting the multiple Doppler compensations (in both angular and Doppler dimension) capability offered by the Doppler interpolation process, better JDL processor performance can be achieved.

The "rule of thumb" regarding the number of samples required for the estimation of the clutter sample covariance matrix is derived using i.i.d. samples. When collecting training data, either in range or time, or both dimensions, the training data are often correlated with each other (non-i.i.d.). Further analysis on the relationship between the number of samples required and the correlation between samples is required. For an airborne bistatic radar system, using the absolute minimum number of training data required will help to prevent widening of the clutter notch, caused by error in the Doppler compensation process. Reducing the training data required will also reduce the computational cost associated with forming the clutter sample covariance matrix, as well as the dwell time required, which will allow a faster scanning rate or narrower beamwidth.

The Doppler interpolation process is considered to more computational intensive than complex phasor multiplication used by Doppler warping. Computationally effective interpolation

[ii] for low mainlobe to sidelobe ratio

processes can be investigated to reduce the computational cost of the proposed Doppler interpolation processor.

Appendix A
Minimum variance estimator (MVE)

Consider a linear uniformly spaced beamformer, the beamformer output, in response to the antenna element inputs $s(n), s(n-1), \ldots, s(n-N+1)$, is given by

$$y(n) = \sum_{k=0}^{N-1} w_k^* s(n-k) \tag{A.1}$$

where $\mathbf{w}$ is the elemental weights of the beamformer, superscript $*$ is the conjugate operator and N is the number of antenna elements used.

For the special case of a sinusoidal excitation, the input at time t is given as

$$u(t) = e^{j\omega t} \tag{A.2}$$

where ω is the angular frequency of the excitation, which is normalised with respect to the sampling rate. For the case of the array illuminated by an isotropic source located in the far field, such that, at time t, a plane wave impinges on the array along a direction specified by the angle θ_0 with respect to the perpendicular to the array. Equation (A.1) is rewritten as

$$y(t) = u_0(t) \sum_{k=0}^{N-1} w_k^* e^{-jk\phi_0} \tag{A.3}$$

where the direction of arrival is defined by the electrical angle ϕ_0 that is related to the angle of incidence, $u_0(t)$ is the electrical signal picked up by the antenna element labelled 0 that is treated as the point of reference.

The constrained optimisation problem to be solved, may be stated as follows:

Find the optimum set of elemental weights $w_{o0}, w_{o1}, \ldots, w_{o,N-1}$ that minimises the mean square value of the beamformer output $y(t)$, subject to the linear constraint

$$\sum_{k=0}^{N-1} w_k^* e^{-jk\phi_0} = 1 \tag{A.4}$$

The beamformer is narrowband in the sense that its response needs to be constrained only at a single frequency. To solve this constrained optimisation problem, the method of Lagrange multipliers (see page 895 of [58]) is used. The real-valued cost function J that combines the two parts of the constrained optimisation problem is defined as

$$J = \sum_{k=0}^{N-1} \sum_{i=0}^{N-1} w_k^* w_i r(i-k) + \mathrm{Re}\Big[\lambda^*\Big(\sum_{k=0}^{N-1} w_k^* e^{-j\phi_0 k} - 1\Big)\Big] \tag{A.5}$$

where λ is a complex Lagrange multiplier. To solve for the optimum values of the elemental weights of the beamformer that minimise J. the gradient vector ΛJ is determined and set equal to zero. The kth element of the gradient vector ΛJ is given as

$$\Lambda_k J = 2 \sum_{i=0}^{N-1} w_i r(i-k) + \lambda^* e^{-j\phi_0 k} \tag{A.6}$$

Let w_{oi} be the ith element of the optimum weight vector $\mathbf{w}_o$. Then the condition for optimality of the beamformer is described by

$$\sum_{i=0}^{N-1} w_{oi} r(i-k) = -\frac{\lambda^*}{2} e^{-j\phi_0 k}, \qquad k = 0, 1, \ldots, N-1 \tag{A.7}$$

This system of N simultaneous equations defines the optimum values of the beamformer's elemental weights. Switching to matrix notation, the system of N simultaneous equations given in equation (A.7) is rewritten simply as

$$\mathbf{R}\mathbf{w}_o = -\frac{\lambda^*}{2}\mathbf{s}(\phi_0) \tag{A.8}$$

where $\mathbf{R}$ is the N-by-N correlation matrix, and $\mathbf{w}_o$ is the N-by-1 optimum weight vector of the constrained beamformer. The N-by-1 steering vector $\mathbf{s}(\phi_0)$ is defined by

$$\mathbf{s}(\phi_0) = [1, e^{-j\phi_0}, \ldots, e^{-j(N-1)\phi_0}]^T \tag{A.9}$$

Solving equation (A.8) for $\mathbf{w}_o$,

$$\mathbf{w}_o = -\frac{\lambda^*}{2}\mathbf{R}^{-1}\mathbf{s}(\phi_0) \tag{A.10}$$

where $\mathbf{R}^{-1}$ is the inverse of the covariance matrix $\mathbf{R}$, assuming that $\mathbf{R}$ is nonsingular.

From equation (A.4),

$$\mathbf{w}_o^H \mathbf{s}(\phi_0) = 1 \tag{A.11}$$

To eliminate λ^* from equation (A.10), Hermitian transpose is carried out on both side of equation (A.10) and postmultiplied by $\mathbf{s}(\phi_0)$. Then using the linear constraint of equation (A.11),

$$\lambda = -\frac{2}{\mathbf{s}^H(\phi_0)\mathbf{R}^{-1}\mathbf{s}(\phi_0)}. \tag{A.12}$$

Substituting equation (A.12) into equation (A.10), the optimum weight vector is given as

$$\mathbf{w}_o = \frac{\mathbf{R}^{-1}\mathbf{s}(\phi_0)}{\mathbf{s}^H(\phi_0)\mathbf{R}^{-1}\mathbf{s}(\phi_0)}. \tag{A.13}$$

Expressing the minimum mean-square value (average power) of the optimum beamformer output as the quadratic form

$$J_{min} = \mathbf{w}_o^H \mathbf{R} \mathbf{w}_o. \tag{A.14}$$

Substituting equation (A.13) into equation (A.14) and simplifying it,

$$J_{min} = \frac{1}{\mathbf{s}^H(\phi_0)\mathbf{R}^{-1}\mathbf{s}(\phi_0)} \tag{A.15}$$

Generalising the result and obtain an estimate of variance as a function of direction by formulating J_{min} as a function of ϕ, the MVE (spatial) power spectrum is defined as

$$S_{MVE}(\phi) = \frac{1}{\mathbf{s}^H(\phi_0)\mathbf{R}^{-1}\mathbf{s}(\phi_0)} \tag{A.16}$$

The MVE (spatial) power spectrum can be expanded into a spatial-temporal power spectrum by replacing the covariance with a space-time covariance matrix and replacing $\mathbf{s}(\phi_0)$ with $\mathbf{s}(\phi_0, \omega_0)$, where ω_0 is the angular frequency of interest.

Appendix B

Relative Doppler frequency, f_r, in term of the look direction of the array, $\cos\beta$

Relating the relative Doppler frequency, f_r (equation (2.3)) with the look direction of the array, $\cos\beta$, equation (2.5) is first solved for $\cos\varphi$. From equation (2.5)

$$\cos\beta = (\cos\varphi\cos\psi + \sqrt{1-\cos^2\varphi}\sin\psi)\cos\theta \quad \text{(B.1)}$$

$$\frac{\cos\beta}{\cos\theta} = \cos\varphi\cos\psi + \sqrt{1-\cos^2\varphi}\sin\psi \quad \text{(B.2)}$$

$$\frac{\cos\beta}{\cos\theta} - \cos\varphi\cos\psi = \sqrt{1-\cos^2\varphi}\sin\psi \quad \text{(B.3)}$$

$$\left(\frac{\cos\beta}{\cos\theta} - \cos\varphi\cos\psi\right)^2 = (1-\cos^2\varphi)\sin^2\psi \quad \text{(B.4)}$$

$$\left(\frac{\cos\beta}{\cos\theta}\right)^2 - 2\left(\frac{\cos\beta}{\cos\theta}\right)\cos\varphi\cos\psi + \cos^2\varphi\cos^2\psi = \sin^2\psi - \cos^2\varphi\sin^2\psi \quad \text{(B.5)}$$

$$\cos^2\varphi\sin^2\psi - 2\left(\frac{\cos\beta}{\cos\theta}\right)\cos\varphi\cos\psi + \cos^2\varphi\cos^2\psi + \left(\frac{\cos\beta}{\cos\theta}\right)^2 - \sin^2\psi = 0 \quad \text{(B.6)}$$

$$\cos^2\varphi(\sin^2\psi + \cos^2\psi) - 2\left(\frac{\cos\beta}{\cos\theta}\right)\cos\varphi\cos\psi + \left(\frac{\cos\beta}{\cos\theta}\right)^2 - \sin^2\psi = 0 \quad \text{(B.7)}$$

$$\cos^2\varphi - 2\left(\frac{\cos\beta}{\cos\theta}\right)\cos\varphi\cos\psi + \left(\frac{\cos\beta}{\cos\theta}\right)^2 - \sin^2\psi = 0 \quad \text{(B.8)}$$

$$\cos\varphi = \frac{2\left(\frac{\cos\beta}{\cos\theta}\right)\cos\varphi\cos\psi \pm \sqrt{\left(2\left(\frac{\cos\beta}{\cos\theta}\right)\cos\varphi\cos\psi\right)^2 - 4\left(\left(\frac{\cos\beta}{\cos\theta}\right)^2 - \sin^2\psi\right)}}{2} \quad \text{(B.9)}$$

$$\cos\varphi = \frac{\cos\beta}{\cos\theta}\cos\psi \pm \sqrt{\left(\frac{\cos\beta}{\cos\theta}\right)^2 \cos^2\psi - \left(\frac{\cos\beta}{\cos\theta}\right)^2 + \sin^2\psi} \quad \text{(B.10)}$$

Substituting equation (2.4) into equation (2.3)

$$f_r = \cos\varphi\cos\theta \quad \text{(B.11)}$$

Substituting equation (B.10) into equation (B.11)

$$f_r = \cos\theta\left(\frac{\cos\beta}{\cos\theta}\cos\psi \pm \sqrt{\left(\frac{cos\beta}{\cos\theta}\right)^2 \cos^2\psi - \left(\frac{\cos\beta}{\cos\theta}\right)^2 + \sin^2\psi}\right) \quad \text{(B.12)}$$

$$f_r = \cos\beta\cos\psi \pm \cos\theta\sqrt{\left(\frac{\cos\beta}{\cos\theta}\right)^2 \cos^2\psi - \left(\frac{\cos\beta}{\cos\theta}\right)^2 + \sin^2\psi} \quad \text{(B.13)}$$

$$f_r = \cos\beta\cos\psi \pm \sqrt{\cos^2\beta\cos^2\psi - \cos^2\beta + \cos^2\theta\sin^2\psi} \quad \text{(B.14)}$$

$$f_r - \cos\beta\cos\psi = \pm\sqrt{\cos^2\beta\cos^2\psi - \cos^2\beta + \cos^2\theta\sin^2\psi} \quad \text{(B.15)}$$

$$(f_r - \cos\beta\cos\psi)^2 = \cos^2\beta\cos^2\psi - \cos^2\beta + \cos^2\theta\sin^2\psi \quad \text{(B.16)}$$

$$f_r^2 - 2f_r\cos\beta\cos\psi + \cos^2\beta\cos^2\psi = \cos^2\beta\cos^2\psi - cos^2\beta + \cos^2\theta\sin^2\psi \quad \text{(B.17)}$$

$$f_r^2 - 2f_r\cos\beta\cos\psi + cos^2\beta - \cos^2\theta\sin^2\psi = 0 \quad \text{(B.18)}$$

$$f_r = \frac{2\cos\beta\cos\psi \pm \sqrt{(2\cos\beta\cos\psi)^2 - 4(cos^2\beta - \cos^2\theta\sin^2\psi)}}{2} \quad \text{(B.19)}$$

$$f_r = \cos\beta\cos\psi \pm \sqrt{(\cos\beta\cos\psi)^2 - (cos^2\beta - \cos^2\theta\sin^2\psi)} \quad \text{(B.20)}$$

Appendix C
Clutter Model

The geometry of an airborne bistatic radar is shown in Figure 2.8. For sensor at x_n, y_n, z_n, the received signal is given as

$$\begin{aligned} s_r(t) &= A_r(\varphi_t, \theta_t, \varphi_r, \theta_r) \exp\Bigg[(j\frac{2\pi}{\lambda}(v_t mT\cos(\varphi_t - \delta_t)\cos\theta_t \\ &\quad + ((x_n + V_r mT)\cos(\varphi_r - \delta_r) + y_n \sin\varphi_r)\cos\theta_r) - z_n \sin\theta_r\Bigg], \\ &\quad m = 1 \ldots M \qquad n = 1 \ldots N \end{aligned} \tag{C.1}$$

where N is the number of array elements.

Since the received clutter echoes are a sum over a larger number of scatterer, they are asymptotically Gaussian. A_r is a circular complex Gaussian-distributed variable (Gaussian amplitude and uniformly distributed phase).

The time delay for sample m to reach the receiver is given as:

$$\begin{aligned} \Phi^{(t)}_{m,k}(\varphi_t, \theta_t, \varphi_r, \theta_r) = \exp\Bigg[j\frac{2\pi}{\lambda}(v_t\cos(\varphi_t - \delta_t)\cos\theta_t \\ + v_r\cos(\varphi_r - \delta_r)\cos\theta_r)(m + l - 1)T\Bigg], l = 1 \ldots L - 1 \end{aligned} \tag{C.2}$$

where L is the number of time dimension data snapshots.

While the extra time delay taken to reach n-th sensor with respect to the sensor at the origin is given as:

$$\Phi^{(s)}_n(\varphi_r, \theta_r) = \exp\left[j\frac{2\pi}{\lambda}(x_n\cos\varphi_r + y_n\sin\varphi_r)\cos\theta_r - z_n\sin\theta_r)\right] \tag{C.3}$$

The clutter model is given as

$$c_{n,m,k} = \int_{\varphi_r=0}^{2\pi} A_r(\varphi_t, \theta_t, \varphi_r, \theta_r) G(\varphi_t, \theta_t) L(\varphi_r, \theta_r) \\ D(\varphi_r, \theta_r) \Phi_{k,m}^{(t)}(\varphi_t, \theta_t, \varphi_r, \theta_r) \Phi_n^{(s)}(\varphi_r, \theta_r) d\varphi \tag{C.4}$$

where $G(\varphi_t, \theta_t))$ stands for the transmitter directivity pattern, $L(\varphi_r, \theta_r))$ stands for the reflectivity of the ground which is general range dependent, while $D(\varphi_r, \theta_r))$ stands for the sensors directivity patterns and is given as

$$\begin{aligned} D(\varphi_r, \theta_r) &= 0.5(1 + \cos(2(\varphi_r - \varphi_0))) \\ & \quad 0.5(1 + \cos(2(\theta_r - \theta_0))) \end{aligned} \tag{C.5}$$

where the angle φ_0 and θ_0 denote the direction of the maximum of the sensor pattern.

Appendix D
Doppler frequency difference between range gates

The Doppler frequency difference between the range gate under test and the training range gate, is determined using both pre-known parameters and the received data.

Using only the pre-known parameters, the Doppler frequency difference is given as

$$\Delta_f = f_k^d - f_r^d \tag{D.1}$$

where f_k^d and f_r^d are the calculated clutter Doppler frequency (at a particular look direction) from range gates k and r respectively. Equation (D.1) does not provide a good estimation of the Doppler frequency difference as it does not take into account the errors that may exist in the pre-known parameters.

In order to consider the errors in the estimation of the pre-known parameters, an extra term $\tilde{f}_K^d$ (obtained from the received data) is added to equation (D.1), which can now be expressed as follow

$$\begin{aligned} \Delta_f &= \frac{\tilde{f}_k^d}{f_k^d}(f_k^d - f_r^d) \\ \Delta_f &= \tilde{f}_k^d(\frac{f_k^d - f_r^d}{f_k^d}) \\ \Delta_f &= \tilde{f}_k^d(1 - \frac{f_r^d}{f_k^d}) \end{aligned} \tag{D.2}$$

where $\tilde{f}_k^d$ is the estimated clutter Doppler frequency (at a particular look direction) from range gate k using the received data. If there is not error in the pre-known parameters ($\frac{\tilde{f}_k^d}{f_k^d} = 1$), and equation (D.2) is equivalent to equation (D.1).

Appendix E
Errors in pre-known parameters for calculation of Doppler frequency difference between range gates

Equation (3.11) is considered to be more robust against errors in pre-known parameters than equation (3.9) as it uses part of the received data. The errors in pre-known parameters are generally caused by sudden change in the transmitter's movement (e.g. acceleration of transmitter platform) which is not communicated to the receiver on time. Such errors include error in the transmitter's velocity, flight direction and position. Error in the transmitter's velocity is used here to develop the equations (3.11) and (3.9) with relation to the error in pre-known parameter. It is assumed that there is no other errors in the pre-known parameters (all parameters are constant except the transmitter velocity).

From equation (3.11),

$$\Delta_f = \tilde{f}_k^d \left(1 - \frac{f_r^d}{f_k^d} \right) \tag{E.1}$$

where $\tilde{f}_k^d$, f_r^d and f_k^d are the estimated clutter Doppler frequency from range gate k using received data, the calculated clutter Doppler frequency from range gates r and k respectively.

$$f_r^d = \frac{v_T \cos(\varphi_{t,r} - \delta_t) \cos\theta_{t,r} + v_R \cos(\varphi_r - \delta_r) \cos\theta_{r,r}}{\lambda} \tag{E.2}$$

and

$$f_k^d = \frac{v_T \cos(\varphi_{t,k} - \delta_t) \cos\theta_{t,k} + v_R \cos(\varphi_r - \delta_r) \cos\theta_{r,k}}{\lambda} \tag{E.3}$$

the angles $\varphi_{t,r}$, $\varphi_{t,k}$, $\theta_{t,r}$ and $\theta_{t,k}$ are the transmit azimuth and depression angles from range gates r and k respectively. The scalar φ_r is the clutter azimuth angle of arrival, $\theta_{r,r}, \theta_{r,k}$ are the depression angles of arrival from range gates r and k respectively. The scalars δ_t and δ_r denote the flight directions of the transmitter and receiver respectively (see Figure 2.8).

In order to simplify the equations (E.2) and (E.3), we let

$$C_{Tr} = \cos(\varphi_{t,r} - \delta_t)\cos\theta_{t,r} \tag{E.4}$$

$$C_{Rr} = v_R\cos(\varphi_r - \delta_r)\cos\theta_{r,r} \tag{E.5}$$

$$C_{Tk} = \cos(\varphi_{t,k} - \delta_t)\cos\theta_{t,k} \tag{E.6}$$

$$C_{Rk} = v_R\cos(\varphi_r - \delta_r)\cos\theta_{r,k} \tag{E.7}$$

then substitute equations (E.4) - (Equation E.7) into equations (E.2) and (E.3), finally equations (E.2) and (E.3) in term of C_{Tr}, C_{Rr}, C_{Tk} and C_{Rk} and then used to express equation (E.1) as follow

$$\Delta_f = \tilde{f}_k^d(1 - \frac{v_T C_{Tr} + C_{Rr}}{v_T C_{Tk} + C_{Rk}}) \tag{E.8}$$

Differentiating Δ_f with respect to v_T, we obtain

$$\begin{aligned}\frac{\mathrm{d}\Delta_f}{\mathrm{d}v_T} &= \frac{\mathrm{d}\tilde{f}_k^d}{\mathrm{d}v_T} - \frac{\mathrm{d}\frac{\tilde{f}_k^d(v_T C_{Tr}+C_{Rr})}{v_T C_{Tk}+C_{Rk}}}{\mathrm{d}v_T} \\ \frac{\mathrm{d}\Delta_f}{\mathrm{d}v_T} &= -\frac{\mathrm{d}\frac{\tilde{f}_k^d(v_T C_{Tr}+C_{Rr})}{v_T C_{Tk}+C_{Rk}}}{\mathrm{d}v_T}.\end{aligned} \tag{E.9}$$

Using differentiation of quotient of two functions:

$$\text{if}\, y = \frac{u}{v},\ \frac{\mathrm{d}y}{\mathrm{d}x} = \frac{v\frac{\mathrm{d}u}{\mathrm{d}x} - u\frac{\mathrm{d}v}{\mathrm{d}x}}{v^2} \tag{E.10}$$

where u and v are functions of x.

$$\frac{\mathrm{d}\Delta_f}{\mathrm{d}v_T} = -\left(\frac{(v_T C_{Tk} + C_{Rk})\frac{\mathrm{d}(\tilde{f}_k^d(v_T C_{Tr}+C_{Rr}))}{\mathrm{d}v_t} - \tilde{f}_k^d(v_T C_{Tr} + C_{Rr})\frac{\mathrm{d}(v_T C_{Tk}+C_{Rk})}{\mathrm{d}v_T}}{(v_T C_{Tk} + C_{Rk})^2}\right)$$

$$\frac{\mathrm{d}\Delta_f}{\mathrm{d}v_T} = -\left(\frac{(v_T C_{Tk} + C_{Rk})(\frac{\mathrm{d}(\tilde{f}_k^d v_T C_{Tr})}{\mathrm{d}v_t} + \frac{\mathrm{d}(\tilde{f}_k^d C_{Rr})}{\mathrm{d}v_t}) - \tilde{f}_k^d(v_T C_{Tr} + C_{Rr})(\frac{\mathrm{d}(v_T C_{Tk})}{\mathrm{d}v_T} + \frac{\mathrm{d}(C_{Rk})}{\mathrm{d}v_T})}{(v_T C_{Tk} + C_{Rk})^2}\right)$$

$$\frac{\mathrm{d}\Delta_f}{\mathrm{d}v_T} = -\left(\frac{(v_T C_{Tk} + C_{Rk})\frac{\mathrm{d}(\tilde{f}_k^d v_T C_{Tr})}{\mathrm{d}v_t} - \tilde{f}_k^d(v_T C_{Tr} + C_{Rr})\frac{\mathrm{d}(v_T C_{Tk})}{\mathrm{d}v_T}}{(v_T C_{Tk} + C_{Rk})^2}\right)$$

$$\frac{\mathrm{d}\Delta_f}{\mathrm{d}v_T} = -\left(\frac{(v_T C_{Tk} + C_{Rk})\tilde{f}_k^d C_{Tr} - \tilde{f}_k^d(v_T C_{Tr} + C_{Rr})C_{Tk}}{(v_T C_{Tk} + C_{Rk})^2}\right)$$

$$\frac{\mathrm{d}\Delta_f}{\mathrm{d}v_T} = -\left(\frac{\tilde{f}_k^d C_{Tr}(v_T C_{Tk} + C_{Rk}) - \tilde{f}_k^d C_{Tk}(v_T C_{Tr} + C_{Rr})}{(v_T C_{Tk} + C_{Rk})^2}\right)$$
$$\frac{\mathrm{d}\Delta_f}{\mathrm{d}v_T} = -\tilde{f}_k^d\left(\frac{C_{Tr}(v_T C_{Tk} + C_{Rk}) - C_{Tk}(v_T C_{Tr} + C_{Rr})}{(v_T C_{Tk} + C_{Rk})^2}\right). \tag{E.11}$$

From equation (3.9)

$$f_s(r,k) = \tilde{f}_k^d - f_r^d \tag{E.12}$$

Using equations (E.4), (E.5) and (E.2) into equation (E.12),

$$f_s(r,k) = \tilde{f}_k^d - \frac{v_T C_{Tr} + C_{Rr}}{\lambda}. \tag{E.13}$$

If we differentiates $f_s(r,k)$ with respect to v_T, we obtain

$$\frac{\mathrm{d}f_s(r,k)}{\mathrm{d}v_T} = \frac{\mathrm{d}\tilde{f}_k^d}{\mathrm{d}v_T} - \frac{1}{\lambda}\frac{\mathrm{d}(v_T C_{Tr} + C_{Rr})}{\mathrm{d}v_T}$$
$$\frac{\mathrm{d}f_s(r,k)}{\mathrm{d}v_T} = -\frac{1}{\lambda}\frac{\mathrm{d}(v_T C_{Tr})}{\mathrm{d}v_T} - \frac{1}{\lambda}\frac{\mathrm{d}(C_{Rr})}{\mathrm{d}v_T}$$
$$\frac{\mathrm{d}f_s(r,k)}{\mathrm{d}v_T} = -\frac{C_{Tr}}{\lambda}. \tag{E.14}$$

Now, let the function $f_{\Delta_f}(v_T) = \Delta_f$, using Taylor series (taking only the first order differentiation into account)

$$f_{\Delta_f}(v_T + \Delta v_T) = f_{\Delta_f}(v_T) + \frac{\mathrm{d}f_{\Delta_f}(v_T)}{\mathrm{d}v_T}\cdot\Delta v_T$$
$$f_{\Delta_f}(v_T + \Delta v_T) - f_{\Delta_f}(v_T) = \frac{\mathrm{d}f_{\Delta_f}(v_T)}{\mathrm{d}v_T}\cdot\Delta v_T$$
$$|\Delta E_{\Delta_f}| = |\frac{\mathrm{d}f_{\Delta_f}(v_T)}{\mathrm{d}v_T}|\cdot|\Delta v_T|$$
$$|\Delta E_{\Delta_f}| = |-\tilde{f}_k^d\left(\frac{C_{Tr}(v_T C_{Tk} + C_{Rk}) - C_{Tk}(v_T C_{Tr} + C_{Rr})}{(v_T C_{Tk} + C_{Rk})^2}\right)|\cdot|\Delta v_T| \tag{E.15}$$

where $|\Delta E_{\Delta_f}|$ is the magnitude of the error in estimating the Doppler frequency difference between range gates r and k, due to error in v_T, when using equation (3.11).

Applying Taylor series to function $f_{f_s(r,k)}(v_T)$, where $f_{f_s(r,k)}(v_T) = f_s(r,k)$, the magnitude of

the error in estimating the Doppler frequency difference between range gates r and k becomes

$$|\Delta E_{f_s(r,k)}| = |\frac{\mathrm{d}\, f_{f_s(r,k)}(v_T)}{\mathrm{d}\, v_T}| \cdot |\Delta v_T|$$
$$|\Delta E_{f_s(r,k)}| = |-\frac{C_{Tr}}{\lambda}| \cdot |\Delta v_T|. \tag{E.16}$$

Appendix F
Derivation of $x_P(g)$

The transmitter-target/scatterer-receiver range measured by a bistatic radar is the sum, $R_{sT} + R_{sR} = d(g)$, (see to Figure 2.8, and defined in equation (3.27)) = $2a_e$. This sum locates the target/scatterer somewhere on the surface of an ellipsoid, the foci of which are the transmitting and receiving locations, separated by the baseline L_e (defined in equation (3.24)), and with major axis of $2a_e$. The ellipsoid is defined by the parameters, a_e, b_e, c_e and L_e, and is the isorange ellipsoid of constant range sum $2a_e$ as shown in Figure F.1 [5].

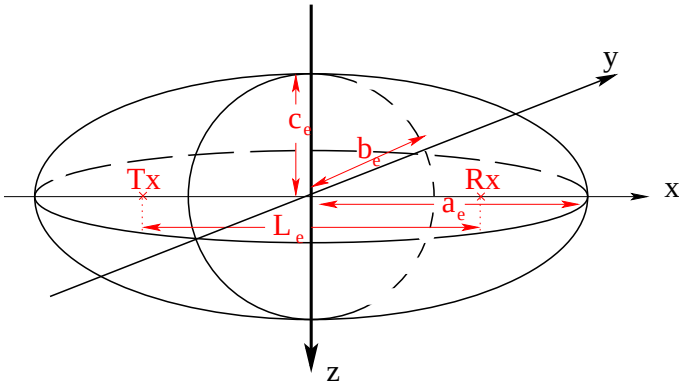

Figure F.1: *Ellipsoid of constant range sum*

Any point on the ellipsoid can be expressed by

$$\frac{x_p(g)}{a_e} + \frac{y_p(g)}{b_e} + \frac{z_p(g)}{c_e} = 1 \tag{F.1}$$

where $x_p(g), y_p(g)$ and $z_p(g)$ are the x, y and z-axes coordinate of the P scatterer from range gate g. Let x_{RP} be the x-axis distance from the receiver,

$$x_{RP} = x_p(g) - \frac{L}{2} \tag{F.2}$$

and

$$a_e = \frac{d(g)}{2} \tag{F.3}$$

$$b_e = c_e = \frac{1}{2}\sqrt{d(g)^2 - L^2}. \tag{F.4}$$

Assuming that the transmitter and receiver are aligned on the flight direction (x-axis), then

$$y_p(g) = x_{RP}\tan(\varphi_r). \tag{F.5}$$

With the transmitter and the receiver are travelling parallel to the ground,

$$z_p(g) = H_T = H_R. \tag{F.6}$$

Substitute equation (F.2) into equation (F.5), we obtain

$$y_p(g) = (x_p(g) - \frac{L}{2})\tan(\varphi_r) \tag{F.7}$$

Finally, we substitute equations (F.3), (F.4), (F.6) and (F.7) into equation (F.1) and solve for $x_p(g)$, it yields the following expression

$$x_P(g) = \frac{1}{2}\left(\frac{4\frac{tan(\varphi_r)^2 L}{d(g)^2 - L^2}}{(4\frac{1}{d(g)^2} + 4\frac{\tan(\varphi_r)^2}{d(g)^2 - L^2})} \pm \begin{matrix} (-\frac{\pi}{2} \le \varphi_r \le \frac{\pi}{2}) \\ (\frac{\pi}{2} < \varphi_r < \frac{3\pi}{2}) \end{matrix} \right.$$
$$\left. \frac{4\frac{\sqrt{-2dtanL^2 - 4d(g)^2 H_R^2 + d(g)^4 - 2d(g)^2 L^2 + L^4 \tan(\varphi_r)^2 + 4L^2 H_R^2 + L^4 - 4dtan\, H_R^2 + dtan\, d(g)^2)}}{d(g)(-d(g)^2 + L^2)}}{(\frac{4}{d(g)^2} + 4\frac{\tan(\varphi_r)^2}{d(g)^2 - L^2})} \right) \tag{F.8}$$

Appendix G
Publications

- K.P. Ong and B. Mulgrew. *"Doppler compensation for JDL for airborne bistatic radar"*. Proceedings of the 2002 IEEE Sensor Array and Multichannel Signal Processing Workshop, SAM2002), pp. 82-86, Rosslyn, VA, USA, August 4-6 2002
- K.P. Ong and B. Mulgrew. *"Angular bin compression for joint domain localised (JDL) processor"*. Proceedings of the twelfth International conference on antennas and propagation, ICAP 2003, pp. 353-356, University of Exeter, UK, March 31 - April 3 2003

DOPPLER COMPENSATION FOR JDL FOR AIRBORNE BISTATIC RADAR

K. P. Ong and B. Mulgrew

University of Edinburgh
Dept. of Electronics and Electrical Engineering
Mayfield Rd., Edinburgh, EH9 3JL, UK
email: kpo@ee.ed.ac.uk, B.Mulgrew@ee.ed.ac.uk

ABSTRACT

In airborne bistatic radar the clutter Doppler is range dependent. STAP processor using training data from other range gate will experience widening of clutter notch. Widening of the clutter notch causes a major problem in detecting slow moving target. In this paper, Doppler compensation using interpolation in the angle-Doppler domain, for joint domain localised processor (JDL) is proposed. Comparison is made with Doppler compensated processor proposed by Kreyenkamp and Klemm [1]. Significant improvement in processor performance is observed across the whole frequency spectrum.

1. INTRODUCTION

Airborne bistatic radar has in recent years, attracted the interest of researchers from different part of the world because of its capability to reduce the probability of the transmitter being intercepted and directional jamming at the receiver [2]. However, being an airborne system, it is by its nature down looking and hence suffers from strong and complex clutter returns. The challenge is to suppress these clutter returns without diminishing the target's echo.

Attempt to remove the clutter returns using one dimensional filtering performed in the Doppler domain, can only achieve adequate rejection over the full spectral bandwidth of the clutter at the expense of attenuating echo from slow moving target. However through the use of adaptive two dimensional filtering (in both spatial and temporal domains), space-time adaptive processing (STAP) can achieve far better clutter suppression performance.

For sidelooking monostatic radar, STAP algorithms are generally performed under ideal conditions; where the clutter spectra in angle-Doppler space is independent of range and is therefore stationary. This allows the estimation of the clutter covariance matrix to be performed using training data obtained in the range dimension. In this ideal situation, the clutter ridge is narrow in angle-Doppler space, hence enable slow moving target to be detected.

However, in airborne bistatic radar the clutter spectra is range dependent. This requires the weights of STAP processor for individual range gate to be computed using their respective range gate clutter covariance matrix $\mathbf{Q}$, which is not obtainable in practice. In the existing literature, these estimated covariance matrix $\widehat{\mathbf{Q}}$ are obtained using training data from other range gates, assuming that its statistics do not change significantly. Difference in the data statistics will result in the widening of the clutter notch, which will increase the system's minimum detectable target's velocity.

In this paper, power correction and Doppler compensation for joint domain localised (JDL) processor is proposed. Doppler compensation through interpolation in angle-Doppler domain, allows clutter from different angles and different frequencies to be Doppler compensated by different amounts. Such multiple Doppler compensation just isn't feasible using the space-time Doppler compensation method suggested by Kreyenkamp.

2. POWER CORRECTION

For any radar system, the power of the clutter/interference differs from range gate to range gate due to the difference in distance travelled. However for airborne bistatic radar, the situation becomes more complicate. The clutter/interference power also changes with direction of arrival in each range gate.

The power of the clutter/interference arriving at the testing range gate, X is estimated by multiplying the power of the clutter/interference arriving at the training range gate, Y with the power correction, P_c.

$$\begin{aligned} P_c &= \frac{P_{r,X}}{P_{r,Y}} \\ &= \frac{\frac{P_t G(\varphi_{t,X},\theta_{t,X}) D(\varphi_{r,X},\theta_{r,X}) L(\varphi_{r,X},\theta_{r,X})}{(4\pi)^3 k T_s B_n R_{sT,X}^2 R_{sR,X}^2}}{\frac{P_t G(\varphi_{t,Y},\theta_{t,Y}) D(\varphi_{r,Y},\theta_{r,Y}) L(\varphi_{r,Y},\theta_{r,Y})}{(4\pi)^3 k T_s B_n R_{sT,Y}^2 R_{sR,Y}^2}} \end{aligned} \quad (1)$$

This work was funded and supported by BAE Systems (Edinburgh).

where P_t stands for transmitted power, $G(.)$ stands for the transmit directivity pattern, $D(.)$ stands for the sensors directivity patterns, $L(.)$ stands for the reflectivity of the ground, kT_sB_n is the thermal-noise power and $R_{sT,Y}$, $R_{sR,Y}$, $R_{sT,X}$ and $R_{sR,X}$ are distance between transmitter(T) / receiver(R) and the ground from range gate Y / X respectively.

Assuming that the sensors directivity pattern and the reflectivity of the ground do not change significantly with near by range gate and $G(\varphi_{t,X}, \theta_{t,X})$ = 1 (since the mainlobe is pointing at that angle),

$$P_c = \frac{\frac{1}{R^2_{sT,X}R^2_{sR,X}}}{\frac{G(\varphi_{t,Y},\theta_{t,Y})}{R^2_{sT,Y}R^2_{sR,Y}}} = \frac{R^2_{sT,Y}R^2_{sR,Y}}{G(\varphi_{t,Y},\theta_{t,Y})R^2_{sT,X}R^2_{sR,X}} \quad (2)$$

3. DOPPLER COMPENSATION

For airborne bistatic radar, the clutter Doppler is range dependent and as a result, the training data does not have same clutter/interference statistics as that of the testing data. Some form of Doppler compensation is hence required before any clutter filter can be designed using the training clutter covariance matrix $\widehat{\mathbf{Q}}$.

The difference in clutter Doppler frequency, Δ_f between testing range gate, X and training range gate, Y is

$$\Delta_f = f_{d,Y}\left(1 - \frac{v_T\cos(\varphi_{t,X}-\delta_t)\cos\theta_{t,X} + v_R\cos(\varphi_r-\delta_r)\cos\theta_{r,X}}{v_T\cos(\varphi_{t,Y}-\delta_t)\cos\theta_{t,Y} + v_R\cos(\varphi_r-\delta_r)\cos\theta_{r,Y}}\right) \quad (3)$$

where $f_{d,Y}$ (obtained using minimum variance estimator) is the clutter Doppler frequency of clutter arriving from angles $\varphi_{r,Y}$ and $\theta_{r,Y}$, while δ_t and δ_r denote the flight directions of the transmitter and receiver respectively.

The azimuth, φ and depression, θ angles can be expressed by clutter P co-ordinates x_p, y_p and slant range R_{sT}, R_{sR}, using equation (4)-(10) shown on the top of next page.

Doppler compensation process is achieved by transforming the clutter data (with power correction), $\mathbf{Y}_{\mathrm{P}k}$ into $\mathbf{Y}_{\mathrm{F}k}$ (in angle-Doppler domain) by applying Fourier transform with zero padding in both space and time, interpolation of clutter data and re-addressing the Doppler bin indices. The angle-Doppler domain data matrix $\mathbf{Y}_{\mathrm{F}}$, $N_a \times M_f \times K$, represents the data at the M_f Doppler bins, N_a angle bins and K data snapshots from the training range gate.

[1] assume that transmitter and receiver is on the same flight path

Interpolation of data allows magnitude of signal with Doppler frequency between the Doppler bins to be determined. Using interpolation such as the cubic spline interpolation, a smooth fit between Doppler bins is achieved. An illustration of the shifting process is given in Figure 1.

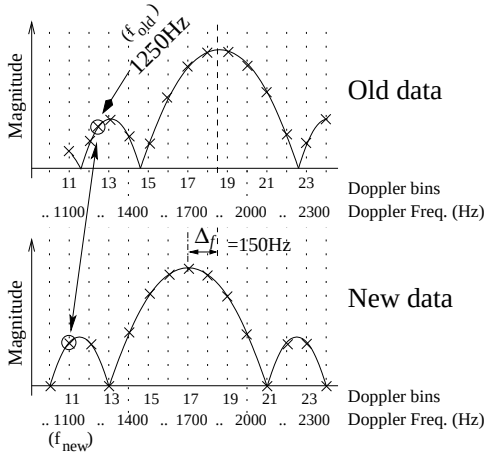

Fig. 1. Illustration of frequency shifting

Let the Doppler frequency f_{new} be the frequency of interest, and its magnitude be $y_{\mathrm{F}new}$. The steps to determine $y_{\mathrm{F}new}$ is given as follows:

1) The corresponding Doppler frequency from the old data, f_{old} is given as

$$f_{new} = f_{old} - \Delta_f; \quad (11)$$

2) Given the magnitude of Doppler frequencies around f_{old}, the magnitude of f_{old}, $y_{\mathrm{F}old}$ could be found using interpolation;

3) The shifting process to Doppler frequency f_{new} is completed by assigning $y_{\mathrm{F}new} = y_{\mathrm{F}old}$.

Doppler compensation process is completed when frequency shifting of the whole data block is carried out.

4. JOINT DOMAIN LOCALISED (JDL) PROCESSOR

In practice, only the few angle-bins covering the angle section centred around the look direction (where most of the transmitted energy is contained) is of interest. On the other hand, all Doppler-bins must be analysed as the target Doppler frequency is unknown to the processor. The angle-Doppler bins of the training data,$\mathbf{Y}_{\mathrm{F}k}$ are divided to form L sub-groups, $\mathbf{Y}_{\mathrm{L}l,k}$ of angle-Doppler bins around the look

$$\Delta_f = f_{d_l Y}\left(1 - \frac{v_T(\frac{x_{TP}(X)}{R_{sT}(X)}\cos(\delta_t) + \frac{y_P(X)}{R_{sT}(X)}\sin(\delta_t)) + v_R(\frac{x_{RP}(X)}{R_{sR}(X)}\cos(\delta_r) + \frac{y_P(X)}{R_{sR}(X)}\sin(\delta_r))}{v_T(\frac{x_{TP}(Y)}{R_{sT}(Y)}\cos(\delta_t) + \frac{y_P(Y)}{R_{sT}(Y)}\sin(\delta_t)) + v_R(\frac{x_{RP}(Y)}{R_{sR}(Y)}\cos(\delta_r) + \frac{y_P(Y)}{R_{sR}(Y)}\sin(\delta_r))}\right) \tag{4}$$

where

$$y_P(g) = {x_{RP}}^1(g)\tan(\varphi_r) \qquad g \in \{X, Y\} \tag{5}$$

$$x_{RP}(g) = x_P(g) - \frac{L}{2} - x_R \tag{6}$$

$$x_{TP}(g) = x_P(g) - \frac{L}{2} - x_T \tag{7}$$

$$L = \sqrt{(x_T - x_R)^2 + (y_T - y_R)^2 + (z_T - z_R)^2} \tag{8}$$

$$x_P(g) = \frac{1}{2}\left(\begin{array}{ll} \frac{4\frac{tan(\varphi_r)^2 L}{Dist(g)^2 - L^2}}{(4\frac{1}{Dist(g)^2} + 4\frac{\tan(\varphi_r)^2}{Dist(g)^2 - L^2})} \pm & (-\frac{\pi}{2} \le \varphi_r \le \frac{\pi}{2}) \\ \frac{4\frac{\sqrt{-2Dist(g)^2 tan(\varphi_r)^2 L^2 - 4Dist(g)^2 H_R^2 + Dist(g)^4 - 2Dist(g)^2 L^2 + L^4 \tan(\varphi_r)^2 + 4L^2 H_R^2 + L^4 - 4\tan(\varphi_r)^2 Dist(g)^2 H_R^2 + \tan(\varphi_r)^2 Dist(g)^4)}}{Dist(g)(-Dist(g)^2 + L^2)}}{(4\frac{1}{Dist(g)^2} + 4\frac{\tan(\varphi_r)^2}{Dist(g)^2 - L^2})} & (\frac{\pi}{2} < \varphi_r < \frac{3\pi}{2}) \end{array}\right) \tag{9}$$

$$Dist(g) = c\,Time(g) \tag{10}$$

while $Time(g)$ is the time taken for the signal to hit the ground in range gate g and back to the receiver.

---

direction φ_r, called the localised processing regions (LPR) [3] as shown in Figure 2.

The indices k in the data matrix is take out in order to simplify the expression. The divided training data $\mathbf{Y}_{\mathrm{L}l}$ and the clutter/interference covariance matrix, $\widehat{\mathbf{Q}}_{\mathrm{L}l}$ ($N_{a0}M_{fl} \times N_{a0}M_{fl}$) becomes

$$\mathbf{Y}_{\mathrm{L}l} = \begin{pmatrix} y^{\mathrm{F}}{}_{r,u_l} & y^{\mathrm{F}}{}_{r,u_l+1} & \cdots & y^{\mathrm{F}}{}_{r,u_l+M_{fl}-1} \\ y^{\mathrm{F}}{}_{r+1,u_l} & y^{\mathrm{F}}{}_{r+1,u_l+1} & \cdots & y^{\mathrm{F}}{}_{r+1,u_l+M_{fl}-1} \\ \vdots & \vdots & \ddots & \vdots \\ y^{\mathrm{F}}{}_{r+N_{a0}-1,u_l} & y^{\mathrm{F}}{}_{r+N_{a0}-1,u_l+1} & \cdots & y^{\mathrm{F}}{}_{r+N_{a0}-1,u_l+M_{fl}-1} \end{pmatrix} \tag{12}$$

where

$$l = 1 \ldots L \tag{13}$$

$$r = \text{looking angle bin} - \mathrm{int}(\frac{N_{a0}}{2}) \tag{14}$$

$$u_l = (\sum_{i=1}^{l-1} M_{fi}) + 1 \tag{15}$$

and

$$\widehat{\mathbf{Q}}_{\mathrm{L}l} = \frac{1}{K}\sum_{k=0}^{K-1} \mathrm{Vec}(\mathbf{Y}_{\mathrm{L}l,k})\mathrm{Vec}(\mathbf{Y}_{\mathrm{L}l,k})^H \tag{16}$$

respectively. $\mathbf{Y}_{\mathrm{L}l}$ is a $N_{a0} \times M_{fl}$ matrix, N_{a0} is the number of angular bin, M_{fl} is the number of Doppler bins in the lth

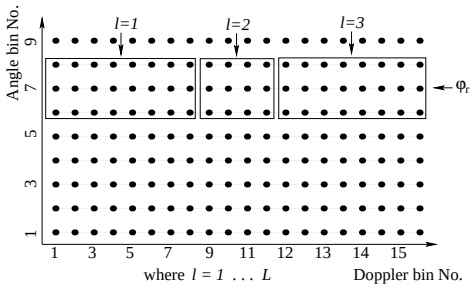

Fig. 2. An example of localised processing regions

group, Vec(·) is a matrix operation that stacks the columns of a matrix under each other to form a new column vector and ^{H} denotes conjugate transpose.

The testing data, $\mathbf{X}_k$ is also transformed into angle-Doppler domain $\mathbf{X}_{\mathrm{F}k}$ and then divided into similar LPR. The clutter/interference covariance matrix from the testing range gate (assuming that there is no target present) becomes

$$\mathbf{Q}_{\mathrm{L}l} = \frac{1}{K}\sum_{k=0}^{K-1} \mathrm{Vec}(\mathbf{X}_{\mathrm{L}l,k})\mathrm{Vec}(\mathbf{X}_{\mathrm{L}l,k})^H \qquad (17)$$

Figure 3 shows the block diagram of the joint Doppler compensation and JDL processor.

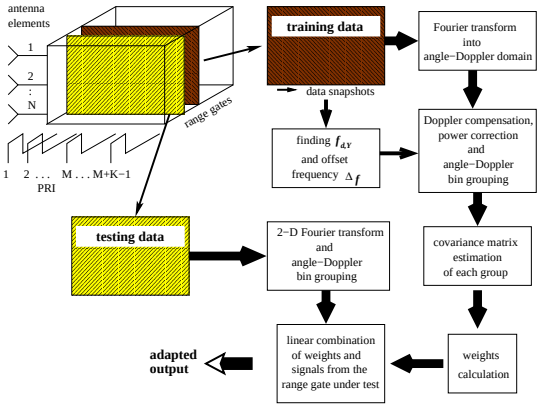

Fig. 3. Block diagram of Doppler compensation for JDL processor

5. SIMULATION AND RESULTS

The efficiency of any linear processor, can be characterised by the improvement factor (*IF*) which is defined as the ratio of signal-to-noise power ratios at the output and input, respectively [4]. For optimum signal-to-clutter + noise ratio (SCNR) processor, $\mathbf{w}_{l(opt)} = \widehat{\mathbf{Q}}_{\mathrm{L}_l}^{-1}\mathbf{s}_{l_{pq}}$

$$IF_{l_{pq}(opt)} = \frac{\mathbf{s}_{l_{pq}}^H \widehat{\mathbf{Q}}_{\mathrm{L}_l}^{-1}\mathbf{s}_{l_{pq}}\mathbf{s}_{l_{pq}}^H \widehat{\mathbf{Q}}_{\mathrm{L}_l}^{-1}\mathbf{s}_{l_{pq}} \cdot \mathrm{tr}(\mathbf{Q}_{\mathrm{L}l})}{\mathbf{s}_{l_{pq}}^H \widehat{\mathbf{Q}}_{\mathrm{L}_l}^{-1}\mathbf{Q}_{\mathrm{L}l}\widehat{\mathbf{Q}}_{\mathrm{L}_l}^{-1}\mathbf{s}_{l_{pq}} \cdot \mathbf{s}_{l_{pq}}^H \mathbf{s}_{l_{pq}}} \qquad (18)$$

where $\mathbf{s}_{l_{pq}}$, $(N_{a0}M_{fl} \times 1)$ is the signal-steering vector in angle-Doppler domain for the pqth bin in lth group, $p \in \{1 \ldots N_{a0}\}$ and $q \in \{1 \ldots M_{fl}\}$.

The radar parameters shown in Table 1 are for pulsed Doppler airborne bistatic radar.

number of antenna elements	N	8
number of pulses delay	M	24
pulse repetition frequency	PRF	20 kHz
wavelength	λ	0.03 m
array geometry	linear forward looking	
receiver & transmitter height	H_R, H_T	1000 m
receiver & transmitter velocity	v_R, v_T	90 m/s
receiver flight angle	δ_r	0°
transmitter flight angle	δ_t	90°
receiver looking direction	φ_r	45°
baseline separation		2000 m
testing range gate	X	27
training range gate	Y	29

Table 1. Radar Parameters

Figure 4 plots improvement factor vs Doppler frequency for Doppler compensated JDL processor, where $N_a = 16$, $M_f = 128$, $L = 1$, N_{a0}=1, M_{f1}=64 and $K = 256$. The dashed and dotted line represent optimum processor performance and processor performance without Doppler compensation respectively, while the solid line represent processor with only Doppler compensation.

Without Doppler compensation, we experience a degrade in improvement factor of at least 10dB (in average) from 0 Hz to 6000 Hz. This degradation will cause target signal in these region to be attenuated. However, with the proposed Doppler compensated JDL processor, the average degradation in improvement factor in the same region reduced to less than 3dB and less than 0.5dB in the rest of the region.

Figure 5 plots improvement factor vs Doppler frequency for processor purposed by Kreyenkamp and Klemm. In their technique, the range dependence is compensated by multiplying the space-time data with a complex phasor matrix $\mathbf{T}$. The dotted line once again represents the processor performance without Doppler compensation.

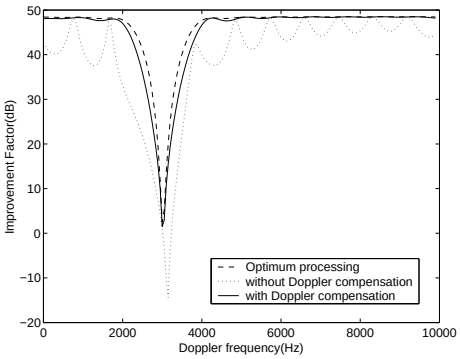

Fig. 4. Doppler compensation for JDL processor

Comparing the performance of the two processors, the proposed Doppler compensated JDL processor has a much narrow clutter notch than the processor purposed by Kreyenkamp. Significant improvement is also observed in region outside the clutter notch.

The difference between the two dotted lines (in Figure 4 and Figure 5) shows the improvement of using just using a JDL processor. A narrower clutter notch can be observed.

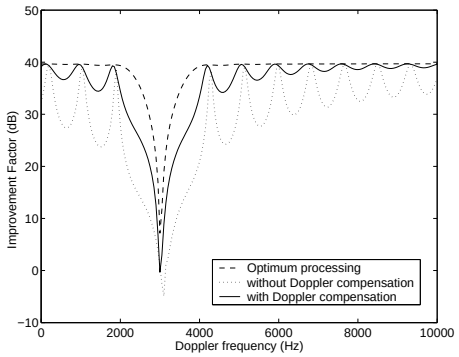

Fig. 5. Doppler compensation with complex phasor

Figure 6 plots the improvement factor for JDL processor using training data with Doppler compensation as well as power correction (solid line). Further improvement in term of improvement factor as compare to processor using just the proposed Doppler compensation can be observed. The proposed combine processor has a performance similar to that of the optimum processor.

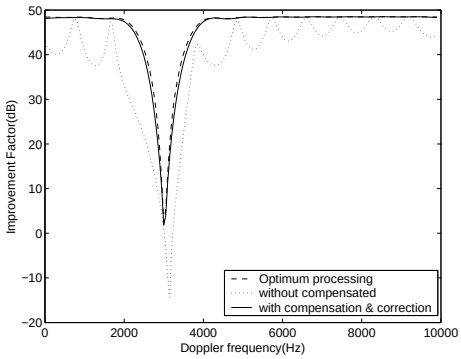

Fig. 6. JDL processor with Doppler compensation and power correction

6. CONCLUSIONS

In this paper, a different Doppler compensation method (using interpolation) is presented. Performing Doppler compensation in angle-Doppler domain allows clutter returns from different angles to be compensated separately. Significant improvement over Doppler compensation with complex phasor can be observed. With power correction as well as Doppler compensation, further performance improvement of up to 5dB is observed. Near optimum performance similar to that of the optimum processor can be achieved.

7. REFERENCES

[1] O. Kreyenkamp and R. Klemm, "Doppler compensation in forward-looking stap radar," *IEE Proceedings: Radar, Sonar and Navigation*, vol. 148, no. 5, pp. 253–258, October 2001.

[2] B. Himed, J.H. Michels, and Y. Zhang, "Bistatic stap performance analysis in radar applications," in *Proceedings of the 2001 IEEE Radar Conference*, Atlanta, Georgia, USA, May 1-3 2001, pp. 198–203.

[3] H. Wang and L.J. Cai, "On adaptive spatial-temporal processing for airborne surveillance radar systems," *IEEE Transactions on aerospace and electronic systems*, vol. 30, no. 3, pp. 660–670, July 1994.

[4] R. Klemm, *Space-Time Adaptive Processing principle and applications*, The Institution of Electrical Engineers, 1998.

ANGULAR BIN COMPRESSION FOR JOINT DOMAIN LOCALISED (JDL) PROCESSOR

K P Ong and B Mulgrew

Institute for Digital Communications
School of Engineering & Electronics
University of Edinburgh, UK
email: kpo@see.ed.ac.uk, B.Mulgrew@see.ed.ac.uk

ABSTRACT

In this paper, we propose a modified joint domain localised (JDL) processor that significantly reduces the computational cost. Space-time adaptive processing (STAP) has been proven to be able to suppress clutter efficiently. However due to the size of its covariance matrix, forming the inverse of the covariance matrix is computational expensive. JDL processor, a reduced dimension version of STAP allows practical implementation through the use of a small dimension covariance matrix (e.g. $[9 \times 9]$ matrix when using a 3×3 JDL). The propose modified JDL reduces the covariance matrix dimension further to a $[3 \times 3]$ matrix by using a tuned discrete Fourier transform.

1. INTRODUCTION

In airborne radar, suppression of Doppler spread clutter without minimising target return (especially low altitude and low relative velocity target) has always been one of the important tasks in radar signal processing. Attempts to remove the clutter using one dimensional filtering performed in the Doppler domain, can achieve adequate rejection over the full spectral bandwidth of the clutter. However at the expense of attenuating returns from low relative velocity target. In contrast, space-time adaptive processing (STAP) further distinguishes the clutter and target return in the angle domain by using antenna array. Number of studies, along with some experimental data have shown that STAP is very efficient for clutter suppression as well as target detection for both airborne monostatic and airborne bistatic radar [1–7]. Doppler compensation is however often required in cases where forward looking antenna array is used (for airborne monostatic radar) [3], or in airborne bistatic radar system [4, 5].

Radar system using STAP typically emits repetitive identical pulses. The reflected echos are collected and sampled at N array elements and M successive pulses for each range gate. The samples are then used to construct the estimated clutter covariance matrix $\widehat{\mathbf{Q}}$. For an optimum signal-to-clutter + noise ratio (SCNR) STAP processor, the weights are given as

$$\mathbf{w}_{(scnr)} = \widehat{\mathbf{Q}}^{-1}\mathbf{s} \tag{1}$$

where $\widehat{\mathbf{Q}}^{-1}$ is the inverse of $\widehat{\mathbf{Q}}$, a $NM \times NM$ matrix, and $\mathbf{s}$, a $NM \times 1$ matrix is the signal-steering vector. Clutter from the range gate under test, as well as the range gates beside it (guard cells) are often excluded from the computation of $\widehat{\mathbf{Q}}$. This is to ensure that $\widehat{\mathbf{Q}}$ is free of any possible target signal.

Real time implementation of STAP processor is considered impossible, as the computational cost of inverting a $NM \times NM$ dimensional matrix, (O$(NM)^3$), is considered too expensive, for large values of N and M. Several methods of reducing the signal vector space and, hence the computational load have since been proposed [2, 7–9]. Among them is the joint domain localised (JDL) processor. Beside reducing the computational costs, reduced dimension/rank STAP serves an increasingly important role in non-homogeneous environment. In environment where the clutter statics is range dependent, collecting data samples over large amount of range gates are subjected to considerable Doppler dispersion. With the dimension reduction of $\widehat{\mathbf{Q}}$, fewer data samples are required, and hence minimising Doppler dispersion.

2. JOINT DOMAIN LOCALISED (JDL) PROCESSOR

JDL algorithm was first introduced by Wang and Cai [7]. It works by transforming the space-time signal vector into angle-Doppler domain using a two-dimension discrete Fourier transform (DFT). The angle-Doppler data is then grouped into region called the localised processing regions (LPR). Adaptive processing is restricted to the LPRs, as shown in Figure 1. Forming LPRs significantly reduced the number of unknowns while retaining maximal gain against thermal noise. The lower degrees of freedom lead to a corresponding reduction in required sample support and computational cost.

In practice, only the few angle-bins covering the angle section centred around the look direction, φ_r (where most of the transmitted energy is contained) is of interest. On the other hand, all Doppler-bins must be analysed as the

This work was funded and supported by BAE Systems (Edinburgh).

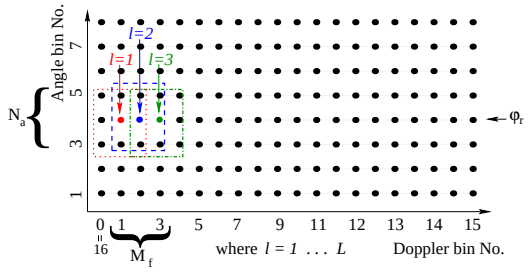

Fig. 1. An example of localised processing regions

target Doppler frequency is unknown to the processor. The angle-Doppler bins of the training data,$\mathbf{Y}_{\mathrm{F}k}$ are divided to form L sub-groups, $\mathbf{Y}_{\mathrm{L}l,k}$ centred around the look direction. Each LPR consists of N_a angle bins and M_f Doppler bins. The choice of N_a and M_f are independent of the number of array elements and the number of pulses. The localisation of the target to a single angle-Doppler bin decouples the number of adaptive degrees of freedom necessary for handling clutter suppression from the size of the data cube, while retaining maximal gain against thermal noise. This is however achieved at the price of fast Fourier transform (FFT) processor.

The indices k in the data matrix is take out in order to simplify the expression. The divided training data $\mathbf{Y}_{\mathrm{L}l}$ and the clutter/interference covariance matrix, $\widehat{\mathbf{Q}}_{\mathrm{L}l}$ ($N_aM_f \times N_aM_f$) are given as

$$\mathbf{Y}_{\mathrm{L}l} = \begin{pmatrix} y_{\mathrm{F}r,u_l} & y_{\mathrm{F}r,u_l+1} & \cdots & y_{\mathrm{F}r,u_l+M_f-1} \\ y_{\mathrm{F}r+1,u_l} & y_{\mathrm{F}r+1,u_l+1} & \cdots & y_{\mathrm{F}r+1,u_l+M_f-1} \\ \vdots & \vdots & \ddots & \vdots \\ y_{\mathrm{F}r+N_a-1,u_l} & y_{\mathrm{F}r+N_a-1,u_l+1} & \cdots & y_{\mathrm{F}r+N_a-1,u_l+M_f-1} \end{pmatrix} \quad (2)$$

where

$$l = 1 \ldots L \quad (3)$$

$$r = \text{looking angle bin} - \text{int}(\frac{N_a}{2}) \quad (4)$$

$$u_l = l - \text{int}(\frac{M_f}{2}) \quad (5)$$

and

$$\widehat{\mathbf{Q}}_{\mathrm{L}l} = \frac{1}{K}\sum_{k=0}^{K-1} \text{Vec}(\mathbf{Y}_{\mathrm{L}l,k})\text{Vec}(\mathbf{Y}_{\mathrm{L}l,k})^H \quad (6)$$

respectively. $\mathbf{Y}_{\mathrm{L}l}$ is a $N_a \times M_f$ matrix, Vec(·) is a matrix operation that stacks the columns of a matrix under each other to form a new column vector, K is the number of training data and ^{H} is the conjugate transpose operator. u_l will be less than 1 for certain $l-th$ LPR. As the Doppler bins repeat itself every pulse repetition frequency (PRF),

$$u_l = D_f + u_l, \qquad \text{for} \qquad u_l < 1 \quad (7)$$

where D_f is the size of the time to Doppler domain DFT.

The testing data, $\mathbf{X}_k$ must also be transformed into angle-Doppler domain $\mathbf{X}_{\mathrm{F}k}$ and then divided into similar LPRs, $\mathbf{Y}_{\mathrm{L}l,k}$. The clutter/interference covariance matrix of the testing range gate (assuming that there is no target presents) becomes

$$\mathbf{Q}_{\mathrm{L}l} = \frac{1}{K}\sum_{k=0}^{K-1} \text{Vec}(\mathbf{X}_{\mathrm{L}l,k})\text{Vec}(\mathbf{X}_{\mathrm{L}l,k})^H \quad (8)$$

3. ANGULAR BIN COMPRESSION

Transforming spatial samples into angular domain using discrete Fourier transform (DFT) with a rectangular window often results in smearing across several angular bins. The smearing depends on number of factors, such as: N, the size of the DFT; the angle of arrival (φ_r); the spatial sampling rate which is determined by the separation between the antenna elements; as well as windowing and zero padding performed on the spatial samples. As a result of the smearing, a number of angular bins, normally $N_a = 3$ angular bins are grouped into each LPR in order to gather a significant portion of the spatial energy.

Figure 2 shows the (angular-domain) 8-point DFT outputs of signals received by a forward looking array. Five individual signals arriving from five different φ_r, with depression angle, $\theta = 27°$ are received during five different experiments and plotted together. It can be seen that, for signals arriving at $\varphi_r = 40°$ and $\varphi_r = 55°$, the DFT output concentrate at bin 3 and bin 4 respectively. On the other hand for signal arriving at $\varphi_r = 45°$, it is attenuated and spread widely across bin 2 and bin 6. This attenuation of the measured value for an angular component that falls in between the DFT bins is known as scalloping loss [10]. Scalloping loss can be reduced by using a tapered window function as well as performing zero padding. However, window tapering will widen mainlobe, while zero padding will increase the DFT size, hence increase computational cost.

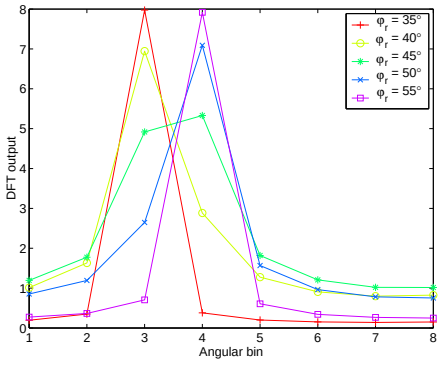

Fig. 2. Output of DFT with varies angle of arrival

In this paper, we propose a tuned DFT that will minimise the scalloping loss and yet reduce the computational

cost significantly. The tuned DFT obtains an unattenuated angular component value, by matching angular bin to the angular component. The systems performance penalty of using only one angular bin is offset by the reduction in scalloping loss. Using just one angular bin, allows the computational cost of calculating the output at other angular bins to be saved. For N = 8, computational saving of up to 87.5% maybe be achieved at this stage. Further computational saving is expected when the dimensional of the LPR is reduced from $[N_a \times M_f]$ to $[1 \times M_f]$.

The output of a tuned DFT for a spatial signal received by a linear array is given as

$$y_{\mathrm{F}a} = \mathbf{w}_{tF}^H \mathbf{y}_s \tag{9}$$

where $\mathbf{y}_s$, represents a $[N \times 1]$ spatial signal vector. $\mathbf{w}_{tF}$, the weight of the tuned DFT is

$$\mathbf{w}_{tF} = (w_{tF1}, w_{tF2}, \ldots, w_{tFN})^H \tag{10}$$

while

$$w_{tFn} = \exp(-j2\pi k(n-1)), n \in \{1 \ldots N\} \tag{11}$$

For a forward looking linear antenna array,

$$k = \frac{\sin\varphi_r \cos\theta}{2}, \qquad k \in \Re \tag{12}$$

while for a sidelooking linear antenna array,

$$k = \frac{\cos\varphi_r \cos\theta}{2}, \qquad k \in \Re \tag{13}$$

The different k values for different linear antenna arrays arises from the ability of the antenna to differentiate between angles. By definition of φ_r, a forward looking array is only able to differentiate $-90 \leq \varphi_r \leq 90$, while a sidelooking array is able to differentiate $0 \leq \varphi_r \leq 180$. The factor of $\frac{1}{2}$ in equ. 12 and equ. 13 is due to the $\lambda/2$ spacing between the antenna elements.

Back to the context of STAP, instead of performing a 2-dimensional DFT for space and time transformation, a normal discrete Fourier transform will follow after the tuned Fourier transform. The normal DFT will transform the time sample output of the tuned DFT ($\mathbf{y}_{\mathrm{F}}a$) into Doppler domain, $\mathbf{y}_{\mathrm{F}}$. Rewriting equ. 9 to take into account of the time samples, the output of tuned DFT becomes

$$\mathbf{y}_{\mathrm{F}a} = \mathbf{w}_{tF}^H \mathbf{Y}_{st} \tag{14}$$

where $\mathbf{Y}_{st}$, a $[N \times M]$ matrix represents the space-time data samples.

The training data in each LPR becomes

$$\mathbf{y}_{\mathrm{L}l} = \begin{pmatrix} y_{\mathrm{F}u_l} & y_{\mathrm{F}u_l+1} & \ldots & y_{\mathrm{F}u_l+M_f-1} \end{pmatrix} \tag{15}$$

4. SIMULATION RESULTS

The efficiency of any linear processor, can be characterised by the improvement factor (*IF*) which is defined as the ratio of signal-to-noise power ratios at the output and input, respectively. For optimum signal-to-clutter + noise ratio (SCNR) processor,

$$IF_{l_{pq}(scnr)} = \frac{\mathbf{s}_{l_{pq}}^H \widehat{\mathbf{Q}}_{\mathrm{L}l}^{-1} \mathbf{s}_{l_{pq}} \mathbf{s}_{l_{pq}}^H \widehat{\mathbf{Q}}_{\mathrm{L}l}^{-1} \mathbf{s}_{l_{pq}} \cdot \mathrm{tr}(\mathbf{Q}_{\mathrm{L}l})}{\mathbf{s}_{l_{pq}}^H \widehat{\mathbf{Q}}_{\mathrm{L}l}^{-1} \mathbf{Q}_{\mathrm{L}l} \widehat{\mathbf{Q}}_{\mathrm{L}l}^{-1} \mathbf{s}_{l_{pq}} \cdot \mathbf{s}_{l_{pq}}^H \mathbf{s}_{l_{pq}}} \tag{16}$$

where $\mathbf{s}_{l_{pq}}$, $(N_a M_f \times 1)$ is the signal-steering vector in angle-Doppler domain for the pqth bin in lth group, $p \in \{1 \ldots N_a\}$ and $q \in \{1 \ldots M_f\}$.

In order to compare the difference between JDL processors that use all angular bins, N_a = 3 angular bins, one normal angular bin and the tuned DFT angular bin, a common ground must be established among them. The common ground is achieved by replacing $\mathbf{Q}_{\mathrm{L}l}$ with $\mathbf{Q}_{\mathrm{LP}l}$.

$$\mathbf{Q}_{\mathrm{LP}l} = \frac{1}{K} \sum_{k=0}^{K-1} \mathrm{Vec}(\mathbf{X}_{\mathrm{LP}l,k}) \mathrm{Vec}(\mathbf{X}_{\mathrm{LP}l,k})^H \tag{17}$$

where $\mathbf{X}_{\mathrm{LP}l,k}$, a $[(N + N_p) \times M_f]$ matrix is the data samples in the l-th LPR group, grouped from angular-Doppler data samples $\mathbf{X}_{\mathrm{P}k}$. N_p is the number of zero padding added to the spatial samples and $\mathbf{X}_{\mathrm{P}k}$, a $[(N + N_p) \times M]$ matrix is obtained by transforming $\mathbf{X}_k$ into the angular-Doppler domain using a 2-dimensional DFT with zero padding on the spatial samples. Zero padding is added to the spatial samples in order to take into account of the energy between the original DFT spatial bins. All $N + N_p$ angular bins are included so that the performance upper limit can be established.

$\mathbf{s}_{l_{pq}}$ needs to be replaced by $\mathbf{s}_{l_{p_{zq}}}$ which is the angle-Doppler signal-steering vector that includes N angular bins as well as the N_p angular bins created by the zero padding. $z \in \{1 \ldots (N + N_p)\}$. Lastly, $\widehat{\mathbf{Q}}_{\mathrm{L}l}^{-1}$ needs to be reconstructed, to have the same matrix size as $\mathbf{Q}_{\mathrm{LP}l}$. The reconstructing is carried out by adding zero in the appropriate position. This is reasonable as the assumption of using less angular bins assumes that the energy in the rest of the angular bin (unwanted bins) is very small ≈ 0.

Figure 3 shows the IF vs Doppler frequency for processor using different number of angular bins as well as the propose tuned DFT angular bin. Some of the parameters used are: $M = 24, N = 8, M_f = 3, N_p = 8, \varphi_r = 55°$. The plot labelled "All bins with zero padding" uses all 16 $(N + N_p)$ angular bins, forms the processor performance upper limit. The plot labelled "All bins without zero padding", uses 8 angular bins formed without zero padding. Of the two plots, the latter shows a performance degradation of about 3dB, which is caused by the scalloping loss.

From Figure 2, we can see that for $\varphi = 55°$, most of the spatial energy concentrates in bin 4, and very little in bin 3 and bin 5. When angular bin 3,4 and 5 are used to calculate the weights of the processor, identical performance as compare with using 8 angular bins is achieved. Slight performance degradation around the notch region is observed when using just one angular bin (bin 4). This is so, as some energy is lost when the energy in bin 3 and bin 5 is assumed to be zero. As expected, the tuned

DFT didn't manage to have any performance improvement over using one angular bin (bin 4), since the energy concentration in bin 4 is already very high.

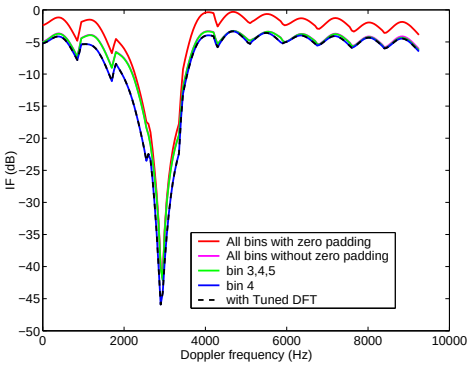

Fig. 3. Performance of angular bin reduction processor

Figure 4 shows the IF vs Doppler frequency for processor with $\varphi_r = 45°$.

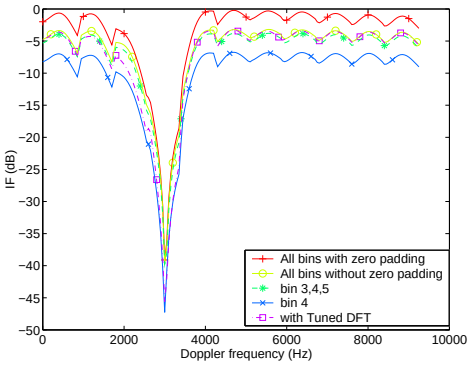

Fig. 4. Performance of angular bin reduction processor

Using bin 3,4 and 5 shows that a comparable performance (as compare to using 8 angular bins) can be achieved by assuming the energy in the rest of the angular bins is approximately zero. A 3dB degrade in performance is however observed when only one angular bin (bin 4) is used. From Figure 2, we can see that significant energy is also present in bin 3 and bin 5, excluding these energy will no doubt degrade the processor performance. The plot that uses the angular bin from the tuned DFT shows that by using one angular bin which is tuned to the maximum energy, performance as good as using 8 angular bins can be achieved. However some performance degradation can be observed at the notch region.

5. CONCLUSION

Effective clutter suppression is achievable practically using reduced rank STAP processor such as JDL. Very significant computational cost saving, in both the transformation of space-time samples into angle-Doppler samples and calculation of the inverse of covariance matrix can be achieved when using the propose tuned DFT. Degrade in processor performance due to using less angular bins, is offset by reduction of scalloping loss. Reducing the covariance matrix size to $[3 \times 3]$ may further reduce the training data support size, hence improving the STAP processor performance in a non-homogeneous environment.

6. REFERENCES

[1] L. Brennan and I. Reed, "Theory of adaptive radar," *IEEE Transactions on Aerospace and Electronic Systems*, vol. AES-9, pp. 237–252, March 1973.

[2] R. Klemm, *Space-Time Adaptive Processing principle and applications*. The Institution of Electrical Engineers, 1998.

[3] G. Borsari, "Mitigating effects on stap processing caused by an inclined array," in *Proceedings of the 1998 IEEE Radar Conference, RADARCON 98*, (Dallas, Texas), pp. 135–140, May 11-14 1998.

[4] K. Ong and B. Mulgrew, "Doppler compensation for jdl for airborne bistatic radar," in *Proceeding of 2002 IEEE Sensor Array and Multichannel Signal Processing Workshop, SAM2002*, (Rosslyn, VA, USA), pp. 82–86, August 4-6 2002.

[5] B. Himed, Y. Zhang, and A. Hajjari, "Stap with angle-doppler compensation for bistatic airborne radars," in *Proceedings of IEEE 2002 National Radar Conference, RadarCon-02*, (Long Beach, California, USA), pp. 311–317, April 22-25 2002.

[6] B. Himed, M. C. Wicks, and P. Zulch, "A new constrained joint-domain localized approach for airborne radars," in *Proceedings of the 2002 IEEE Radar Conference*, (Long Beach, California), pp. 403–407, April 22-25 2002.

[7] H. Wang and L. Cai, "On adaptive spatial-temporal processing for airborne surveillance radar systems," *IEEE Transactions on aerospace and electronic systems*, vol. 30, pp. 660–670, July 1994.

[8] Z. Bao, S. Wu, G. Liao, and Z. Xu, "Review of reduced rank space - time adaptive processing for airborne radars," in *Proceedings of 1996 IEEE CIE International Conference on Radar*, (Beijing, China), pp. 766–769, Oct 8-10 1996.

[9] R. DiPietro, "Extended factored space-time processing for airborne radar systems," in *Proceedings of 26th Asilomar Conference on Signals, Systems & Computers*, (Pacific Grove, California, USA), pp. 425–430, October 26-28 1992.

[10] B. Mulgrew, P. Grant, and J. Thompson, *Digital Signal Processing: Concept and Applications*. Palgrave Macmillan Press Ltd., 2 ed., 2001.

References

[1] B. Himed, "Effects of bistatic clutter dispersion on stap systems," in *Proceedings of IEE International Radar Conference, Radar2002*, (Edinburgh, UK), pp. 360–364, October 15-17 2002.

[2] M. I. Skolnik, ed., *Radar handbook*. New York: McGraw-Hill, 1 ed., 1970.

[3] A. Farina and G. Galati, "Surveillance radars: State of the art, research and perspectives," *Alta Frequentia*, vol. LIV, no. 4, pp. 261–277, 1985.

[4] V. S. Chernyak, *Fundamentals of Multisite radar systems: Multistatic Radars and Multiradar Systems*. Gordon and Breach Science Publishers, 1998.

[5] N. J. Willis, *Bistatic Radar*. Technology Service Corporation, 2 ed., 1995.

[6] Y. Guo and H. Uberall, "Bistatic radar scattering by a chaff cloud," *IEEE Transactions on Antennas and Propagation*, vol. 40, pp. 837–841, July 1992.

[7] A. Prentice, "A digitally beamformed phased array receiver for tactical bistatic radar," in *Proceedings of IEE Colloquium on 'Active & Passive Components for phased Array system' 1992*, (London, UK), pp. 11/1–4, April 24 1992.

[8] G. Stimson, *Introduction to Airborne Radar*. SciTech Publishing, Incorporated, 2nd ed., May 1999.

[9] R. Fante, "Ground and airborne target detection with bistatic adaptive space-based radar," *IEEE Aerospace and Electronic Systems Magazine*, vol. 14, pp. 39–44, Oct 1999.

[10] L. Yang and Z. Sun, "Identification of false targets in bistatic radar system," in *Proceedings of 1997 IEEE National Aerospace and Electronics Conference*, vol. 2, (Syracuse, NY, USA), pp. 878–883, May 13-15 1997.

[11] Y. Chen and Z. Sun, "A new algorithm for multiple targets tracking in bistatic radar system," in *Proceedings of IEEE Proceedings of the National Aerospace and Electronics Conference*, vol. 1, (Dayton, KY, USA), pp. 187–189, May 22-26 1995.

[12] Y. Chen and Z. Sun, "Information fusion for multiple target tracking in bistatic system," in *Proceedings of 1996 IEEE National Aerospace and Electronics Conference*, (Dayton, KY, USA), pp. 177–179, May 20-23 1.

[13] Y. Chen, Z. Sun, and H. Cheng, "A Study on Multi-Stage Tracking Technique in T/R-R Bistatic System," in *Proceedings of IEEE 1995 National Aerospace and Electronics Conference, NAECON 1995*, vol. 1, (Dayton, NJ, USA), pp. 210–214, May 22-26 1995.

[14] W. Wang, "An adaptive tracking algorithm for bistatic radar system with an independent receiver," in *Proceedings of IEEE Proceedings of the National Aerospace and Electronics Conference*, vol. 1, (Dayton, KY, USA), pp. 43–46, May 22-26 1995.

[15] P. Howland, "Passive Tracking of Airborne Targets Using Only Doppler and DOA Information," in *Proceedings of IEE Computing and Control Division Colloquium on Algorithms for Target Tracking*, 104, (London, UK), pp. 7/1–7/3, May 16 1995.

[16] H. Cheng and Z. Sun, "A nonlinear optimized location algorithm for bistatic radar system," in *Proceedings of IEEE Proceedings of the National Aerospace and Electronics Conference*, vol. 1, (Dayton, KY, USA), pp. 201–205, May 22-26 1995.

[17] Y. Chen and J. Wu, "Bistatic location & tracking based on intermittent data fusion," in *Proceedings of 1997 IEEE National Aerospace and Electronic Conference*, vol. 2, (Syracuse, NY, USA), pp. 998–1001, May 13-15 1997.

[18] L. He and Z. Sun, "Location and tracking technique in a multistatic system established by multiple bistatic systems," in *Proceedings of the IEEE 1991 National Aerospace and electronics Conference NAECON 1991*, vol. 1, pp. 437–441, 1991.

[19] L. He, Z. Sun, and X. Xie, "Location error analysis and a tracking algorithm in a bistatic system," in *Proceedings of the IEEE 1992 National Aerospace and electronics Conference, NAECON 1992*, vol. 2, pp. 592–597, 1992.

[20] Q. Liu, H. Zhu, Z. Sun, and X. Song, "Analysis of position location with two coordinate measurements in bistatic system," in *Proceedings of 1996 IEEE CIE International Conference on Radar*, (Beijing, China), pp. 539–542, Oct 8-10 1996.

[21] H. Wang and L. He, "The location method and accuracy analysis for bistatic systems," in *Proceedings of the IEEE 1994 National Aerospace and Electronics Conference NAECON 1994*, vol. 1, pp. 62–65, 1994.

[22] H. Cheng and Z. Sun, "On the influence of coordinate transform upon measurement error of bistatic radar system," in *Proceedings of 1997 IEEE National Aerospace and Electronic Conference*, vol. 2, (Syracuse, NY, USA), pp. 896–903, May 13-15 1997.

[23] Q. Liu, Z. Sun, and X. Song, "Position location approach and accuracy analysis with two coordinate measurements in bistatic system," in *Proceedings of 1996 IEEE National Aerospace and Electronics Conference*, vol. 1, (Dayton, KY, USA), pp. 173–176, May 20-23 1996.

[24] Q. Liu, H. Cheng, L. Mo, Z. Sun, and X. Song, "Analysis of detection distance and location performance in airborne-ground bistatic system," in *Proceedings of 1997 IEEE National Aerospace and Electronic Conference*, vol. 2, (Syracuse, NY, USA), pp. 975–980, May 13-15 1997.

[25] B. Sweetman, *F-22 Raptor*. Motor International, April 1998.

[26] B. Sweetman, *Lockheed Stealth*. Motorbooks International, May 2001.

[27] J. C. Goodall, *America's Stealth Fighters and Bombers*. Motorbooks International, September 1992.

[28] S. Pace, ed., *B-2 Spirit: The Most Capable War Machine on the Planet*. McGraw-Hill Professional, August 1999.

[29] B. Sweetman, ed., *Inside the Stealth Bomber*. Motorbooks International, June 1999.

[30] P. F. Crickmore, A. J. Crickmore, and A. Crickmore, eds., *F-117 Nighthawk*. Motorbooks International, July 1999.

[31] W. G. Holder, B. Holder, and M. Wallace, *Lockheed F-117 Nighthawk: An illustrated History of the Stealth Fighter*. Schiffer Publishing, Ltd, January 2000.

[32] G. Stimson, *Introduction to Airborne Radar*, ch. 39, pp. 493–498. SciTech Publishing, Incorporated, 2nd ed., May 1999.

[33] G. Stimson, *Introduction to Airborne Radar*, ch. 42, pp. 525–534. SciTech Publishing, Incorporated, 2nd ed., May 1999.

[34] B. Chambers, "Symmetrical radar absorbing structures," *Electronics Letters*, vol. 31, pp. 404–405, March 1995.

[35] H. Kuschel, "Vhf/uhf radar part 1: Characteristics," *IEE Electronics and Communication Engineering Journal*, vol. 14, pp. 61–72, April 2002.

[36] H. Kuschel, "Vhf/uhf radar part 2: Operational aspects and applications," *IEE Electronics and Communication Engineering Journal*, vol. 14, pp. 101–111, June 2002.

[37] R. Boyle, "Comparison of monostatic and bistatic bearing estimation performance for low rcs targets," *IEEE Transactions on Aerospace and Electronic Systems*, vol. 30, pp. 962–967, July 1994.

[38] T. Lane and N. Alexander, "The Bistatic Coherent Measurement System (BICOMS)," in *Proceedings of the 1999 11th IEEE/AESS Radar Conference*, (Piscataway, NJ, USA), pp. 154–159, Apr 20-22 1999.

[39] L. Brennan, J. Mallet, and I. Reed, "Adaptive arrays in airborne mti radar," *IEEE Transactions on Antennas and Propagation*, vol. AP-24, pp. 607–615, 1976.

[40] S. Hayward, "Effects of motion on adaptive arrays," *IEE Proceedings on Radar, Sonar and Navigation*, vol. 144, pp. 15–20, February 1997.

[41] J. McWhirter, H. Rees, S. Hayward, and J. Mather, "Adaptive radar processing," in *Proceedings of the IEEE 2000 adaptive systems for signal processing, Communications, and Control Symposium 2000. AS-SPCC*, (Lake Louise, AB, Canada), pp. 25–30, October 1-4 2000.

[42] I. Gupta and A. Ksienski, "Effect of mutual coupling on the performance of adaptive arrays," *IEEE Transactions on Antennas and Propagation*, vol. 31, pp. 785–791, Sept 1983.

[43] R. Adve, T. Sarkar, and R. Schneible, "Accounting for the effects of mutual coupling in adaptive antennas," in *Proceedings of the IEEE National Radar Conference 1997*, (Syracuse, NY), pp. 361–366, May 13-15 1997.

[44] R. Adve and T. Sarkar, "Compensation for the effects of mutual coupling on direct data domain adaptive algorithms," *IEEE Transactions on Antennas and Propagation*, vol. 48, pp. 86–94, January 2000.

[45] O. Kreyenkamp, "Clutter covariance modelling for stap in forward looking radar," in *Proceedings of DGON International Radar Symposium 98*, (Munich, Germany), Sept. 15-17 1998.

[46] H. Wang and L. Cai, "On adaptive spatial-temporal processing for airborne surveillance radar systems," *IEEE Transactions on aerospace and electronic systems*, vol. 30, pp. 660–670, July 1994.

[47] K. Ong and B. Mulgrew, "Doppler compensation for jdl for airborne bistatic radar," in *Proceeding of 2002 IEEE Sensor Array and Multichannel Signal Processing Workshop, SAM2002*, (Rosslyn, VA, USA), pp. 82–86, August 4-6 2002.

[48] K. Ong and B. Mulgrew, "Angular bin compression for joint domain localised (jdl) processor," in *Proceedings of the twelfth International conference on antennas and propagation, ICAP 2003*, vol. 1, (University of Exeter, UK), pp. 353–356, April 2003.

[49] R. Klemm, "Comparison between monostatic and bistatic antenna configurations for stap," *IEEE Transactions on Aerospace and Electronic Systems*, vol. 36, pp. 596–608, April 2000.

[50] L. Brennan and I. Reed, "Theory of adaptive radar," *IEEE Transactions on Aerospace and Electronic Systems*, vol. AES-9, pp. 237–252, March 1973.

[51] R. Klemm, *Space-Time Adaptive Processing principle and applications*. The Institution of Electrical Engineers, 1998.

[52] G. Borsari, "Mitigating effects on stap processing caused by an inclined array," in *Proceedings of the 1998 IEEE Radar Conference, RADARCON 98*, (Dallas, Texas), pp. 135–140, May 11-14 1998.

[53] B. Himed, Y. Zhang, and A. Hajjari, "Stap with angle-doppler compensation for bistatic airborne radars," in *Proceedings of IEEE 2002 National Radar Conference, RadarCon-02*, (Long Beach, California, USA), pp. 311–317, April 22-25 2002.

[54] B. Himed, M. C. Wicks, and P. Zulch, "A new constrained joint-domain localized approach for airborne radars," in *Proceedings of the 2002 IEEE Radar Conference*, (Long Beach, California), pp. 403–407, April 22-25 2002.

[55] F. Staudaher, *"Airborne MTI" in Radar handbook: SKOLNIK, M. (Ed.)*, ch. 18, pp. 18.1–18.16. McGraw-Hill, 1970.

[56] W. Tam and D. Faubert, "Displaced phase centre antenna clutter suppression in space based radar applications," in *Proceedings of IEE International Conference on Radar - 87*, (London, UK), pp. 385–389, Oct 19-21 1987.

[57] E. Hofstetter, C. Weinstein, and C. Muehe, "A theory of multiple antenna amti radar," Technical note 1971-21, Massachusetts Institute of Technology, 1971.

[58] S. Haykin, *Adaptive filter theory*. Prentice Hall, 3 ed., 1996.

[59] Y. Wang, Y. Peng, and Z. Bao, "Space-time adaptive processing for airborne radar with various array orientations," *IEE Proceedings: Radar, Sonar and Navigation*, vol. 144, pp. 330–340, December 1997.

[60] P. Richardson, "Analysis of the adaptive space time processing technique for airborne radar," *IEE Proceedings: Radar, Sonar and Navigation*, vol. 141, pp. 187–195, August 1994.

[61] G. M. Herbert, "Space-time adaptive processing (stap) for wide-band airborne radar," in *Record of the IEEE 2000 International radar conference*, (Alexandria, Virginia, USA), pp. 620–625, May 8-12 2000.

[62] G. Liao, Z. Bao, and Z. Xu, "Evaluation of adaptive space-time processing for inclined sideways looking array airborne radars," in *Proceedings of 1996 IEEE CIE International Conference on Radar*, (Beijing, China), pp. 78–81, Oct 8-10 1996.

[63] R. Klemm, "Adaptive airborne mti: Comparison of sideways and forward looking radar," in *Proceedings of the 1995 International Radar Conference*, (Alexandria, VA, USA), pp. 614–618, May 8-11 1995.

[64] R. Richardson and S. Hayward, "Adaptive space time processing for forward looking radar," in *Proceedings of the 1995 International Radar Conference*, (Alexandria, VA, USA), pp. 629–634, May 8-11 1995.

[65] T. Nohara, P. Weber, A. Premji, and T. Bhattacharya, "Airborne ground moving target indication using non-side-looking antenna," in *Proceedings of the 1998 IEEE Radar Conference, RADARCON 98*, (Dallas, Texas), pp. 269–274, May 11-14 1998.

[66] Y. Wang, Z. Bao, and Y. Peng, "Stap with medium prf mode for non-side-looking airborne radar," *IEEE Transactions on Aerospace and Electronic Systems*, vol. 36, pp. 609–620, April 2000.

[67] W. Melvin, M. Callahan, and M. Wicks, "Bistatic stap: application to airborne radar," in *Proceedings of the IEEE Radar Conference, 2002, RadarCon-02*, (Long Beach, California, USA), pp. 1–7, April 22-25 2002.

[68] R. Klemm, *Principles of space-time adaptive processing*. The Institution of Electrical Engineers, 2 ed., 2002.

[69] G. Herbert and P. Richardson, "On the benefits of space-time adaptive processing (stap) in bistatic airborne radar," in *Proceedings of IEE Radar 2002*, (Edinburgh, UK), pp. 365–369, Oct 15-17 2002.

[70] G. Herbert and P. Richardson, "Benefits of space-time adaptive processing (stap) in bistatic airborne radar," *IEE Proceedings: Radar, Sonar and Navigation*, vol. 150, pp. 13–17, February 2003.

[71] Z. Gu, R. Blum, W. Melvin, and M. Wicks, "Comparison of stap algorithms for airborne radar," in *Proceedings of the IEEE National Radar Conference 1997*, (Syracuse, NY), pp. 60–65, May 13-15 1997.

[72] H. Wang, "An overview of space-time adaptive processing for airborne radars," in *Proceedings of 1996 IEEE CIE International Conference on Radar*, (Beijing, China), pp. 789–794, Oct 8-10 1996.

[73] R. Adve, T. Hale, and M. Wicks, "A two stage hybrid space-time adaptive processing algorithm," in *Record of the 1999 IEEE Radar Conference*, (Waltham, Massachusetts, USA), pp. 279–284, April 20-22 1999.

[74] A. Farina and L.Timmoneri, "Nonlinear stap processing," *Electronic and Communication Engineering Journal*, vol. 11, pp. 41–48, February 1999.

[75] M. Wicks, W. Melvin, and P. Chen, "An efficient architecture for nonhomogeneity detection in space-time adaptive processing airborne early warning radar," in *Proceedings of the 1997 Radar Edinburgh International Conference, IEE Publ. no. 449*, (Edinburgh, UK), pp. 295–299, IEE, Oct 14-16 1997.

[76] W. Melvin and M. Wicks, "Improving practical space-time adaptive radar," in *Proceedings of the IEEE National Radar Conference 1997*, (Syracuse, NY), pp. 48–53, May 13-15 1997.

[77] Y. L. Wang and J. W. Chen, "Robust stap approach in nonhomogeneous clutter environments," in *Proceedings of Radar 2001, CIE International conference*, (Beijing, China), pp. 753–757, October 15-18 2001.

[78] N. Goodman, "Statistical analysis based on a certain multivariate complex gaussian distribution," *Annals Mathematical Statistics*, vol. 34, pp. 152–177, March 1963.

[79] J. Johnson, H. Li, E. Culpepper, E. Blasch, and A. klopf, "Learning algorithms for suppressing motion clutter in airborne array radar," in *Proceedings of 1997 IEEE National Aerospace & Electronics Conference (NAECON)*, vol. 2, (Dayton, OH, USA), pp. 840–845, Jul 14-17 1997.

[80] H. Akaike, "Block toeplitz matrix inversion," *SIAM Journal of Applied Mathematics*, vol. 24, 1973. 234-241.

[81] M. Gover and S. Barnett, "Inversion of certain extensions of toeplitz matrices," *Journal of Mathematical Analysis and Applications*, vol. 100, pp. 339–353, 1984.

[82] S. Kadambe and Y. Owechko, "Computation reduction in space time adaptive processing (stap) of radar signals using orthogonal wavelet decompositions," in *Conference Record of 34th Asilomar Conference on Signals, Systems and Computers, 2000*, vol. 1, (Pacific Grove, CA, USA), pp. 641–645, October 29 - November 1 2000.

[83] Y. M. Li and C. H. Cheong, "Fft-based conjugate gradient method for optimal stap," in *Proceedings of Radar 2001, CIE International conference*, (Beijing, China), pp. 778–782, October 15-18 2001.

[84] J. Ward, "Space-time adaptive processing for airborne radar," Tech. Rep. 1015, MIT:Lincoln Laboratory, 13 December 1994.

[85] J. R.T. Compton, *Adaptive Antennas, Concepts and Performance*. Prentice-Hall, 1988.

[86] A. Farina, *Antenna-Based Signal Processing Techniques for Radar Systems*. Artech House, Jan 1992.

[87] A. Farina and L. Timmoneri, "Parallel algorithms and processing architectures for space-time adaptive processing," in *Proceedings of 1996 IEEE CIE International Conference on Radar*, (Beijing, China), pp. 770–774, Oct 8-10 1996.

[88] A. Farina and L.Timmoneri, "Real-time stap techniques," *Electronic and Communication Engineering Journal*, vol. 11, pp. 13–22, February 1999.

[89] L. Brennan, F. Staudaher, and D. Piwinsky, "Comparison of space-time adaptive processing approaches using experimental airborne radar data," in *Proceedings of the IEEE National Radar Conference*, (Boston, MA), pp. 176–185, April 20-22 1993.

[90] A. Jaffer, "Constrained partially adaptive space-time processing for clutter suppression," in *Conference record of the Twenty-Eighth Asilomar Conference on Signals, Systems and Computers, 1994*, vol. 1, (Pacific Grove, California, USA), pp. 671–676, Oct. 31 - Nov. 2 1994.

[91] R. Brown and R. Linderman, "Algorithm development for an airborne real-time stap demonstration," in *Proceedings of the IEEE National Radar Conference*, (Syracuse, NY), pp. 331–336, May 13-15 1997.

[92] W. Gruener, J. Toernig, and P. Fielding, "Active-electronically-scanned-array based radar system features," in *Proceedings of the 1997 Radar Edinburgh International Conference, IEE Publ. no. 449*, (Edinburgh, UK), pp. 339–343, IEE, Oct 14-16 1997.

[93] P. Sanyal, R. Brown, M. Little, R. Schneible, and M. Wicks, "Space-time adaptive processing bistatic airborne radar," in *Proceedings of the 1999 11th IEEE/AESS Radar Conference*, (Piscataway, NJ, USA), pp. 114–118, Apr 20-22 1999.

[94] W. H. Press, S. A. Teukolsky, W. T. Vetterling, and B. P. Flannery, *Numerical Recipes in C, The art of Scientific Computing*. Cambridge University Press, 2 ed., 1992.

[95] P. Richardson, "Space-time adaptive processing for manoeuvring airborne radar," *Electronic and Communication Engineering Journal*, vol. 11, pp. 57–63, February 1999.

[96] Y. Wang, Y. Peng, and Z. Bao, "Adaptive space-time processing for non-side-looking airborne radar," in *Proceedings of the CIE international Radar conference CIE IRC'96*, (Beijing, China), pp. 91–95, Oct. 1996.

[97] H. N. Nguyen, *Robust steering vector mismatch techniques for reduced rank adaptive array signal processing*. PhD thesis, Virginia Polytechnic Institute and State University, Fallschurch, Virginia, 10 October 2002.

[98] T. Barton and S. Smith, "Structured covariance estimation for space-time adaptive processing," in *Proceedings of the Adaptive Sensor Array Processing (ASAP) Workshop*, (MIT Lincoln Laboratory, Lexington, MA), March 15-17 1995.

[99] M. Zatman and D. Marshall, "Forwards-backwards averaging for adaptive beamforming and stap," in *Proceedings of 1996 IEEE International Conference on Acoustics, Speech, and Signal Processing (ICASSP-96)*, vol. 5, (Atlanta, Georgia), pp. 2630 –2633, May 7-10 1996.

[100] S. Pillai, J. Guerci, and Y. Kim, "Generalized forward/backward subaperture smoothing techniques for sample-starved stap," in *Proceedings of the IEEE International Conference on Acoustics, Speech and Signal Processing, 1998 (ICASSP'98)*, vol. 4, (Seattle, WA, USA), pp. 2501–2504, May 12-15 1998.

[101] J. Guerci and E. Feria, "Application of a least squares predictive-transform modeling methodology to space-time adaptive array processing," *IEEE Transactions on Signal Processing*, vol. 44, pp. 1825–1833, July 1996.

[102] J. Roman, D. Davis, and J. Michels, "Multichannel parametric models for airborne phased array clutter," in *Proceedings of the IEEE National 1997 Radar Conference*, (Syracuse, NY, USA), pp. 72–77, May 13-15 1997.

[103] R. Brown, M. Wicks, Y. Zhang, Q. Zhang, and H. Wang, "A space-time adaptive processing approach for improved performance and affordabliliy," in *Proceedings of the 1996 IEEE National Radar Conference*, (Ann Arbor, Michigan, USA), pp. 321–326, May 13-16 1996.

[104] Y. Wang and Y. Peng, "Space-time joint processing method for simultaneous clutter and jammer rejection in airborne radar," *IEE Electronics Letters*, vol. 32, pp. 258–259, February 1996.

[105] Z. Bao, S. Wu, G. Liao, and Z. Xu, "Review of reduced rank space - time adaptive processing for airborne radars," in *Proceedings of 1996 IEEE CIE International Conference on Radar*, (Beijing, China), pp. 766–769, Oct 8-10 1996.

[106] Y. Zhang and H. Wang, "Further results of sum and difference stap approach to airborne surveillance radars," in *Proceedings of the IEEE national Radar conference*, (Syracuse, New York, USA), pp. 337–342, May 13-15 1997.

[107] J. Maher, *Jammer pre-suppression in cascade with sum and difference channel space-time adaptive processing*. PhD thesis, Syracuse University, Syracuse, NY, USA, June 1998.

[108] J. Maher, "Space-time adaptive processing with sum and difference beams for airborne radars," in *Proceedings of SPIE's 13th Annual International Symposium on AeroSense*, vol. 3704, (Orlando, FL, USA), pp. 160–169, April 5-9 1999.

[109] R. Brown, R. Schneible, M. Wicks, H. Wang, and Y. Zhang, "Stap for clutter suppression with sum and difference beams," *IEEE Transactions on Aerospace and Electronic Systems*, vol. 36, pp. 634–646, April 2000.

[110] R. DiPietro, "Extended factored space-time processing for airborne radar systems," in *Proceedings of 26th Asilomar Conference on Signals, Systems & Computers*, (Pacific Grove, California, USA), pp. 425–430, October 26-28 1992.

[111] W. Gabriel, "Adaptive digital processing investigation of dft subbanding vs transversal filter canceler," tech. rep., Naval Research Laboratory Report 8981, 1986.

[112] A. Jaffer, M. Baker, W. Ballance, and J. Staub, "Adaptive space-time processing techniques for airborne radars," tech. rep., Rome Lab Tech. Report 91-162, July 1991.

[113] W. Melvin and B. Himed, "Comparative analysis of space-time adaptive algorithms with measured airborne data," in *Proceedings of 7th International Conference on Signal Processing Applications and Technology*, pp. 1479–1483, Oct 7-10 1996.

[114] A. Haimovich, "The eigencanceler: adaptive radar by eigenanalysis methods," *IEEE Transactions on Aerospace and Electronic Systems*, vol. 32, pp. 532–542, April 1996.

[115] J. Goldstein, P. A. Zulch, and I. S. Reed, "Reduced rank space-time adaptive radar processing," in *Proceedings of 1996 IEEE International Acoustics, Speech and Signal Processing, ICASSP-96*, vol. 2, (Atlanta, Georgia), May 7-10 1996.

[116] P. Richardson, "Effects of manoeuvre on space time adaptive processing performance," in *Proceedings of the 1997 Radar Edinburgh International Conference, IEE Publ. no. 449*, (Edinburgh, UK), pp. 285–289, IEE, Oct 14-16 1997.

[117] E. J. Baranoski, "Improved pre-doppler stap algorithm for adaptive clutter nulling in airborne radars," in *Conference Record of the Twenty-Ninth Asilomar Conference on Signals, Systems and Computers, 1995*, vol. 2, (Pacific Grove, California, USA), pp. 1173–1177, Oct 30 - Nov 1 1995.

[118] E. J. Baranoski, "Constraint optimization for partially adaptive subspace stap algorithms," in *Conference Record of Thirty-Second Asilomar Conference on Signal, Systems & Computers, 1998*, vol. 2, (Pacific Grove, CA, USA), pp. 1527–1531, Nov 1-4 1998.

[119] P. Moo, "Gmti performance of $Sigma$D$elta$-stap for a forward looking radar," in *Proceedings of the 2001 IEEE Radar Conference*, (Atlanta, Georgia, USA), pp. 258–263, May 1-3 2001.

[120] J. Guerci, "Principal components, covariance matrix tapers, and the interference modulation problem," in *Proceedings of the Adaptive Sensor Array Processing (ASAP) Workshop*, (Lexington, MA, USA), MIT Lincoln Laboratory, March 10-11 1999.

[121] J. Guerci, "Principal components, covariance matrix tapers, and the subspace leakage problem," *IEEE Transactions on Aerospace and Electronic Systems*, vol. 38, pp. 152–162, January 2002.

[122] J. Goldstein, S. Kogon, I. Reed, D. Willisms, and E. Holder, "Partially adaptive radar signal processing: the cross-spectral approach," in *Conference Record of the Twenty-Ninth Asilomar Conference on Signals, Systems and Computers, 1995*, vol. 2, (Pacific Grove, California, USA), pp. 1383–1387, Oct 30 - Nov 1 1995.

[123] J. Goldstein and I. Reed, "Subspace selection for partially adaptive sensor array processing," *IEEE Transactions on Aerospace and Electronic Systems*, vol. 33, pp. 539–544, April 1997.

[124] T. Hale and B. Welsh, "Secondary data support in space-time adaptive processing," in *Proceedings of the 1998 IEEE Radar Conference, RADARCON 98*, (Dallas, Texas), pp. 183–188, May 11-14 1998.

[125] J. Guerci, J. Goldstein, and I. Reed, "Optimal and adaptive reduced-rank stap," *IEEE Transactions on Aerospace and Electronic Systems*, vol. 36, pp. 647–663, April 2000.

[126] N. Hien, J.D.Hiemstra, J. Goldstein, T. Pratt, and J. Allnutt, "A robust steering vector mismatch technique for the multistage wiener filter," in *Proceeding of 2002 IEEE Sensor Array and Multichannel Signal Processing Workshop, SAME2002*, (Rosslyn, VA, USA), pp. 383–387, August 4-6 2002.

[127] M. Weippert, J. Hiemstra, M. Zoltowski, and J. Goldstein, "Insights from the relationship between the multistage wiener filter and the method of conjugate gradients," in *Proceeding of 2002 IEEE Sensor Array and Multichannel Signal Processing Workshop, SAM2002*, (Rosslyn, VA, USA), pp. 388–392, August 4-6 2002.

[128] P. Ferrazzoli, L. Guerriero, and D. Solimini, "Comparison between predicted performances of bistatic and monostatic radar in vegetation monitoring," in *Proceedings of International Geoscience and Remote Sensing Symposium (IGARSS)*, vol. 3, (Pasadena, CA, USA), pp. 1850–1852, Aug 8-12 1994.

[129] T. Ma and L. Griffiths, "A solution space approach to achieving partially adaptive arrays," in *Proceedings of the International Conference Acoustics, Speech, Signal Processing, 1988*, (New York, USA), pp. 2869–2872, April 11-14 1988.

[130] I. Scott and B. Mulgrew, "Sparse lcmv beamformer design for suppression of ground clutter in airborne radar," *IEEE Transactions on Signal Processing*, vol. 43, pp. 2843–2851, December 1995.

[131] H. Yang and M. Ingram, "Design of partially adaptive arrays using the singular-value decomposition," *IEEE Transactions on Antennas and Propagation*, vol. 45, pp. 843–850, May 1997.

[132] H. Wang, H. Park, and M. Wicks, "Recent results in space-time processing," in *Proceedings of the IEEE National Radar Conference*, (Atlanta, GA, USA), pp. 104–109, March 29-31 1994.

[133] B. Himed, M. C. Wicks, and G. J. Genello, "Accounting for array effects in joint-domain localized stap processing," in *Proceeding of IEE Radar 2002*, (Edinburgh, UK), pp. 186–190, Oct 15-17 2002.

[134] R. Adve and M. Wicks, "Joint domain localized processing using measured spatial steering vectors," in *Proceedings of the 1998 IEEE Radar Conference, RADARCON 98*, (Dallas, Texas), pp. 165–170, May 11-14 1998.

[135] W. Wang, S. Li, and S. Mao, "Modified joint domain localized reduced-rank stap," in *Proceedings of Radar 2001, CIE International conference*, (Beijing, China), pp. 773–777, October 15-18 2001.

[136] C. Peckham, A. Haimovich, T. Ayoub, J. Goldstein, and I. Reed, "Reduced-rank stap performance analysis," *IEEE Transactions on Aerospace and Electronic Systems*, vol. 36, pp. 664–676, April 2000.

[137] H. Wang, Y. Zhang, and Q. Zhang, "Lessons learned from recent stap experiments," in *Proceedings of 1996 IEEE CIE International Conference on Radar*, (Beijing, China), pp. 761–765, Oct 8-10 1996.

[138] J. Goldstein and I. S. Reed, "Theory of partially adaptive radar," *IEEE transactions on Aerospace and Electronic Systems*, vol. 33, pp. 1309–1324, October 1997.

[139] B. Himed and J. H. Michels, "Performance analysis of the multi-stage wiener filter," in *Record of the IEEE 2000 International radar conference*, (Alexandria, Virginia, USA), pp. 729–734, May 8-12 2000.

[140] P. Zulch, "Comparison of reduced-rank signal processing techniques," in *Conference Record of Thirty-Second Asilomar Conference on Signal, Systems & Computers, 1998*, vol. 1, (Pacific Grove, CA, USA), pp. 421–425, Nov 1-4 1998.

[141] S. Hayward, "Adaptive beamforming for rapidly moving arrays," in *Proceedings of 1996 CIE International Conference of Radar*, (Beijing, China), pp. 480–483, October 8-10 1996.

[142] M. Zatman, "Circular array stap," in *Record of the 1999 IEEE Radar Conference*, (Waltham, Massachusetts, USA), pp. 108–113, April 20-22 1999.

[143] S. Kogon and M. Zatman, "Bistatic stap for airborne radar systems," in *Proceeding of Adaptive Sensor Array Processing (ASAP) Workshop*, (MIT Lincoln Laboratory), pp. 1–6, March 14-15 2000.

[144] M. Zatman, "The properties of adaptive algorithms with time varying weights," in *Proceedings of the 2000 IEEE Sensor Array and Multichannel Signal Processing Workshop*, (Cambridge, Massachusetts, USA), pp. 82–86, March 16-17 2000.

[145] O. Kreyenkamp and R. Klemm, "Doppler compensation in forward-looking stap radar," *IEE Proceedings: Radar, Sonar and Navigation*, vol. 148, pp. 253–258, October 2001.

[146] F. D. Lapierre and J. Verly, "The range-dependence problem of clutter spectrum for non-sidelooking monostatic stap radars," in *Proceedings of 21st Benelux Meeting on Systems and Control*, (Veldhoven, The Netherlands), March 19-21 2002.

[147] F. D. Lapierre and J. Verly, "Evaluation of a monostatic stap radar range-compensation method applied to selected bistatic configurations," in *Proceedings of 3rd IEEE Benelux Signal Processing Symposium (SPS-2002)*, (Leuven, Belgium), pp. S02 1–4, March 21-22 2002.

[148] W. Melvin, M. Callahan, and M. Wicks, "Adaptive clutter cancellation in bistatic radar," in *Conference Record of 34th Asilomar Conference on Signals, Systems and Computers, 2000*, vol. 2, (Pacific Grove, CA, USA), pp. 1125–1130, October 29 - November 1 2000.

[149] R. Blum, W. Melvin, and M.Wicks, "An analysis of adaptive dpca," in *Proceedings of IEEE national Radar conference, 1996*, (Ann Arbor, MI, USA), pp. 303–308, May 13-16 1996.

[150] B. Himed, J. Michels, and Y. Zhang, "Performance analysis in radar applications," in *Proceedings of the 2001 IEEE Radar Conference*, (Atlanta, Georgia, USA), pp. 198–203, May 1-3 2001.

[151] M. Rangaswamy and J. Michels, "A parametric multichannel detection algorithm for correlated non-gaussian random processes," in *Proceedings of the IEEE National Radar Conference 1997*, (Syracuse, NY), pp. 349–354, May 13-15 1997.

[152] B. Himed, "Effects of bistatic clutter dispersion on stap systems," *IEE Proceedings on Radar, Sonar and Navigation*, vol. 150, pp. 28–32, Feb 2003.

[153] B. Mulgrew, P. Grant, and J. Thompson, *Digital Signal Processing: Concept and Applications*. Palgrave Macmillan Press Ltd., 2 ed., 2001.

[154] E. Jacobsen and R. Lyons, "The sliding dft," *IEEE Signal Processing Magazine*, vol. 20, pp. 74–80, March 2003.

[155] J. Capon, R. Greenfield, and R. Kolker, "Multidimensional maximum-likelihood processing of a large aperture seismic array," *Proceeding of IEEE*, vol. 55, no. 5, pp. 192–211, 1967.

[156] J. Capon, "High resolution frequency wavenumber spectrum analysis," *Proceeding of IEEE*, vol. 57, no. 8, pp. 1409–1418, 1969.

[157] C. Boor, *A Practical Guide to Splines*. Springer Verlag, reprint ed., August 26 1994.

[158] T. Schanze, "Sinc interpolation of discrete periodic signals," *IEEE Transactions on Signal Processing*, vol. 43, pp. 1502–1503, June 1995.

[159] E. Meijering, "A chronology of interpolation: From ancient astronomy to modern signal and image processing," *Proceedings of the IEEE*, vol. 90, pp. 319–342, March 2002.

[160] T. geometry of bistatic radar systems, "M.c. jackson," *IEE Proceedings Part F*, vol. 133, pp. 604–612, December 1986.

[161] M. I. Skolnik, *Radar Handbook (2nd ed.*, ch. 25, p. 25.14. McGraw-Hill,New York, 1990.

[162] H. L. V. Trees, *Optimum array processing*. 4, John Wiley & Sons, 2002.

[163] L. Harkness, *Airborne pulsed Doppler radar*, ch. 6, p. 117. Artech house, 2 ed., 1996.

[164] C. Band, C. Finlay, A. Kinghorn, R. Lyon, and M. Smith, "Impact of radomes on airborne pulse-doppler radar performance," in *Proceeding of IEE Radar 2002*, (Edinburgh, UK), pp. 291–294, Oct 15-17 2002.

[165] G. Morris and L. Harkness, eds., *Airborne Pulse Doppler Radar*. Artech House, 2 ed., 1996.

[166] R. J. Schlesinger, *Principles of Electronic Warfare*. Peninsular Publishing, 1961.

[167] I. Reed, J. Mallett, and L. Brennan, "Rapid convergence rate in adaptive array," *IEEE Transactions on Aerospace and Electronic Systems*, vol. 10, pp. 853–863, November 1974.

[168] R. A. Monzingo and T. W. Miller, *Introduction to adaptive arrays*. John Wiley & Sons, Inc., 1980.

[169] D. D. Feldman and L. J. Griffiths, "A projection approach for robust adaptive beamforming," *IEEE Transactions on signal processing*, vol. 42, pp. 867–876, April 1994.